

DOE/NASA/0372-1
NASA CR-180890
MTI 87TR57

1N-35
1.1.1.1.1
2/1/88

Conceptual Design of an Advanced Stirling Conversion System for Terrestrial Power Generation

(NASA-CR-180890) CONCEPTUAL DESIGN OF AN
ADVANCED STIRLING CONVERSION SYSTEM FOR
TERRESTRIAL POWER GENERATION Final Report
(Mechanical Technology) 376 p CSDL 10B

N89-12504

G3/85 Unclass
0166498

Mechanical Technology Incorporated
Sanders Associates, Inc.
Thermacore, Inc.
and
Pioneer Engineering and Manufacturing Company

January 1988

Prepared for
NATIONAL AERONAUTICS AND SPACE ADMINISTRATION
Lewis Research Center
Under Contract DEN 3-372

for

U.S. DEPARTMENT OF ENERGY
Conservation and Renewable Energy
Office of Solar Heat Technologies

DISCLAIMER

This report was prepared as an account of work sponsored by an agency of the United States Government. Neither the United States Government nor any agency thereof, nor any of their employees, makes any warranty, express or implied, or assumes any legal liability or responsibility for the accuracy, completeness, or usefulness of any information, apparatus, product, or process disclosed, or represents that its use would not infringe privately owned rights. Reference herein to any specific commercial product, process, or service by trade name, trademark, manufacturer, or otherwise, does not necessarily constitute or imply its endorsement, recommendation, or favoring by the United States Government or any agency thereof. The views and opinions of authors expressed herein do not necessarily state or reflect those of the United States Government or any agency thereof.

Printed in the United States of America

Available from

National Technical Information Service
U.S. Department of Commerce
5285 Port Royal Road
Springfield, VA 22161

NTIS price codes¹

Printed copy: A17

Microfiche copy: A01

¹Codes are used for pricing all publications. The code is determined by the number of pages in the publication. Information pertaining to the pricing codes can be found in the current issues of the following publications, which are generally available in most libraries: *Energy Research Abstracts (ERA)*; *Government Reports Announcements and Index (GRA and I)*; *Scientific and Technical Abstract Reports (STAR)*; and publication, NTIS-PR-360 available from NTIS at the above address.

Conceptual Design of an Advanced Stirling Conversion System for Terrestrial Power Generation

Mechanical Technology Incorporated
Latham, New York

Sanders Associates, Inc.
Nashua, New Hampshire

Thermacore, Inc.
Lancaster, Pennsylvania

and

Pioneer Engineering and Manufacturing Company
Madison Heights, Michigan

January 1988

Prepared for
National Aeronautics and Space Administration
Lewis Research Center
Cleveland, Ohio 44135
Under Contract DEN 3-372

for
U.S. DEPARTMENT OF ENERGY
Conservation and Renewable Energy
Office of Solar Heat Technologies
Washington, D.C. 20545

CONTENTS

	Page
1.0 INTRODUCTION	1
2.0 SUMMARY AND CONCLUSIONS	8
3.0 SYSTEM DESCRIPTION	17
4.0 ENGINE DESCRIPTION	21
5.0 ENGINE ANALYSIS	40
6.0 ALTERNATOR DESIGN AND ANALYSIS	63
7.0 SYSTEM ANALYSIS	75
8.0 DEVELOPMENT STATUS AND NEEDS	108
9.0 REFERENCES	115
APPENDIXES	
I RECEIVER DESIGN AND ANALYSIS	117
II HEAT TRANSPORT SYSTEM DESIGN AND ANALYSIS	179
III COST PERFORMANCE TRADE-OFF BASIS	213
IV PRELIMINARY DESIGN DESCRIPTION	229
V MANUFACTURING COST ESTIMATE	243

1.0 INTRODUCTION

A free piston Stirling engine coupled to an electric generator or alternator with a nominal 25 kWe power output absorbing thermal energy from a nominal 100 square meter parabolic solar collector and supplying electric power to a utility grid was identified within the DOE Solar Power Development Program at Sandia National Laboratories as a system with economic potential. In response to an RFP for an Advanced Stirling Conversion System (ASCS) MTI proposed a system, based on existing in-house technology, in which a linear alternator is directly coupled to a free piston engine in an hermetically sealed arrangement. MTI received a contract, DEN3-372, from NASA-Lewis with funding from Sandia National Labs in December 1986. This report documents the results of the conceptual design study of an ASCS. A manufacturing cost estimate generated by The Pioneer Engineering Company is summarized in section 2.5. and reported in detail in Appendix V.

1.1 Objectives of the Study

The objectives of the study as outlined in Reference 1 are as follows:

1. Define the ASCS configuration; major component form, critical tolerances, major system dimensions, materials, construction and component operating conditions to meet the ASCS requirements
2. Provide a manufacturability and cost evaluation for the ASCS
3. Predict ASCS performance over the range of solar input required to produce power
4. Estimate system and major component weights
5. Define engine and electrical power conditioning control requirements

6. Define key technology needs not ready by the late 1980's in meeting efficiency, life, cost and weight goals for the ASCS

The requirements for an ASCS as delineated in Reference 1 are summarized in Table 1.1.

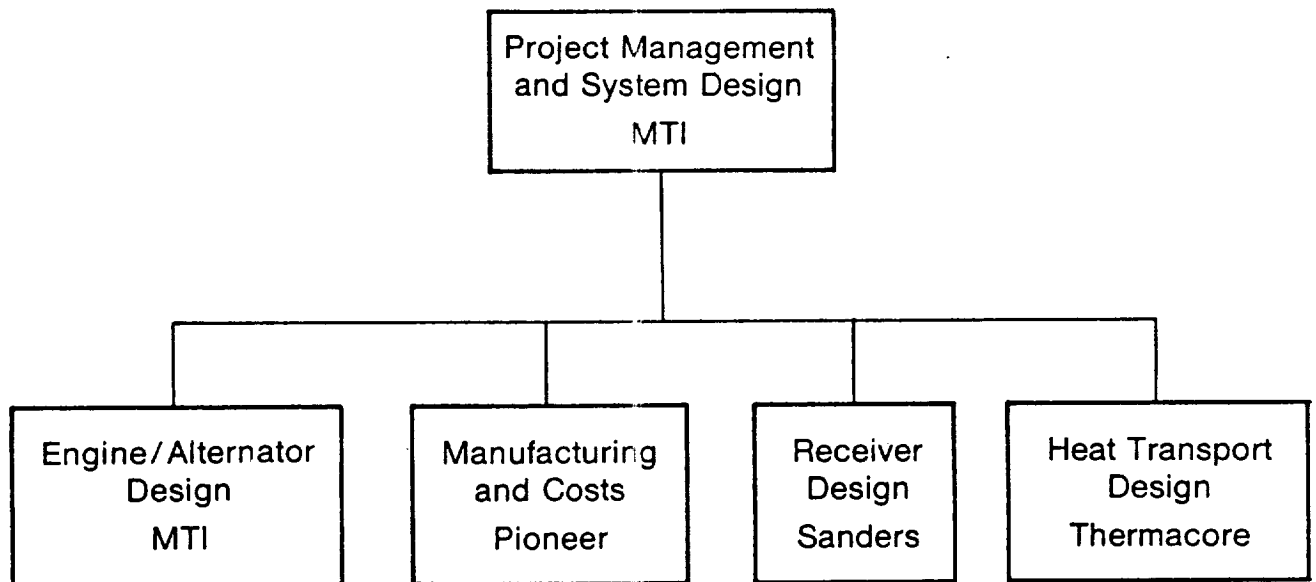
1.2 Program Outline

As indicated in the proposal [2], the team assembled to address all phases of the study was Mechanical Technology Inc., Sanders Associates Inc., Thermacore Inc. and Pioneer Engineering Company. As shown in the organization chart, Fig. 1.1, MTI was responsible for project management, system design, and engine-alternator design. Sanders and Thermacore, under subcontract, developed the design of the receiver and heat transport system, which are intimately interrelated. The contract directed that Pioneer Engineering be selected to perform manufacturing and cost studies. This direction, which applied to both this program and the parallel program being conducted on a Stirling engine hydraulically coupled to a rotary alternator, is intended to minimize bias in the cost estimates conducted on the alternate approaches.

The effort was broken down into three phases, i.e. preliminary conceptual design, final conceptual design and cost analysis. Design review meetings were planned and held at the end of the two design phases at NASA-LeRC. Feedback from the first design review was reflected into the design during the second phase. This report covers both the technical work done during the first two phases and the cost analysis performed during the third phase. Figure 1.2 outlines the work breakdown and schedule.

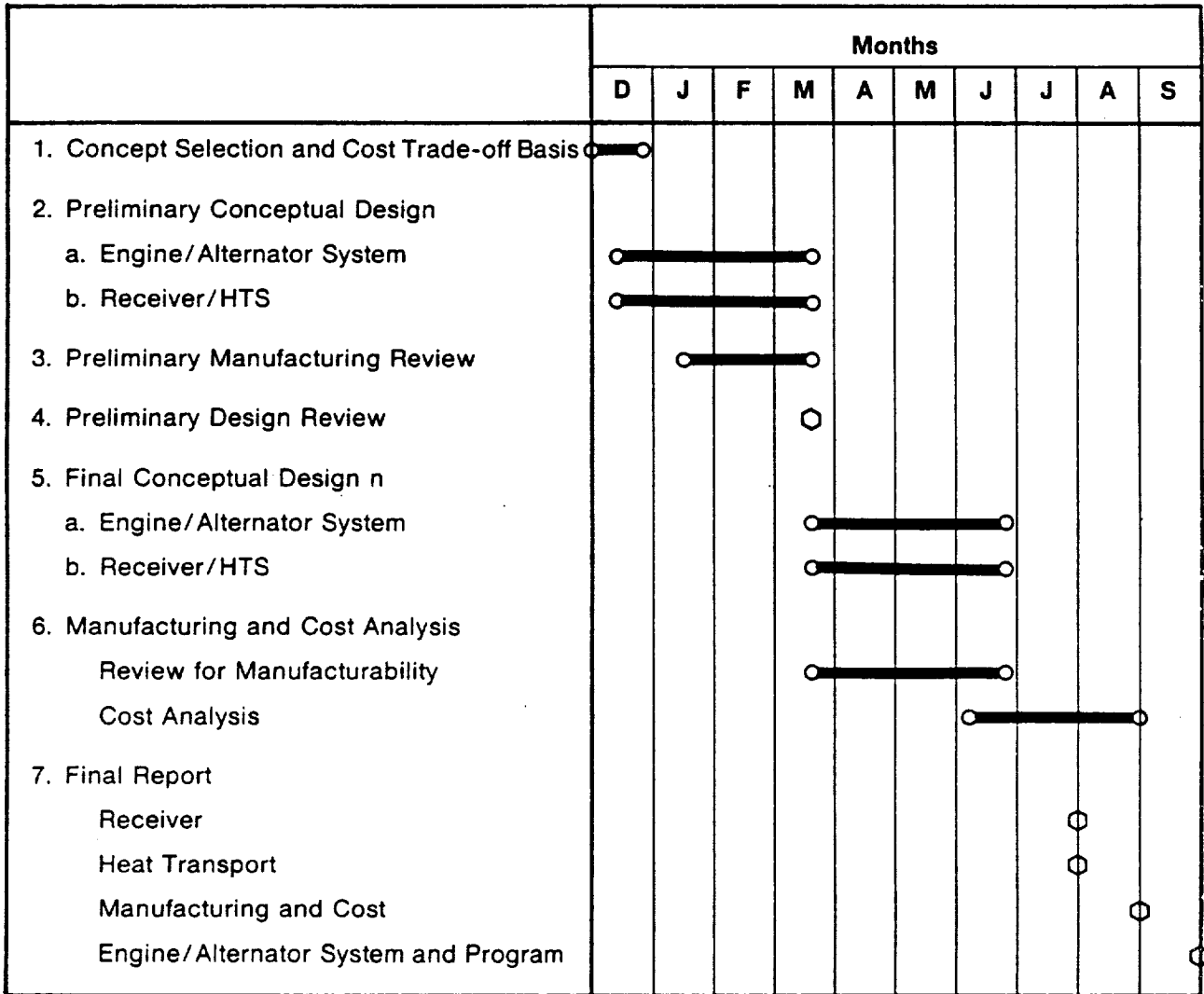
1.3 Conceptual Approach

The conceptual approach utilizes an hermetically sealed free-piston Stirling engine with an integral, direct-coupled linear alternator (FPSE/LA) to convert solar thermal energy to electric power. The heat input to the engine is from a receiver located at the focal plane of a parabolic solar collector (~ 100 square meters). The receiver is directly attached to the engine and heat is transferred from the receiver heated surface to the engine using a liquid metal heat pipe approach. Electric power generated by the alternator is supplied via suit-



Program Organization

Figure 1.1



Program Schedule

Figure 1.2

able controls to a utility power grid. The basic concept is very similar to the Space Power Demonstrator Engine (SPDE) currently on test at MTI which was built to demonstrate thermal to electric power conversion for long life unattended operations in outer space using a nuclear reactor heat source.

MTI has been developing Stirling engine technology since the middle of the 1970's. This has encompassed both kinematic (rotating crankshaft) engines and free-piston (sealed linear drive) engines. Seal wear in kinematic engines is expected to require engine maintenance at intervals of a few thousand operating hours. For the Solar application (over 50000 hrs) this introduces an undesirable maintenance requirement which is avoided in free piston engines by using non-contacting seals in hermetically sealed engines. Power generation and heat activated heat pumps requiring a maintenance free long life are the applications currently being developed. At MTI free-piston engines started at relatively low power levels, (i.e. less than 1.0 kW) but over the years have been steadily increased. Success of a 3 kW engine alternator led to the current Space and Heat Pump Programs. The space engine (SPDE) used two 12.5 kW modules in a linearly opposed arrangement to eliminate vibration. This engine has been converted into two separate 12.5 kW engines referred to as Space Power Research Engines (SPRE). The next space engine which is scheduled to be designed and built in 1988-89 is a 25 kW single module and studies are in process to evaluate the performance capability of even larger engines. A nominal 25 kW output from a 100 square meter solar dish coupled with the long life, low maintenance requirements can be met with a FPSE/LA using technology that has been developed at MTI in the above-mentioned programs.

1.4 Cost Performance Trade-offs

A basis for determining the trade-offs between cost, performance and life was formulated at the beginning of the study and is included as Appendix III.

The five key parameters which were identified that involved a trade-off were:

Hot Side Temperature (800°C vs. 700°C)

Alternator Concept - Permanent Magnet vs. Saturated Iron

Seal Concept (Clearance vs. Piston Rings)

Cooling System Size

Ceramic vs. Stainless Steel Power Piston

While detailed costs of all alternates were not generated, the simplified formulations at the end of Appendix III, along with rough estimates of the probable cost and performance of alternates were used as a guideline in selecting the baseline design defined in the preliminary conceptual design phase.

Considerations of development status and technical uncertainties as opposed to cost and performance were the primary basis for changes between the preliminary and final conceptual designs.

The trade between maintenance cost, and installed cost, provided a very clear incentive to devise a system which is essentially maintenance free.

Table 1.1

ASCS SPECIFIED REQUIREMENTS

Insolation:	Design Point	950 W/sq. m.
	Peak	1100 W/sq. m.
Baseline Head Temperature:		800°C
Costs:	Life Cycle Cost	Minimum
	E/A Cost Goal	300\$/kWe @ 10,000/year
Life:	ASCS	30 years (60,000 h)*
	E/A	40,000 h.
Test Installation:		TBC (Sandia)
Collector Diameter		11 m (95 sq. m.)
Heat into Receiver		75 kWt @ 950 W/sq. m.
Weight Limit		2000 lbs
Moment Limit		4000 ft lbs
Vibratory Force Limit		150 lbs
Receiver:	Aperture	8.0 in.
HTS Concept:		Heat Pipe or Reflux Boiler
	Fluid	Liquid Metal
Ambient Temps - Operating		20 to 92°F
Shutdown		-20°F
Power Output - Voltage		1φ/120-240/60 Hz
Power Factor		>.85
Distortion		<2.5%
Controls - Normal Operation		Automatic
Faults		Automatic
*At 3000 hr/yr	30 yrs = 90,000 hrs.	

2.0 SUMMARY AND CONCLUSIONS

2.1 Design Approach and System Performance

The design approach is to maximize the ratio of seasonal power output to ASCS system cost within the following constraints:

- 30 year life without major replacements
- Negligible planned maintenance
- Avoid elements that have potential reliability problems
- Minimize the use of technology that might not be available in the 1980's

Based upon the interrelationship of creep-rupture strength of pressure vessel materials, operating hours per year and operating temperature it was determined that no significant advantage occurred from designing to less than the full plant operating life of 30 years.

There is some uncertainty with respect to the long-time behavior of materials exposed to sodium. The approach taken is to limit the materials exposed to sodium to one structural material (Inco 600) and one wick material (Nickel). These materials are expected, based upon their metallurgical character, to be resistant to long-time attack. As the design evolved the operating temperature was reduced from 800°C to 700°C to minimize the risk of long-term attack to the maximum extent practical.

Since the engine is designed with noncontacting seals and bearings on the moving parts to preclude wear mechanisms, and since it is an all-welded, hermetically-sealed system there is no planned maintenance on components within the engine helium or receiver sodium boundaries. Vibration control is by a passive device (mass on springs) with no active control required.

The normal control system is elegantly simple. For all normal operations the two parameters controlled are head temperature and minimum cooler temperature. Head temperature is controlled by adjusting the turns ratio of an autotransformer which couples the engine/alternator to the grid. This produces a smooth transition during start-up and all normal operational transients. The minimum cooler temperature is maintained by thermostatic control of the radiator fan, such as in a car engine.

The additional controls required to limit the damage from potential single point failures are also simple. They include a solenoid-actuated damping valve within the engine to kill the engine in the event electrical control is lost. Signals used to trigger emergency shutdown are heater temperature, cooler temperature casing acceleration, current and voltage in the electrical output circuit.

2.2 Key Features of the System

Figure 3.1 shows the layout of the system and Figure 4.1 shows a cross section through the engine-alternator.

The key features are summarized in Table 2.1 and a weight breakdown is shown in Table 2.2.

2.3 Evolution of System

Table 2.3 summarizes the key characteristics of the system at the proposal, preliminary design review and final design review stages of design evolution.

Table 2.4 shows the performance and weight calculated at the various stages of the design evolution.

In addition to the performance reported in the proposal, the preliminary design and the final design reviews, the potential gains to be made by incorporating a foil regenerator and ceramic piston in future 700°C engines is shown in the fourth column. The last column, which is a repeat of the PDR column shows the further gain possible if 800°C operation in a sodium environment could be justified.

Table 2.1

KEY FEATURES OF SYSTEM

Receiver/Heat Transport System

- Single heat pipe wick on hemispherical shell with gravity return of condensed liquid

Engine/Alternator

- Annular Regenerator/Cooler
- Tubular Heater - only one structural material in contact with sodium
- Sintered Wire Regenerator (Felt Metal)
- Non-Contacting Seals
- Hydrodynamic Gas Bearings (Spinning Pistons)
- Stainless Steel Power Piston and Cylinder
- Permanent Magnet Alternator
- Heater Head Temperature Controlled by Ground-Mounted Autotransformer in Electric Circuit
- Passive Vibration Absorber and Soft Engine Mounts
- Ground-Mounted Cooling System Similar to Automobile
- Ground-Mounted Capacitors in Load Circuit Assure Stable Engine Operation at all Conditions
- Inherent Control of Power Factor
- Pneumatic Damping Valve to Kill Engine if Alternator Coil is Open Circuited

Table 2.2

SYSTEM WEIGHT BREAKDOWN

Dish Mounted Equipment

(Design Limit 2000 lbs)

Engine Alternator	700 lbs
Receiver	150 lbs
Vibration Absorber	200 lbs
Structure	250 lbs
	<hr/>
	1300 lbs
Moment	3200 lb ft
(Design Limit 4000 lb ft)	

Auxiliaries*

Cooling System	✓200 lbs
Controls (Variac) and Capacitors	✓100 lbs

*Ground Mounting is an option - Dish Mounting is preferred.

Table 2.3
SUMMARY OF KEY SYSTEM CHARACTERISTICS

	Proposal	F.D.R.	F.D.R.
Receiver - max	87 kWt	87 kWt	87 kWt
Receiver - design pt	75 kWt	75 kWt	75 kWt
Heater - Temperature	800°C	800°C	700°C
Ambient Air Temperature	33°C	33°C	33°C
Net Power Output	25.0 kWe	26.5 kWe	23.2 kWe
Annual Power Output	59,000 kWh	70,000 kWh	59,000 kWh
Number of Cycles	1 or 2	1	1
General Arrangement	Modified SPDE	Simplified SPDE	Simplified SPDE
Heat Pipe Concept and Fluid	Single or Multiple Various	Single Sodium	Single Sodium
Bearings and Seals	Hydrostatic or Hydrodynamic Rings or Clearance	Hydrodynamic Clearance	Hydrodynamic Clearance
Alternator	Magnets or Iron Pl.	Magnets (Neod)	Magnets (Neod)
Regenerator	Screen or Sintered	Foil	Sintered
Controls (Th, P.F.)	Displacer Damping and Mean Pressure	Auto-transformer	Auto-transformer (Control) Pneumatic Damping (Fault)
Power Piston	Unspecified	Ceramic	Stainless Steel
Vessel Material (Hot)	Unspecified	Inco 713LC	Inco 713LC (or Inco 718)
Heater Tubes and Receiver Structure	Unspecified	Incolloy 800	Incolloy 800
Frequency Tolerance	Unspecified	Unspecified	± 1% (.6 Hz)
Mount Frequency	Unspecified	Unspecified (Fairly High)	5 Hz
Alternator and Gas Spring Cooling	External	External	Internal

Table 2.4

PERFORMANCE AND WEIGHT SUMMARY

	<u>Proposal</u>	<u>PDR</u>	<u>FDR</u>	<u>Future</u>
Thot (°C)	800	800	700	800
Vessel Material	-	Inco 713LC	Inco 713LC	Inco 713LC
Regenerator	Sintered	Foil	Sintered	Foil
Power Piston	-	Ceramic	S.S.	Ceramic
Design Point Power at 75 kw	~ 25.0	26.5	23.2	25.0
Seasonal Output (kWh)	~58600	70500	59200	65000
Weight of Dish (lbs)	<2000	1200	1300	1000
Moment at Mount (ft.lb.)	<4000	3200	3500	2700
Max. Vibration Force (lb)	<150	-*	<40	<150
Weight on Ground (lb)	-	500	500	500

*Sensitivity to Line Frequency was Identified.

Table 2.5

RECAP OF MANUFACTURING COST FOR
MTI 25 KW SOLAR DRIVEN STIRLING ENGINE ELECTRICAL GENERATOR
1984 COST

PAGE KEY		MATERIAL COST	DIRECT LABOR COST	BURDEN COST	SCRAP ALLOWANCE	MANUFACTURING COST	LABOR MINS.
5	1.	Receiver Shell Arteries Wicking	\$ 521.02	\$ 7.88	\$ 46.95	\$ 581.64	39.50
15&59	2.	Stirling Engine With Vibration Absorber	3,483.15	101.22	252.81	3,874.51	504.15
68	3.***	Linear Alternator	863.27	28.73	141.72	1,043.12	141.60
86	4.*	Temperature Sensors Accelerometers Auto Transformer Tuning Capacitors	398.65	6.86	27.44	433.30	7.54
98	5.**	Radiator Fan & Driver Water Pump & Driver	811.02			811.02	
		Pareto's Extension @ 125% On Cost	\$ 6,077.11	\$144.69	\$468.92	\$ 6,743.59	692.79
			\$ 7,596.39	\$180.86	\$586.15	\$ 8,429.49	692.79

* As quoted from engineering information as supplied.

** Cost adjusted for comparison, engineering information not complete for direct comparison.

***No material cost adjustment as magnetic materials not quotable in 1984.

Estimated Tooling Cost: \$802,200

Estimated Capital Equipment: \$4,108,200

2.4 Development Status and Needs

Some of the design details of the heat transport system have not been fully demonstrated on a similar system. While major difficulties in reducing the design to a satisfactory operating system are not expected, some of the features should be demonstrated before incorporating the receiver-heat transport components into a fully operational system. The fabrication and satisfactory operation of the relatively large sintered wick on the thin sheet receiver structure should be demonstrated. A tentative program outlined in Section 8 incorporates this approach. The particular design was selected over a pool boiler because for a production engine it is smaller and potentially less costly. For near-term demonstration of the engine/alternator a pool boiler is an acceptable alternate approach.

Since the engine/alternator is based on the same technology as the 12.5 kWe per cylinder space power engine currently on test at MTI, the basic feasibility of the engine/alternator concept is well established. The one feature that has not yet been fully demonstrated is the use of hydrodynamic bearings. Since initial assessment of hydrodynamic bearings is currently in progress on the space engine, and since they are significantly simpler (less costly) and more efficient than hydrostatic bearings, they have been selected for the production solar engine. If demonstration of their performance on the space engine is delayed, the first solar test engine could incorporate both hydrostatic and hydrodynamic bearings.

In a brand new design there is always some uncertainty in the performance predictions. Significant understanding of both engine thermodynamic behavior and loss mechanisms in and around the linear alternator on the space engine have been obtained. Ongoing work is producing further improvements in the methodology used to design free-piston engines and linear alternators. Basing a new design on this understanding reduces the risk of large errors in performance prediction.

2.5 Manufacturing Cost Estimate.

Appendix V presents the details of the cost estimate performed by Pioneer Engineering Company.

The results of the cost study are summarized in Table 2.5. The Manufactured Cost for the complete system is \$8429. The installed cost goal (see Appendix III) is \$13000. Costs have been translated into 1984 dollars to be consistent with the DOE 5 year plan which established the cost goal. An estimate of the factor by which the manufacturing cost must be raised to represent an installed cost was not made. Both the manufacturing cost estimate and the cost goal have significant uncertainties in them. At this stage the projected manufacturing cost is in the range where development of the Free Piston Stirling Engine can be justified.

The largest cost element is the Stirling engine proper. This constitutes about 60% of the system total. The two most costly elements of the engine are the heater head and regenerator. These are estimated at 35% and 16% of the engine cost or 21% and 10% of the system cost respectively. These two components are where further effort to reduce their cost will have a significant impact.

If XF818 can be substituted for Inco713LC (see section 5.1 for further discussion) significant savings might be attained depending on a more detailed determination of manufacturing cost.

Introduction of a foil regenerator (development on other programs is anticipated) has the potential of reducing cost and more importantly of increasing performance.

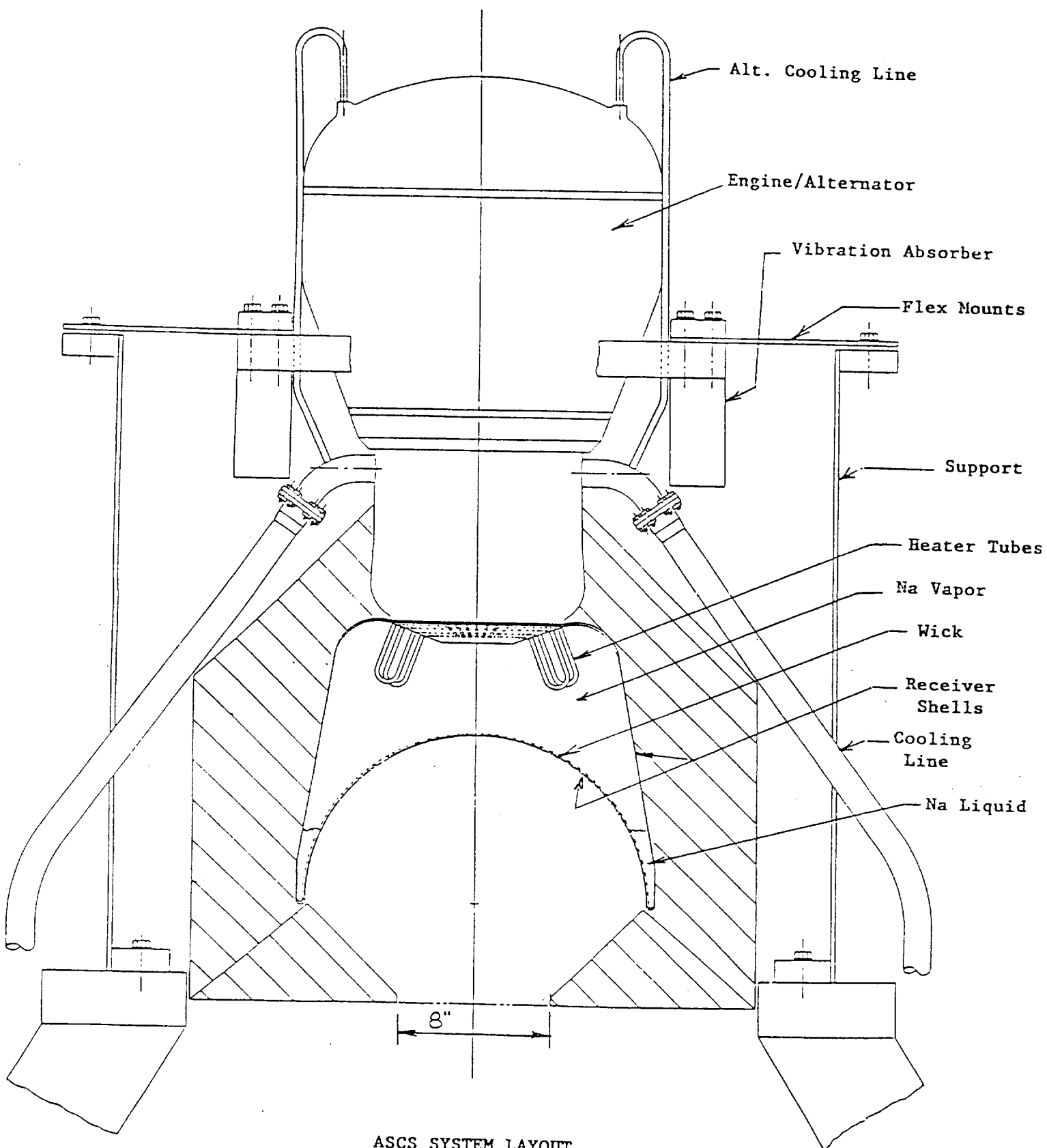
3.0 SYSTEM DESCRIPTION

The elements of the system are:

1. Receiver/Heat Transport System
2. Engine-Alternator
3. Vibration Absorber
4. Engine Mounts
5. Cooling System
6. Power Control System

Each of the above are explained in detail in subsequent sections of the report. Coverage in this section is limited to a description of the overall arrangement and subsystem interfaces. Elements 1 through 4 are located on the solar collector, the main components of 5, 6 and 7 can be located on the ground or on the collector. Mounting on the collector is preferred since it would permit the complete system to be assembled at the factory and minimize the effort (cost) of installation. This approach adds weight to the equipment mounted on the dish. The final selection should be based on further study. Figure 3.1 shows the system arrangement on the solar collector. The mounting ring configuration applies to the Sandia Test Bed Collector. The clearance within the mounting ring is 31.25 inches and the supporting bolt circle diameter is 36.0 inches. These dimensions were taken from Sandia Drawing No. S60104, Part No. 2.

The receiver/heat transport system is described in detail in Appendices I and II. As shown in Figure 3.1, the receiver comprises a hemispherical shell which collects the thermal energy from a parabolic solar collector which focuses the incident insolation through an 8 inch diameter aperture in the face of the collector. The hemispherical shell, the ellipsoidal head on the engine and the interconnecting shell form a cavity into which the engine heater tubes project. A layer of sintered porous metal containing arteries to aid fluid distribution is located on the back face of the hemispherical head and about one pound of sodium is contained within the cavity. Heat transfer between the heated hemispherical shell and the engine heater tubes is based on the same principle used in conventional tubular heat pipes, except gravity is used to return the condensed vapor to the sump. This is covered in detail in Appendix II. The



ASCS SYSTEM LAYOUT

Figure 3.1

engine-alternator, which is described in Section 4, interfaces with the system at the heater tubes, the cooler assembly and the alternator power output terminals. Heat input at the heater tubes is from vaporized sodium in the receiver cavity which condenses and gives up its latent heat of vaporization. The condensed sodium returns by gravity to the sump and is distributed by capillary action in the wick over the heated shell surface. Heat is conducted across the walls of the heater tubes and the helium in the engine cycles back and forth through the tubes and absorbs the heat by forced convective heat transfer. Heat which is not converted to electrical power is rejected to the cooling system at the engine and alternator coolers. The cooling lines are shown in Figure 3.1. The coolant is a water/glycol mixture which is circulated through an air-cooled radiator. The radiator, motor-driven fan, water pump and thermostatic control comprises the cooling system, which is covered further in Section 7.

The power control system incorporates a bank of capacitors and a motor-driven autotransformer between the alternator and the grid. The capacitors adjust the reactance of the alternator to assure stable system operation over the full operating range.

Since the grid voltage is essentially constant the autotransformer controls voltage at the alternator terminals. As explained in Section 7, this permits power level to be adjusted to match changes in power input while maintaining the head temperature at its design point, and thus maximizing engine efficiency.

The vibration absorber is an undamped mass on a set of springs. The mass and spring stiffness is selected so that the resonant frequency of the absorber is the same as the nominal operating frequency of the engine (i.e. 60 Hz). As explained further in Section 7, the vibratory motion of the engine casing can be virtually eliminated at the design frequency. Due to small variations in line frequency, a residual vibration cannot be avoided at the specified 1% variation extreme. To reduce the force transmitted to the collector in this situation, a relatively soft support structure is used. The set of flat plates shown on Figure 3.1 are designed to limit the force transmitted due to this residual vibration at off-frequency operation. The soft mounts would actually limit force transmission to the 150 lb level specified in Table 1.1 without a vibration absorber. It is currently thought prudent to include a vibration

absorber to minimize g-loading on the receiver and further reduce off-frequency force transmission to the collector.

A breakdown of the system weight is shown in Table 2.2. The total weight on the dish of 1300 lbs is well below the 2000 lbs allowed per Table 1.1. As indicated above, it may be preferable to locate the cooling and control components on the dish.

4.0 ENGINE-ALTERNATOR DESIGN DESCRIPTION

4.1 Design Requirements and Options

The design requirements can be summarized as:

- High Efficiency
- Low Cost at 10,000 Units/Year Production Rate
- Long Life (30 Years at 3000 Hours/Year)
- High Reliability
- Low Maintenance Costs
- Minimal New Development

High efficiency is obtained by understanding the loss mechanisms and minimizing them within the constraint of a producible design. The engine, as designed, has an estimated shaft efficiency of 38.5% and an overall efficiency including alternator, auxiliary and control losses of 33.7%. At 59% and 52% of Carnot efficiency respectively, these constitute fairly high performance for a 25 kW, single-cylinder free-piston engine operating on helium and utilizing low cost piston and displacer materials.

Every effort has been made to develop a design that is amenable to low cost production in fairly large quantities. The final cost numbers developed by manufacturing engineers at Pioneer as reported in Appendix V suggest that acceptable production costs are attainable.

No significant cost savings or performance gains were identified for designing to less than the full design life of an operating plant (30 years).

High reliability and low maintenance requirements, along with avoidance of undemonstrated features to the maximum extent practical were reflected in the final concept selections.

Table 4.1 shows the options considered and the final options selected.

Table 4.1

Concept Seletion

(Final Selection Underlined)

- | | |
|--------------------------|--|
| 1. Seals | <u>Noncontacting</u> vs. Contacting |
| 2. Bearings | <u>Hydrodynamic</u> vs. Hydrostatic vs. Contacting |
| 3. Arrangement | <u>Annular HX</u> vs. Canister HX |
| 4. Heater Temperature | <u>700°C</u> vs. 800°C |
| 5. Regenerator | <u>Feltmetal</u> vs. Weave vs. Foil |
| 6. Power Piston Material | <u>St. Steel</u> vs. Ceramic |
| 7. Alternator Concept | <u>Perm. Magnet</u> vs. Sat. Plunger |

Items 1 through 6 will be discussed further in Section 4.4. Item 7 is covered in Section 6.

4.2 General Arrangement

Figure 4.1 shows a cross section of the final conceptual design of the engine alternator. It is comprised of the following elements:

1. Displacer Assembly
2. Heat Exchanger/Pressure Vessel Assembly
3. Power Piston Assembly
4. Power Piston Cylinder Assembly
5. Outer Stator Assembly
6. Pressure Vessel Closure

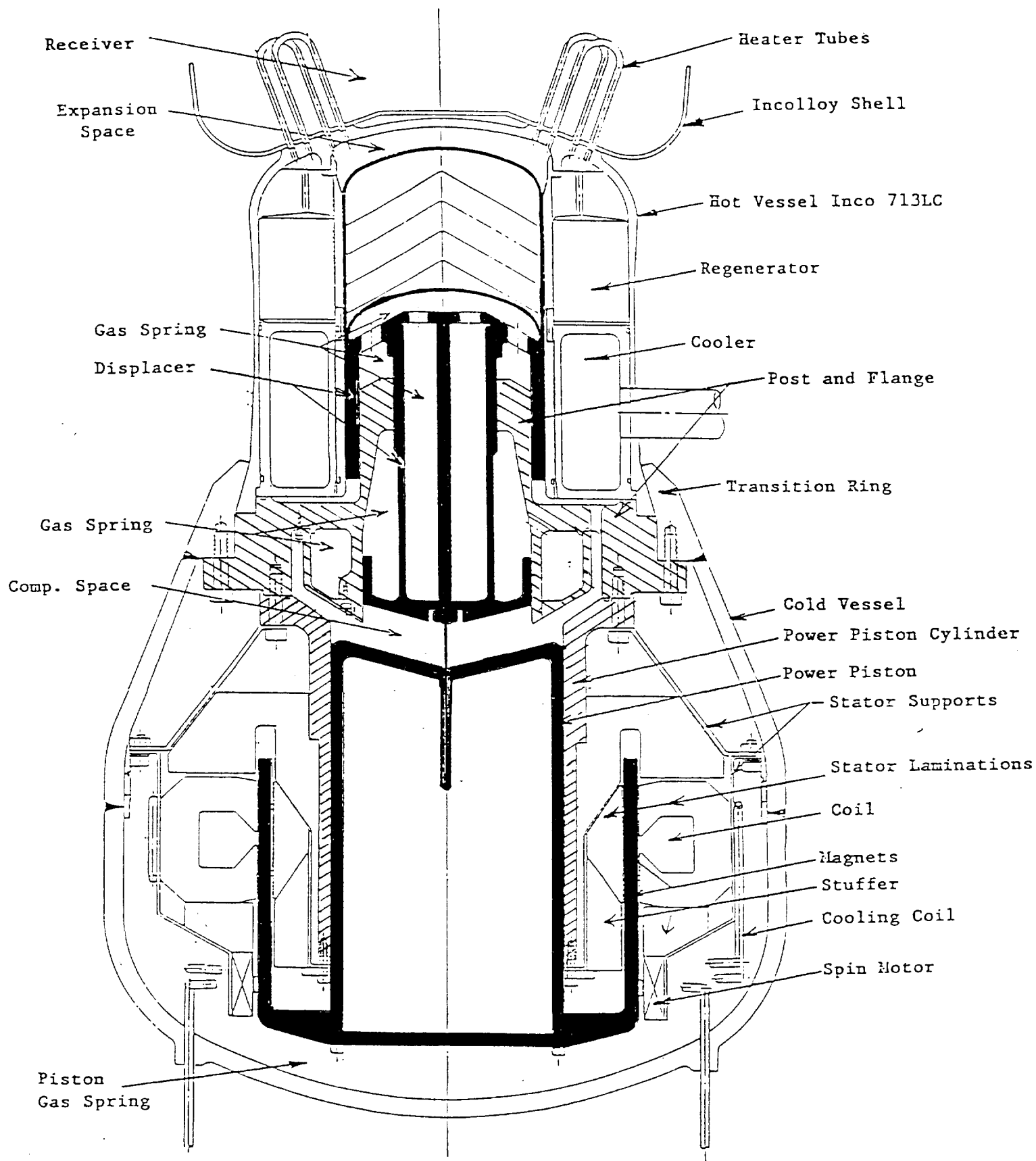
Figures 4.2 and 4.3 show these assemblies in partially exploded format.

The design as it existed at the preliminary design review is covered in Appendix IV. The figures therein also show the arrangement of the components

In Figure 4.1 the two moving elements (the power piston and displacer) are shown in heavy shading. The post and flange and power piston cylinder which guide the moving parts is shown crosshatched.

The working fluid of the engine is helium at a mean pressure of 105 Bar (1520 psi). Hydrogen would result in higher efficiency, but the long-term permeation characteristics, particularly into the heat pipe receiver make it unacceptable for long life, replacement-free operation. The design operating temperature of the heater (sodium condensation temperature) is 700°C (973°K). Based upon the thermodynamics of a Stirling cycle engine the attainable efficiency is a function of the ratio of the absolute temperature of the heater and cooler. The cooler temperature is established by ambient atmospheric conditions to be in the range 300 to 330°K.

For a solar system, since there is no control on the energy source the delivered power is directly proportional to system efficiency. To maximize this the engine should be operated at as high a temperature as materials will allow for the conditions of pressure and life required. From creep strength on high temperature alloys it was determined that 800°C (1073°K) would be possible,



ASCS ENGINE ALTERNATOR

Fig. 4.1

Table 4.2
ENGINE PARAMETERS

Working Gas		Helium
Heater Tube Surface Temperature	T(H)	700°C
Cooler Tube Surface Temperature	T(C)	60°C
Mean Pressure	P(M)	105 bar
Frequency	F	60 Hz
Design Point Heat Input	(QIN)	68.8 kW
Piston Diameter		7.5 ins.
Displacer Diameter		6.0 ins.
Piston Half Stroke (Design Point)		.71 ins.
Displacer Half Stroke (Design Point)		.58 ins.
Displacer Phase (Ahead of Piston)		60 deg
Rod Area		1.2 sq.in.
Heater		
No. of Tubes		96
Tube O.D.		5.0 mm
Tube I.D.		4.0 mm
Heated Length		9.85 in.
Regenerator		
Type		Sintered Wire
Thickness		.001 in.
Porosity		90%
Length		2.81 ins.
Cooler		
No. of Tubes		360
Tube O.D.		4.0 mm
Tube I.D.		3.0 mm
Cooled Length		4.5 ins.
Power Piston Mass		55 lbs
Displacer Mass		24.0 lbs
Casing Mass		630.0 lbs
Absorber Effective Mass		100.0 lbs
Displacer Spring Constant		9546 lb/in.
Power Piston Spring Constant		6836 lb/in.
Absorber Spring Constant		36,781 lb/in.
Displacer Damping		.535 lb-s/in.
Power Piston Damping		.323 lb-s/in.
Absorber Damping		0.0 lb-s/in.
Coil Inductance		.0057 henry
Coil Resistance		.0642 ohm
Core Resistance		63.5 ohm
Tuning Capacitance		.00144 farad

however, due to uncertainties in the long-term behavior of alloys exposed to sodium, 700°C was selected as the reference hot side temperature to reduce the probability of unacceptable attack of alloys and/or joints in the receiver and engine heater materials. The selection of the basic parameters of the system, which are listed in Table 4.2 were established to maximize the system efficiency.

The overall length of the engine-alternator is 34 inches and the maximum diameter is 20 inches. Overall weight is approximately 700 lbs. A weight breakdown is shown in Table 4.3.

4.3 Principle of Operation

There are two moving parts in the engine, i.e. the displacer and the power piston.

The displacer is constrained by the post and flange to move in the axial direction and similarly the power piston is guided by the power piston cylinder. A set of magnets is housed in the alternator plunger attached to the end of the power piston.

During operation the displacer and power piston move back and forth in a reciprocating motion at 60 cps (3600 cpm), the displacer leading the power piston by about 60°. The displacer motion causes the high pressure (105 Bar) helium gas in the engine to flow back and forth between the hot expansion space and the cold compression space. During this cyclic flow the gas absorbs heat at the heater tubes, interchanges heat with one regenerator and rejects heat at the cooler. The work of the thermodynamic cycle is used to drive the alternator plunger, which is attached to the power piston, and also to overcome mechanical losses in the gas springs and seals.

The magnetic field from permanent magnets on the plunger is caused to traverse the coil of the alternator and induce 60 Hz single phase power in the coil, which is extracted at the alternator terminals.

For a free-piston engine, stable operation over the full power range requires careful selection and tuning of the parameters which affect the engine dynamics,

i.e. displacer and piston mass, displacer and piston gas spring stiffness, alternator inductance and load characteristics. Engine and system dynamics is covered in more detail in Section 7. The rod area (difference between the frontal area of the displacer in the expansion space to that in the compression space) is also a major parameter affecting displacer stroke. The numerical values of the final dynamic parameters are shown in Table 4.2.

4.4 Subassembly Concept Selection and Description

4.4.1 Heat Exchanger and Pressure Vessel

The general arrangement of the heater, regenerator and cooler, along with heater temperature and pressure vessel material selection, involves interdependent considerations of material strength and engine performance. The key parameter is the regenerator length. Stress conditions on the pressure boundary are most severe in the pressure wall at the ends of the regenerator. This is because the stresses due to the temperature gradient along the regenerator wall are most severe at these locations and combine with stresses due to the oscillating helium pressure to produce a severe fatigue situation. The severity of this is approximately inversely proportional to the ratio of regenerator length to regenerator wall diameter.

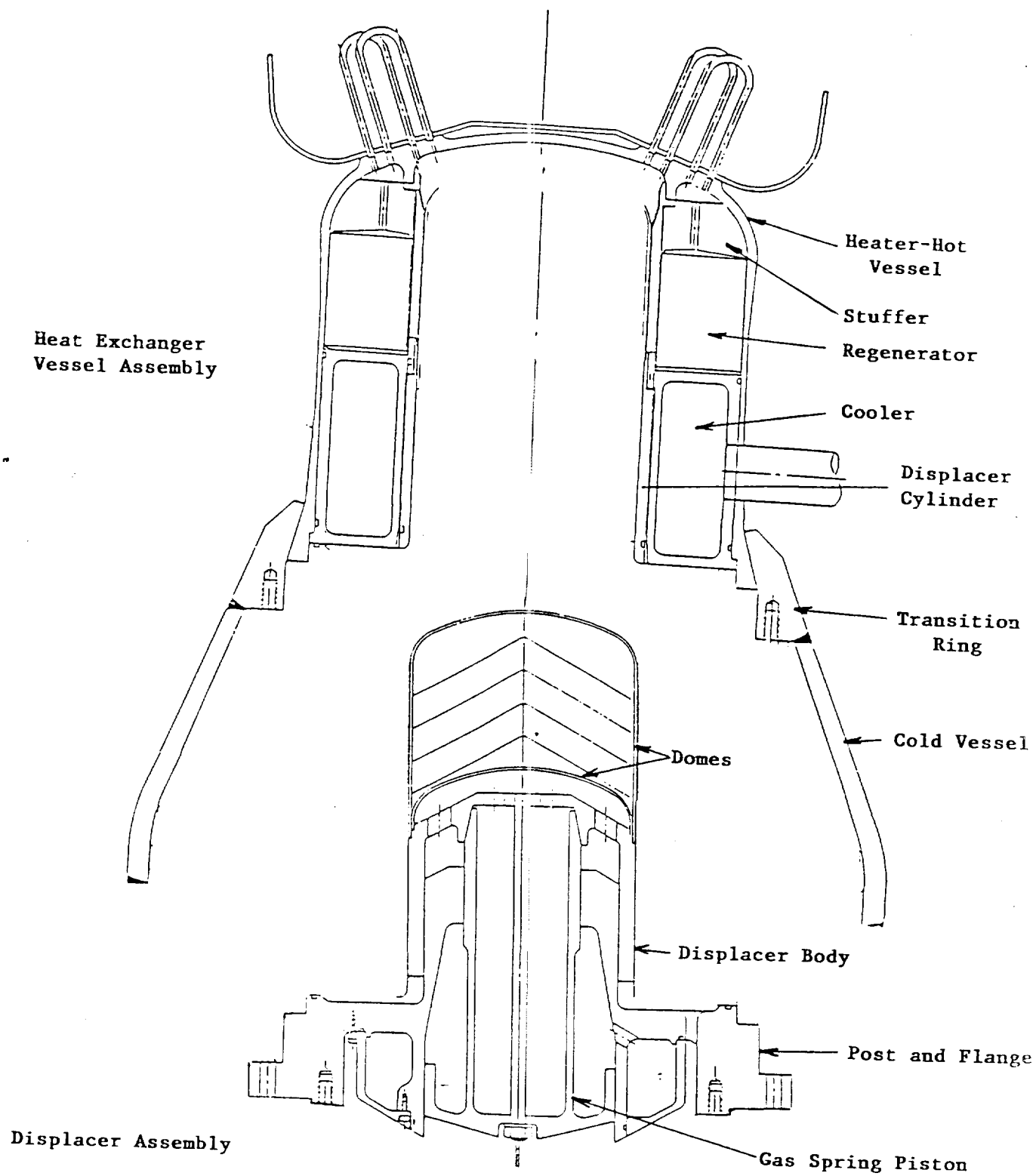
The regenerator area, length, porosity and type are important parameters which must be carefully selected in a high efficiency engine.

Two of the general arrangements of the regenerator and cooler which have been applied in Stirling engines are referred to as annular and canister designs. The annular arrangement is as shown in Figure 4.1 with the regenerator and cooler in an annulus inside the main vessel. In the canister arrangement the regenerator and cooler are located outboard of the main pressure vessel in a set of several modules or canisters. Figure 4.4 shows a typical arrangement generated for the solar engine. The main advantage of the canister arrangement is the diameter of the pressure wall around the regenerator is much smaller than in the annular design and, consequently, the stress conditions are less severe. The disadvantage is the design tends to be more complex and heavier and, as a consequence, more costly to fabricate. Readers familiar with the ASE MOD I and MOD II

Table 4.3

ENGINE ALTERNATOR MATERIAL AND WEIGHT BREAKDOWN

<u>Component</u>	<u>Material</u>	<u>Weight</u>
Pressure Vessel Assembly		33
Hot Vessel	INCO 713LC	5
Tubes	Incolloy 800	160
Cold Vessels	Low Alloy Steel and 300 SS	13
Displacer Cylinder	Steel and INCO 625	
Displacer Assembly		55
Post and Flange	Cast Iron	23
Displacer and Piston	Cast Iron	2
Dome	INCO 625	
Regenerator	300 SS Foil	21
Cooler	300 SS	19
Power Piston and Cylinder		30
Piston	Stainless Steel	70
Piston Cylinder	Stainless Steel	2
End Cap	Aluminum	20
Hardware	Steel	
Alternator and Plunger		140
Stators	Steel Lams.	60
	Copper	25
Hardware	Steel	18
Magnets	Neodymium	6
Plunger Hardware	Aluminum and Plastic	
Spin Motor	Copper and Steel	13
Total		<hr/> ~700 lbs.



Heat Exchanger and Displacer Assemblies

Fig. 4.2

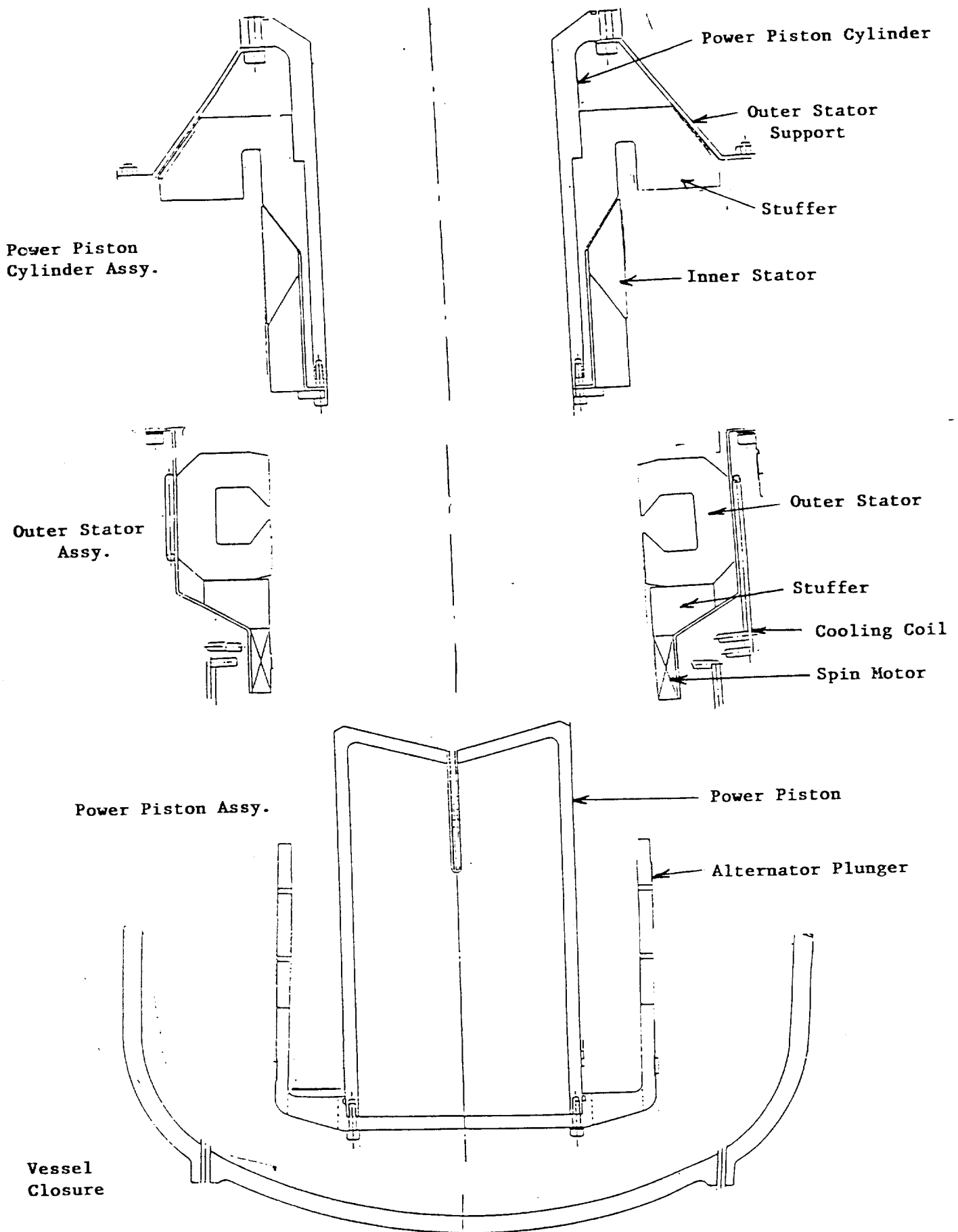


Fig. 4.3 - Power Piston, Power Piston Cylinder and Outer Stator Assemblies

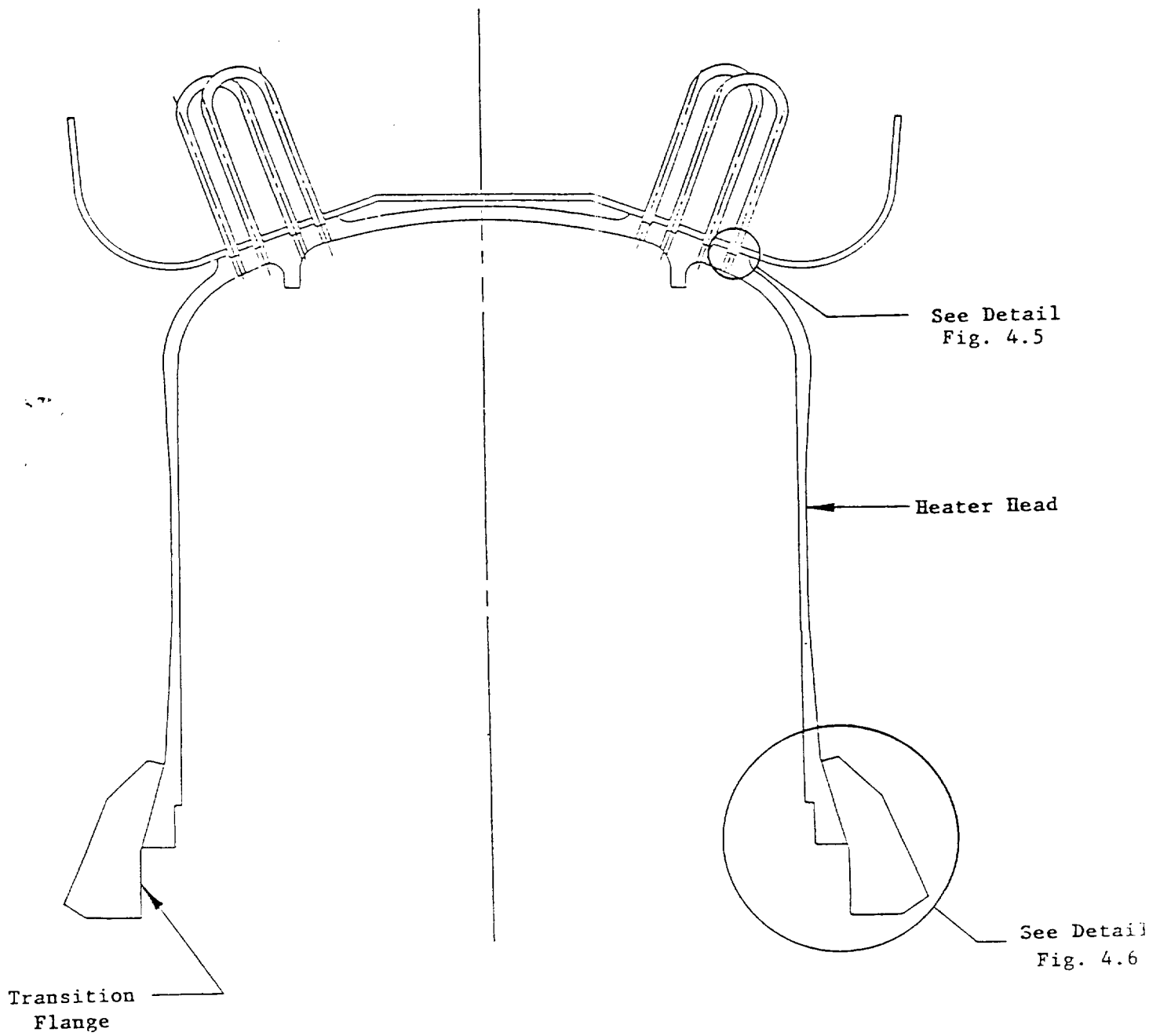


Fig. 4.4 - Heater Head Brazing Assembly

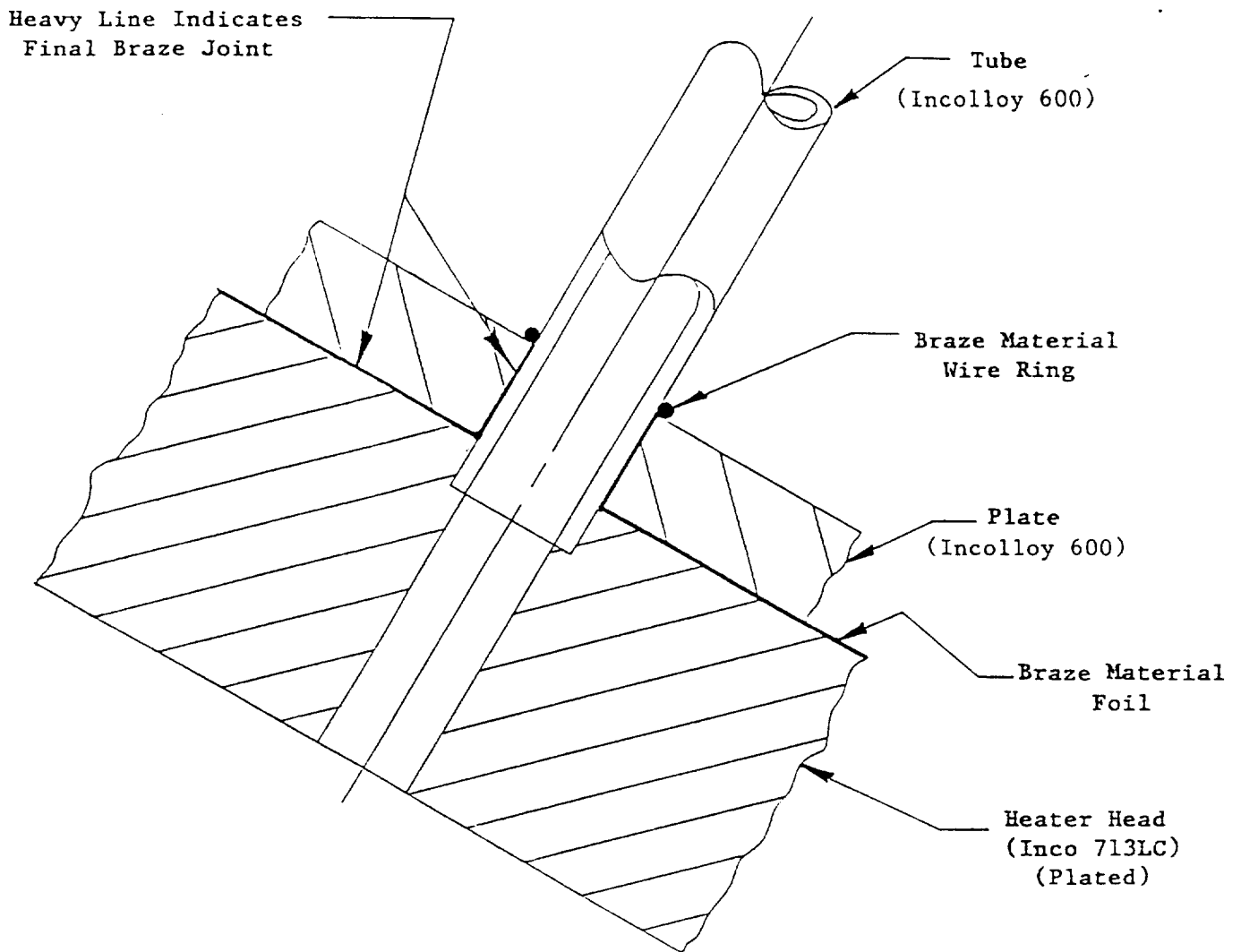


Fig. 4.5 - Tube Detail

engines will recognize that an annular arrangement was selected for MOD II over the MOD I canister design for the same reason.

For the solar engine the annular design was selected. Even though the high temperature materials applicable to this design are fairly expensive, the inherent simplicity was judged more important in meeting the engine design requirements.

As shown in the Summary Table 2.3, the combinations of vessel material, heater temperature and regenerator type which can be used in our annular design are:

1. Inco 713LC or Inco 718	700°C	Feltmetal
2. XF 818	700°C	Foil
3. Inco 713LC	800°C	Foil

Combination (1) is selected for this study since the development requirements and potential sodium corrosion problems are minimized by this selection. Combination (2) can be considered after foil regenerators are developed, and Option 3 is a possible longer term option of sodium compatibility at 800C can be shown to be acceptable.

The heater head assembly, the heater tube to vessel joints and the vessel wall joint are shown on Figures 4.2, 4.4 and 4.5 respectively.

For the heater tubes and receiver boundary, the primary concerns are to provide reliable joints where the tubes containing high pressure helium enter and leave the head, and also avoid potential attack of materials exposed to sodium liquid and vapor. The approach shown in Figures 4.3 and 4.4 avoids direct sodium contact of the structural material of the vessel head and also results in a single structural alloy exposed to the sodium in the receiver. Incolloy 600 is selected as a reference based upon its resistance to sodium attack and the relatively small difference between its thermal expansion characteristics and that of nickel minimizes potential spalling problems in the sintered wick on the back of the receiver dome.

At the heater tube to vessel interface the Inco 713LC head is plated with suphamate nickel then an Incolloy 600 sheet is brazed to the head. Holes are then drilled for the heater tubes (96 U-shaped tubes in two rows), as shown, the tubes inserted and then brazed into place. A fillet at the tube to hole interface is desired to avoid a crevice at this location and minimize sodium attack. Even though the heater tubes contain high pressure (about 1700 psi max.) the wall stresses are small due to the large thickness to inside diameter ratio. Thus, even though Inco 600 is not an ultrahigh strength material, it is adequate for this application.

The joint in the vessel wall shown in Figure 4.6 is required to transition from the high cost Inco 713LC used for the hot pressure vessel to the low cost alloy steel used for the cold pressure vessel. The primary concern is the axial load due to engine pressure.

Friction welding was identified as an approach to join dissimilar metals which was discarded following the preliminary design based on the high projected cost of suitable production equipment. The brazing approach shown in Figure 4.6 was selected because the braze is primarily a seal and the interlocking arrangement of a tapered joint backed up by the rigid flange of the post and flange gives an inherently safe design. This joint will probably not exist on the first test engine, since the requirements for disassembly and replacement are expected to dictate a bolted joint be used at this location.

4.4.2 Displacer Assembly, Bearings and Dynamic Seals

The design of the displacer and the selection of bearings and seals on both the displacer and the power piston involve trade-offs between:

- Cost
- Performance (Mechanical Losses)
- Life

A major advantage of free-piston engines using noncontacting bearings and seals is that there is no wear, such as is inherent in contacting bearings and seals. Noncontacting bearings and seals require very small clearances between the moving elements and adjacent stationary elements. Typical radial clearances

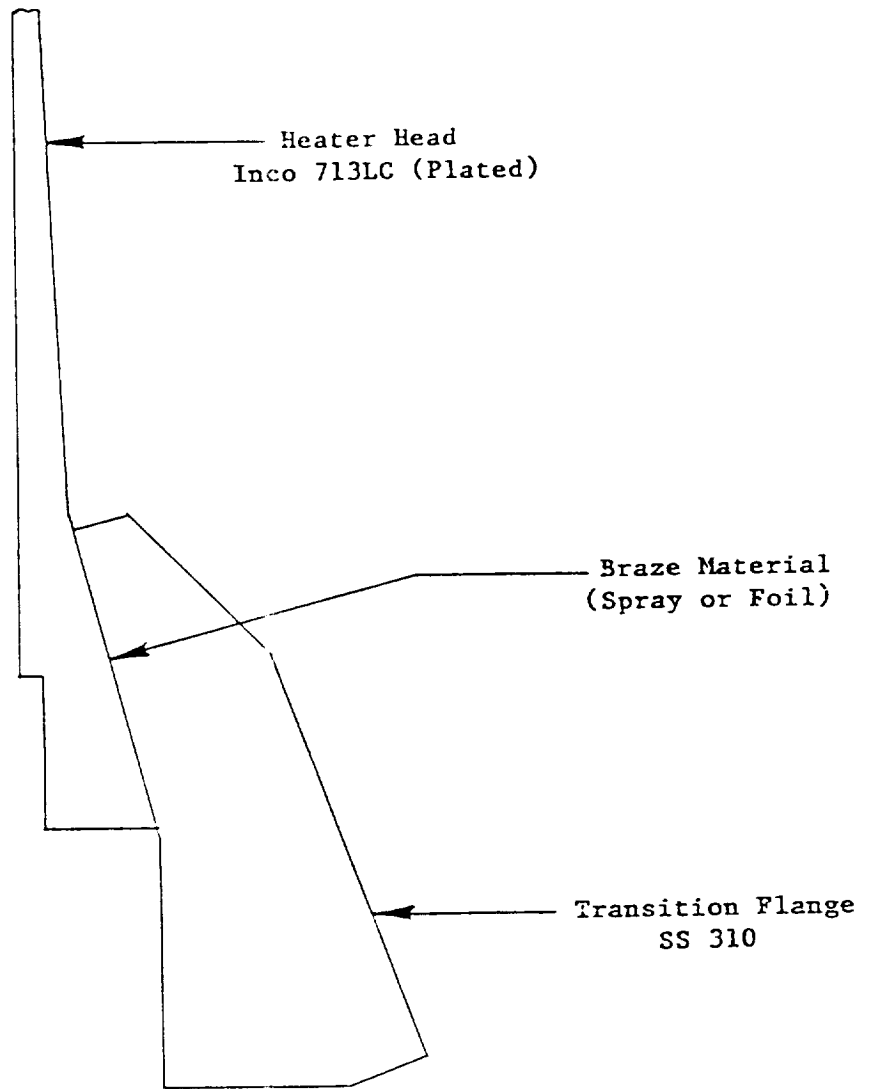
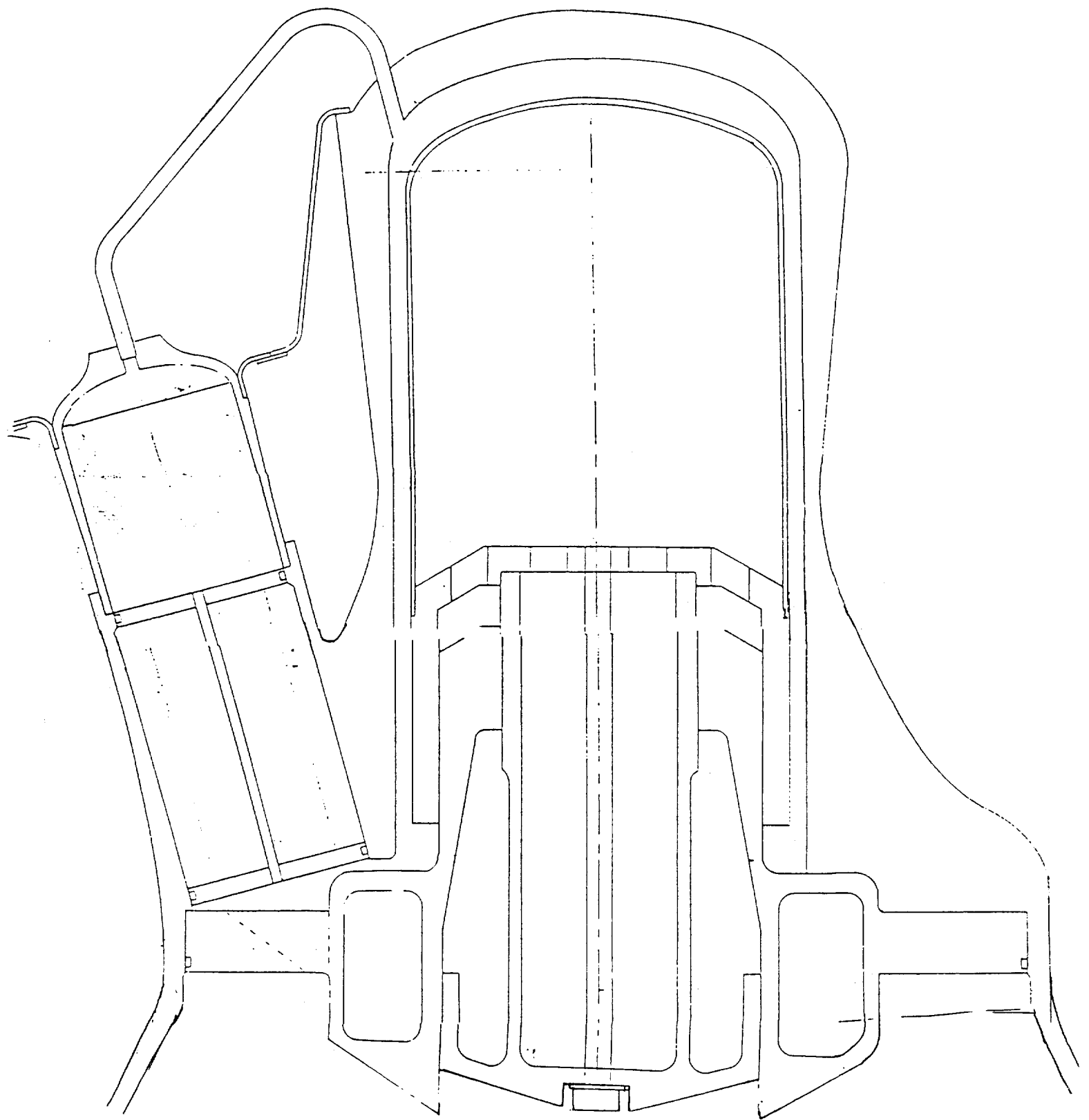


Fig. 4.6 - Lower Braze Joint Detail



General Arrangement - Canister Concept

Figure 4.7

range from .0005 to .0009 inches, depending on seal diameter and seal length. Simple arrangements such as the power piston are less susceptible to difficulty than displacer arrangements. Because practical displacer designs require two gas springs, at least one joint is required in the moving assembly and at least three concentric clearances are required. The particular arrangement used in the solar engine has been evolved at MTI to meet the cost/performance/life requirements on engines with commercial product potential. Indications from Pioneer Engineering are that the clearance and tolerance requirements for the design arrangement shown in Figure 4.2 are well within the range of current production techniques. A similar finding was made by a consultant who reviewed the same concept being applied to MTI's heat pump engine.

Based upon the above, it was judged that the relatively small initial cost savings that could be expected from using contacting seals would not outweigh the performance loss and cost associated with wear out and periodic replacement of contacting seals.

The choice available for noncontacting bearings is either hydrodynamic (spinning pistons) or hydrostatic (nonspinning pistons) gas bearings. Based upon simplicity and the small power requirement to drive them, hydrodynamic bearings are preferred if it can be shown that they can be made to operate stably. Hydrostatic bearings in which high pressure helium is supplied to sets of orifices in the stationary walls of the bearing journals have been used extensively on laboratory engines. They are somewhat more complicated in that a source of pressure somewhat above engine mean pressure is required to supply them. An internal pumping arrangement, such as clipping the pressure wave of one of the gas springs, is possible but difficult to incorporate in an engine which operates over a wide range of power, stroke, and gas spring pressure amplitude. An external pump or booster is an alternate approach which is also possible, but introduces an additional power loss associated with the pump's inefficiency. Anticipating successful demonstration on the space engine program hydrodynamic bearings are selected for the conceptual design of the production solar engine. The power piston of SPRE has been successfully run on hydrodynamic bearings in motoring tests so that feasibility is demonstrated.

4.4.3 Power Piston and Power Piston Cylinder Assembly - Power Piston Material Selection

The power piston assemblies and power piston cylinder are shown in Figure 4.3. The weight of the power piston assembly is a dominant factor affecting the engine performance. The inertia force of the piston is balanced by a combination of pressure force from the compression space and pressure force from the gas spring. As the weight of the piston is increased above that which is balanced by compression space pressure amplitude, the gas spring pressure amplitude must be increased. Hysteresis power losses in the gas spring increase as the square of pressure amplitude. They are also proportional to the surface area exposed to gas in the gas spring. At the preliminary design stage a ceramic piston and cylinder were identified as a good selection to control piston weight. This also resulted in a rigid assembly in which the seal clearance at the piston outer diameter did not change due to cyclic pressure loads on the piston and cylinder. In keeping with the desire to avoid using undemonstrated approaches to the maximum extent possible, this decision was reconsidered and even though using non-magnetic stainless steel resulted in about 2% less power output, it was felt the incorporation of a ceramic piston and cylinder be postponed for later consideration. This also minimizes difficulties in making cost estimates on relatively new technology where production levels have not been demonstrated.

The alternator plunger containing the magnets is attached to the end of the piston. The magnets with plastic spacers are bonded into fiberglass layers on the two surfaces to form a composite assembly, which is then bonded to the aluminum carrier. The carrier is bolted to the end of the piston as shown.

The inner stator of the alternator is attached to the end of the power piston cylinder. A plastic stuffer is included to reduce the gas spring volume. It is also designed to minimize surface area in the gas spring.

The outer stator support is bolted into position at the power piston cylinder flange prior to installing the outer stator.

4.4.4 Outer Stator Assembly

The outer stator assembly is comprised of the outer stator, the spin motor, cooling coils and stuffer as shown in Figure 4.3. The stator is supported at its outer diameter. The support arrangement permits the stator to be located concentric with the power piston bore using a fixture which pilots on the bore. The bolts in the stator support are tightened after the stator is located. This assures concentricity without depending on close tolerances between the stator and its supporting structure. A flexible seal between the stator support and the weld backing ring on the vessel is shown in Figure 4.1. This is used to close off the gas spring and reduce its volume to the required magnitude. The spin motor is the drive for the hydrodynamic bearings. The power draw of this motor is very small (less than 50 watts).

5.0 ENGINE ANALYSIS

5.1 Introduction

Stress analyses were conducted to select materials of construction and the dimensions and layout of the engine components. These were particularly important in selecting the materials and configurations of the components on the hot side of the engine.

Thermodynamic and system performance calculations at the design point, and also over the full range of operating conditions, were conducted to maximize the performance of the engine within prescribed constraints. In the preliminary design stage the performance was based upon 800°C heater temperature, foil regenerator and ceramic power piston. For the final design the performance was based upon 700°C heater temperature, sintered wire (feltmetal) regenerator and stainless steel power piston.

Engine thermodynamic performance and structural design are closely interrelated at the pressure vessel around the regenerator where regenerator length determines the thermal stress conditions in the vessel wall due to the axial gradient along the wall. As discussed in Section 4.4.1 this was a dominant factor in selecting the basic arrangement of the heat exchangers and the hot vessel material.

Engine dynamics and stability analyses are covered in Section 7.0 (System Analysis) since they involve the interaction of the engine, the alternator and the external load circuit.

The approach taken is to optimize the engine to maximize shaft power at the alternator at the design point, adjust the dynamic parameters to produce the strokes and phase required for this optimization, then evaluate the system at power levels above and below the design point. As shown in Section 7, the system efficiency is relatively constant over most of the operating range.

5.2 Stress Analysis and Material Selection

5.2.1 Analyses and Structural Criteria

Table 5.1 summarizes the analyses performed and the material selections made for various components of the engine.

Table 5.2 summarizes the structural criteria applied to all engines designed by MTI. The criteria is based upon providing a conservatively calculated factor of safety of 1.5 for structural failure mechanisms and where appropriate restricting deformation such that engine performance is not affected by dimensional changes.

Analyses which will be covered in detail due to their importance to the concept selection are stresses in the hot pressure vessel and deformation in the power piston clearance gap.

5.2.2 Hot Pressure Vessel

For all Stirling engines the selection of material and the design of the vessel which contains the high pressure working gas on the hot side of the engine is critical. Ideally a simple geometry and an inexpensive material is desired to minimize cost. Engine efficiency increases with temperature and engine size decreases with increasing pressure. These factors tend to drive designs to high pressure and high temperature. The creep rupture strength of the vessel material dictates its temperature/life capability and the hot section of the vessel is restricted to a relatively small number of alloys. Figure 5.1 shows the creep-rupture strength characteristics of several alloys that have been considered for Stirling engine applications. The head thickness which is required to carry the pressure load assuming a 2 to 1 ellipsoidal head on a 10.0 inch diameter vessel is shown in Figure 5.2. The nominal overall design point efficiency required for the ASCS is about 33% (i.e. 25 kWe power from 75 kWt into the receiver). This dictates that the head temperature be in the range of 700°C to 800°C. The economic trade-off between performance and engine cost was determined to be about \$1200/kWe. A 100°C change in head temperature at 700°C translates into about 1.2 kW more power, which is equivalent to about \$1400 in capital cost. Since the difference between using high cost alloys and lower cost iron base alloys is expected to be a few hundred dollars at most in production quantities, the economic trade-off favors the selection of high operating temperatures. For

Table 5.1

STRESS ANALYSIS AND MATERIAL SELECTION

1. Pressure Vessel (Hot End)	INCO713LC with INCO600 Sodium Barrier
<ul style="list-style-type: none"> • Creep due to "steady" pressure • Low cycle fatigue due to thermal transient • High cycle fatigue due to pressure cycling 	
2. Heater Tubes	INCO600
<ul style="list-style-type: none"> • Creep • High Cycle Fatigue 	
3. Pressure Vessel (Cold End)	Low Alloy Steel 4130 or Equivalent
<ul style="list-style-type: none"> • Burst due to steady pressure • High cycle fatigue due to pressure cycles 	
4. Power piston and cylinder	Ceramic (SiC)
Loss of seal clearance due to cyclic pressure	
5. Displacer (Cold End) and Displacer Cylinder	Nodular Cast Iron Alloy Steel
Loss of seal clearance due to cyclic pressure	
6. Displacer (Hot End)	INCO625
<ul style="list-style-type: none"> • Buckling • High cycle fatigue 	

Table 5.2

STRUCTURAL CRITERIA

1. PRIMARY MEMBRANE STRESS $\leq S_m$

$$S_m \leq \frac{2}{3} S_y$$

S_y = Yield Strength at
Op. Temp.

and

$$S_m \leq \frac{1}{2} S_u$$

S_u = Ultimate Strength

and

$$S_m \leq \frac{2}{3} S_r$$

S_r = Stress to cause rupture
in design life.

and

$$S_m \leq S_{c-1\%}$$

$S_{c-1\%}$ = Stress to cause 1 % creep
in design life.

2. PRIMARY SURFACE STRESS (Membrane + Bending)

$$S_s < 1.5 S_m$$

3. PRIMARY + SECONDARY SURFACE STRESS

$$S_s^1 < 3 S_m$$

4. CYCLIC STRESSES SHALL NOT INDUCE FAILURE WITH A FACTOR OF SAFETY OF 1.5 WHEN PLOTTED ON A GOODMAN DIAGRAM.

5. DYNAMIC CHANGE IN SEAL CLEARANCES < 1.0%

6. BOLT PRELOADS 150% MINIMUM REQUIRED.

DEFINITIONS

PRIMARY STRESS

A stress which is not relieved by plastic deformation if the elastic limit (yield) is exceeded.

SECONDARY STRESS

A stress which is relieved by plastic deformation if the elastic limit (yield) is exceeded.

MEMBRANE STRESS

Is the average stress through the cross section of a structural element.

SURFACE STRESS

Is the stress at the material surface due to the combined effect of direct plus bending loads - but excluding stress concentration.

PEAK STRESS

Is the surface stress increased by the effect of local stress concentration.

MEAN STRESS

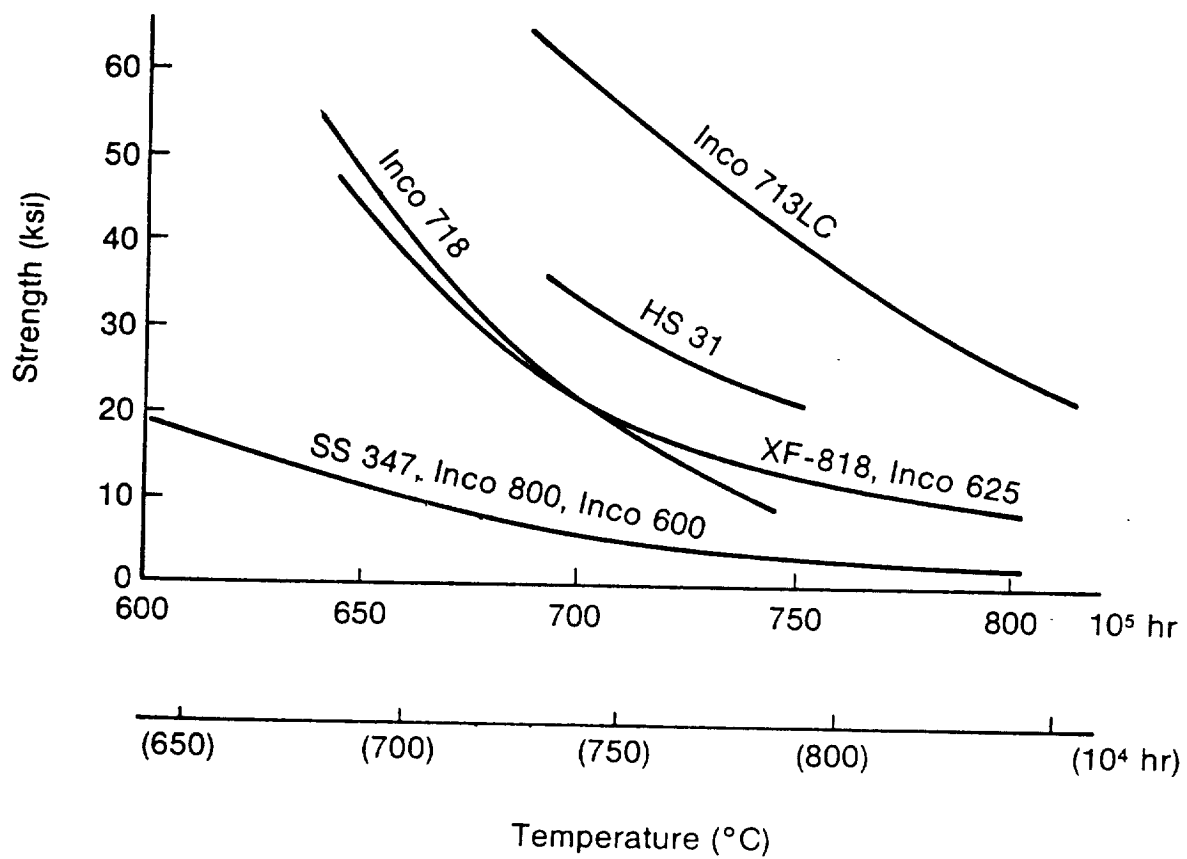
Is the average peak stress during cyclic loading.

ALTERNATING STRESS

Is half the stress range (e.g. stress amplitude) during cyclic loading.

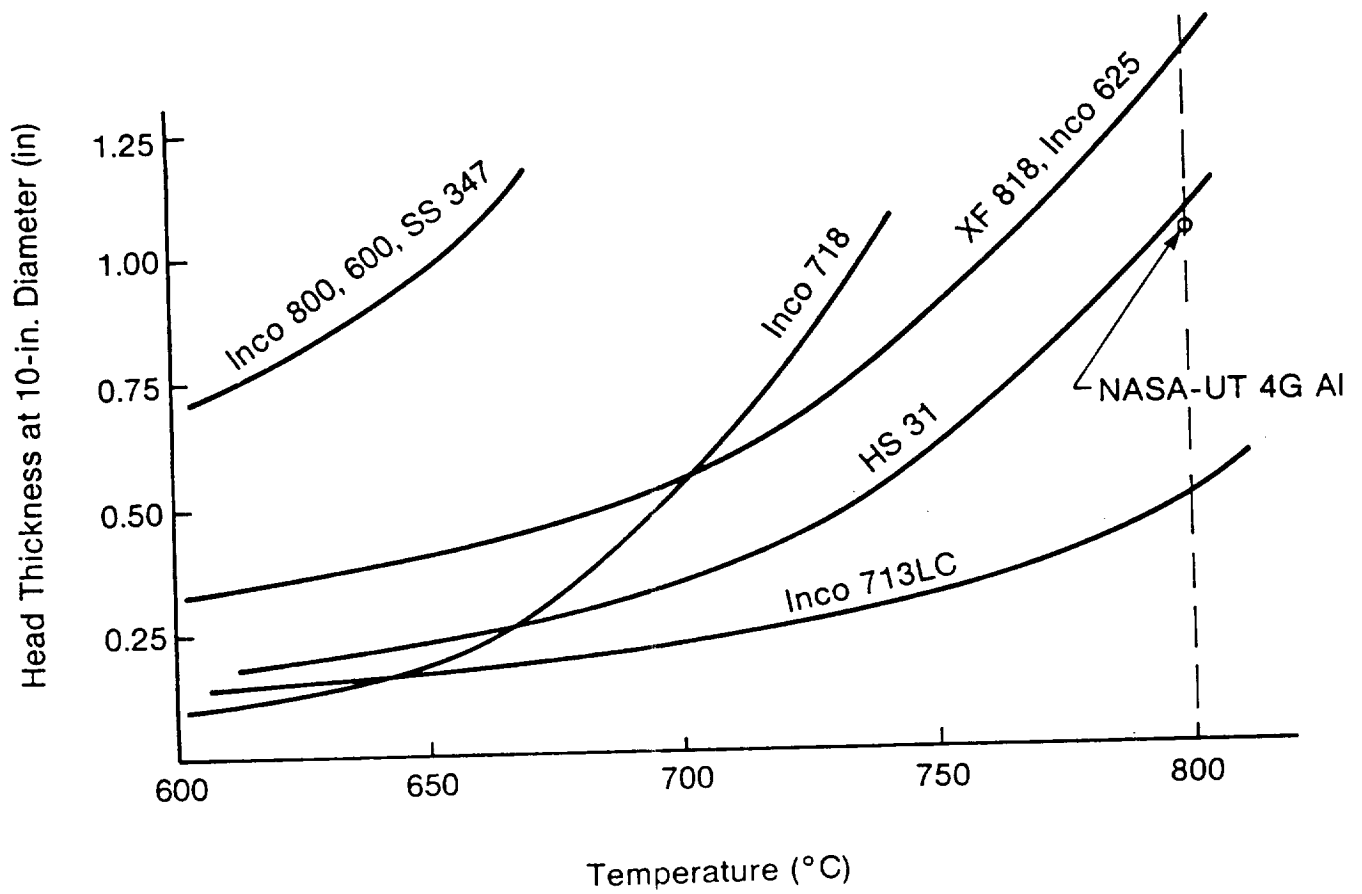
EFFECTIVE STRESS

Is the equivalent uniaxial stress determined from Von Mises formulation for treating biaxial and triaxial stress conditions.



Stress-Rupture Data

Figure 5.1



Hot Vessel Head Thickness

Figure 5.2

the preliminary design 800°C and INCO 713LC was selected. This was decreased to 700°C for the final design based on other considerations (i.e. liquid metal attack of the receiver materials).

For the annular heat exchanger arrangement (the concept selection reasons are covered in Section 4), a vessel strength requirement, which is equally as important as creep strength, is the fatigue strength.

Conditions which cause stresses in the pressure vessel are:

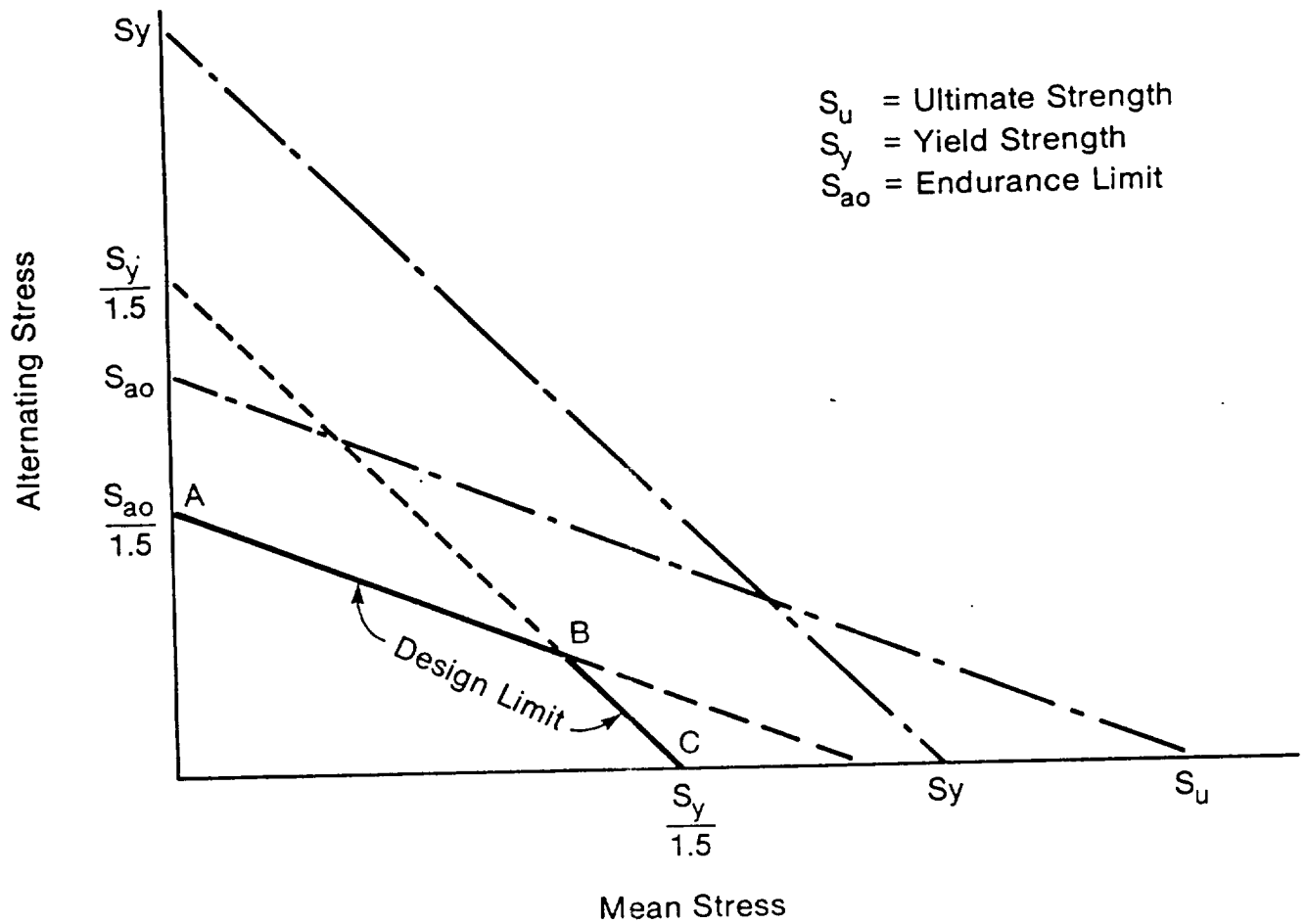
1. Mean Engine Pressure 105 Bar (1522 psi)
2. 60 Hz Cyclic Engine Pressure ± 16.3 Bar (± 237 psi) at maximum power point
3. Thermal stresses due to the temperature gradient along the vessel wall adjacent to the regenerator = 640°C

Two start/stop cycles per day give 20,000 cycles in 20 years.

The dominant fatigue condition is the pressure cycling (2) superposed on the steady stresses due to mean pressure (1) and thermal gradient (3).

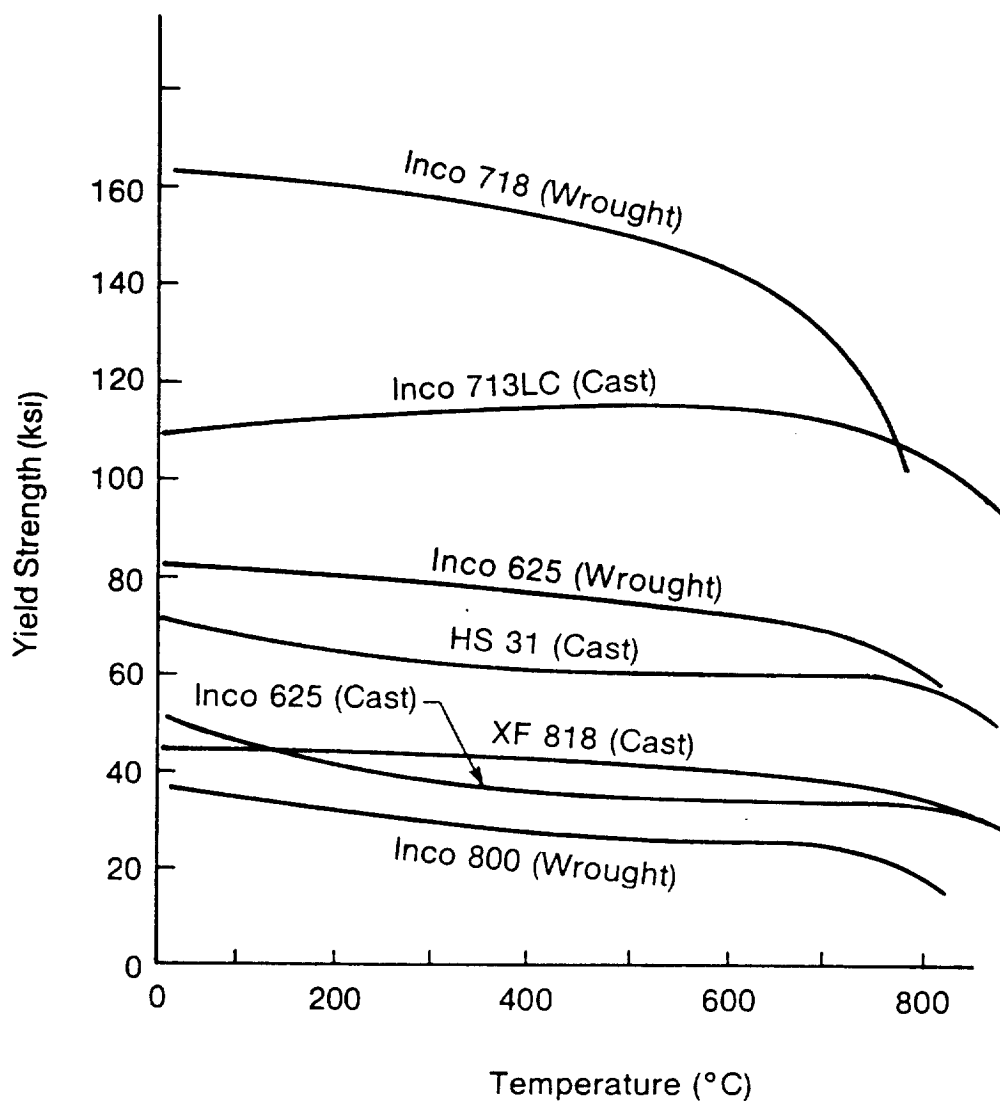
The fatigue condition due to the superposition of the thermal cycling (3) on the mean pressure (1) is generally less severe than the pressure cycling condition.

The allowable fatigue stress levels are shown on a Goodman Diagram. A conservative diagram can be constructed for high cycle fatigue as shown in Fig 5.3. The region of particular interest to the vessel fatigue stress conditions due to pressure cycling is the region between B and C. As seen in the diagram, the maximum stress (mean stress + alternating stress) in this region is limited by the yield strength of the material. Figure 5.4 shows the yield strength of several high temperature alloys. Figures 5.5, 5.6, 5.7 show sample head geometries that were analyzed during the program. Geometry A shows the Inco 713LC head for 800°C operation with a 5.0 in. long foil regenerator selected as baseline for the preliminary design review. Geometry B shows the Inco 713LC head



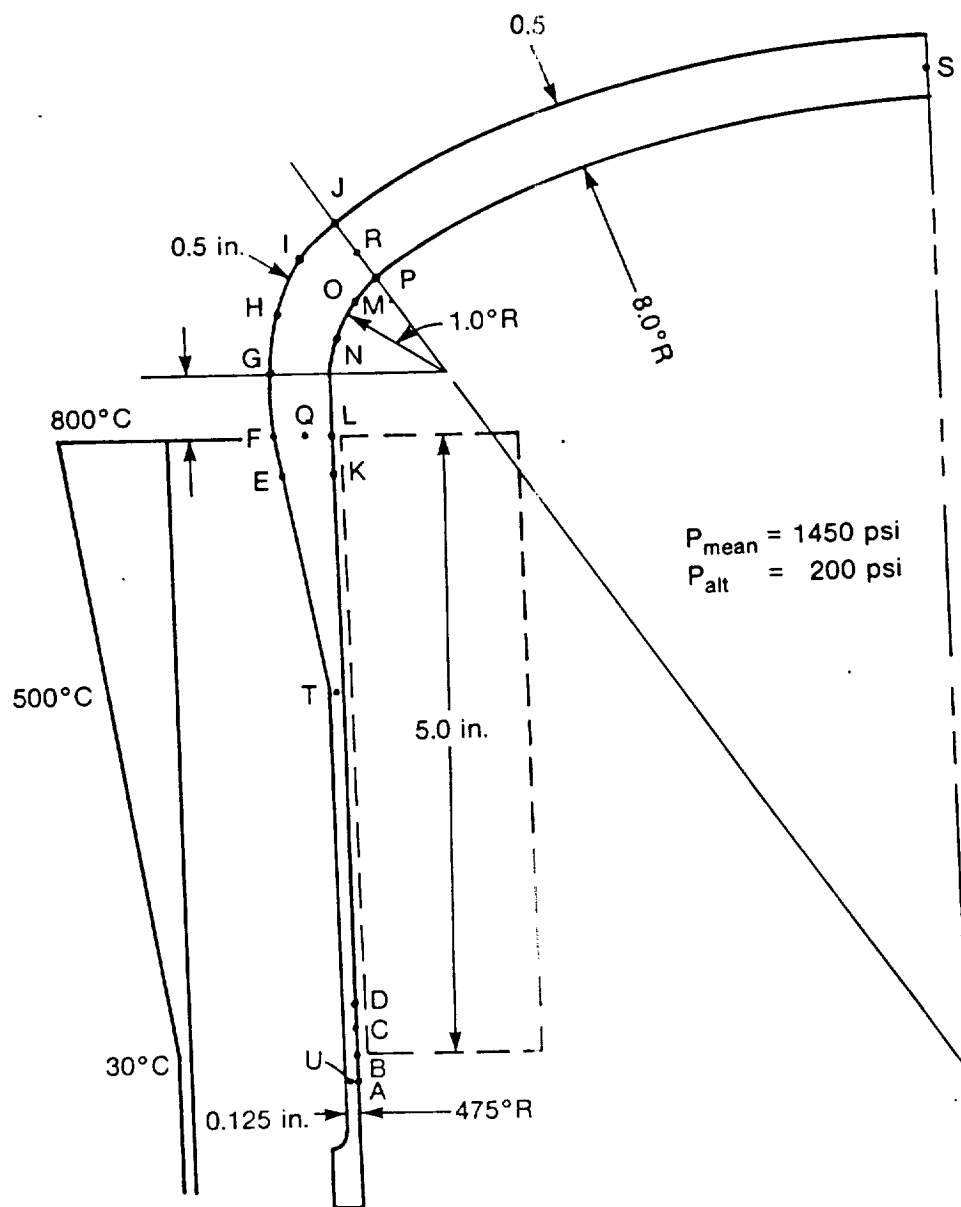
High Cycle Fatigue Diagram Construction

Figure 5.3



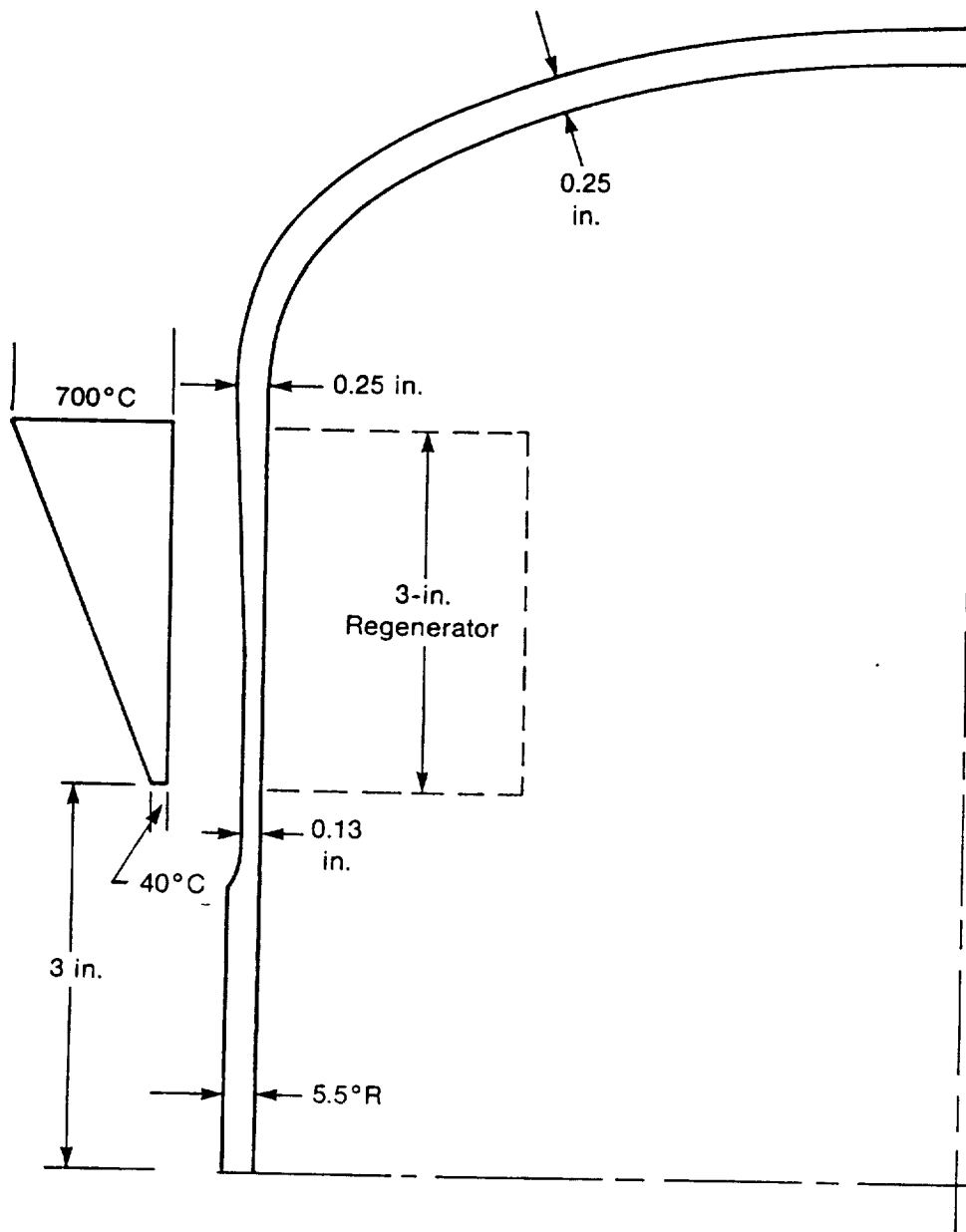
Yield Strength of High Temperature Alloys

Figure 5.4



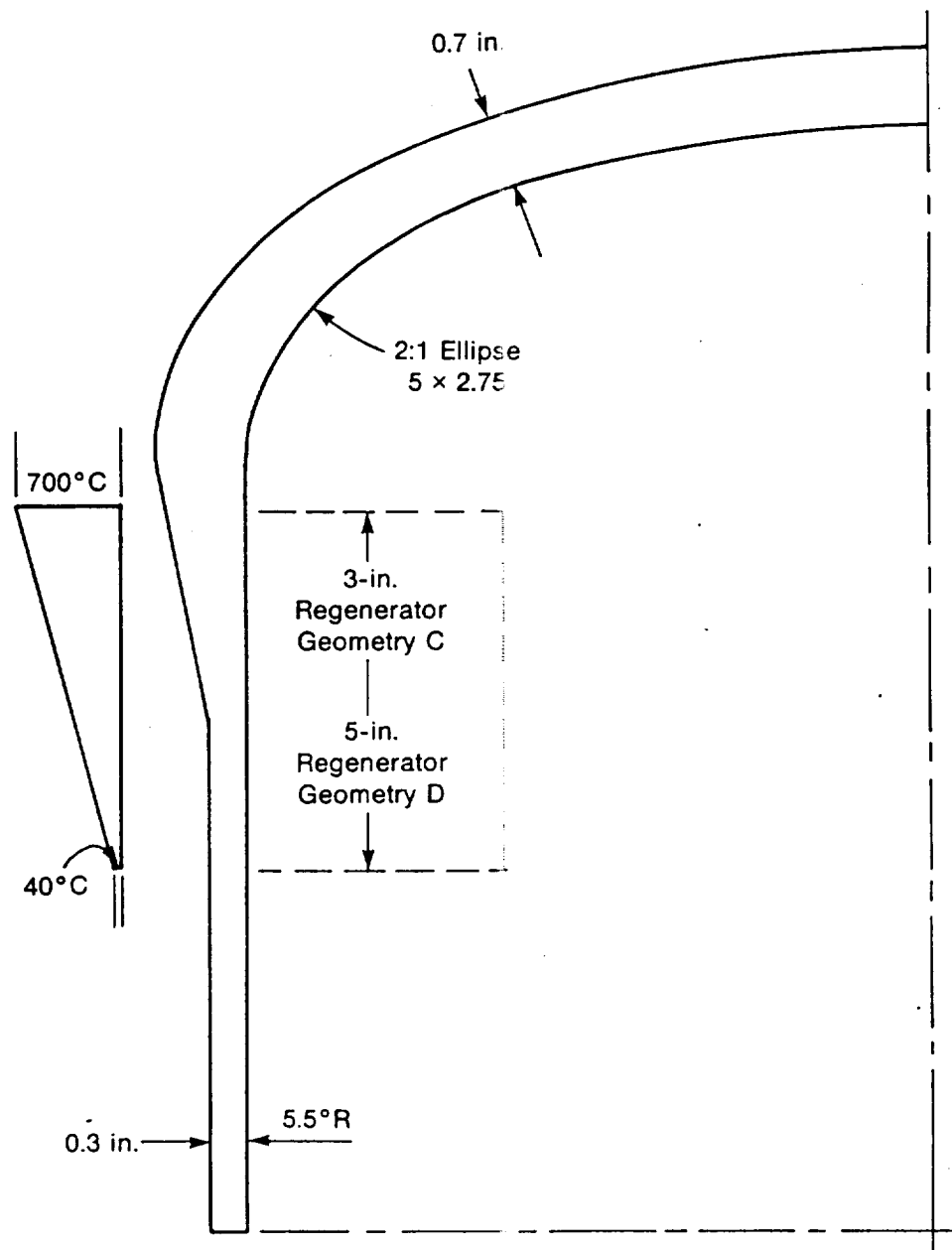
Vessel Geometry A (Inco 713CC - 800C)

Figure 5.5



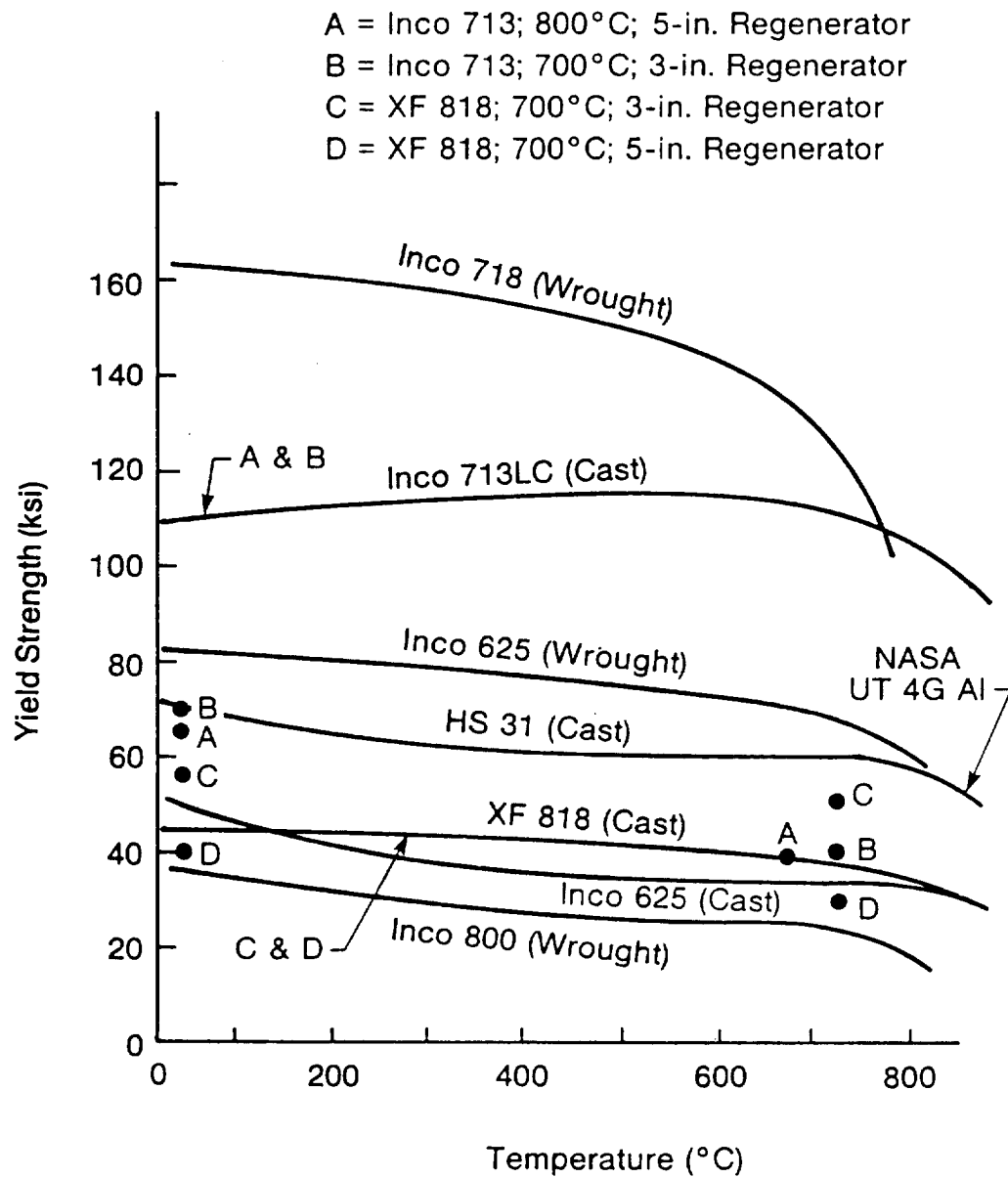
Vessel Geometry 'B' (Inco 713CC - 700C)

Figure 5.6



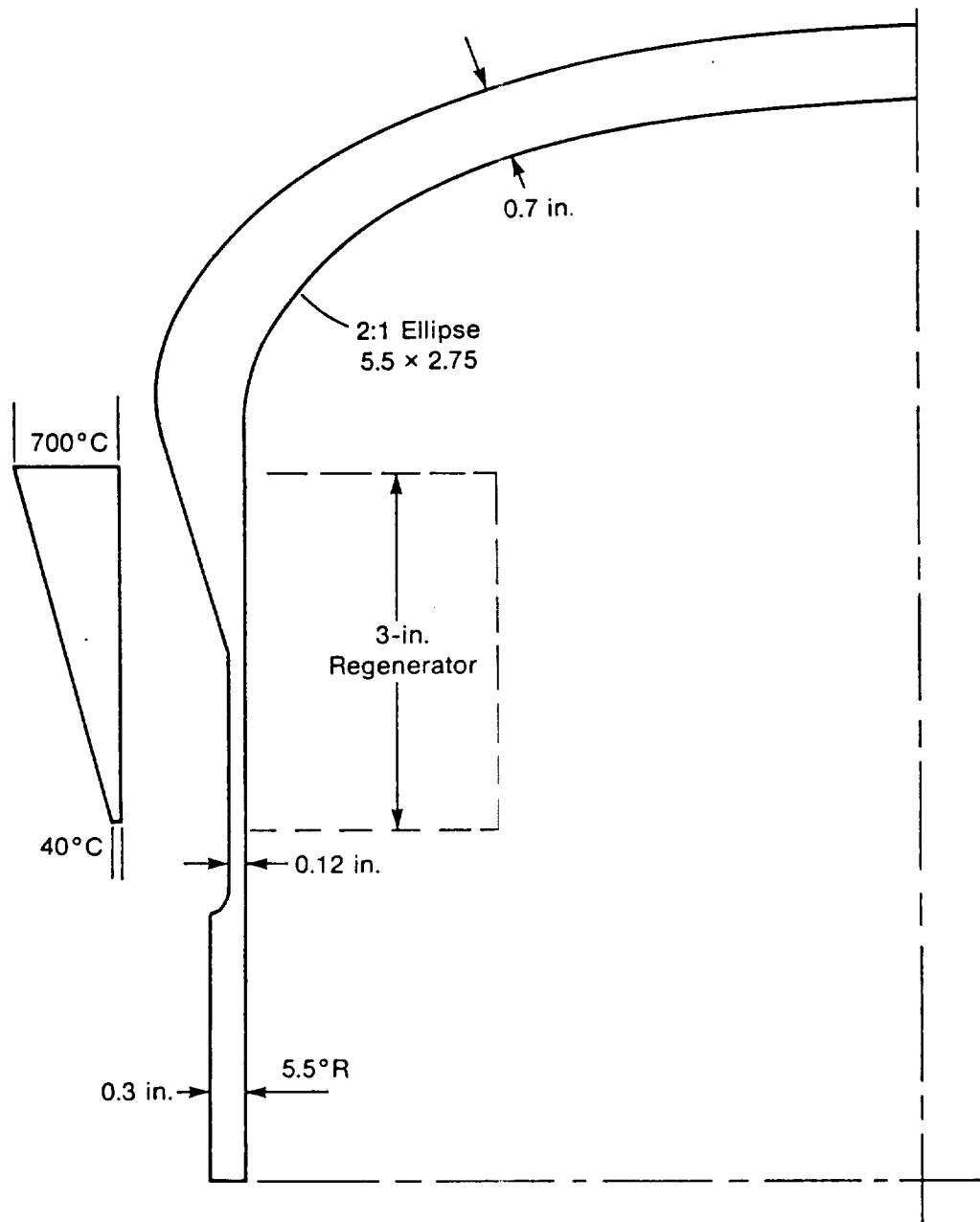
Vessel Geometry C and D - (XF818 - 700C)

Figure 5.7



Maximum Stresses in Vessel Wall

Figure 5.8



Vessel Geometry 'E' (Inco 718 - 700C)

Figure 5.9

for 700°C operation and a 3.0 in. long sintered regenerator selected for the final conceptual design. Geometries C and D were trials made to evaluate XF818 as a head material. The results of analyses on these geometries are shown in Figure 5. It can be seen that the only two materials identified with adequate margin of safety for the final conceptual design (Geometry B) are Inco 713LC and Inco 718.

An Inco 718 head at 700°C with 3.0 in. long regenerator would be similar to XF818 at the hot end similar to Inco 713LC at the cold end. This is an acceptable alternate and is designated Geometry E. and is shown in Figure 5.9. The conclusions reached are that for the hot vessel the following are the minimum strength requirements:

Stress Rupture Strength at 700°C and 10 ⁵ hrs	20.0 ksi
Yield Strength at R.T.	90.0 ksi
Yield Strength at 700°C	75.0 ksi

The reference material selected is Inco 713LC with Inco 718 identified as an acceptable alternate.

5.2.3 Power Piston Seal Clearance

The two dominant parameters related to the power piston assembly which have a significant affect on the performance of the machine are:

1. Piston Mass
2. Clearance between Piston and Cylinder

Up to a piston mass of about 40 lbs the gas spring can be quite soft. Up to this level most of the inertia force associated with the reciprocating motion of the piston is balanced by the pressure in the compression space. As the weight increases above this level the gas spring must be made stronger (smaller volume) and the cyclic pressure amplitude increased. Hysteresis losses in the gas spring are proportional to the square of pressure amplitude and the wetted area. There are practical limitations on how much the wetted area can be reduced, so that the magnitude of gas spring pressure dominates the hysteresis loss.

Table 5.3

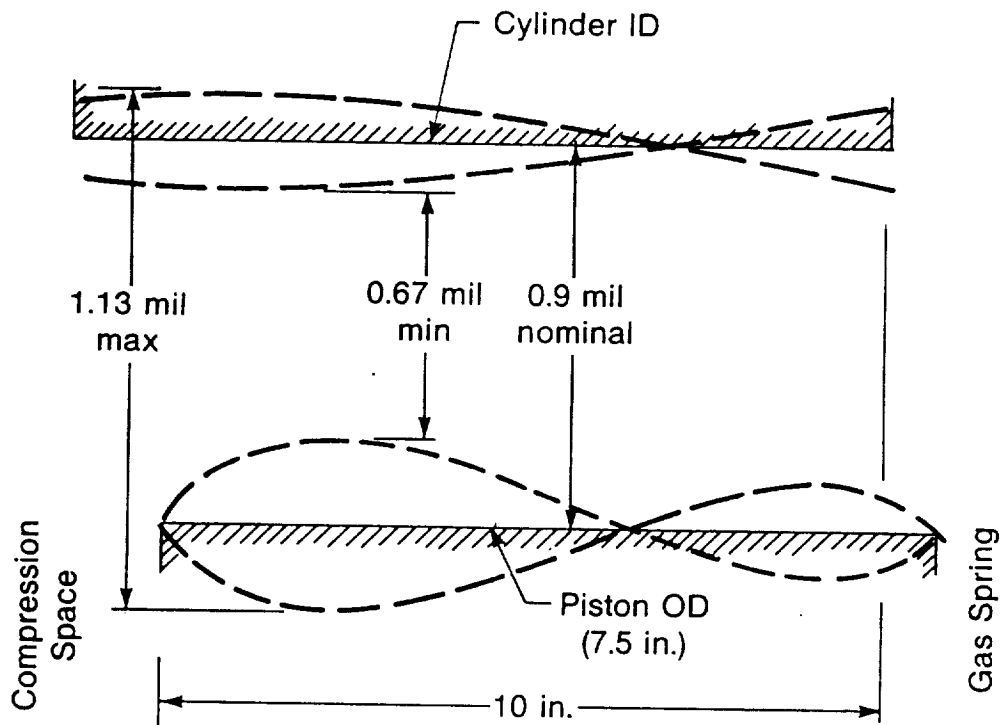
STAINLESS STEEL VS. CERAMIC PISTON

		<u>S.S.</u>	<u>CERAMIC (SiC)</u>
MODULUS OF ELASTICITY	$\frac{\text{PSI}}{10^6}$	28.6	48.0
DENSITY	LB/CU. IN.	.285	.12
E/ ρ	IN/ 10^8	1.0	4.0
PISTON WALL THICKNESS	INS.	.375	.50
CYLINDER WALL THICKNESS	INS.	.75/.375	.50
PISTON/PLUNGER WEIGHT	LBS	55	40
COMPRESSION SPACE PRESSURE AMPLITUDE AT DESIGN STROKE	BAR	14.2	14.2
CHANGE IN SEAL CLEARANCE DUE TO PRESSURE CYCLING	MILS	$\pm .23$	$\pm .05$
GAS SPRING PRESSURE AMPLITUDE	BAR	7.6	2.0
GAS SPRING SURFACE AREA	SQ. M	1.6	3.0
GAS SPRING HYSTERESIS	WATTS	980	280

FOR NEAR-TERM NONMAGNETIC STAINLESS STEEL IS SELECTED.

FOR LONGER-TERM - CERAMIC IS WORTH DEVELOPING.

ORIGINAL PAGE IS
OF POOR QUALITY



Clearance Gap Change Due To Pressure
(Stainless Steel Piston And Cylinder)

Figure 5.10

To minimize losses associated with leaking magnetic fields around the alternator, it is desirable for the power piston cylinder and power piston to be nonmagnetic and nonconducting.

In addition to the gas spring hysteresis loss, the mechanical loss associated with pumping gas along the seal at the outer diameter of the piston must be controlled. Since this loss increases as the third power of clearance, very small clearances must be selected and maintained.

From material property considerations ceramics such as silicon carbide are ideal materials for the power piston and its cylinder. These properties are high stiffness and low density, which results in a piston and cylinder with very low deformation in the seal clearance due to cyclic pressure loading while meeting the low piston weight requirement. Additionally they are nonmagnetic and dimensionally stable materials. Since they are not widely used in similar applications there is some uncertainty in the production cost projection for the tolerances required.

Nonmagnetic stainless steel is the most suitable conventional material for this application, but does introduce some additional losses since the piston weight exceeds the optimum. For the final conceptual design stainless steel was selected to avoid uncertainties associated with ceramics at this particular time. Table 5.3 compares the characteristics of a stainless steel and ceramic piston. A ceramic piston arrangement is shown in Appendix IV which covers the design presented at the preliminary design review.

Figure 5.10 shows the cyclic deformation in the seal clearance. The nominal clearance of .7 mils was increased to .9 mils to accommodate this.

5.3 Engine and System Performance

5.3.1 Introduction

The seasonal performance of the system is characterized by the electric power delivered to the grid during a typical year. The specified distribution of insolation on the collector is shown in Table 5.4. The thermal energy at the

Table 5.4

ANNUAL SOLAR INSOLATION DISTRIBUTION

<u>Insolation</u> Watts/m ²	<u>Time</u> Hours/Year
0 to 99	5091
100 to 199	276
200 to 299	201
300 to 399	216
400 to 499	181
500 to 599	229
600 to 699	261
700 to 799	444
800 to 899	674
900 to 999	1021
1050 to 1099	<u>168</u> 8762

receiver is also specified as 75 kWt for an insolation level of 950 watts per square meter. This is also defined as the design point for the system. The system is required to accept up to 1100 watts per square meter of insolation. As shown in Section 7, the system has been designed to generate power over the full range of useful insolation intensity (approx. 200 to 1100 watts per square meter). For this study the collector efficiency has been assumed constant:

$$\text{i.e. } Q_R = (I \times 75 \text{ kWt})/950$$

Where Q_R is heat into the receiver

I is insolation on collector in watts per square meter

The total energy available at the receiver is calculated on this basis to be 205,000 kWh/year.

The objective is to convert as much of this energy to electricity as is economically practical within life, reliability and maintenance constraints. This reduces to minimizing losses to the extent practical in the following categories:

- 1) Receiver Thermal Losses
- 2a) Engine Thermodynamic Losses
- 2b) Engine Mechanical Losses
- 3) Alternator Power Losses
- 4) Auxiliaries and Controls Power Requirements and Losses

The losses in the receiver are covered in detail in Appendix I. Since the receiver operates at constant temperature the loss is essentially independent of power level. For the final conceptual design with a nominal receiver temperature of 700°C the loss is 6.2 kWt (i.e. receiver efficiency 91.7% at the design point). For the baseline temperature of 800°C, which was being considered up to the P.D.R., the corresponding loss was 7.5 kWt (i.e. 90% efficiency).

The performance of the alternator is covered in Section 6 and the performance of the auxiliaries along with the design of the subsystems to control the dynamic

behavior of the engine is covered in Section 7. Emphasis in this section will be on optimizing the engine thermodynamics and mechanical (shaft) power.

For a heat engine operating on the Stirling cycle the maximum efficiency theoretically attainable is the Carnot efficiency given by:

$$\text{ETA (Carnot)} = (T_H - T_C) / T_H$$

where T_H is the temperature of the heat source

T_C is the temperature of the heat sink

The heat source in the solar engine is the sodium which condenses on the heater tubes. This is 700°C in final design (800°C in the preliminary design). The heat sink is the engine cooler.

At the design point the average temperature of the metal outer wall in the cooler is estimated to be 30°C above the ambient air temperature due to temperature drops in the cooling system. Ambient air temperature is assumed to average 30°C. This results in a design point cooler wall temperature of 60°C (333°K). For simplicity this was conservatively assumed to be constant over the full operating range. The nominal temperatures of the heater tube surface and cooler tube surface are 973°K (700°C) and 333°K (60°C). These values result in a Carnot efficiency of 65.8%, hence the maximum theoretical power from an idealized engine is $68.8 \times .658 = 45.3$ kW. The objective is to design the engine to convert as much of this available energy as is practical to shaft power at the alternator plunger.

The basic thermodynamic analysis of the Stirling cycle utilizes the HFAST computer code, which has been developed at MTI over the past few years. The latest version of this code has been correlated against experimental measurements on both free-piston and kinematic engines. These cover a wide range of pressure level, pressure amplitude, and temperature ratio with both helium and hydrogen as working gases. In addition to gross correlation such as power and efficiency, the code also correlates well against engine pressure amplitude and heat exchanger temperature distribution in SPDE. Temperature correlation has been a major factor in understanding and predicting engine performance. There are still uncertainties in the accuracy of analytical predictions on Stirling

engine thermodynamics, particularly for a new design which has conceptual differences from engines that have been tested. HFAST predictions for the solar engine should be reasonably accurate since it has some inherent advantages over the space engine with regard to loss predictions. These are:

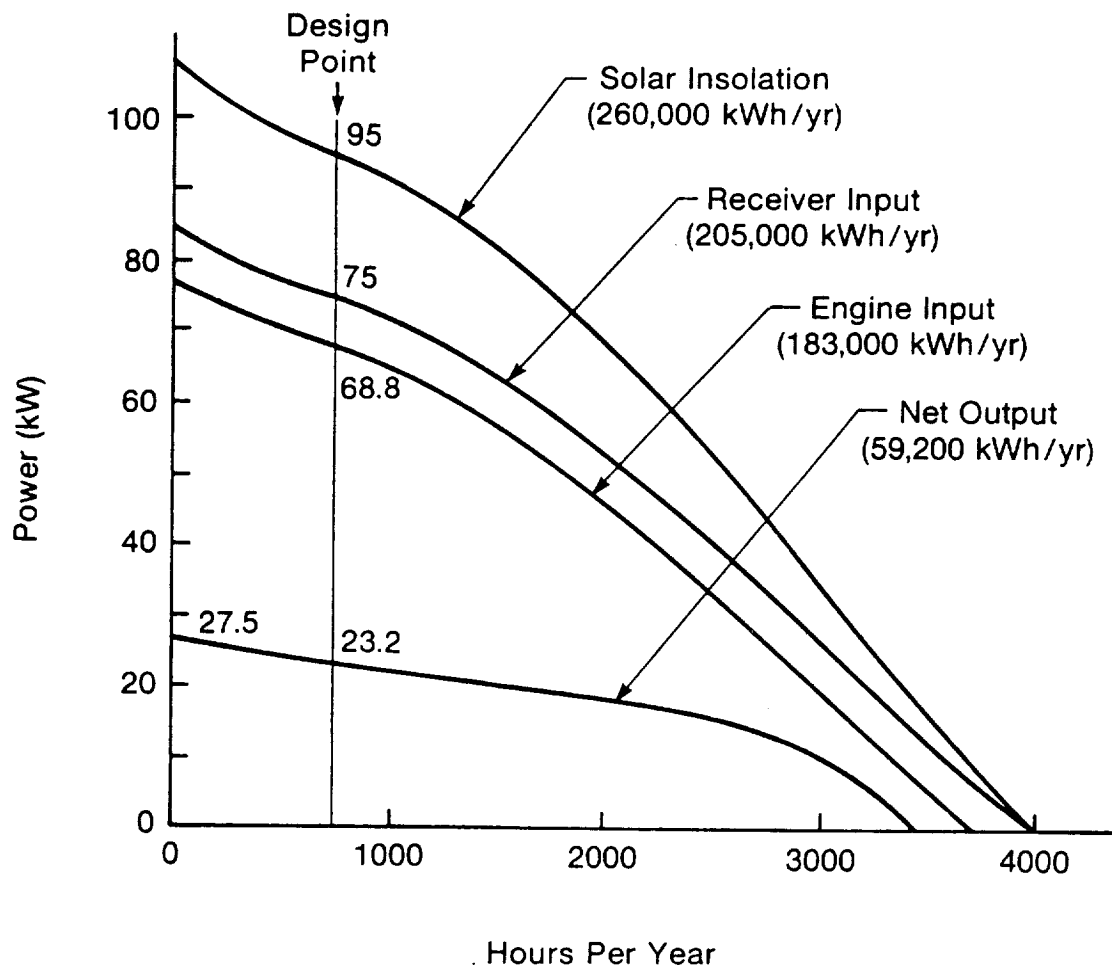
Temperature Ratio	3.0 vs. 2.0
Pressure Level	105 Bar vs. 150 Bar
Frequency	60 Hz vs. 100 Hz

The HFAST code can be coupled to an optimization routine, a gas spring loss calculation routine, and an input generation routine to select an optimum set of engine parameters within prescribed limits which maximize the shaft power delivered to the alternator. A system dynamics routine is also coupled into the overall solution to adjust parameters such as gas spring volumes, and moving element masses to produce the optimum strokes and phase of the moving elements. This routine also determines the dynamic behavior at various power levels above and below the design point from which the power performance at these conditions is determined.

The engine efficiency is almost constant from 30% to 115% of the design point power level. System efficiency is not quite so flat because thermal losses from the receiver and losses associated with cooling and control subsystems become significant at very low power levels. Since only a small fraction of the available energy is at insolation levels below 300 watts per square meter, the seasonal efficiency of 29% is only about 2% below the design point efficiency.

Table 4.2 summarizes the engine parameters selected to optimize the engine performance. Table 5.5 summarizes the power losses and efficiencies at the design point for the baseline engine presented at the preliminary design stage (heater temperature 800°C) and the final design (heater temperature 700°C).

Figure 5.11 shows the seasonal performance for $T_H=700C$. The curve shows the annual distribution of insolation at the collector, thermal power into the receiver, thermal power into the engine and electrical power delivered to the grid. The annual energy to the grid for the final design (700°C - sintered regenerator - S.S. piston) is calculated to be 59,200 kWh/yr or 29% of the total energy available to the receiver.



Seasonal Performance

Figure 5.11

6.0 LINEAR ALTERNATOR DESIGN AND ANALYSIS

6.1 Introduction

Two alternator concepts were identified in the proposal as being potentially suitable for the ASCS application. These are referred to as:

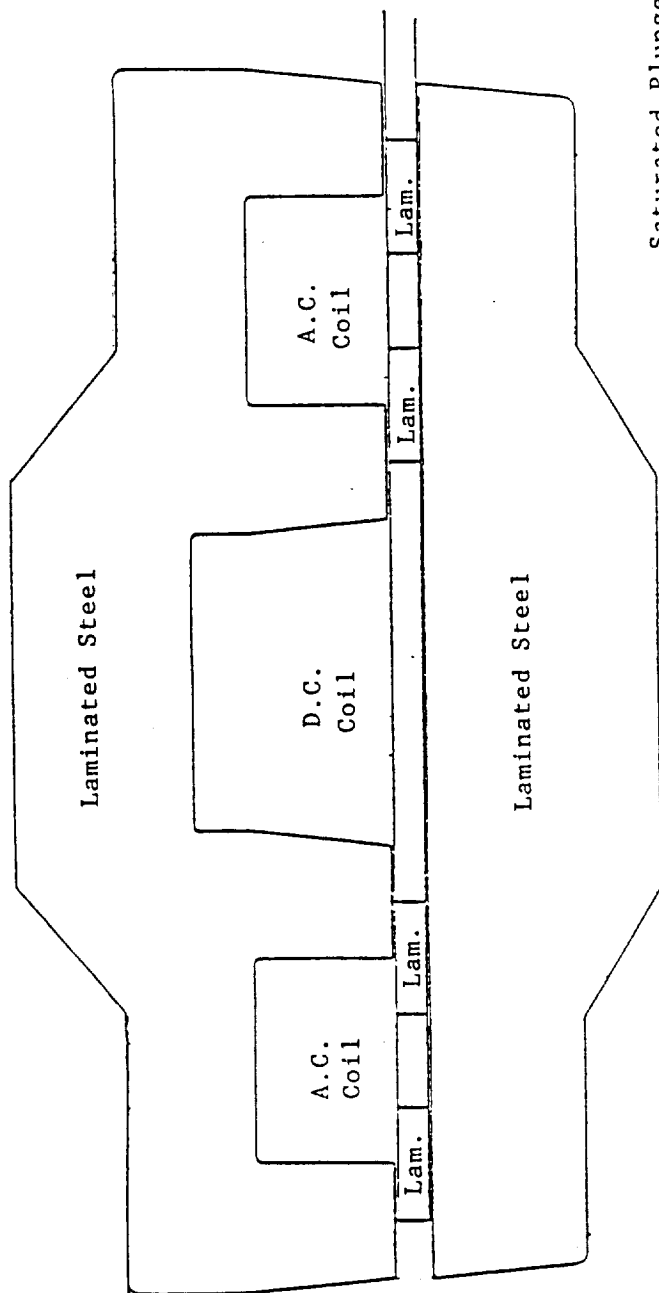
1. Permanent Magnet Alternator
2. Saturated Plunger Alternator

Designs based on each concept were generated and evaluated. The permanent magnet concept, using Neodymium-Boron-Iron magnets was selected at the preliminary design stage and has been retained in the final conceptual design.

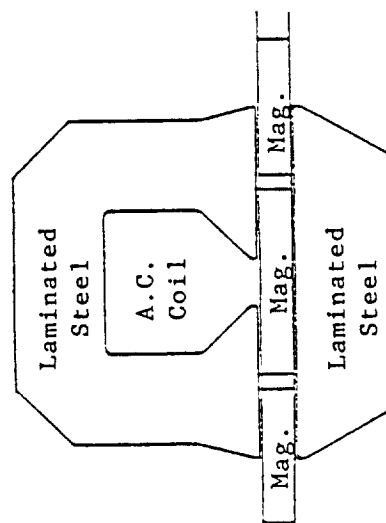
Figure 6.1 shows a comparison of cross-sections of each alternator type for the ASCS application.

The PM alternator consists of inner and outer stator cylindrical stators with a single AC output coil wound cylindrically in the outer stator. The PM plunger consists of three cylindrical magnet rings. The two outer ring are magnetized radially outward and the center ring is magnetized radially inward. The magnets in each ring are segmented cylindrically to reduce magnet eddy currents. When the plunger is fully to the left, the magnet flux links the AC coil in a clockwise direction primarily as a result of flux generated by the middle magnet (under the left pole) and the right outer magnet (under right pole). When the plunger is fully to the right, the flux links the AC coil in a counter clockwise direction due to the effect of the left outer and middle magnets. When the plunger is at the center position the magnet fluxes link each through the poles without linking the AC coil. As the plunger reciprocates sinusoidally, the variation in magnet flux linking the AC coil generates a periodic voltage in the coil. This voltage is referred to as the generated voltage and is referred to E_{gen} .

The saturated plunger alternator similarly consists of inner and outer cylindrical stators with a reciprocating plunger in the radial gap between the stators. However, the saturated plunger alternator has two cylindrical AC output coils



Saturated Plunger
Alternator



Permanent Magnet
Alternator

Figure 6.1

COMPARISON OF SATURATED PLUNGER AND PERMANENT MAGNET ALTERNATORS

wound in the outer stator and, in addition, a DC coil wound in the outer stator in the region separating the two AC coils. The saturated alternator plunger does not use permanent magnets, rather it's active magnetic material consists of laminated soft iron elements located under the stator pole regions. The elements are designed to saturate at moderate induction levels (1.3 Tesla), and the AC and DC coil amp-turns are selected so that the plunger iron under the pole regions remains fully saturated during alternator operation. (Typically, this requires that the AC amp-turns be limited to somewhat less than half the DC amp-turns during normal alternator operation.) This is referred to as "fully saturated" operation, and this operating mode is chosen to limit the alternator inductance.

When the saturated alternator plunger is fully to the left, the magnetically active zones are located under the left poles of each AC coil, and the DC coil flux primarily links the left AC coil. When the plunger is fully to the right, the magnetically active zones are under the right poles of each coil, and the DC coil flux primarily links the right AC coil. Because the flux linkage switches back and forth between the left and right AC coils with plunger motion, the alternator is called a flux switching (as opposed to a flux reversing) design.

As can be seen from Figure 6.1, the PM and saturated plunger designs are different in size, with the saturated plunger being approximately three times as large. The reason for the size difference can be justified by noting that the saturated plunger alternator can be considered to be made up of three parts: two end parts which are similar in size and shape to a single PM alternator, and a middle section. The end sections containing the AC coils are similar in size and shape to PM alternators, but each generates about half the output of a similar sized PM unit because of the flux switching as opposed to flux reversing characteristic of the saturated plunger machines. In addition to the two AC units, the saturated plunger alternator requires a DC coil region to generate the DC flux needed to energize the plunger elements. This DC coil region is about the same size as the two AC units, and consequently the overall alternator is about three times as large as a single equivalent PM unit.

In addition to size, the PM alternator tends to be more efficient than the saturated plunger machine. This is primarily the result of the additional copper

losses associated with the using the DC coil and the additional AC coil on the saturated plunger machine.

In selecting the PM alternator over the saturated plunger alternator, the primary selection criteria used was life cycle cost, and specifically the cost of the magnet on the PM alternator versus the cost of lost output power on the lower efficiency saturated plunger machine.

6.2 Permanent Magnet Alternator

6.2.1 Alternator Description

The permanent magnet alternator for the solar FPSE shown in Figure 4.1 is a monocoil design similar to that used in SPDE. It consists of four basic elements: an outer stator, an inner stator, an AC coil, and an armature carrying the permanent magnets. The alternator is mounted outside of and concentric with the power piston cylinder. The AC coil is packaged in the outer stator, and the armature is cantilevered off the rear of the power piston.

6.2.2 PM Alternator Configuration Selection

Figure 6.2 shows three potential permanent magnet alternator structures. These three structures are related in a simple fashion: the second evolves from the first by adding two wing magnets to the center magnet, and the third evolves from the second by widening the coil opening and lengthening the center magnet. (The SPDE alternator can be considered as a further evolution of the third in which the coil is further widened with the center magnet consequently split into two magnets separated axially by a nonmagnetic spacer.) Comparatively, for magnets strongly susceptible to demagnetization, the upper configuration will typically have the highest plunger mass, the mid-configuration the least, and the bottom configuration an intermediate value. On that basis, i.e., demagnetization, the mid-configuration is preferable. However, as a result of the large AC leakage fluxes associated with the tapered portion of the coil slot, the inductance of the mid-configuration will typically be higher than that of the bottom configuration (and significantly so in large gap machines of the type proposed). The leakage reactance can be reduced by opening the bottom of the coil slot and moving towards the bottom configuration. However, as indicated

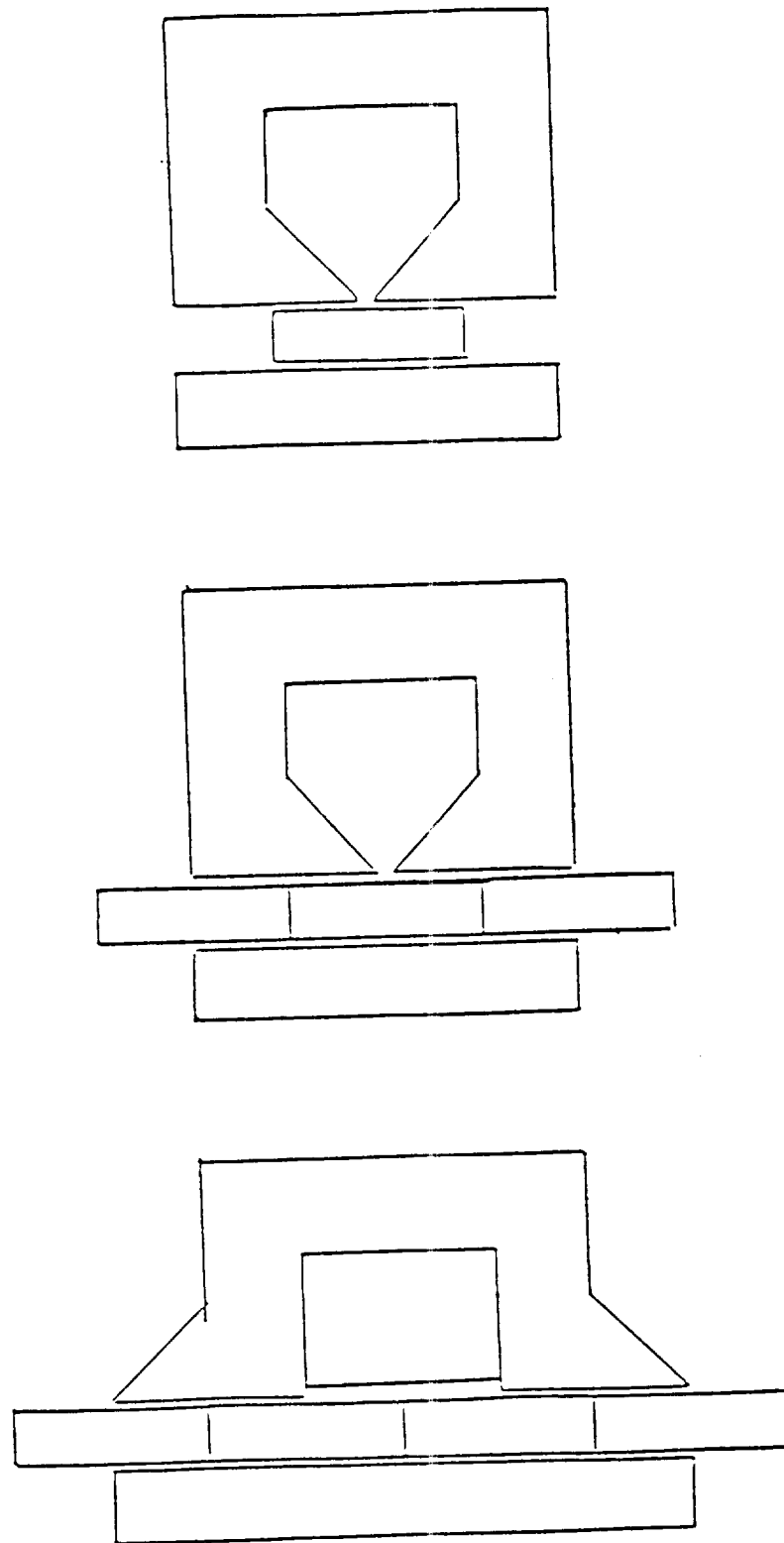


Figure 6.2

PERMANENT MAGNET ALTERNATOR CONFIGURATIONS

previously, this requires increasing the length (i.e. mass) of the center magnet, and consequently the mass of the plunger.

For the solar engine system, a configuration lying between the mid and bottom configurations has been selected. This configuration retains the higher resistance to demagnetization of the two lower configurations, while effecting a compromise between the lower plunger mass of the mid-configuration and the lower reactance of the bottom configuration.

6.2.3 Magnets and Demagnetization

The alternator design utilizes Neodymium-Iron-Boron magnets. These magnets are somewhat more powerful than Samrium Cobalt magnets, at least in terms of residual induction and peak energy product, and have the added advantage of being made from more available and, hence, potentially lower cost materials. The fabrication process for these magnets involves six basic steps: generation of alloy in finely powdered form; pressing (at room temperature) into rough shape (typically at 60 to 80 kpsi in a magnetic field); sintering in a inert gas or vaccum furnace (typically a controlled time temperature process extending over a period of 10 to 12 hours with a peak temperature of 1100 degC), abrasive machining; magnetization, inspection, and grading; and finally, armature installation. Shinkage of the magnets during the sintering process prevents the direct casting of fine details.

Despite the higher relative induction of NIB magnets relative to Samarium Cobalt magnets, they have significantly lower demagnetization resistance; higher temperature sensitivity (i.e., the residual induction and demagnetization resistance decrease per degree of temperature rise is relatively high); and the usable temperature limit for NIB magnets (150 degC) is much less than for SaC magnets (greater than 300 degC). Of the above, reduced resistance to demagnetization has the biggest impact on solar alternator design.

Demagnetization refers to the loss of magnetic induction which occurs when a demagnetizing field is imposed on the magnets. Typically the loss in residual induction is quite small until the demagnetizing force becomes large enough to push the magnet past the "knee" on the demagnetization curve, after which significant irreversible or permanent demagnetization occurs rapidly with

increasing field strength. In the proposed permanent magnet alternator, a demagnetization field is applied to the magnets by the AC coil when the flux induced by the AC coil is opposed to the magnetization direction of a given magnet. Since the strength of the demagnetization field depends on the AC coil current, the alternator is designed to avoid demagnetization for fault conditions as well as normal operation. This requires restricting the magnitude of the operating demagnetizing field strength so that demagnetization does not occur under the worst fault condition, or limiting the current by suitable external circuitry. This is discussed further in Section 7.5.

Alternator shorts normally generate the worst demagnetizing transients, and typically the worst short is a short across the output wires just downstream of the alternator tuning capacitor. (A short in this location results in an alternator circuit with very low series impedance which, for fixed alternator stroke, would result in a rapid rise in alternator current to very high values.) Fortunately, a short at this location overdamps the engine and hence results in an engine shutdown. The alternator current rises during the first few cycles after the short, and then quickly decays with the decaying piston stroke. A transient analysis of this process indicated that the short results in approximately twice the steady state current prior to the first current zero crossing, and has a peak transient current equal to approximately three times steady state value. The worst time for the short to occur is on a hot day (the magnets are more susceptible to demagnetization at higher temperatures), and at peak insolation conditions (the steady state current is highest at this condition).

Limiting the steady state demagnetization field is equivalent to limiting the AC flux density, B_{ac} , induced by the AC coil current in the alternator pole region. Limiting B_{ac} reduces the power output of the alternator and adversely affects the alternator specific power. The value to which B_{ac} must be limited to avoid demagnetization can be raised by:

1. selecting an alternator structure which has an inherently high resistance to demagnetization
2. using magnets with a relatively high resistance to demagnetization
3. operating the magnets at lower temperatures (i.e., increasing the effectiveness of the back end cooling system)

4. placing an active or passive current limiting device at the alternator output terminals.
5. designing the alternator so that the iron saturates as and inhibits demagnetization at AC current levels which would normally result in demagnetization without saturation.

6.2.4 Inductance and Coil Loss Considerations

In a given alternator design, the AC flux density (and hence magnet mass) may be limited by considerations other than demagnetization; i.e.:

1. alternator inductance
2. stator pole face saturation
3. AC coil loss

For the Solar application, coil inductance is limited by stability considerations as discussed in Section 7.2. The stability requirement is typically stated nondimensionally in terms of the ratio of the inductive voltage drop in the AC coil, V_i , to the magnet induced voltage E_{gen} . This ratio is called the alternator "beta". For a given alternator operating at fixed stroke and frequency, E_{gen} is fixed. For these conditions, the power output, the coil inductive voltage, and hence "beta." are proportional to the coil current. If the alternator is "inductance limited", then the coil current, and hence the power output, must be limited to values consistent with the allowable β value.

In the proposed alternator, despite the upper limit on alternator inductance imposed by stability considerations, demagnetization is the more limiting AC flux density consideration. (From an inductance viewpoint $B_{ac}=0.75$ Teslas is acceptable, whereas simple demagnetization considerations in the proposed design limit B_{ac} to approximately half this value.)

The proposed design utilizes the first two of the above elements to reduce the impact of demagnetization considerations. It utilizes magnets with a high magnetization resistance (e.g. NEO 30H from Thomas & Skinner, Inc.); and anticipates employment of a relatively effective aft end cooling system (the magnets are assumed to operate at 60 degC (140degF) at the 95 degF day operating point).

Demagnetizing currents due to fault conditions can be controlled by incorporating a current limiting circuit in the system. A simple circuit built around a TRIAC switching is one simple way of performing this function.

6.2.5 Design Calculations

Design calculations were performed to select the size and geometry of the magnets, coil and iron structures. The sidepull gradient was also estimated. The final geometry was selected to optimize alternator efficiency while meeting the constraints on power, inductance (engine stability) and cost (weight of magnets).

The results of these calculations are shown in Tables 6.1, 6.2 and 6.3.

Table 6.1

ALTERNATOR SUMMARY

- Electrical Output
 - 30 kWe
 - 60 Hertz
 - 1 ϕ
 - 240 Volts
- Mechanical Input
 - 31.9 kWe
 - 60 Hertz
 - Linear Reciprocating
 - 36 mm Stroke
- Efficiency - 94%
- Structural - Floating P.M. Design Similar to SPDE
- Salient Features
 - NIB Magnets (Low Cost - Availability)
 - Low Inductance ($B = 1.0$)
 - Light Weight (2 Kg/Kw)

Table 6.2

DESIGN PARAMETERS

• Frequency	60 hertz
• Stroke	36 mm
• Magnets	NIB-30H @ 60°C
• Br	1.1 Tesla
• Hci	13 KOe
• μ	1.05
• β	1.0 (Vi/Egen)
• K	.346 (B_{ac}/B_r)
• Demag SF	3.0
• Dp	.279 m (11 inches)
• M mag	7.4 Kg (17.4 lbm)
• M outer	34.6 Kg (76.2 lbm)
• M inner	10.9 Kg (24.1 lbm)
• M copper	7.3 Kg (16.0 lbm)
• M total	60.7 Kg (134 lbm)
• Specific mass	2 Kg/Kw (4.5 lbm/Kg)
• η	94%

Table 6.3

ALTERNATOR LOSS BREAKDOWN

		Calculated Value	Loss Factor	Estimated Value
Copper	Direct I ² R Losses in AC Coil	.020	1.0	.020
Iron	Eddy and Hysteresis Loss	.004	2.0	.008
Magnet	Magnet and Coil Induced Eddy Currents in Magnets	.012	1.0	.012
Stray	Structural Eddy Currents in Support Structure and Pressure Level	TBD	N.A	.020
TOTAL				.060

$$\eta = 94\%$$

7.0 SYSTEM DESIGN CONSIDERATIONS

In this section the system design considerations of the basic ASCS system are presented. The material presented includes a brief description of the major subsystems, a description of the dynamic behavior of the power module during normal operation, a review of system requirements and the conceptual design approach to meet these requirements, a description of system performance, and finally a description of system start-up, normal shut down and emergency shut down procedures.

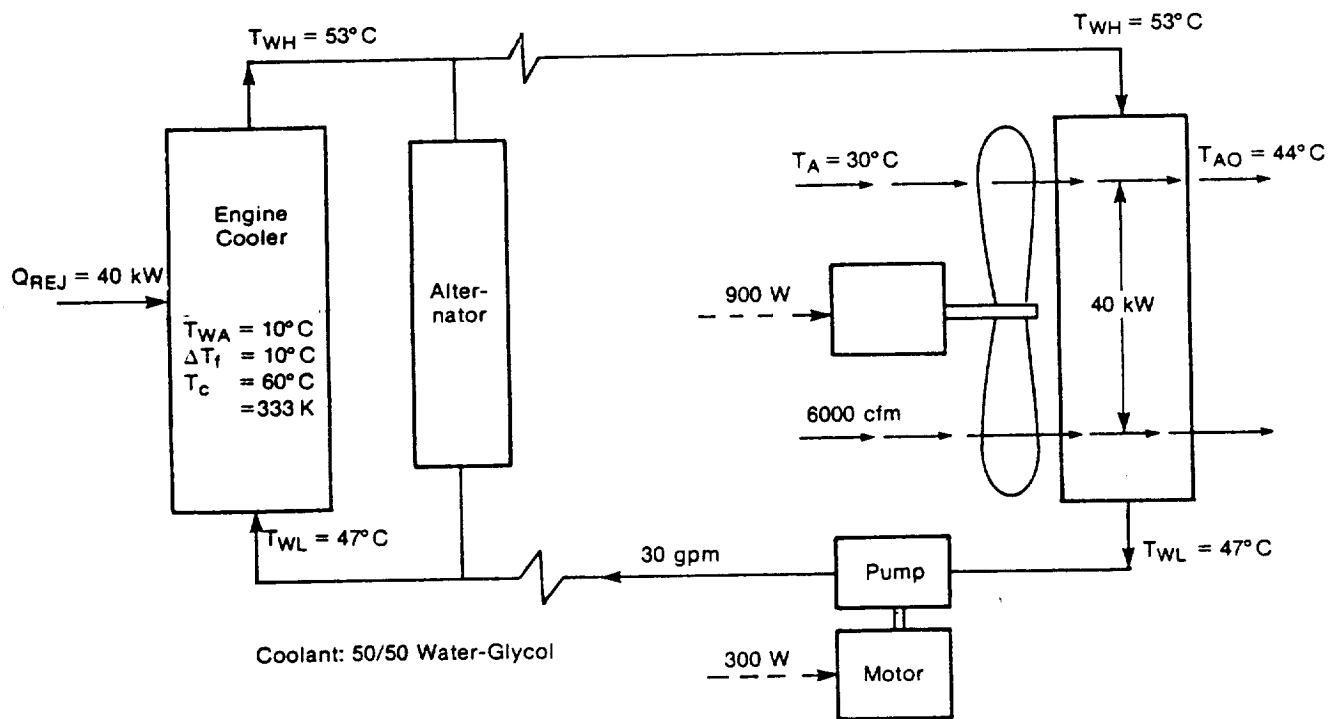
7.1 System Overview

From overall system operation considerations, the basic ASCS system can be conveniently divided into four major subsystems, which are:

1. Heat supply subsystem
2. Power module subsystem
3. Heat reject subsystem
4. Control subsystem

The heat supply subsystem consists of a receiver and a thermal energy transport medium. The purpose of the receiver is to receive concentrated solar flux from the collector and convert it efficiently into thermal energy. The resultant thermal energy is transferred to the engine by evaporation of liquid sodium at the receiver surface and condensation of sodium vapor on the engine heater tubes. The receiver surface is provided with heat pipe wicks to ensure distribution of liquid sodium over the entire receiver surface.

The purpose of the power module is to convert the thermal energy supplied to the engine heater tubes into electrical power and to feed that electrical power into the utility grid. The power module consists of a displacer type free piston Stirling engine directly connected to a linear alternator. The linear alternator is connected to the grid in series with a tuning capacitor and an autotransformer.



Radiator:	
Face Area (ft)	3×3
Air Flow (cfm)	6000
Velocity (fpm)	670
Fins/in.	125
4 Pass	
30 gpm	
$(\Delta p \times Q)_{AIR} \text{ (W)}$	500

Cooling System

Figure 7.1

The purpose of the heat reject subsystem is to remove waste heat from the power module (engine and alternator) and to reject it to the atmosphere. The heat reject subsystem is a standard closed loop cooling system consisting of a radiator, blower fan, coolant pump, and two parallel coolant loops; one for the engine cooler and the other for the alternator stator. A schematic drawing of heat reject subsystem is shown in Figure 7.1.

The purpose of the control subsystem is to maintain proper operation of the ASCS within the system requirements under normal operating conditions, and to respond automatically to major and minor system faults. The control subsystem consists of 1) an autotransformer, which modulates the engine heater heat flux rate to match the solar insolation rate received by the receiver, 2) radiator fan motor on-off control which allows safe and proper ASCS operation over the desired ambient temperature range, and 3) a solenoid operated pneumatic valve in the engine to kill the engine if electrical control is lost.

7.2 Power Module Dynamic Behavior

Figure 7.2 shows the block diagram of the ASCS power module consisting of a free piston engine coupled to a permanent magnet linear alternator.

The free piston engine consists of two moving parts: a displacer piston (mass M_d) and a power piston (mass M_p). Each piston is acted on by their respective gas spring dynamic elements. In addition, the two pistons dynamically interact with each other through the engine working gas. The motion of the displacer piston and power piston result in a pressure wave which lags the piston motion. The amplitude and the phase angle of the pressure wave are defined by the volumetric displacement of the two pistons, the working gas temperature profile, and the parasitic losses in the engine working spaces. The pressure drop in the engine heat exchangers results in pressure waves in the compression and expansion spaces (P_c and P_e respectively) which are slightly out of phase with each other. The cycle power available at the power piston is proportional to the vector dot product of compression space pressure wave and power piston velocity. The heater heat flux rate required by the engine is proportional to the dot product of the expansion space pressure wave and the displacer velocity, and to the first order is independent of heater temperature. Therefore, a change in

Dynamics Model

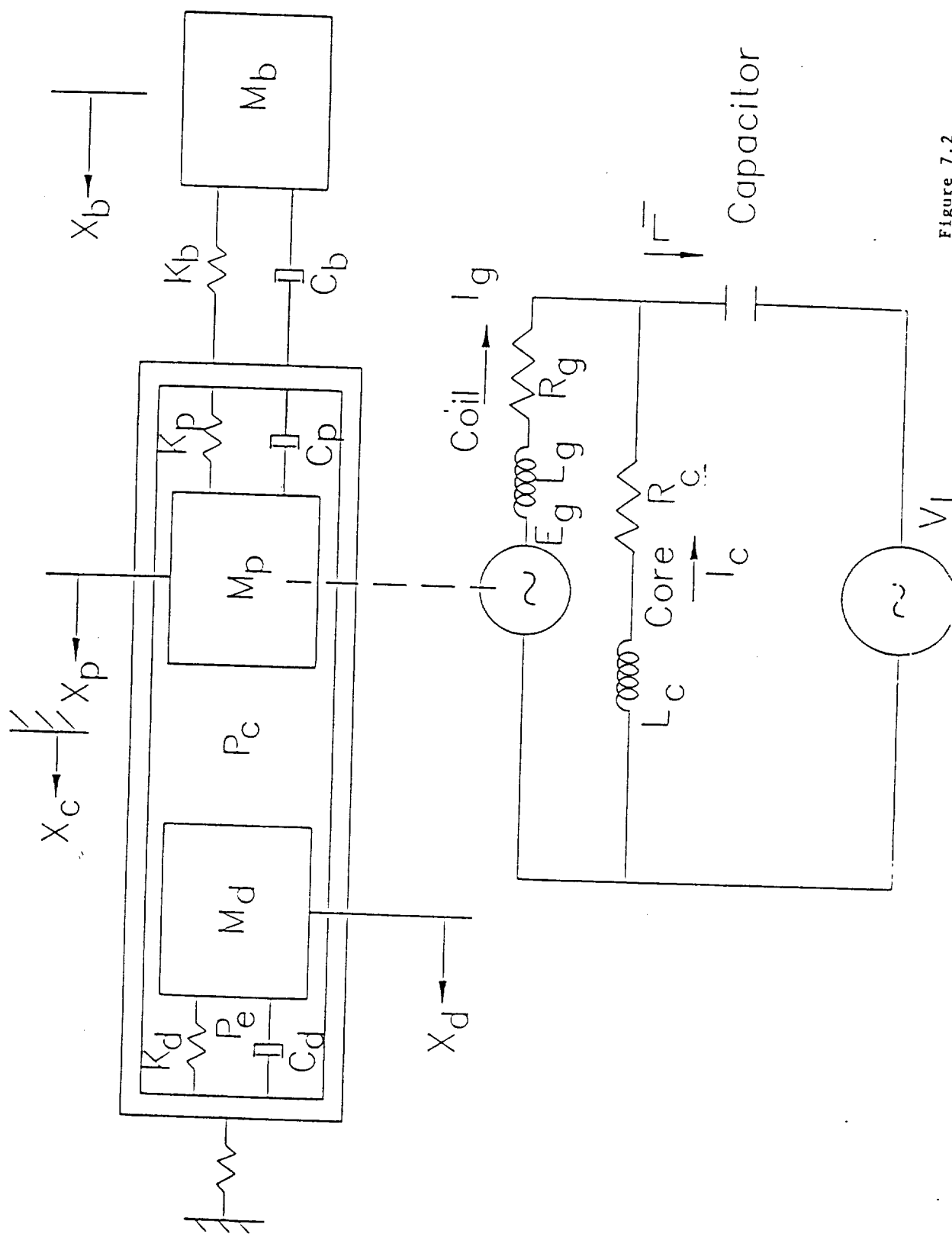


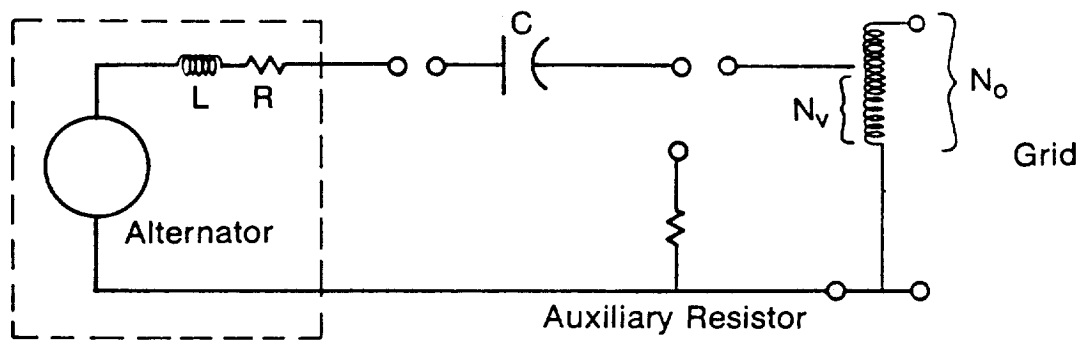
Figure 7.2

heater heat flux rate requires either a change in engine mean pressure or a change in volumetric displacement of the displacer or power piston. In the present ASCS the engine heater heat flux rate is matched to the solar insolation rate by modulating the volumetric displacement of the displacer and power piston. This action is performed by an autotransformer as mentioned earlier.

The alternator is a permanent magnet linear alternator with plunger rigidly coupled to the power piston. The alternator block diagram shown in Figure 7.2 depicts two parallel electrical loops; one for the iron core circuit and the other for the copper coil circuit. As shown in Figure 7.3, the linear alternator is connected to the utility grid in series with a tuning capacitor and an autotransformer. The need for a tuning capacitor arises from stability considerations, which is discussed next.

During transient operation, rate of change of engine power is primarily a function of rate of change in the displacer stroke and therefore is defined by the displacer time constant (displacer mass and stiffness). The rate of change of power dissipation is primarily a function of rate of change in the load current, and therefore is defined by the electrical circuit time constant (inductance and capacitance in the electrical circuit). Stable operation requires that the rate of change in power dissipation be higher than the rate of change in power generation. Therefore, stable engine-load interface can be ensured by maximizing the displacer mass (slow down the engine) and minimizing the electrical circuit inductance (increase the electrical circuit response). However, higher displacer mass results in higher gas spring losses and/or larger displacer gas spring piston area and volume. Lower alternator inductance requires thicker magnets and therefore higher piston gas spring losses and/or larger piston gas spring area and volume. A measure of the alternator inductance is the ratio between the voltage drop in the inductance and the magnet induced voltage (alternator generated voltage). This ratio is referred to as "alternator voltage ratio - β ". Dynamic analysis of the conceptual design indicated that without a series capacitor in the circuit alternator voltage ratio has to be less than or equal to 0.5 for stable operation. With the capacitor in the circuit, the system is stable for alternator voltage ratio of less than or equal to 3.

For alternator voltage ratio of 0.5, the alternator size became excessive. Overall system performance studies indicated that alternator designed with



Circuit Diagram - Alternator To Grid

Figure 7.3

voltage ratio of 1 resulted in a a good compromise between performance, stability and weight (alternator plus capacitor).

The following describes the power module-load interaction. The alternator plunger motion results in a change in coil flux linkage which induces voltage in the coil, E_g , at a frequency equal to that of the plunger oscillation. The product of E_g and I_g (coil current) is the shaft power of the alternator which is supplied by the engine. Since a permanent magnet alternator does not employ separate field excitation, the magnitude of E_g can be changed only by varying the velocity of the plunger (same as the power piston velocity since the two are rigidly coupled). For fixed frequency operation E_g is therefore linearly proportional to the piston displacement amplitude. For a grid connected system, the engine/alternator behaves essentially as an externally excited vibratory system with the grid voltage acting as a system forcing function. During steady state operation, the following dynamic characteristics hold true:

- The amplitude of oscillation of the displacer and power piston is proportional to the grid voltage (or the voltage applied at the alternator terminals if a transformer is placed between the power module and the grid). This is because the power piston motion is proportional to E_g , and in turn E_g is proportional to the voltage supplied at the alternator terminals.
- The frequency of oscillation is equal to the source (grid) frequency.

By changing the turns ratio of the autotransformer, voltage V_1 (see Figure 7.3) is varied which results in power piston (and displacer piston) stroke variation. This results in control of heater heat flux demand.

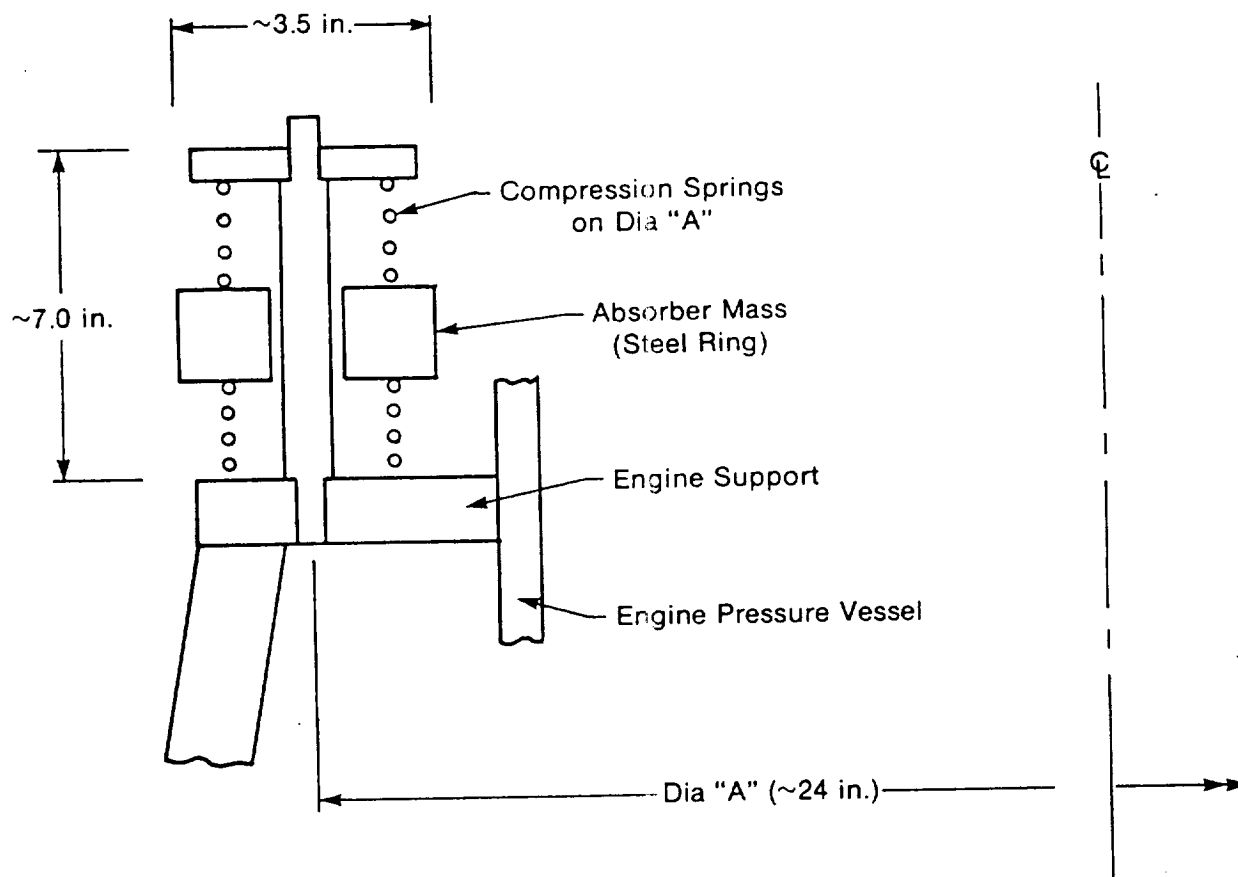
The engine and the alternator are enclosed in a casing (mass M_c) which is supported on a soft mount. The purpose of the soft mount is to minimize vibratory force transmission to the solar concentrator dish. The soft mount consist of 12 low alloy steel rectangular plates (4.5" x 8.0" x .12") with a total stiffness of 3000 lb/inch. The plates have a mean stress of 45 ksi and undergo a maximum alternating stress of 5 ksi.

The displacer and power piston motion in a single cylinder free piston Stirling engine impose a net vibratory force on the engine casing. To limit the casing vibration to an acceptable level (defined by the maximum "g" loading that the receiver and thermal transport subsystem can tolerate) a vibration absorber (Mass M_b) has been included. The vibration absorber consists of an absorber mass and mechanical springs as shown in Figure 7.4. The effective reciprocating mass of the absorber is 100 lbs; 75 lbs of moving mass and 25 lbs contributed by the compression springs. For an undamped absorber, if the natural frequency of the absorber is equal to the system operating frequency, the net force acting on the casing is zero for all operating conditions. If the operating frequency drifts from the absorber natural frequency, the casing will vibrate, and the amplitude of vibration for a given change in frequency will depend on the mass ratio between the absorber and the casing.

The above describes the dynamic behavior of the system under normal operation.

7.3 System Requirements and Performance

Table 7.1 lists the major system requirements along with the approach taken to meet these goals. The following section describes the ASCS predicted performance and shows that the proposed design meets the system requirements.



Number of Spring Pairs	28
Spring Diameter (n.)	2.0
Wire Diameter (in)	3.75
Number of Turns	6
Moving Mass (lb)	75
Spring Mass (lb)	75
Posts and End Caps (lb)	<u>60</u>
Total Mass (lb)	210

Vibration Absorber

Figure 7.4

Table 7.1

SYSTEM REQUIREMENTS AND CONTROL

THERMODYNAMIC

Solar insolation range 0 - 85.8 kW	Auto Transformer
-6C to 33C operation	Fan control
Coolant freeze protection to -29C	Inherent

ELECTRICAL

Power factor greater than 0.85 inductive	Inherent
Harmonic distortion less than 2.5%	Inherent
Operating frequency variation $\pm 1\%$	Inherent

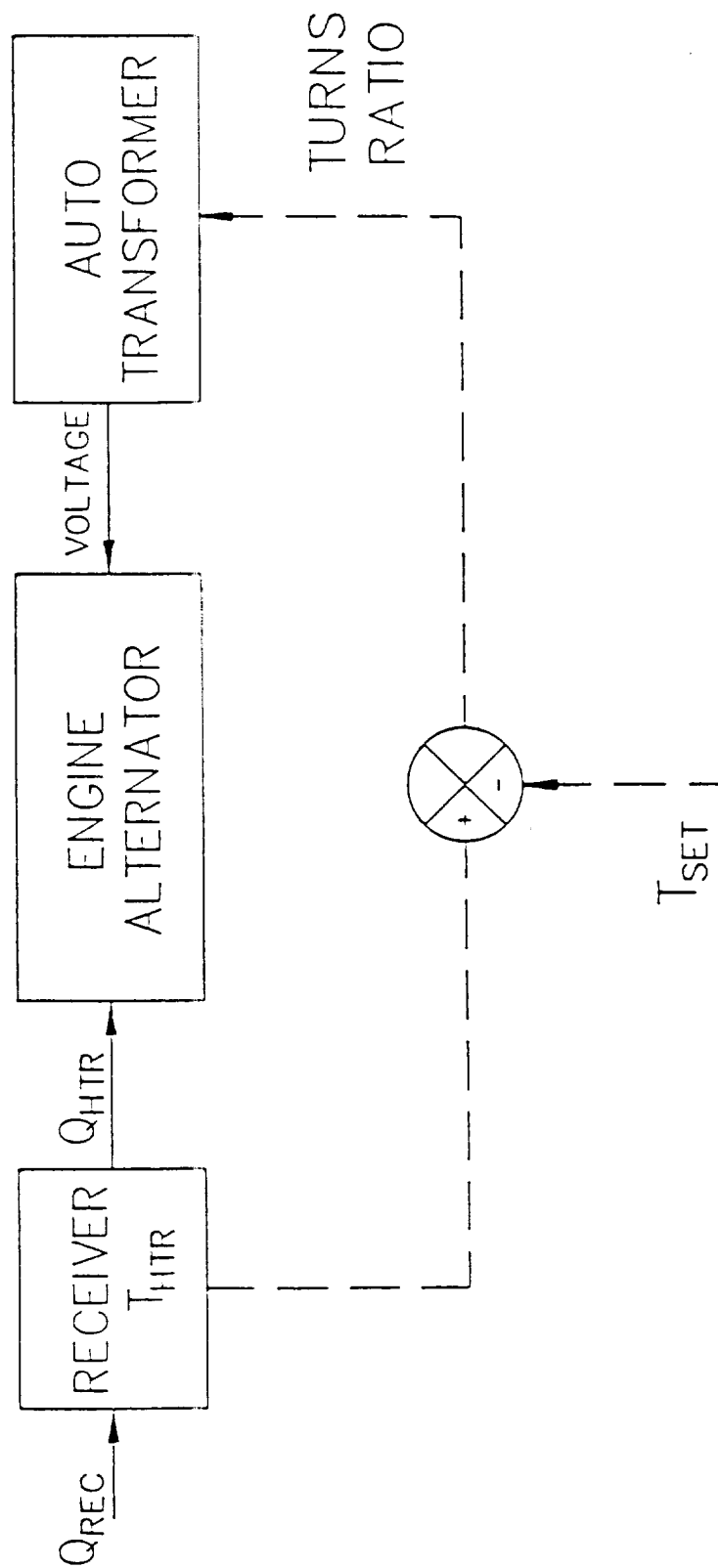
CONTROLS

Automatic start-up and shutdown	Auto Transformer
Emergency shutdown	Automatic

MECHANICAL

667N net unbalanced force to mounts	Soft mounts
	Vibration absorber

HEATER TEMPERATURE CONTINUOUS FEEDBACK CONTROL



Heater Temperature Continuous Feedback Control

Figure 7.5

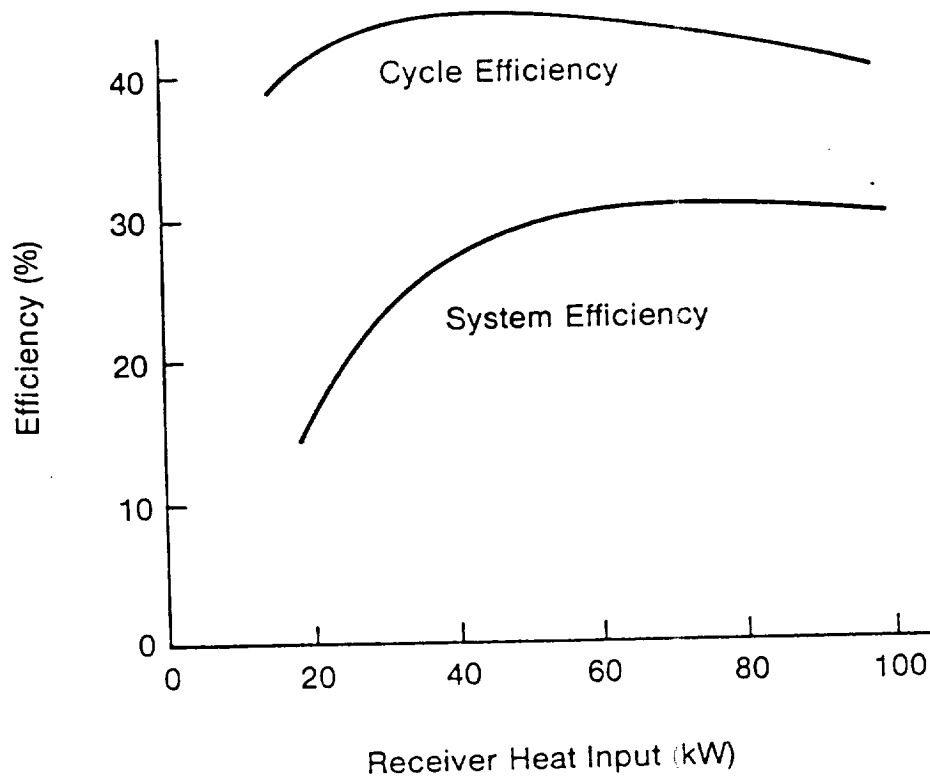
7.3.1 Solar Insolation Operating Range

The ASCS is required to operate over a solar insolation range as shown in Table 5.4. This results in a heat energy input to the receiver from 0 to 85.8 kW with the nominal design point of 75 kW.

As solar insolation changes from the design level, the engine operation has to be adjusted to avoid a large change in the engine heater temperature. As mentioned in the above the autotransformer is provided to control the heater head temperature as shown schematically in Figure 7.5. Q_{rec} is the solar insolation into the receiver. Q_{htr} is the heat flux rate absorbed by the engine. T_{htr} is the average heater temperature, and T_{set} is the desired temperature of the heater. If Q_{rec} increases due to higher solar insolation, T_{htr} increases which sends a positive error signal to the motor of the autotransformer. This signal in turn moves the transformer brush to increase the turns ratio thereby increasing the voltage amplitude at the alternator terminals. The variable autotransformer is connected as shown on Figure 7.3. The alternator voltage is $(N_v/N_0)/V_{grid}$.

Increased voltage at the alternator terminals increases the power piston and displacer amplitude resulting in increased Q_{htr} which lowers the error signal. If Q_{rec} decreases, a negative error signal results, and the sequence of operation is reversed resulting in decrease in Q_{htr} . This is a very simple control scheme which maintains high engine cycle efficiency over a large operating range. Figures 7.6 thru 7.10 show system efficiency, cycle efficiency, power supply to grid, power factor, and displacer and piston amplitudes, displacer phase angle and transformer turns ratio plotted against solar insolation absorbed by the receiver. These plots show that:

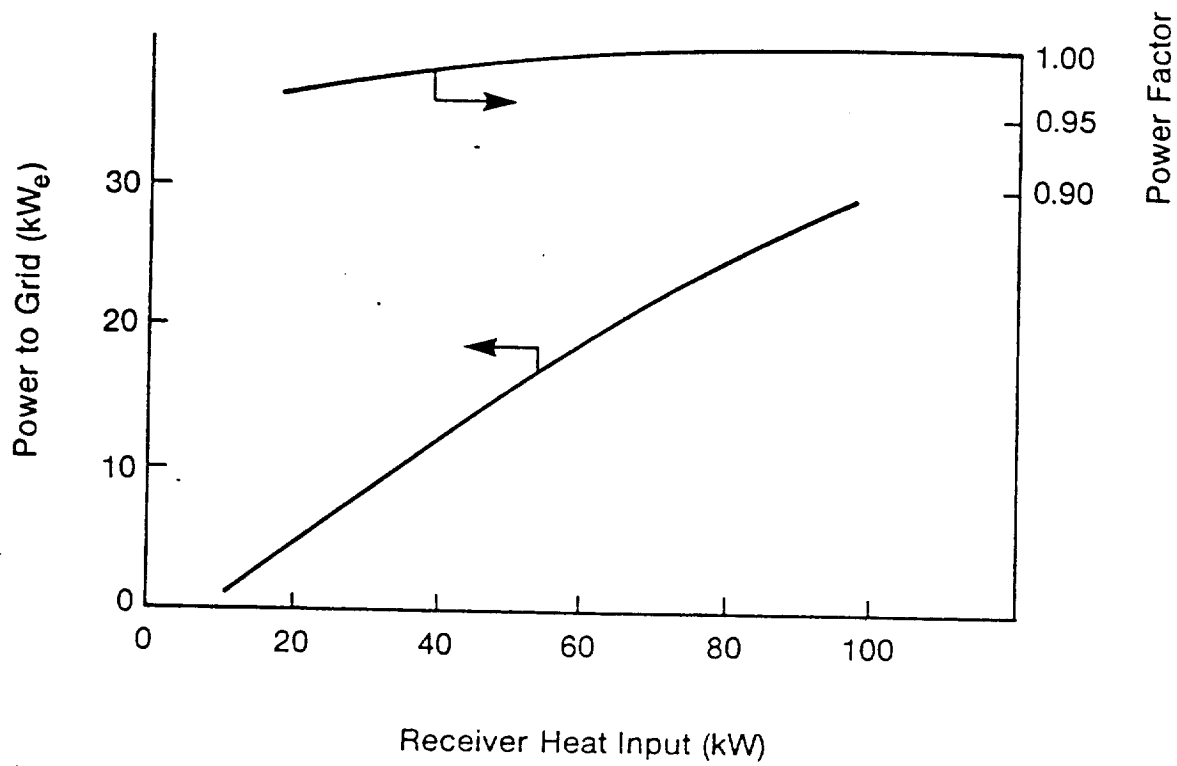
- ASCS produces net electrical power at a receiver heat input as low as 13 kW. ASCS can accept a maximum receiver input of 94 kW.
- Engine thermodynamic cycle efficiency is essentially flat over the whole operating range.
- Power factor is close to unity over the whole range.



(a)

Efficiencies vs Heat Input

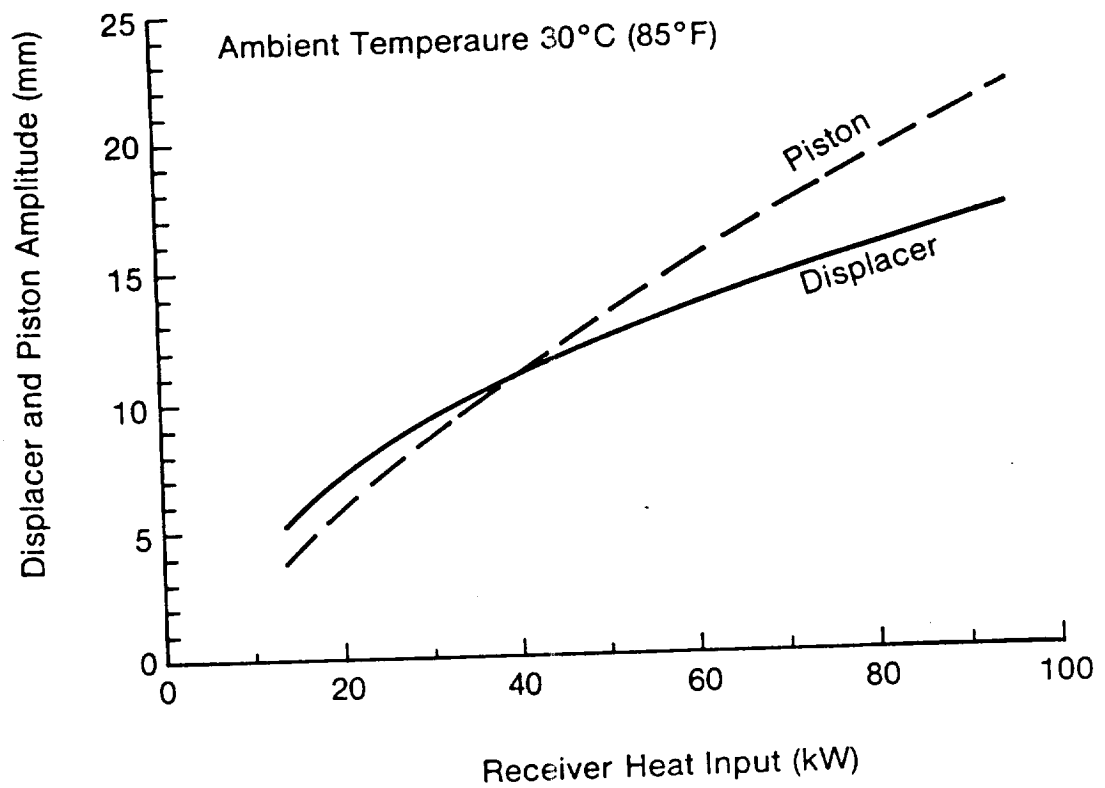
Figure 7.6



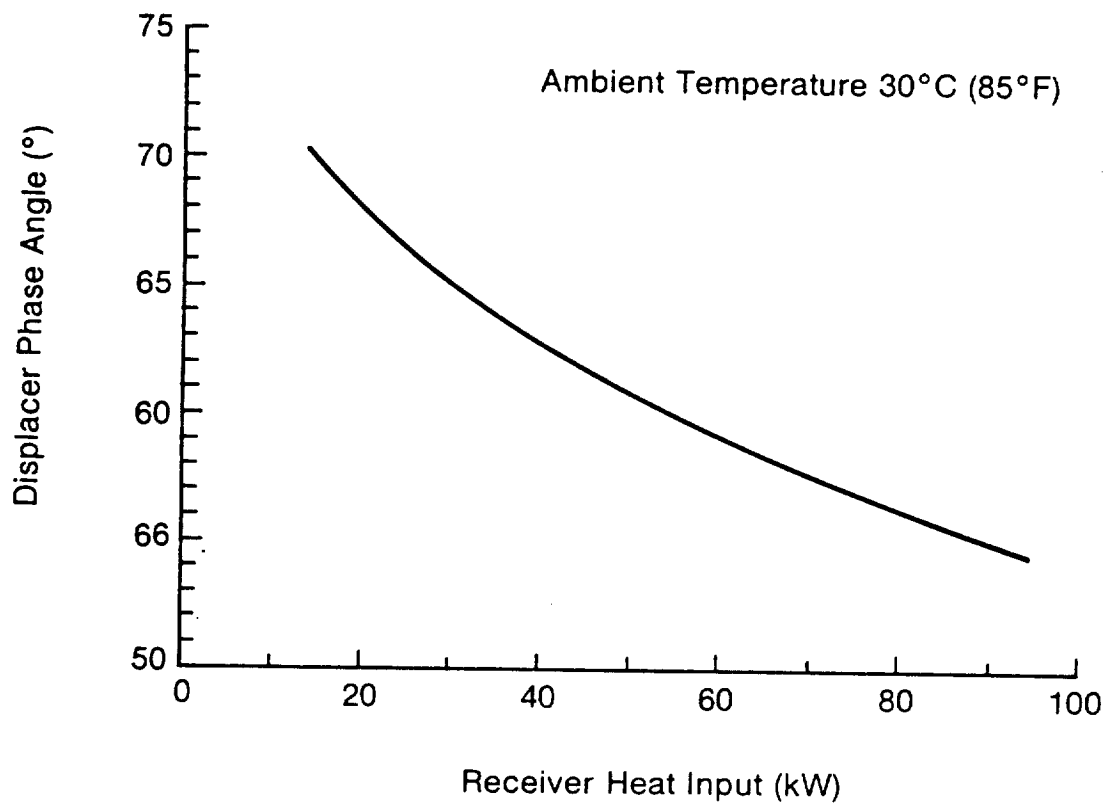
(b)

Net Power Output vs Heat Input

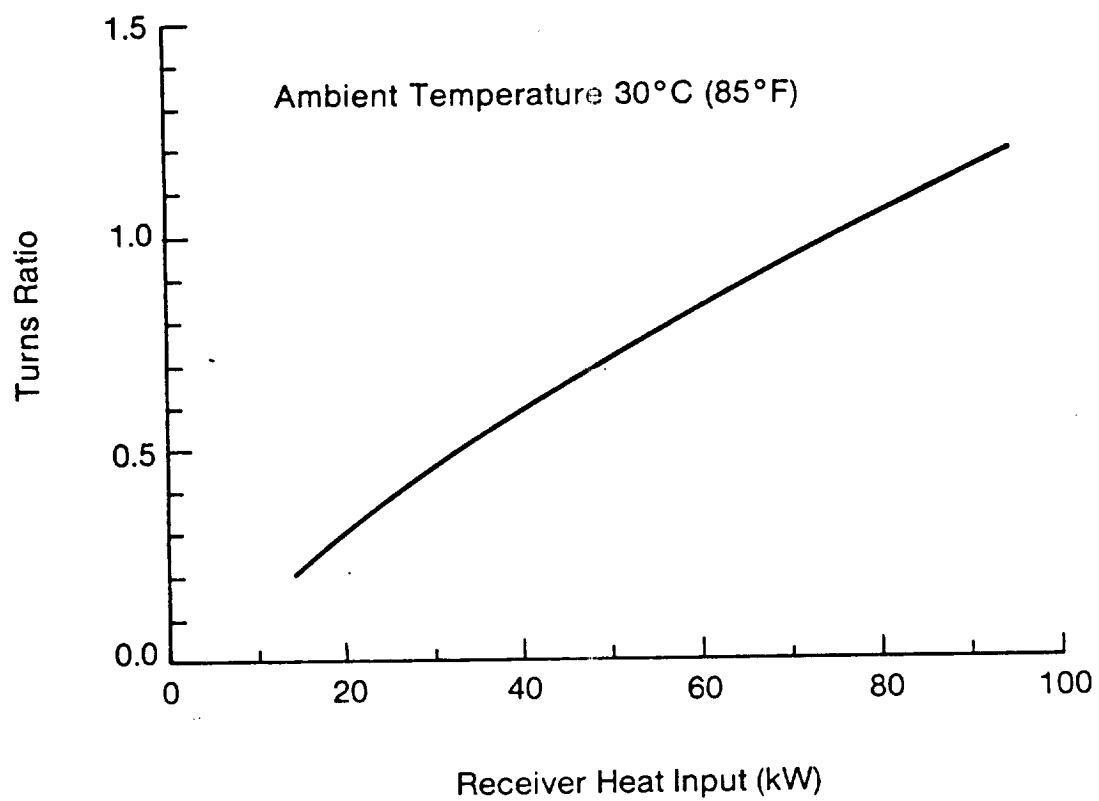
Figure 7.7



Displacer And Piston Amplitude vs Receiver Heat Input
Figure 7.8



Displacer Phase Angle vs Receiver Heat Input
Figure 7.9



Turns Ratio vs Receiver Heat Input

Figure 7.10

7.3.2 Operation Over Ambient Temperature Range

The ASCS is required to operate over an ambient temperature range of -6°C to 33°C . (The ASCS is designed to operate to over 40°C .) Coolant freeze protection is required to -29°C . A 50-50 water glycol solution is used as coolant which has a freezing point of -34°C and boiling point of 120°C .

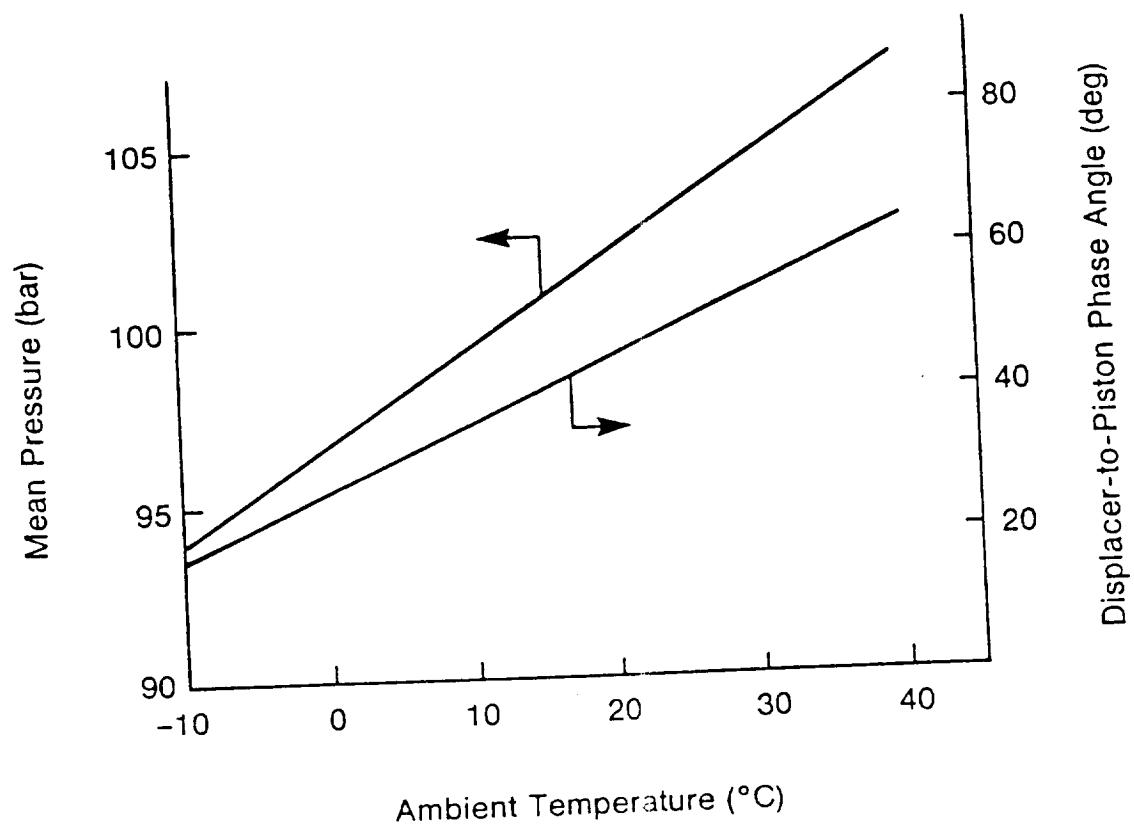
A free piston Stirling engine is sensitive to the variation in ambient temperature due to the effect of compression space and cooler temperatures on engine mean pressure. A change in mean pressure affects the natural frequency of the displacer and the power piston which causes a change in engine dynamics. As ambient temperature increases from the nominal design level, the engine mean pressure increases resulting in a higher displacer-to-piston phase angle, causing higher volumetric displacement. As ambient temperature decreases from the nominal level, the engine mean pressure decreases resulting in a lower displacer-to-piston phase angle, causing lower volumetric displacement. Therefore as ambient temperature decreases the capability of the engine to absorb solar insolation decreases. The sensitivity of the engine to variation in ambient temperature can be reduced by providing controls which ensure proper engine dynamic operation over the whole ambient temperature range. The possible control schemes are:

- Engine mean pressure control
- Displacer or piston gas spring control
- Cooler metal temperature control

Based upon cost and reliability considerations cooler metal temperature control was selected and is discussed next.

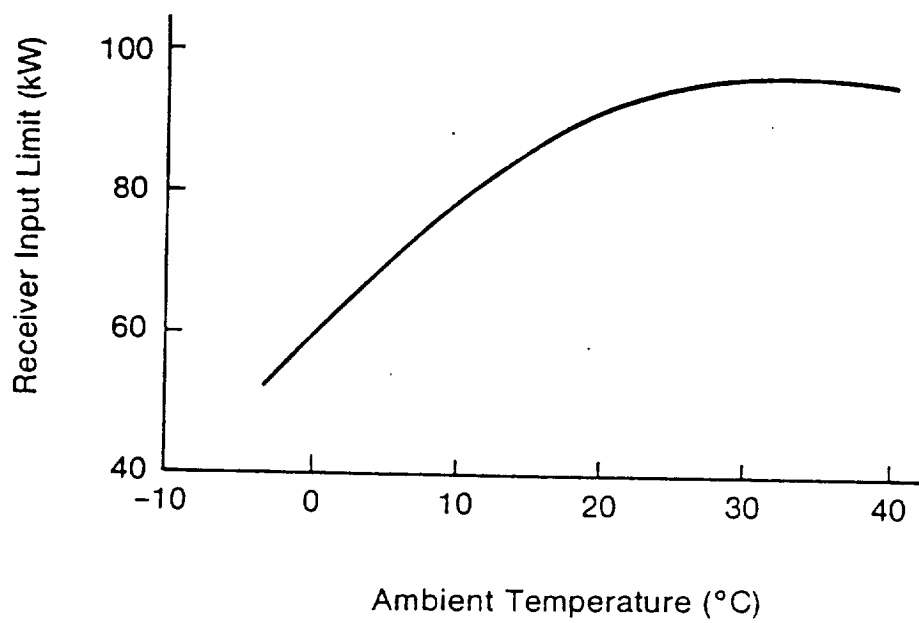
The ASCS nominal design point ambient temperature is 30°C . At 30°C ambient temperature the engine average cooler wall temperature is about 60°C . The heater wall average temperature is 700°C for all conditions.

Figure 7.11 shows a plot of engine mean pressure at various ambient temperatures. Figure 7.12 shows a plot of the maximum solar energy that the ASCS (with out cooler wall temperature control) can absorb at various ambient temperatures. At ambient temperature levels of 20°C and above the ASCS can absorb the maximum



(a)

Mean Pressure vs Ambient Temperature
Figure 7.11



(b)

Receiver Input Limit vs Ambient Temperature

Figure 7.12

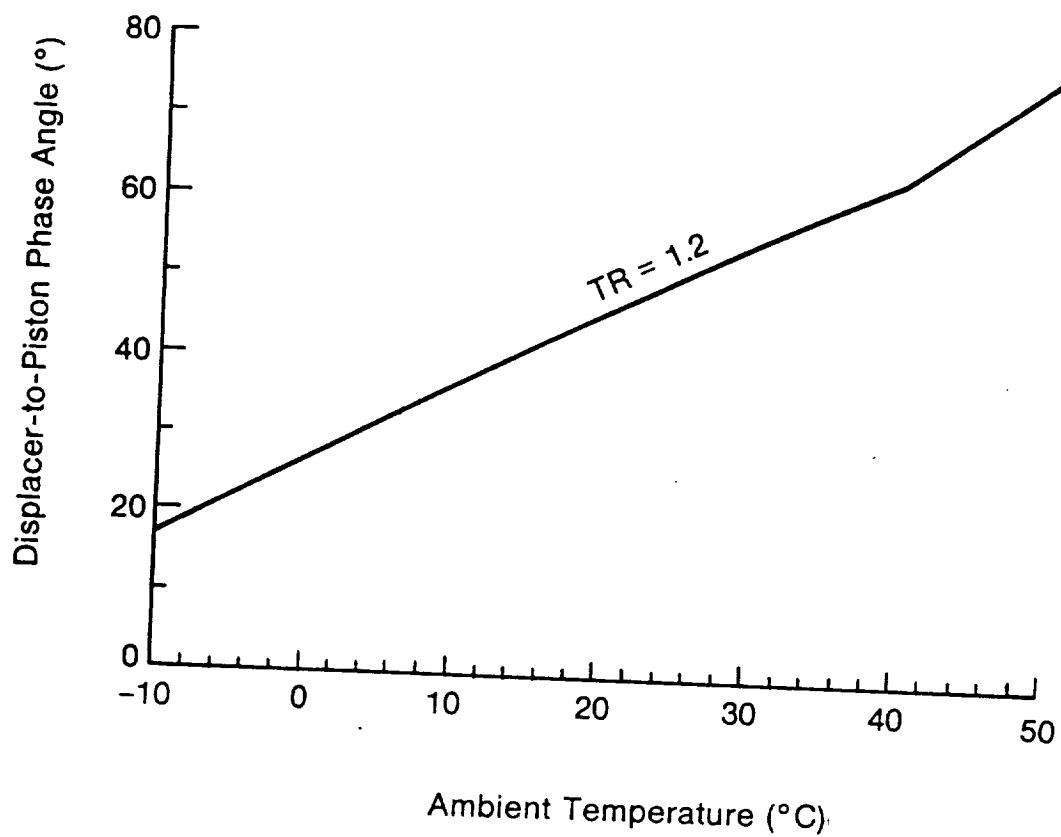
required solar insolation. Below 20°C the capability of the engine to absorb solar insolation decreases with decreasing ambient temperature. This is mainly due to decrease in displacer-to-piston phase angle as shown in Figure 7.13. The decrease in displacer phase angle is due to the reduction in the engine mean pressure which is caused by the lowering of the cooler wall temperature at lower ambient temperatures. Therefore a simple means of maintaining the desired heater heat flux rate at all ambient temperatures is by not allowing the cooler wall temperature to drop below 50°C (cooler wall temperature corresponding to 20°C ambient temperature) as shown in Figure 7.14. For low ambient temperature conditions, the cooler wall temperature will be held at about 50°C by on-off control of the radiator fan. This scheme is shown in Figure 7.15. The cooler wall temperature is compared to the desired minimum wall temperature, and if the resulting error signal is negative the radiator fan is turned off and if the error is positive the radiator fan is turned on.

7.3.3 Sensitivity to the Grid Frequency Variation

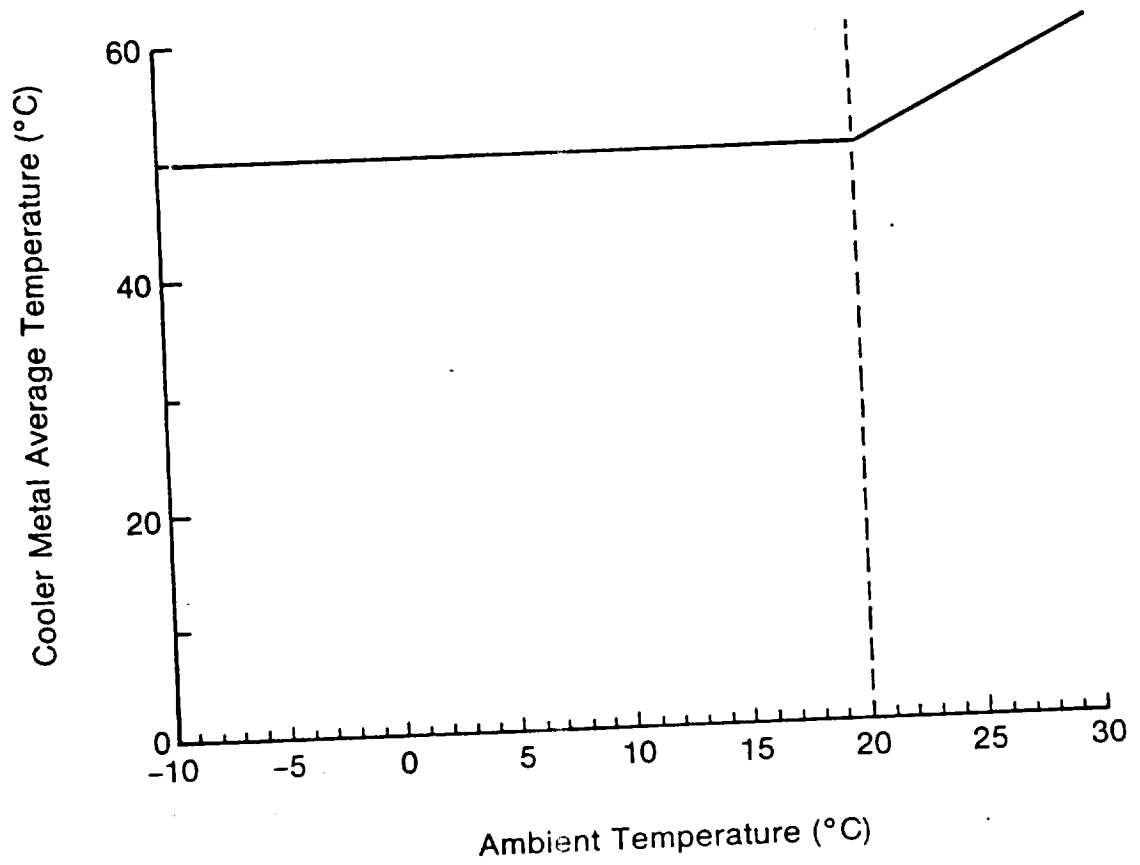
The ASCS is required to operate over a frequency range of 59.4 hz to 60.6 hz. As mentioned earlier the ASCS is provided with a vibration absorber tuned to 60 hz frequency. Therefore at 60 hz the casing vibration and vibratory force transmission to the concentrator dish is negligibly small. If the operating frequency drifts from the vibration absorber natural frequency, the casing vibration amplitude will increase.

Figures 7.16 a thru f show the sensitivity of the following parameters to variation in operating frequency (these plots are predicted for the autotransformer turns ratio set at 1.0).

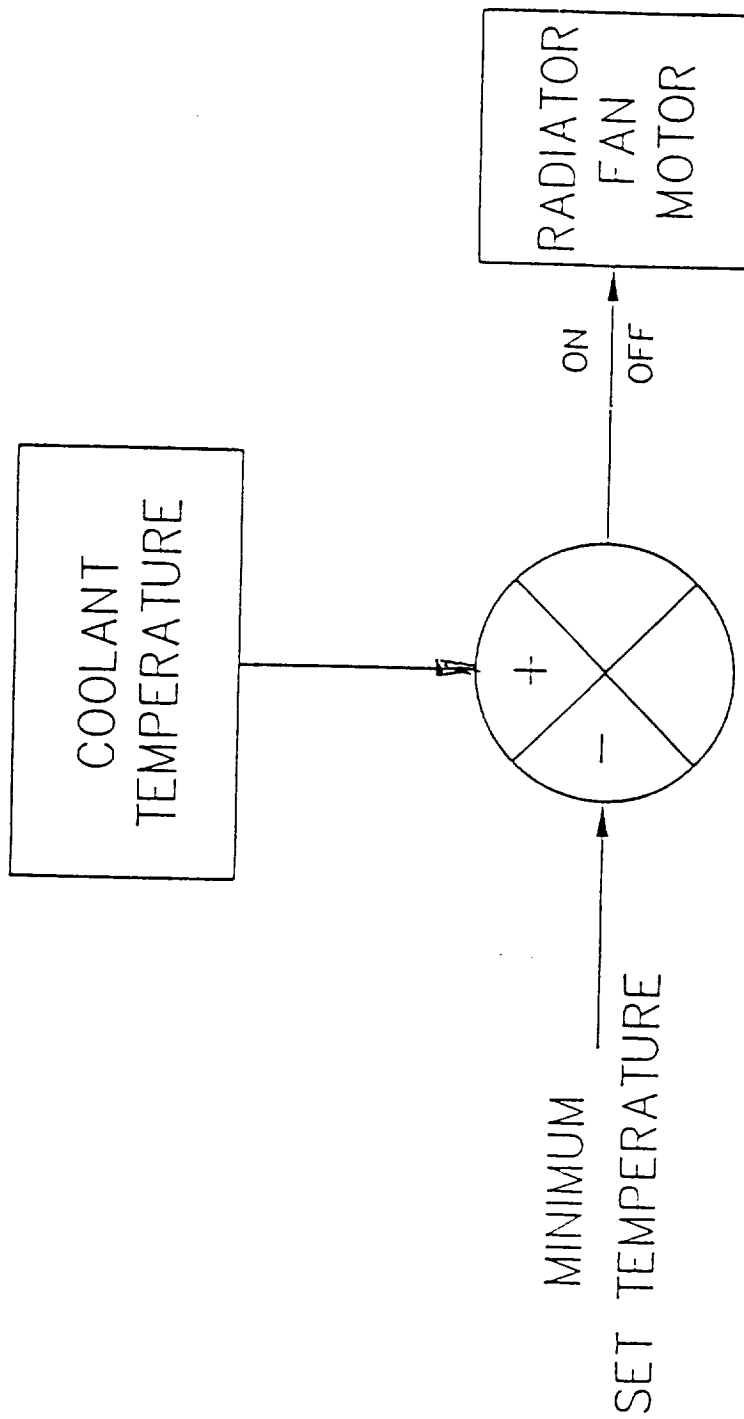
- Casing motion amplitude,
- Vibratory force transmission to the structure holding concentrator dish,
- "g" loading on the receiver and heat transport subsystem due to casing motion,
- solar insolation absorbed by the receiver (thermal energy absorbed by the engine plus receiver losses),



Displacer-to-Piston Phase Angle vs Ambient Temperature
Figure 7.13

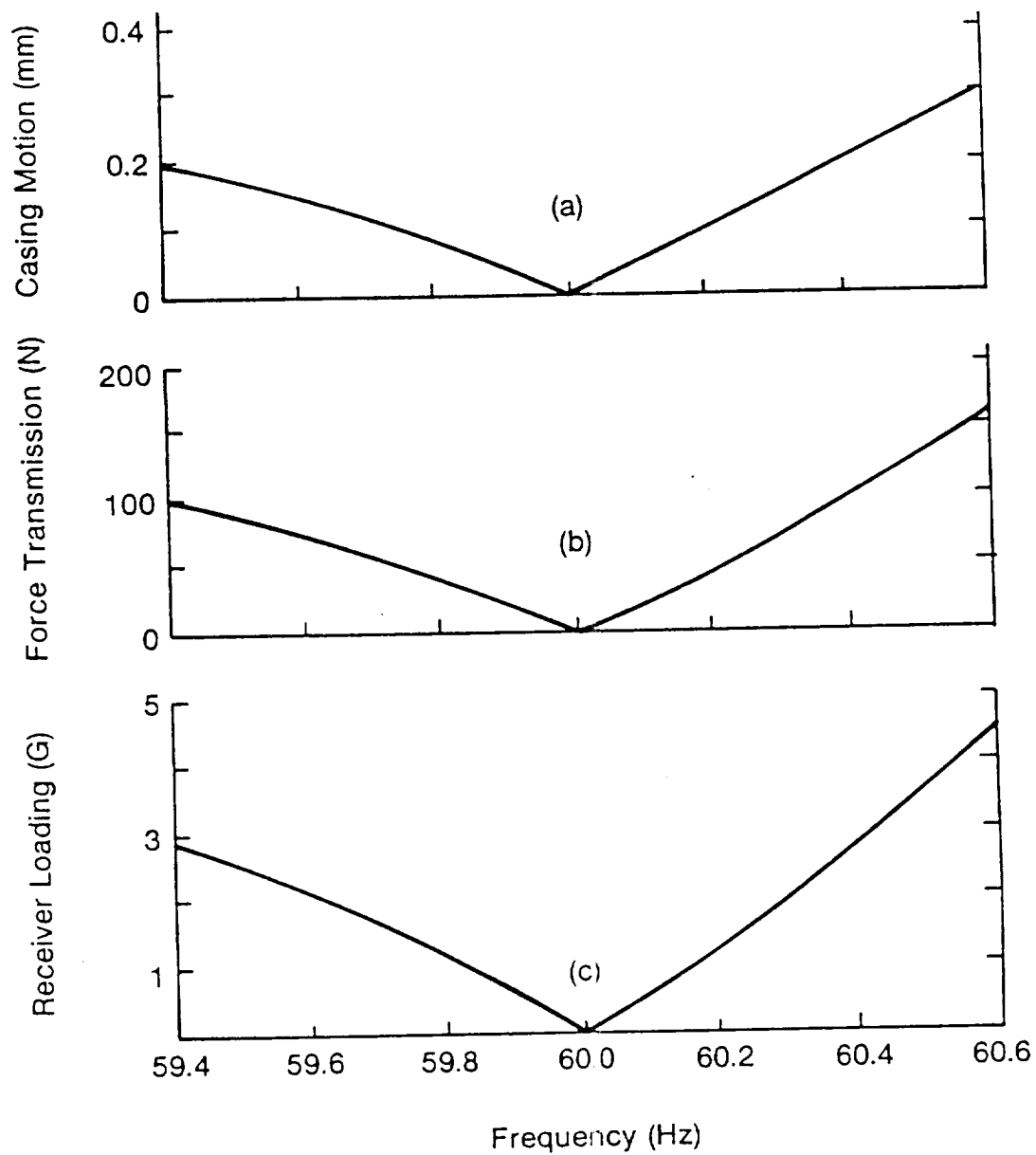


Cooler Metal Average Temperature vs Ambient Temperature
Figure 7.14



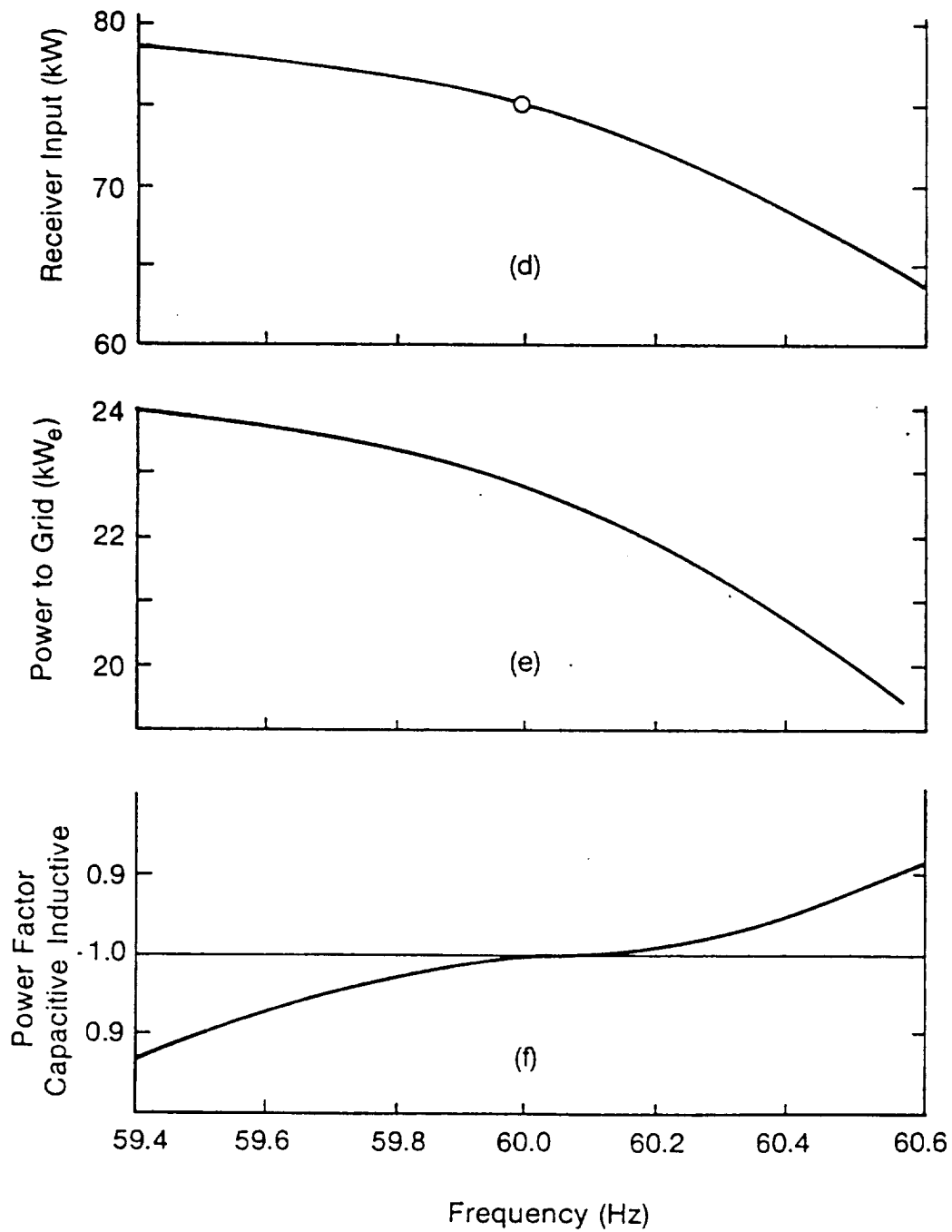
COOLANT MINIMUM TEMPERATURE CONTROL

Figure 7.15



Sensitivity To Grid Frequency Variation

Figure 7.16 a,b,c



Sensitivity To Grid Frequency Variation

Figure 7.16 d,e,f

- power delivered to the utility grid, and
- power factor.

The following is concluded from the above plots:

- The maximum vibratory force transmitted to the concentrator dish structure is well below the maximum acceptable value of 667 newtons.
- The maximum loading on the receiver is about 5 g's which has been assessed to be within acceptable levels.
- At 60.6 hz operating frequency the maximum thermal energy that the receiver can absorb is 63 kW at a turns ratio setting of 1.0. At a turns ratio of 1.2 , 90 kW of thermal energy can be absorbed.
- The power factor is well above 0.85 over the whole operating frequency range.

7.3.4 Harmonic Distortion

Free piston Stirling engine generator systems inherently have very low harmonic distortion in the alternator line voltage and current. Low harmonic distortion is due to low engine pressure amplitude, high power piston inertia and linear characteristics of the permanent magnet linear alternator.

For the ASCS system, because it is 'slaved' to the utility grid, voltage at the ASCS electrical terminals is the same as the grid.

Table 7.2 lists the measured voltage and current harmonics at the SPDE alternator terminals. The total harmonic distortion in the alternator line current is 1.52%.

The current harmonic distortion in the ASCS is expected to be even less than the SPDE measured value because the SPDE alternator was connected to a resistive

Table 7.2

TOTAL HARMONIC DISTORTION - SPDE

Harmonic #	Voltage		Current	
	Amplitude	Phase	Amplitude	Phase
1	711.71	27.95	55.40	96.34
2	1.62	95.51	0.20	-52.10
3	9.25	110.74	0.77	123.20
4	0.54	-24.42	0.10	142.87
5	1.84	-136.14	0.26	176.35
<hr/>				
Total Harmonic Distortion	1.35%		1.52%	

load through a rectifier circuit which introduces higher harmonics than an auto-transformer grid connection.

7.4 Start-up and Shutdown Procedures

In this section an overview of the system operation for a typical day is presented. System start-up and normal shutdown procedures are outlined, and system response to a cloud passage is described.

7.4.1 Start-up

Grid connected engines are inherently easy to start since the grid itself provides the required start-up excitation. The ASCS is particularly easy to start because of the following capabilities provided to the system:

- In the engine shutdown mode, the displacer piston and power piston are passively centered at their mid-stroke position. The centering force for the power piston is provided by the alternator plunger magnets. The displacer centering force is provided by magnets attached to displacer gas spring pistons.
- Bearing spin motor is continuously run, even in the shutdown mode, to minimize start-up and shutdown surface contact wear.
- The autotransformer, placed between the alternator and the grid, changes the alternator terminal voltage amplitude in a continuous and smooth manner from zero to full load voltage, thus limiting the start-up transients to very low levels.

Normally the system is started after an overnight shutdown. Before the start-up, the receiver is off the solar disk, the heat input and heat reject subsystems are in shutdown mode, the ASCS system is disconnected from the grid, and the autotransformer turns ratio is set at zero. Depending on the receiver temperature, the heat transport medium, sodium, may be in liquid or solid phase.

If sodium in the receiver reservoir is in the solid phase (identified by the reservoir temperature), it is melted with electrical heater elements (see Appendix I for a discussion of the details).

The ASCS system is next connected to the grid and the coolant pump is turned on. A signal to the autotransformer motor moves the brush from zero turns ratio to 0.5 turns ratio (start-up turns ratio). This process takes about a few seconds. In this mode, the piston stroke is about 10 mm, and depending upon the ambient temperature, the displacer stroke is about 4 to 6 mm, the displacer-to-piston phase angle is between -10°C to $+10^{\circ}\text{C}$, and a maximum of about 2 kW electrical power is supplied from the grid to the alternator. Because of the low displacer-to-piston phase angle, the engine operates in a gas spring mode. Out of 2 kW electrical power supplied, 1.5 kW is rejected by the cooler to the cooling subsystem and 0.5 kW is rejected by the heater to the heat transport subsystem.

The solar insolation is next focused on to the receiver. The heater head temperature starts to rise. When the heater head temperature reaches about 200°C (heater head temperature at which the ASCS system self sustains), the control subsystem (heater temperature control and radiator fan motor on-off control) is activated. With engine on the grid, normal control operation will control the engine in response to the low heater head temperature, and the heater head temperature will continue to rise until it reaches the steady state reference design set value (700°C). The radiator fan will start automatically when the cooler wall temperature rises above the set level of 50°C . This completes the start-up process (from shutdown mode to steady state operation). As is evident the start-up procedure is simple and will be automatically controlled with a single push button start.

7.4.2 Shutdown

The normal shutdown process is initiated automatically by the autotransformer. At solar insolation of about 13 kW to the receiver the autotransformer turns ratio is about 0.2 and the ASCS system is barely self sustaining. The minimum turns ratio during engine operation is set at 0.2, and therefore as solar insolation to the receiver drops below 13 kW, the heater head temperature begins to drop. When the head temperature reaches 200 C, the control subsystem prompts

the field operator for a command to commence shutdown process (this is to avoid complete system shutdown triggered by passing clouds).

If the operator response is negative (standby command, cloud cover expected for only short period of time), the ASCS system continues to operate at about 20% of power piston stroke, and heater temperature continues to drop till it reaches a steady state value (slightly above ambient temperature). In this mode of operation electrical power (few hundred watts) is supplied from the grid to the alternator. After the clouds pass, the solar insolation to receiver increases, heater head temperature starts to rise. The heater temperature control scheme modulates the piston stroke to match the solar insolation to the receiver.

If the operator response is positive (shut down command), the control system automatically switches the transformer primary winding from the grid to an auxilliary resistive load. The heat reject system continues to operate until the engine temperature falls below a selected level to avoid cold side hot soak.

The above shutdown process is the normal response to low solar insolation. Shutdown can be initiated intentionally (emergency shutdown) by pointing the collector off the solar disk and then following the low solar insolation shutdown procedure.

7.5 Fault Protection

To automatically respond to abnormal operating conditions, the ASCS system has been provided with the following fault sensors which are continuously monitored by the system controller.

1. Heater and receiver temperatures
2. Cooler wall temperature
3. Casing acceleration
4. Autotransformer primary and secondary voltage and current

As a part of the fault protection system the ASCS power module is provided with electrical and pneumatic power module "kill" mechanisms which are activated by the system controller.

The electrical "kill" mechanism is an auxiliary load resistance as shown in Figure 7.3. Switching of the autotransformer primary winding from the grid to the auxiliary resistance will stop the engine even if it is operating at the maximum power level.

The pneumatic "kill" mechanism is a solenoid operated valve, which when open, connects the compression space to mean pressure volume thus providing enough damping on the displacer and power piston to almost instantaneously stop the engine.

7.5.1 Fault Responses

High heater temperature is an indication of power module malfunction. Loss of the engine working fluid and/or mechanical seizure of displacer or power piston will result in high heater temperature. The controller will respond by commencing the emergency shutdown procedure.

High receiver temperature can also result from failure of concentrator tracking system. In the event of loss of track, the solar disk will gradually move off the aperture and across the face of the receiver, resulting in high receiver face plate temperature. The controller will first respond by starting the receiver coolant flow (receiver face plate cooling has been included in the conceptual design) and then will commence the normal shutdown procedure.

High cooler wall temperature can result from malfunction in the cooling subsystem (coolant leakage, breakdown of radiator fan or coolant pump motor). The controller will initiate the shutdown procedure.

Abnormal casing acceleration can result from malfunction of the vibration absorber or overstroking of the displacer or power piston. The controller will activate the engine damping valve and initiate the shutdown procedure.

In case of an alternator coil open circuit, the alternator line current will drop to zero, which will signal the controller to activate the engine damping valve and start the emergency shutdown procedure.

If the autotransformer turns ratio is above 0.2 and the heater head temperature is in the normal operating range, flow of power from the grid to the alternator will signal a power module malfunction (alternator short circuit, mechanical seizure of the displacer or power piston, or leakage of engine working fluid). The controller will start the emergency shutdown procedure.

Zero rms current flow at the primary winding of the autotransformer can result from open circuit in the utility grid. The controller will connect the power module to the auxiliary load resistance and then will start the emergency shutdown procedure.

8.0 DEVELOPMENT STATUS AND NEEDS

8.1 Introduction

A program leading to the commercialization of a 25 kW free-piston Stirling engine would proceed through various stages.

These stages will logically:

1. Demonstrate on test engines that the potential of the concept can be attained in practice
2. Demonstrate on preproduction engine systems that the production model will meet all system requirements

Step 1 may involve more than one iteration to reach an optimum system, but it is clear that successful operation of the first test engine and demonstration that the concept selected has the potential to meet the primary system requirements is key to the future success of free-piston Stirling engines in solar applications.

The major differences between the first test engine and later preproduction and production engines are:

1. All components in the engine would be removable for inspection and replacement or modification if required. This implies bolted joints in the vessel and O-ring seals on some components which would be eliminated in a hermetically sealed production model.
2. Internal diagnostic instrumentation such as pressure transducers, stroke measuring transducers and thermocouples will be required on the first test engine. For a production engine all internal instrumentation would be eliminated.

The most important considerations at this stage are development issues that impact the first test engine. These can be broken down into:

1. Features which are not yet fully demonstrated which are essential to system operation
2. Inaccuracies in performance prediction.

Undemonstrated features essential to system operation have been intentionally kept to a minimum. They are currently:

1. The sintered wick in the heat transport system
2. Hydrodynamic bearings in the engine displacer and power piston

8.2 Receiver/Heat Transport System

The receiver/heat transport system concept and arrangement was selected because its simple axisymmetric configuration leads to a compact design which is expected to be cost effective in production quantities.

Reducing the design to practice is not expected to incur unusual difficulties, but no existing sodium heat transport systems use a wick construction of the configuration proposed.

For the first test engine two options are available:

1. Demonstrate the proposed configuration in a component test(s) prior to incorporating it into a complete system. (This could be scheduled to occur while the rest of the system was being designed, built and checked out.) or

2. Use a pool boiler for the first test engine. This may have a somewhat lower development risk since it does not involve the sintered wick on a large curved sheet surface.

Final decision should be based on cost comparisons which have not yet been completed by Pioneer Engineering, and also the availability of funds for development activities on the first engine.

Hydrodynamic Bearings

Hydrodynamic bearings will not be an excessive development risk on the first test engine since the development currently in process on the space engine is expected to provide a basis for assessing this during the next few months.

If, at the time design decisions have to be made, the development risk is judged to be unacceptable for the first test engine, it would be quite practical to incorporate both hydrodynamic and externally pumped hydrostatic bearings. The advantages of hydrodynamic bearings over hydrostatic bearings on a production engine make them the clear choice in the long run, i.e. simpler hence more economical and lower power loss.

Hydrostatic bearings require that the engine working gas be drawn from a source in the engine, pumped to about 10 Bar above mean pressure, delivered to the bearings and returned to the source. This can be done with an external pump which requires power to drive it. Techniques for pumping off internal gas springs are possible but difficult to incorporate in an engine which varies stroke to modulate power.

While validated analytical tools are not available for predicting the performance of high pressure hydrodynamic gas bearings in which rotation and reciprocation are combined, MTI experts believe stable operation can be attained. Surface grooving can be incorporated to increase bearing stability. Tests are planned to determine if such treatment is necessary on the SPRE power piston during this fiscal year.

A.D.L. has demonstrated hydrodynamic bearings with both rotation and reciprocation at low pressure and Sunpower has demonstrated limited operation on a Stirling engine displacer.

As this report goes to press (February 1988) successful operation of the SPRE power piston in a motoring mode has been demonstrated. Basic feasibility is thus demonstrated. Details with regard to surface grooving will have to be established for the solar engine power piston and displacer.

8.4 Performance Predictability

8.4.1 Thermodynamics

Understanding the thermodynamic behavior of Stirling engines and developing accurate analytical predictive tools are an ongoing activity. For engines in which the characteristics are similar to engines which have been characterized experimentally, the uncertainties are relatively small. In a new design the uncertainty in prediction is a function of both modelling and thermodynamic calculation accuracy.

The solar engine is geometrically similar to the space engine in many respects, but there are subtle differences which must be modelled correctly. The code HFAST correlates quite well on several other engines, but there is still some uncertainty since it does not hit all test measurements exactly. At this point for an engine such as solar the predictive accuracy is expected to be within about 15%. To reach the upper end of the predicted performance range changes based on empirical measurements on the test engine will probably be needed.

8.4.2 Alternator Performance

There is no theoretical reason to believe that high alternator efficiencies cannot be attained. Success depends upon understanding the effects of many details which introduce loss mechanisms and, based upon this understanding, minimize the losses to the extent practical. MTI has expended significant effort over the last year to develop an understanding of the causes of loss in a permanent magnet linear alternator. This effort will be continued as part of the Space Engine Development Program. A laboratory is being set up which will

be dedicated to the development of linear electrical machinery. This will permit dynamometer evaluation of linear motors and alternators independent of the equipment in which they are used.

In addition to the above-mentioned experimental activities, MTI has acquired and is evaluating and applying advanced computer techniques to the design and analysis of linear electrical machines. The application of these techniques, coupled with experimental measurements of alternator hardware, followed by modifications as suggested by the evaluations is expected to produce an alternator with an efficiency in the 90 to 95% range.

8.5 Test Program Outline

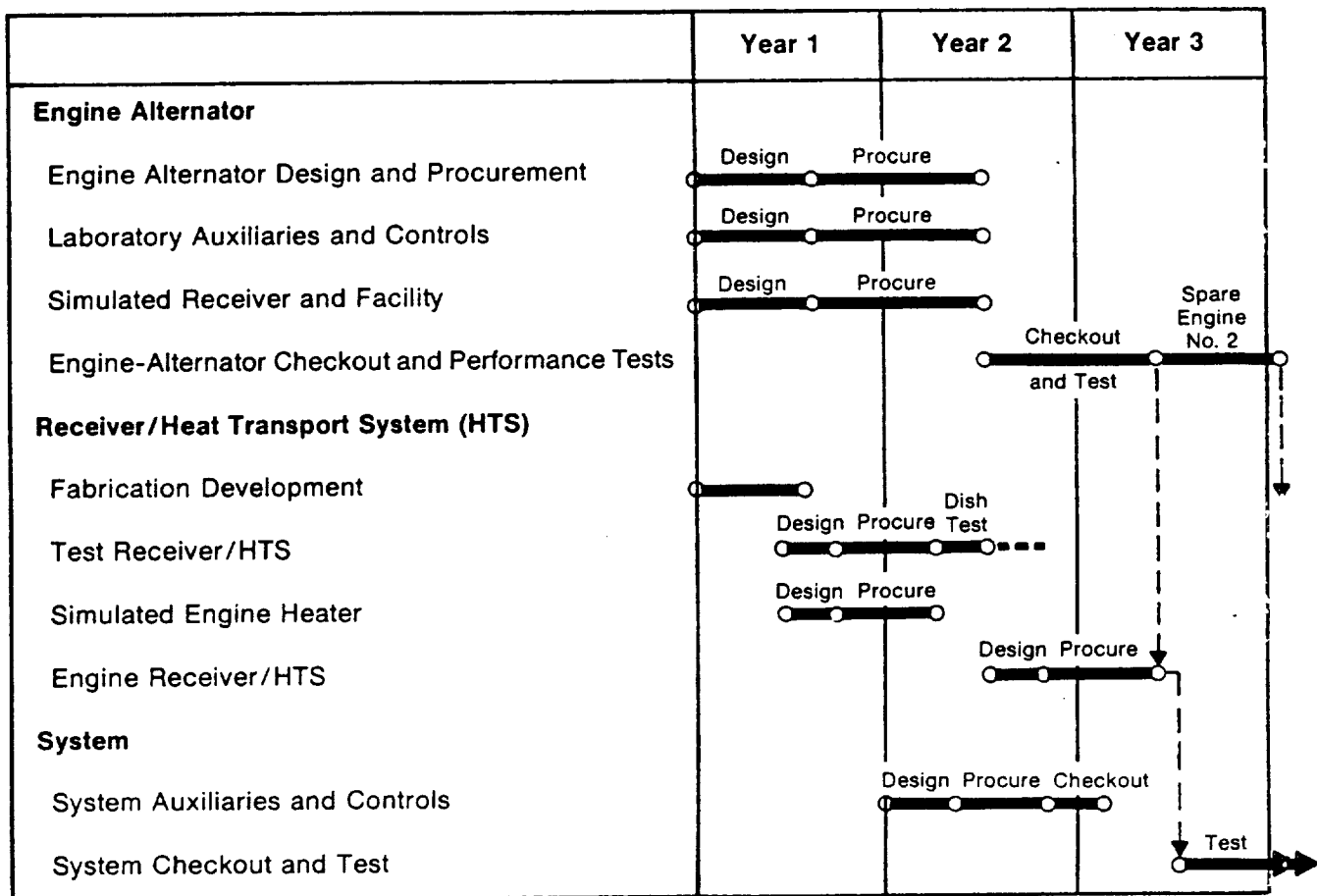
Figure 8.1 is a very preliminary outline of a test program culminating in the demonstration of one (ore more) solar dish-mounted Stirling engine power systems.

The outline suggests that the engine-alternator and the receiver-heat transport system be checked out independently before being married into a system and tested on a solar collector. The engine-alternator activity is laid out in the sequential phases of design, procurement, check out, laboratory performance characterization, and system tests on a solar dish.

The design and procurement phases could be accomplished in about 18 months in a well expedited program. The time required to check out and characterize a new engine is somewhat unpredictable. It depends upon the problems encountered in debugging brand new hardware. For planning purposes, about 12 months is recommended.

It is expected that laboratory equipment required to check out and characterize the engine would take less time to procure than engine hardware and would not dictate the schedule. The receiver and heat transport system should be built and checked out independent of the engine. The hardware is much simpler than for the engine. The roughly 30 months assigned to getting the engine ready for system installation should be ample time for receiver-heat transport system development. If funds permit, this time could be gainfully used developing the sintered wick concept. A tentative schedule is shown in Figure 8.1.

If a pool boiler approach is selected, the same general approach of checking out individual elements of the system is advisable. This maximizes the probability of success in a timely fashion for the integrated system.



Tentative Development Program Schedule

Figure 8.1

9.0 REFERENCES

1. Contract DEN3-372. Appendix A.
2. MTI G6-188 Volume I Technical Proposal "Conceptual Design Of Solar Electric Advanced Stirling Power System"

APPENDIX I

CONCEPTUAL DESIGN OF A SOLAR RECEIVER FOR A kWe
SOLAR ELECTRIC ADVANCED STIRLING POWER SYSTEM

FINAL REPORT

June 26, 1987

Prepared For:
Mechanical Technology Inc.

CONTENTS

	Page
1.0 INTRODUCTION	1
2.0 PROGRAM OUTLINE	1
3.0 STRESS ANALYSIS	3
4.0 RECEIVER LIFE ANALYSIS	17
5.0 THERMAL ANALYSIS	23
6.0 RECEIVER MECHANICAL LAYOUT	34
7.0 RECEIVER COLD STARTING REQUIREMENTS	40
8.0 CONCLUSIONS AND RECOMMENDATIONS	43

APPENDIXES:

A Hand Calculations for Heat Pipe Vessel Stresses	49
B Calculations to Determine Specular and Diffuse Solar Reflections from the Cavity	53
C Preliminary Absorber Surface Coating Recommendations	58

1.0 INTRODUCTION

This report contains the design of a solar receiver for a Stirling engine. The prior history of problems associated with the first generation of heater head/solar receiver designs has lead DOE to solicit a more reliable cost effective solution. At the request of the DOE, MTI, Sanders and Thermacore have considered employing a heat pipe scheme to this application.

A heat pipe solar receiver has several key advantages which were not inherent in the early designs. The early receiver Stirling designs involved directly irradiating a bundle of heater head tubes and were found to be unreliable. Failures were related to the unpredictability of high solar fluxes and the presence of non-uniform hot spots (gradients). The principle advantage of the new proposed cavity heat pipe solar receiver is its ability to isothermalize the heater head while the receiver is exposed to spacially variant solar flux.

In the concept of figure 1, solar energy is absorbing energy on a large cavity-type evaporator. Condensation of the liquid metal occurs on a conventional tubular heater head arrangement as vapor flows freely in the heat pipe cavity behind the absorber shell. The geometry of the heat pipe cavity is configured such that the condensed liquid drains by gravity back to the transport arteries at the base of the evaporator shell. This approach also has the distinct advantage of allowing independent optimization of heater head tube geometry and the solar cavity.

2.0 Program Outline

The first phase of this program involved establishing the size and flux limits of the cavity heat pipe concept. Because of the competing nature of design issues involving the wick and the absorber, a range of cavity sizes and shapes were selected for analysis. Solar flux levels 20 to 50 W/cm² were determined to be acceptable for gravity feed heights of 15 to 25 inches. The concept presented in this report is a 19 inch hemisphere with a peak flux level of approximately 40 W/cm².

The most critical receiver objective is to verify that system life goals can be reached. These goals were specified to be 80,000 hours with 20,000 cycles. Because of these stringent requirements, a large portion of our study involved performing a stress/life analysis on the absorber/evaporator shell. This work is described in section 3. Section 4 describes the selection of cost effective materials and receiver life projections. The receiver design point efficiency analysis was initiated after the preliminary stress analysis was completed. This work is presented in section 5. Next, the structural layout was prepared and is described in section 6. As a result of the PDR additional work was conducted to study the starting requirements of the heat pipe and propose a scheme to avert possible problems. A discussion of the remaining key issues of future recommendations form the last two sections 7 and 8 in this report.

3. Stress Analysis

The determination of solar flux profiles is the first step in performing the stress analysis. The ultimate solar flux distribution on a variety of axisymmetric conic section cavities was accomplished with a Monte Carlo ray tracing scheme. We believe this analytical technique is the most flexible means for quantitatively representing the concentrator's optical characteristics. This Fortran routine was also easily integrated with the thermal, stress, and wick design analyses. Although the model is rigorous in terms of its consideration of concentrator surface properties, it does not provide a prediction of actual anomalies which are common to cost-effective concentrators. However, it is important to consider the stress effects produced by the so called hot spots. High resolution data from concentrator testing shows not only spacially but time varying flux spikes. Moreover, these variations over the absorber surface intensity often occur even when relatively smooth data is obtained at the focal plane.

The adverse solar flux profile can introduce three types of uncertainties into the stress analysis. Primarily, the absolute flux maybe greater then the smooth theoretical prediction, leading to increased thermal (hoop) stresses in the shell. Secondly, the circumferential gradient may contribute additional components to the von mises stress field. Thirdly, the time varying nature of the flux can produce thermal fatigue cycles.

Because of these potential unknowns we devised a plan to consider the independent and combined effects of these possible flux variations. Therefore, some alterations were made to the nominal flux values predicted by the ray tracing routine to achieve the desired analysis conditions. Based on Sanders prior experience base of working with low cost concentrator systems a hypothetical worst case set of conditions was derived. These conditions are presented in general terms in table 1.

CONCENTRATOR ASSUMPTIONS

Power in 8" Aperture	75kW
Insolation	950 W/m ²
Specularity Standard Deviation	2.5 mrad
Surface Normal Standard Deviation	2.5 mrad
Reflectivity	0.9
Sun Disk Image Angle	4.6 mrad
F/D	0.6
Peak Power @ 1100w/m ²	86.8kW
Design Flux Safety Factor @ 1100w/cm ²	1.2
Worst Case Flux Gradient (downward)	3:1 per linear inch

Table 1-Assumptions used as inputs to the Monte Carlo ray tracing analysis to achieve the global power characteristics specified in the RFP. Also, included are Sanders projections for worst case flux gradients and suggested flux safety factor.

The first step in the stress analysis involved the consideration of one dimensional (1-D) thermal and pressure stresses. These simple relations given by equations 1 and 2 are obviously limited in their applicability to the problem.

$$\rho_p = -q3a^3/(2(a^3-b^3)) \quad \text{Eq. 1}$$

$$\rho_t = \pm E\alpha\Delta T/2(1-\nu) \quad \text{Eq. 2}$$

Where q is the pressure, a is the outer radius, b is the inner radius, ν is Poisson's ratio, and α is the coefficient of expansion.

One limitation in the thermal stress equation arises because the composite materials have dissimilar properties. The most notable are a change in the modulus of elasticity (E), and in the thermal conductivity (K). Also, these relations give no insight into the three dimensionality of the stress field which arises due to the transverse (circumferential) thermal gradients and the edge restraining conditions. By understanding these effects the potentially critical shear stresses which might cause separation at the powdered metal/absorber interface can be also predicted. Finally the effect of the more massive rib-like arteries spanning the relatively thin evaporator shell must be investigated. Therefore, in summary, the following list of stress issues were addressed in sequence.

- (1) Simple 1-D stresses at nominal flux value predictions.
- (2) 1-D computer modeled solution involving the spatially dependent E , α , K composite properties.
- (3) Axisymmetric (2-D) flux profile predictions with simple edge constraints using a finite element method model (FEM).
- (4) Axisymmetric flux profile with more realistic edge constraints using FEM.
- (5) 3-D flux profile on a symmetric 60° sector of the dome.
- (6) Axisymmetric flux profile incorporating a severe flux gradient (hot spot) and realistic edge constraints.
- (7) The addition of a circumferential artery passing through the peak flux zone in test case 6.

When designing the composite absorber/evaporator, it becomes evident that there are several competing effects which affect the selection of the absorber shell and wick thicknesses. For example, a thinner absorber wall reduces the thermal stress while increasing the magnitude of the pressure stresses. Theoretically, the minimum combined stress would occur at a thickness where these two stresses are nominally equal. In addition to this there are fabrication and handling concerns which limit the range of acceptable thicknesses. Also, of great significance is the issue of sodium induced wall corrosion which, over the exceptionally long life of thirty years could consume a substantial percentage of the base material. Oxidation on the environmental side of the absorber shell might produce a similar erosion of metal as well as pitting and stress concentration points.

The design of the wick also involves stress, performance and cost trades. The wick thickness and permeability controls the amount of liquid which can be transported over a given distance while consuming a given amount of capillary head. Hypothetically, a thicker wick is less likely to dry out due to high local evaporation rates than a thinner wick. However, the wick thickness is critical in that it directly relates to the amount of super heating of the sodium in the wick. Excessive super heat results in an undesirable transition into a nucleate boiling regime and the associated potential of the bubbles to impede the liquid transport through the wick. The proposed Thermacore technique of locating a geometric pattern of primed arteries on the absorber affects the required liquid transport distance and hence provides another controllable variable .

The selected wick design approach was to initially choose an acceptable wick thickness based on super heat criteria and manufacturing details and then determine the pattern and distance between the arteries for given cavity dimensions and corresponding flux levels. For the flux levels and the cavity dimension ranges previously stated it was determined to apply a constant wick thickness of 0.06 inches.

Figure 2 illustrates the 1-D thermal stress model. This model shows that maximum thermal hoop stress is likely to be compressive at the heated surface. Because of the lower modulus of the wick materials, the tension on the outer wick surface is proportionally lower in magnitude. Somewhere in between the two surfaces there exists a plane of zero hoop stress. This plane could occur on either side of the wick/wall interface. To obtain this 1-D stress profile it is necessary to simultaneously solve Fourier's 1-D conduction equation with the stress relation in equation 1. In this analysis (case 2) the moments on either side

ONE DIMENSIONAL STRESS CALCULATION FOR COMPOSITE WICK/ABSORBER

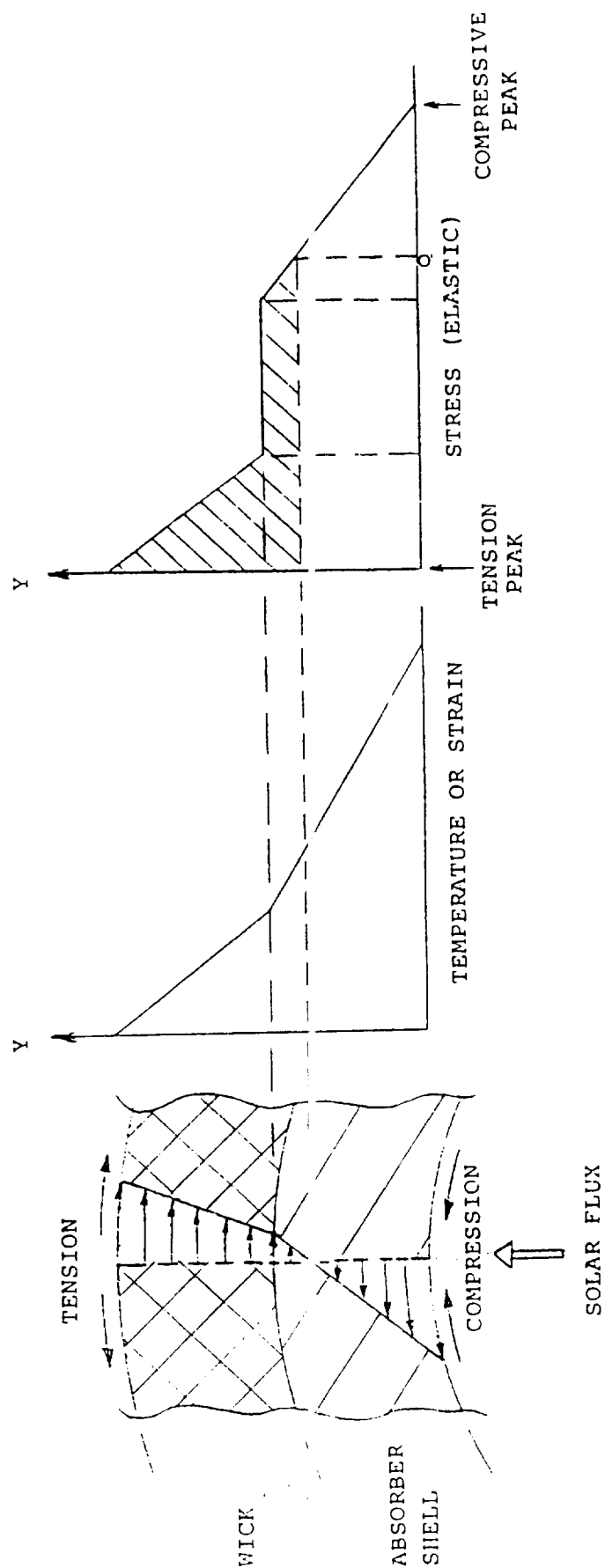


Figure 2. Model includes continuous variable properties in thickness dimension (coef. of expansion, thermal conductivity, modulus of elasticity)

of the zero stress interface must be equal and opposite. When applying this criteria a quadratic equation is obtained which predicts the position of the 0 stress axis (figure 2). From this point, the temperature drop to either edge, can be applied to the equation 1. The Fortran model which performs this calculation also takes into consideration the temperature dependency of material characteristics.

The pressure exerted by the less than atmospheric sodium vapor pressure (.47 ATM @ 800°C, .15 ATM @ 700°C) acts to put the entire shell in tension. Given the range of absorber thicknesses considered, and coupled with the .06 inch wick, this component of total stress is still several times lower than the thermal stress at the peak flux point.

Manufacturing and corrosion criteria suggest that the absorber thickness be not less than .02 inches. Figure 3 represents the results of the 1-D model showing the effect of absorber thickness on peak compressive and tensile stresses. In this case the incident flux profile developed for the 19 inch diameter hemisphere is presented.

The next step in the stress analysis was to compare the 1-D results with a more comprehensive finite element model (FEM). A 2-D axisymmetric model was created with PAFEC*¹ to consider the flux profile generated with the Monte Carlo analysis. The FEM performed both a thermal (conduction) and stress analysis of this data. First, the simplest pin type edge constraints were implemented. Having initially verifying the effect of various boundary conditions a more realistic edge support structure was modeled. The model configuration and exaggerated displacements of this configuration under thermal and pressure loads is shown in figure 4. The results for the 19 inch diameter test case showed that the lateral conductive leveling effect is very small. By far the dominant thermal transfer is purely through the wall thickness. The example temperature profiles are shown in figure 5. This analysis assumed that the wick/vapor interface is maintained at the wick surface by evaporation at a vapor temperature of 800°C. The data is generated at every degree of arc and is somewhat jagged due to the selected resolution of the Monte Carlo analysis. More ray tracing smooths this out but we felt that the jagged data is more realistic and would provide a better assessment of the conductive leveling effect.

The peak compressive stresses obtained from this analysis have been located on the 1-D parametric curve in figure 3. This illustrates the close agreement of the two models and the apparent one-dimensionality of the nominal operating conditions at the peak flux point.

2.D AXISYMMETRIC FINITE ELEMENT THERMAL STRESS ANALYSIS

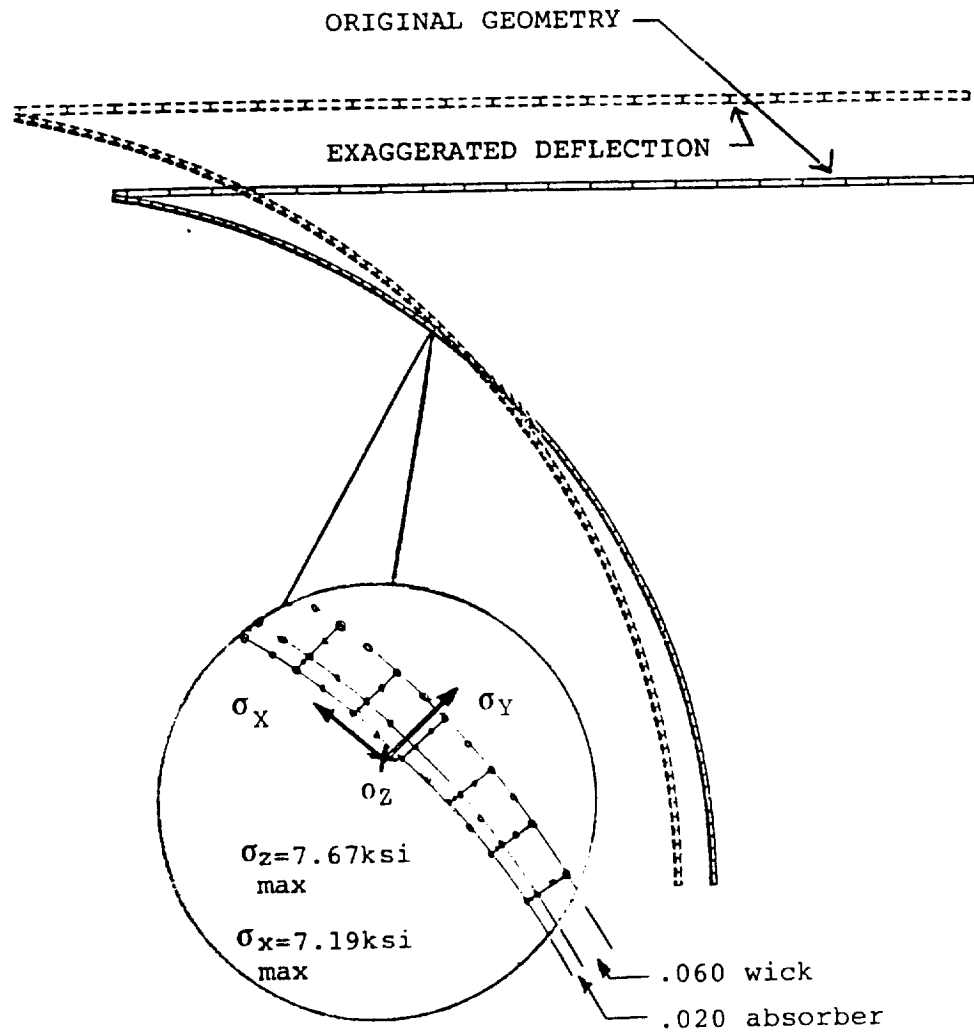


Figure 4. High Resolution Node Arrangement

Monte Carlo Generated Axisymmetric
Temperature Profile for 19 inch
Hemisphere

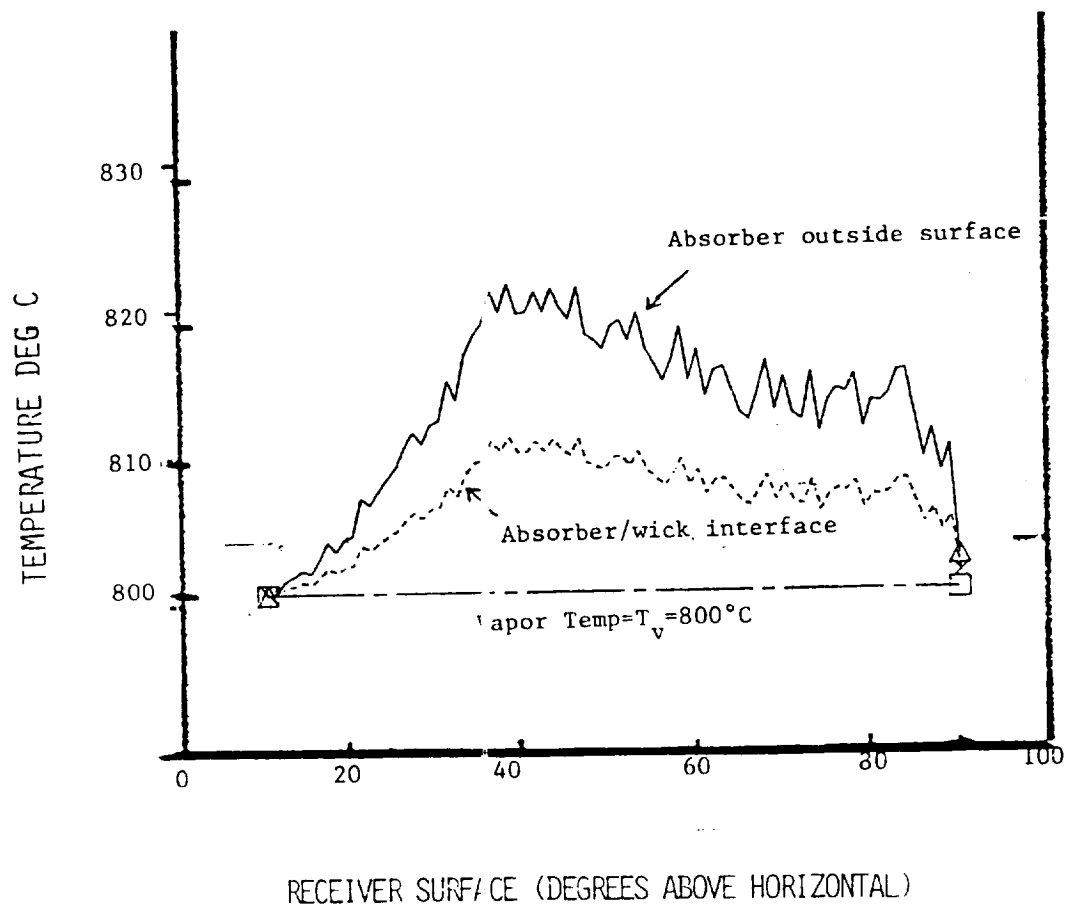


Figure 5.

In a somewhat parallel modeling effort a 3-D FEM model was designed to incorporate a severe temperature gradient in both the circumferential and azimuthal directions. The input conditions, contrived to fit the criteria of table 1, were chosen for a 60° sector and this pattern was repeated sinusoidally sixty times to form a dome. Figure 6 shows this element configuration. Preliminary results of this analysis again showed that the stresses are directly influenced by the absolute magnitude of the incident flux and were not substantially affected by the sharp gradient. However, an unexpected lack of resolution in the element mesh prohibited proper convergence of the routine at certain nodes. It was therefore determined not to be feasible to further refine this model to obtain an accurate estimate of the individual effects of the sharp thermal gradients. Rather, the gradient effects could be reassessed using the 2-D axisymmetric model. This model also required additional element refinement, but only in the region of the imposed gradient. This exercise therefore provided simpler and directly comparable case study of the gradient effects.

While revising the axisymmetrical model, we took the opportunity to incorporate the geometry of an arterial rib passing over the peak flux zone. Because of the symmetry in the model, it was necessary for this artery to also be circumferential. Although the actual artery layout is radial (figure 7), we do not expect this to significantly misrepresent the stress problem. It was previously determined that the edge effects due to the low fluxes near the rib produced relatively small stresses. Therefore we expect that the local effects of the artery in the peak flux zone are most important. This configuration will provide the ability to assess the possible stress concentration and additional thermal stresses induced by the rib-like artery. Figure 8 illustrates the FEM nodal layout which includes the artery.

As indicated in Table 2, the peak compressive stress on the absorber was not affected by the artery. However, tensile stresses in the sintered nickel wick rose by 32%. Also, the shear stresses at the composite interface increased by 60% for the .02 inch absorber test case. The significance of these magnitudes will be discussed later in this section.

3-Dim FEM Analysis of 6° Sector

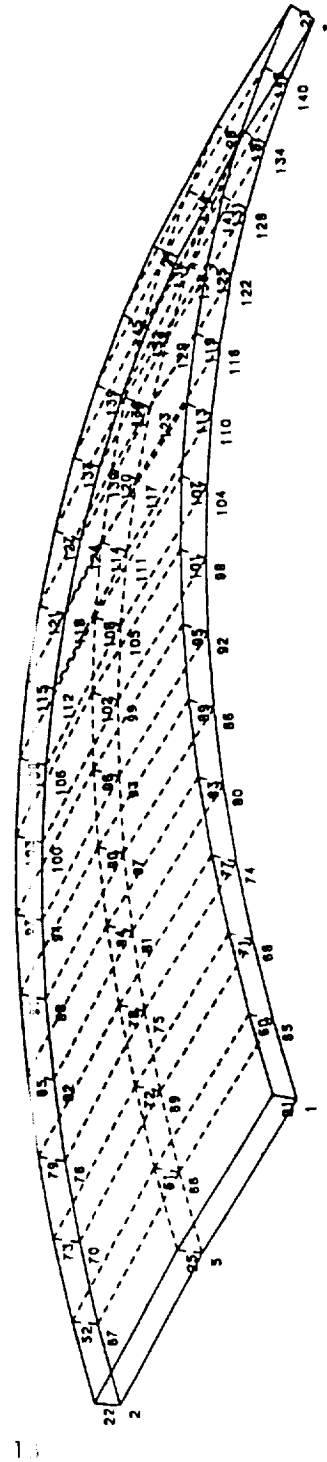


Figure 6. 3-D element grid used in PAFEC analysis to investigate flux distortions on the composite absorber/wick structure.

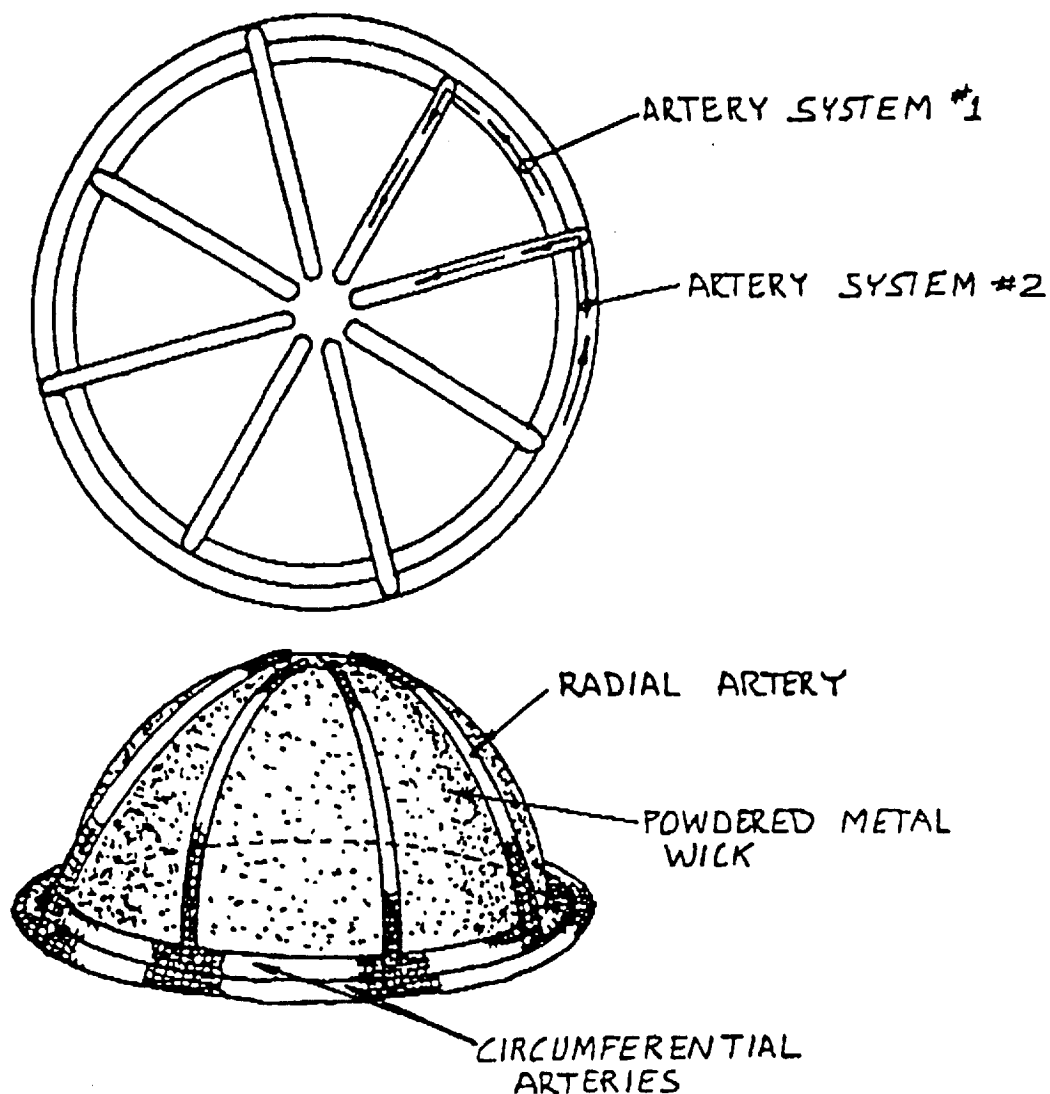


Figure 7. Thermacores Artery Layout. Redundant circumferential and radial criteria are provided. The artery has approximately 0.1 inch circular passage surrounded with an .06 inch wick.

FINITE ELEMENT STRESS ANALYSIS OF ABSORBER/EVAPORATOR

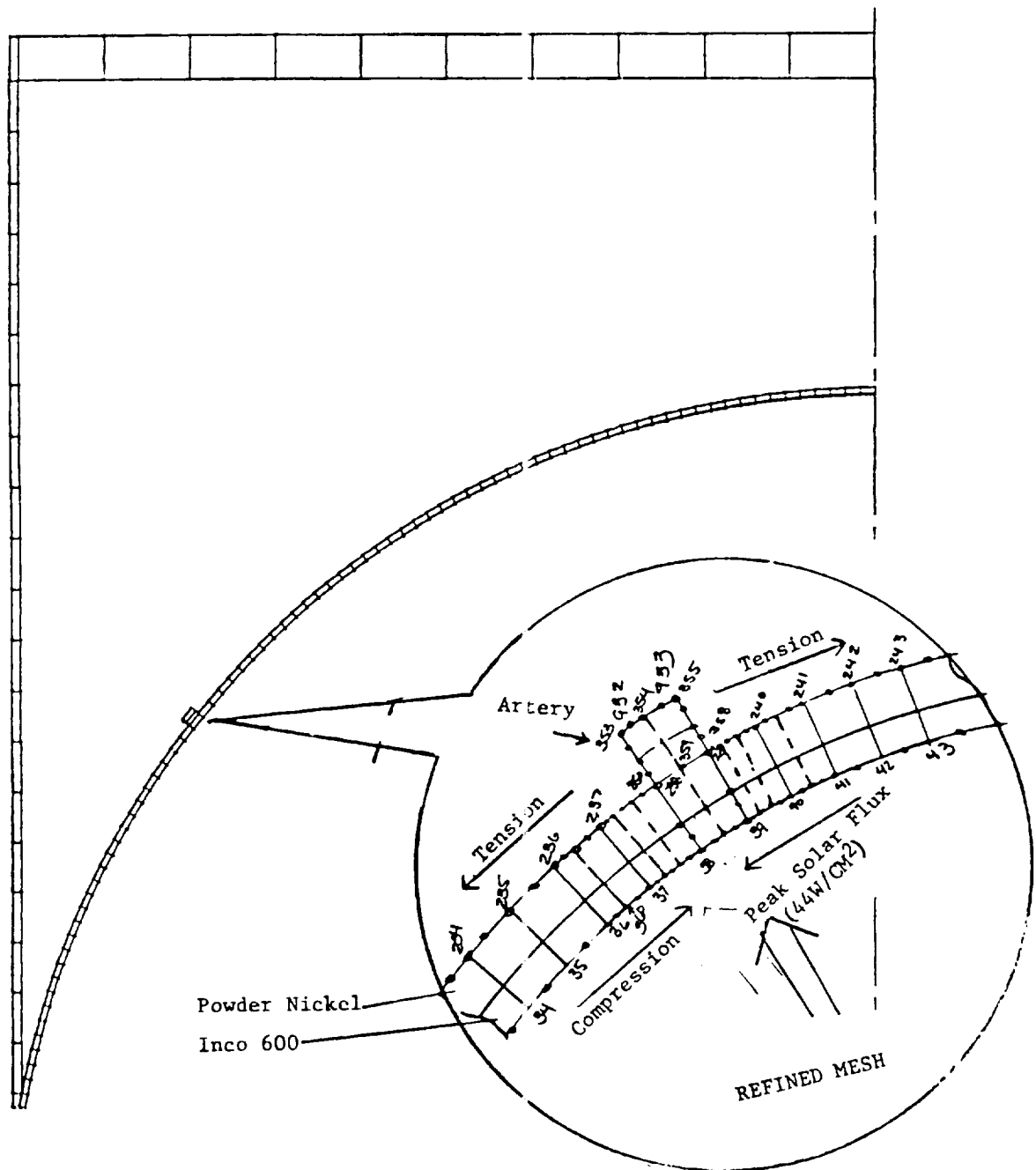


Figure 8. PAFEC nodal grid illustrating circumferential (axisymmetric) artery

Table 2. MAXIMUM STRESS SUMMARY FOR 0.02 INCH ABSORBER AND 0.06 INCH WICK.

Model Conditions	Location	σ_{\max} (ksi)	τ_{\max} (ksi)	τ'_{\max} (ksi)
No Artery No Gradient	Collector IN600	7.7	3.7	.33
	Sintered NI201	2.5	1.3	
With Artery No Gradient	Collector IN600	7.6	3.8	.527
	Sintered NI201	3.3	1.4	
With Artery With Gradient	Collector IN600	7.9	4.0	.72
	Sintered NI201	3.2	1.3	

Where:

σ_{\max} is the maximum principle stress

τ_{\max} is the maximum principal shear stress.

τ'_{\max} is the maximum shear stress between the IN600 layer and the sintered nickel layer.

* Note all of the stresses reported above were reported at around $\theta = 38^\circ$

GENERAL DESIGN OF PIER QUALITY

The effect of the sharp thermal gradient was analyzed next. This gradient varies from 1/3 of the predicted value up to the full predicted value in a distance of about 1 inch. This, from our experience, is as sharp a gradient as we should expect under real conditions. The input temperature profile assumed for this test is shown in figure 9. The results of this study showed only a small rise in the maximum stress value. The only other significant variation was an additional rise in the composite interfacial shear stress of about 40%. In all, the shear stresses at this critical point more than doubled between the original non-artery case and an adverse artery case, but the absolute magnitude is still rather low.

A preliminary analysis was conducted of the stresses in the heat pipe vessel at several locations not on the evaporator dome. Special attention was given to the zones around the interfaces between the conical shell and the evaporator on one end, and the engine on the other end. At the evaporator, the conical vessel must be wide enough to accept the hemispherical dome with the two circumferential arteries around its perimeter. To connect the dome to the heat pipe shell, both a lip in the dome or a separate annular ring were considered to provide the clearance for the arteries. These two alternatives were analyzed and the separate annular ring was selected. Appendix A presents the calculations used to evaluate the stresses in this zone. The fabrication details associated with this design are presented section 6.

At the engine end, the conical heat pipe shell tapers down to provide a slope for the liquid sodium to return to the wick when the receiver is in a near horizontal operating position. The minimum diameter of the heat pipe vessel at this point is set by the diameter of the heater tube arrangement.

As illustrated in figure 1 the conical vessel mates with a flange which is integral with the cylinder head. Calculations used to evaluate stresses in this vicinity are presented in Appendix A.

Section 4 Receiver Life Analysis

The allowable stresses for this system are primarily defined in terms of fatigue life criteria. The criteria for acceptable life is 20,000 thermal and pressure cycles. The phenomena associated with fatigue such as cracking and absorber/ sintered wick delamination of the composite have been found to be difficult to predict. These issues are not fully calculable and therefore part of this section will address recommendations for experimental component testing.

MODIFIED TEMPERATURE DISTRIBUTION ON RECEIVER FOR FINITE ELEMENT ANALYSIS

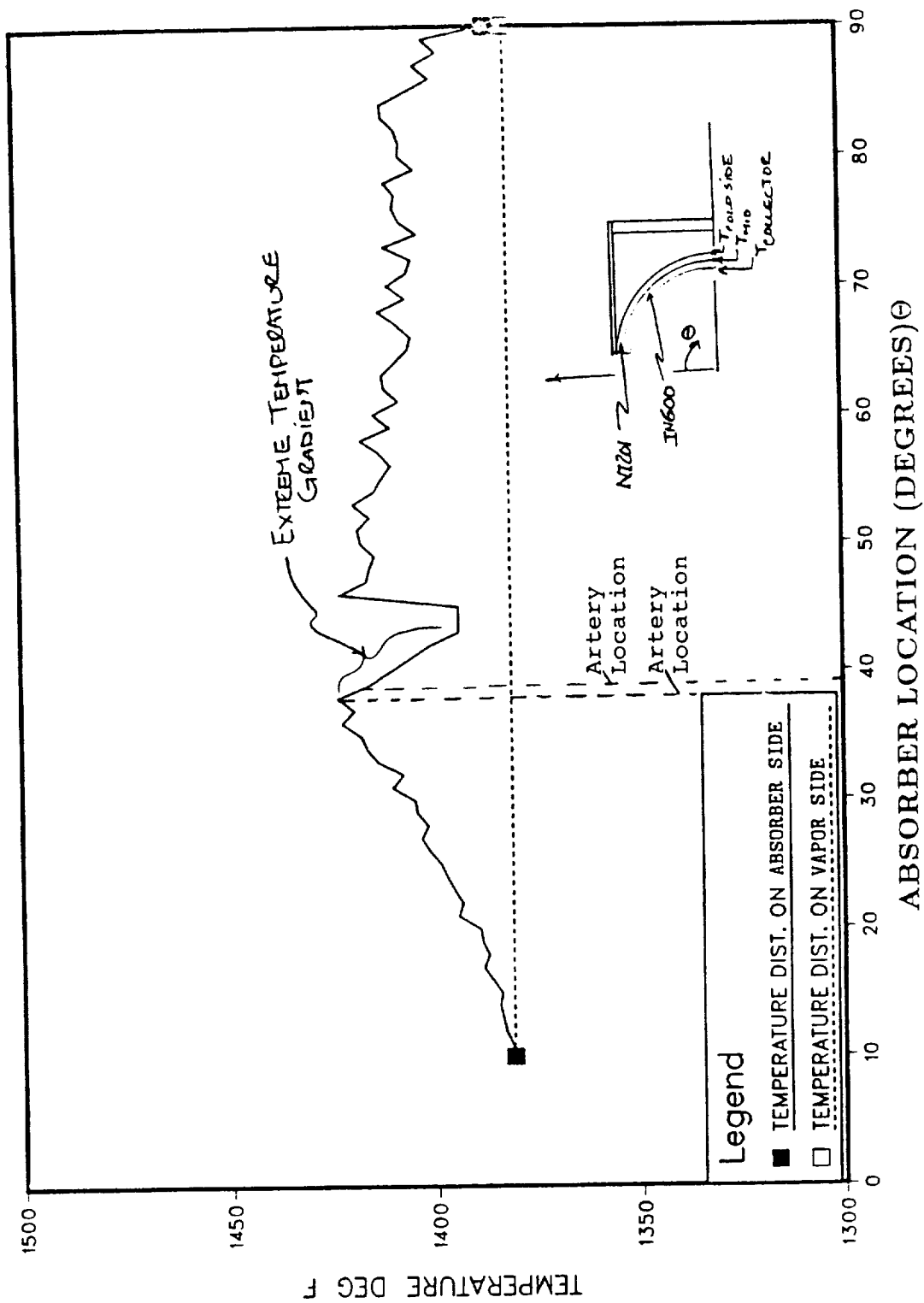


Figure 9.

**ORIGINAL PAGE IS
OF POOR QUALITY**

A modified Goodman diagram has been constructed for each material by employing the Method of Universal Slopes.*² This plot of alternating stress against mean stress incorporates a safety factor of 1.5 at 20,000 cycles. The alternating stress and mean stress about which the system oscillates during the operating and non-operating cycles are obtained from the steady state values. These values represent the peak operating stresses. When not operating, the entire shell experiences a 0.60Ksi tensile stress due to the pressure load. Under these nominal cycles the absorber cycles between a peak compressive stress of about 10.9 Ksi (0.04 inch thick absorber with 20% solar safety factor) and a peak tensile stress of 0.6Ksi. The wick, at the same time, operates between a peak tensile stress of 5.6ksi and a lesser non-operating tensile stress. These points have been located on the modified Goodman diagrams in figure 10. The strict interpretations of these values represents the stresses associated with the strain range for the first thermal cycle only. Both characteristic stress points located on the Goodman diagrams are well below the Universal Slopes threshold. Therefore this implies that additional safety factor (>1.5) exists.

The preceding approach assumes that no permanent plastic deformation takes place in either material. This of course is not actually the case. In fact, both wick and wall peak stress values are well above the creep rupture limits for the 60,000 hour life at 700°C.

These strict creep limitations do not apply in terms of the conventional time/temperature (Larsen/Miller) data. Since the dominant stresses are thermally induced, creep leads to a relaxation of the stresses. For typical day/night temperature cycles, the strain range remains nominally constant while the peak stresses reduce in magnitude due to permanent plastic deformation. Under conditions of extreme plastic deformation the operating stresses will have time to decrease to a level where creep becomes negligible. Since no appreciable creep takes place in the cold condition, the hot stresses will decrease with every cycle. Similarly the cold stress will continue to rise, limited by the magnitude of the original hot stress but with opposite sign. With such a progression, it is obvious that additional safety factor will develop for two reasons. First, as illustrated on the Goodman diagram, a representative stress point will move horizontally towards the Y-axis. Secondly, the ultimate stress, which is a strong function of temperature, will increase causing the X-Y intercept points of the Universal Slopes curve to rise. This leads us to the conclusion that the original assessment, excluding creep, yields a conservative result.

FATIGUE STRESS ALLOWABLES BY THE METHOD OF UNIVERSAL SLOPES

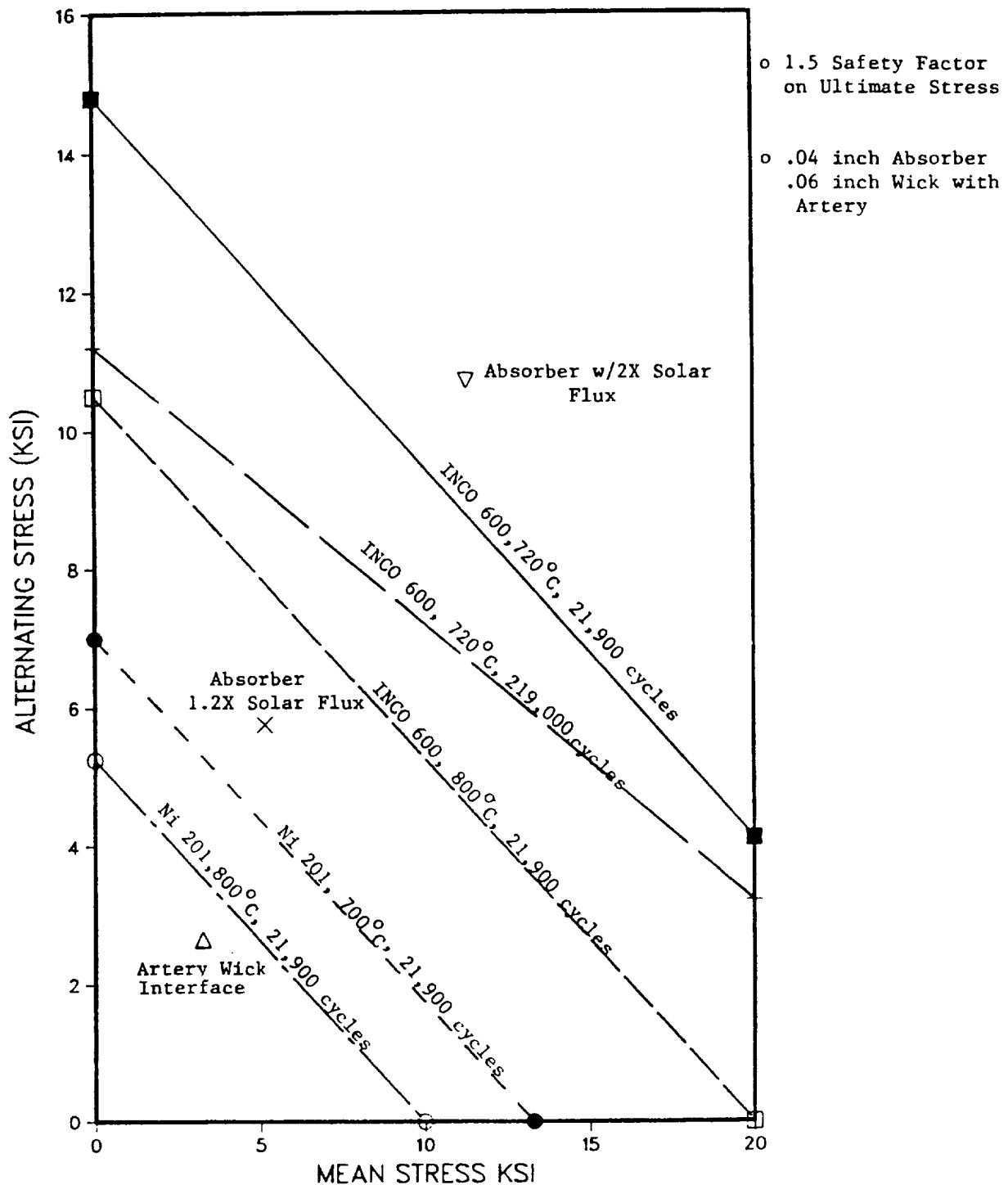
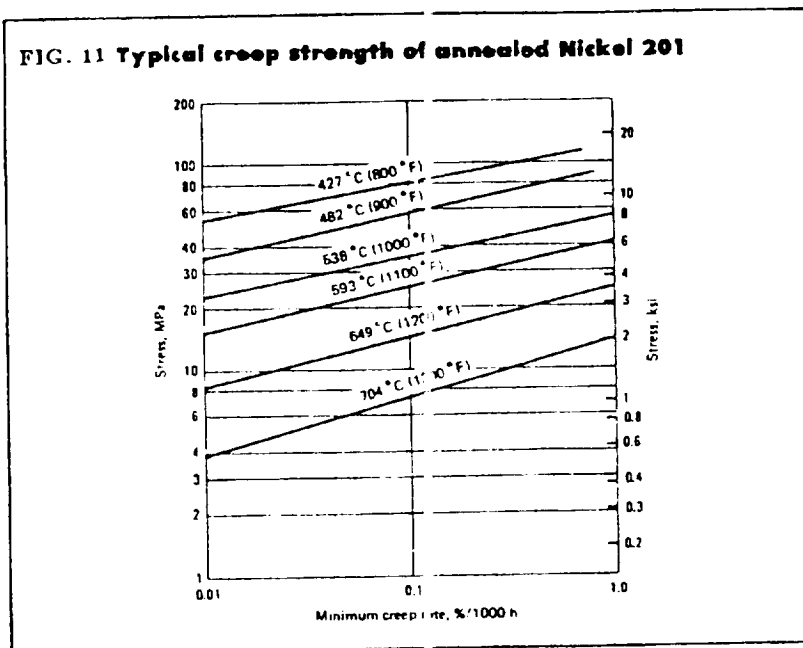


Figure 10. Modified Goodman diagram for wick (Ni201) and absorber (Inco600) material.

ORIGINAL PAGE IS
OF POOR QUALITY

The tensile stresses and shear stresses in the wick produce much greater creep rate than those in the absorber even though the stresses are lower in magnitude. Figure 11 illustrates the very weak characteristics of nickel 201 at the 700°C operating temperature. This data is for bar stock and may differ from the sintered powdered material. Unfortunately, no comparable data with a powdered metal was found. We therefore conducted the analysis using this handbook data. Sanders and Thermacore are presently trying to improve on our data base in this area.



The same trend as previously described for the absorber will take place in the wick. However, as evident from data in figure 11, the creep rate in the nickel will be much greater than in the absorber. This also implies that the period for complete relaxation of tensile stress, which maximizes cold compressive stress, is relatively short.

Before proceeding with this study the potential inapplicability of the method of Universal Slopes should be mentioned. This technique was developed for predicting the fatigue life of a broad, but metallurgical by similar, category of steels and superalloys. We feel that the application of this method to the absorber Inco 600 is acceptable. However, applicability to the powdered metal wick, due to its 50% porosity and very low strength at the operating temperature, is somewhat suspect. The modulus of elasticity, in particular, is less than half of the typical Universal Slopes candidates. Again experimental data for this material should be obtained.

Extrapolation of the nickel 201 handbook data creep rates at the design temperature leads us to the conclusion that the nickel will relax to a stress of less than 1ksi in only a few cycles. A linear extrapolation of the creep data on figure 11 implies that about 0.1% creep relaxation would occur in only 10 hours at the most highly loaded zone on the absorber. Since only about 0.04% elongation is required in the outer edge of the wick to completely eliminate the thermal stress, it is evident that the relaxation is quite rapid. Therefore the greatest tendency for crack generation in the wick would also exist in the first few cycles. For this reason, Thermacore's successful operating experience with this material under similar conditions may be the best insurance for the satisfactory creep performance.

To help avert the potential for abrupt crack generation in the wick during the early stages of operation, a gradual break-in period would be helpful. Since the stress, like the solar flux profile, varies significantly over the dome surface, gradual thermal ageing could be conducted at a low concentrator power level.

Cracking within the 0.06 inch thick wick can occur in two ways. Uniformly distributed microcracks, smaller than the mean capillary pore size of 2×10^{-5} meters (0.8mils) would not affect the heat pipe performance. If the peak wick strain is multiplied by the hemiperimeter, a characteristic length is obtained. If this dimension is uniformly distributed over the absorber surface and, for example in the limit, divided by the number of grain boundaries, no appreciable effect will result.

However, if cracks congregate locally in zones of high flux, a gap significantly greater than the pore may result. Cracks larger than the mean pore size of the evaporator surface could impede liquid replenishment to portions of the wick. This would not necessarily be catastrophic if sufficient safety factor is built into the wick/liquid transporter system. There is really no practical way to predict this occurrence and, therefore, future work in this area should focus on initially performing some laboratory tests.

It is most important to avoid cracking of the arteries. Relatively large cracks compared to the pore size would reduce the available pumping head of this system or in the limit deprive the artery. Also, the highest stress determined from the FEM was shown to be in the vicinity of the artery junction at the surface. Figure 8 illustrates the stress conditions involving the artery. Since the outer wick surface is in tension, a sharp corner at the artery bond to the evaporator would give rise to a stress concentration point. Also the hole in the center of the artery presents another text book stress concentration condition. However, with generous radiusing of the corner, local stresses should not appreciably exceed the FEM predictions.

Once developed, crack propagation could be perpetuated by mechanisms other than stress. Both corrosion and volumetric expansion of the sodium, which occurs in transition from frozen to liquid states, can play an important role. Mechanical forces imposed during the phase change are associated with start-up issues and will be discussed in section 7.

5. Thermal Analysis

The thermal loss from the receiver is shown in table 3 to be composed of six dominant mechanisms. Most of the analysis for this study centered about the first two on this list: shell conduction and cavity reradiation.

Because of the near isothermal conditions within this cavity, it was possible to evaluate these cavity losses and the external shell losses independently without sacrificing accuracy. The heat pipe surface temperature, under the design flux load has been shown to vary by less than 20°C.

The conical cavity walls under radiative equilibrium steady state conditions will also achieve a temperature close to the nominal absorber temperature. This wall will actually exhibit a thermal gradient from the aperture lip minimum temperature to the junction at the absorber which is assumed to be at the sodium vapor temperature. This general trend exists because the tapered wedge of insulation is smallest at the aperture and this zone has the greatest view factor to the ambient. In addition to these factors, ambient convection, both natural and forced (wind), can play an important role in the losses at this edge. However, the analysis of these convection effects will be deferred to future programs.

A Monte Carlo ray tracing routine was used to model the concentrator and generate flux and temperature profiles on the absorber dome. In this analysis the outer edge of the wick was assumed to be at the vapor temperature of 700°C or 800°C. Again, lateral conduction in the shell was shown to be quite small through use of the FEM thermal stress study. Thus the simple 1-D approach is justified. Data from this analysis was fed into a SINDA model which analyzed various shell insulation schemes. Figure 12 illustrates an example of the nodal arrangement used in the SINDA analysis. Careful attention was given to modeling the conical wedge-shaped insulation surrounding the aperture. Previous Sanders receiver tests have shown correlation of results in this zone to be difficult.

RECEIVER ENERGY LOSS MECHANISMS

	Percent of 75KW Thermal Input	
	800°C	700°C
Shell Insulation	2	1
Cavity Reradiation	3.5	2.5
Dish Shadeing	0.7	0.7
Transient Start-up*	0.7	0.7
Diffuse Cavity Reflection	2.3	2.3
Cavity Convection		
- Horizontal	(?)	1
- Vertical	<1	
Net Receiver Efficiency (Vertical)	90	91.8

Assumed Conditions:

o $T_{\infty} = 25^{\circ}\text{C}$

o Total Solar Energy input on 950w/m^2 day $= 2.1 \times 10^5 \text{KJ}$

o 6" insulation

Table 3.

ORIGINAL PAGE IS
OF POOR QUALITY

CONCEPT OF INSULATION

A range of insulation thicknesses were considered in a trade study of thermal losses. However, in the final design, the insulation thickness may be set by the constraint to be within the existing TBC mounting ring. Figure 13 presents the effect of increased insulation thickness on total shell heat loss.

Alternative shell geometry for the front cover was considered in an attempt to provide more insulation in the critical area. Figure 14 illustrates the SINDA model design for a conical front cover which increases the thickness of insulation in that vicinity. This concept was not found to be compatible with the existing TBC water cooled aperture ring. However, a future low cost production receiver could integrate these receiver design aspects with the aperture shield design.

Table 4 lists the insulation materials considered for this design and their pertinent data. For cost reasons it was recommended that a composite insulation scheme utilizing both refractory blanket and fiberglass could be effectively employed. The low cost fiberglass is limited in temperature and therefore can only be used in the outer cooler section. Therefore the more expensive Mansville product will be confined to the hot zone in contact with the heat pipe and around the aperture.

In our earlier Brayton designs, a precast insulation product was used effectively by Sanders to form the cavity entrance cone. This approach would form the conical cavity from a precast piece of insulation thus eliminating the need for the metal cone liner which extends from the aperture to the absorber. However, with an open cavity, the insulation would be susceptible to weather damage. Water saturated insulation is, of course, very undesirable.

To minimize the potential for exposing the insulation to moisture, we have proposed to employ the conical metal cavity liner with bat-type insulation behind it. We believe that this approach is less expensive in production than the cast insulation. The stainless steel entrance cone is fastened to the aperture lip of the external receiver shell. As shown in figure 1 a thermal break is provided at this junction by clamping a ceramic gasket between the metal parts. At the absorber end of the cone, a clearance gap allows for unrestrained thermal growth of the cavity parts.

Heat Loss vs. Insulation Thickness

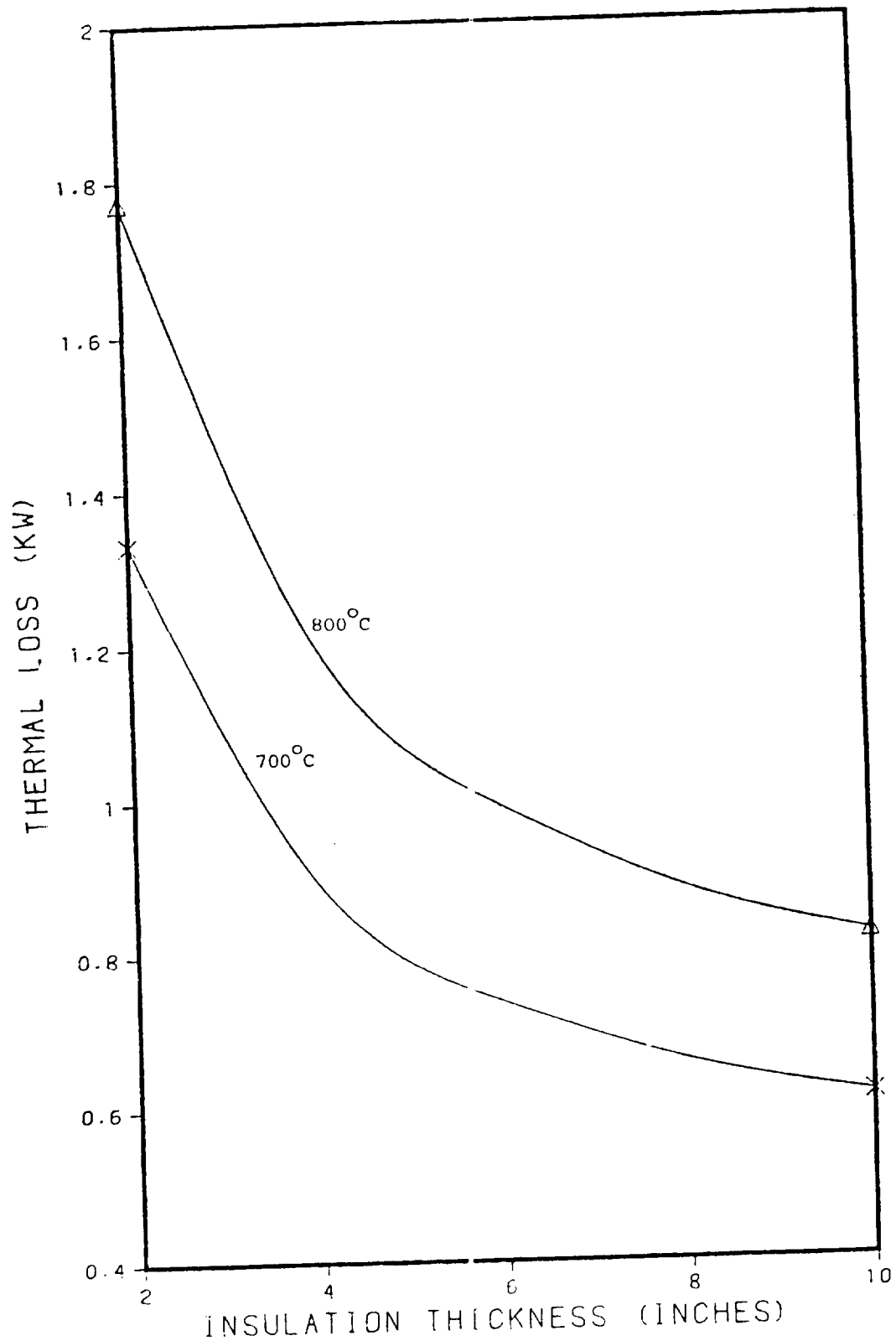


Figure 13. Shell insulation losses using composite insulation scheme analyzed **with** SINDA nodal

781	684	564	435	251	76					
781	684	564	435	251	75					
781	683	564	434	250	73					
780	682	561	432	248	71					
777	669	546	420	239	66					
789	690	595	489	375	210	61				
793	714	628	541	446	341	189	57			
794	721	643	564	484	398	302	165	53		
793	711	641	568	494	422	345	261	141	50	
790	663	595	538	477	414	354	290	217	117	46
452	389	435	422	382	337	291	239	179	97	44
	249	301	286	265	235	197	148	82	42	
	160	158	191	181	156	118	69	40		
		140	134	118	93	58	38			
		85	94	88	72	50	37			
			64	65	57	45	36			
				50	47	39	35			
					43	37	34			
						35	34			
						38	33			

ORIGINAL PAGE IS
OF POOR QUALITY

TABLE NO. 4 INSULATION OPTIONS CONSIDERED

Product	Mfg	Unit Cost (\$/ft ² in)	Conductivity (BTU in/ft ² hr°F)	Service Temp Limit (°F)	Density (lb/ft ³)	Specific Heat (BTU/lb°F)
SGR 3* Fiberglass Blanket	Manville	0.16	1.23 @ 900°F	1000	2	
			0.67 @ 600°F			
			0.39 @ 300°F			
Cera wool* Blanket	Manville	2.00	2.4 @ 1600°F	1600	8	0.26 @ 1200°F
			1.6 @ 1200°F			
			0.8 @ 800°F			
MIN-K	Manville	50.00	0.5 @ 1600°F	1800	20	0.27 @ 1200°F
			0.35 @ 1200°F			
			0.25 @ 800°F			

* Selected

The first order analysis of receiver cavity solar reflection losses shows that this is an area worth paying attention to. It was assumed that the solar reflections are purely diffused from both the absorber and the secondary reflections off the entrance cone. The diffuse assumption would lead to the minimum reflection loss prediction. Under the assumption of total specularity, more energy would be lost from the cavity. Appendix B shows the hand calculations for this limiting case, as well as the purely diffuse case. The specular analysis is also interesting because it predicts that for a shallow cavity, where the center of curvature of the absorber is near the aperture plane specular losses will increase to a maximum. For a 19 inch diameter absorber all specularly reflected rays will be lost on the first "bounce" when the center of curvature is within 1.7 inches of the focal plane. In the recommended design this dimension is 5.5 inches and therefore many of the reflected rays hit the conical cavity walls.

In actuality, the solar reflection losses should fall between the diffuse and specular limiting cases presented in Table 5. Some representative data is available for the wavelengths of interest. Figure 15 shows that for high roughnesses and low angles of incidence, (30°) which is our case, we should not expect a significant specular reflection component of energy. This is a reasonable assumption when considering the surface effects of partially oxidized Inconel 600. That is, the "optical roughness," defined by the characteristic (rms) roughness dimension wavelength, is predominantly greater than 1. The monochromatic data in figure 15 is representative of the solar spectrum which peaks at a wave length of about $0.5\mu\text{m}$.

The calculation of diffuse reflections has been based on the assumption of a solar absorption of 85% for both absorber and entrance cone. Figures 16 and 17 present data showing that this is reasonable for rough, weathered, oxidized Inconel. Thus a cavity of our dimensions will have a total reflection out of the aperture of approximately 2.3%. These calculations are presented in Appendix B.

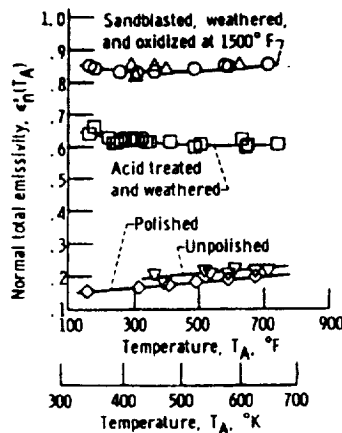


FIGURE 17. Effect of surface condition and oxidation on normal total emissivity of stainless steel type 18-8. (Data from [5]).

CAVITY REFLECTIVITY PREDICTIONS

<u>REFLECTIVITY</u>	<u>SPECULAR LOSS</u>	<u>DIFFUSE LOSS</u>
15%	2.9%	2.26%
10%	1.83%	1.43%
30%	6.69%	5.2%

Table 5.F For the calculation presented in Appendix B, both specular and diffuse cases have been considered. The reflectivity of the absorber is set equal to the reflectivity of the cavity walls which are considered diffuse in both calculations.

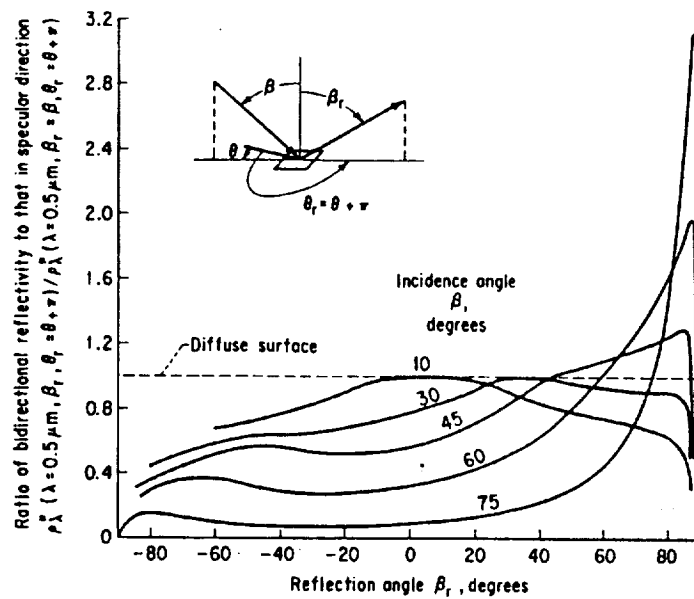


Figure 15. Bidirectional reflectivity in plane of incidence for various incidence angles; material, aluminum (2024-T4), aluminum coated; rms roughness, $\sigma_0 = 1.3 \mu m$; wavelength of incident radiation, $\lambda = 0.5 \mu m$. (From [14]).

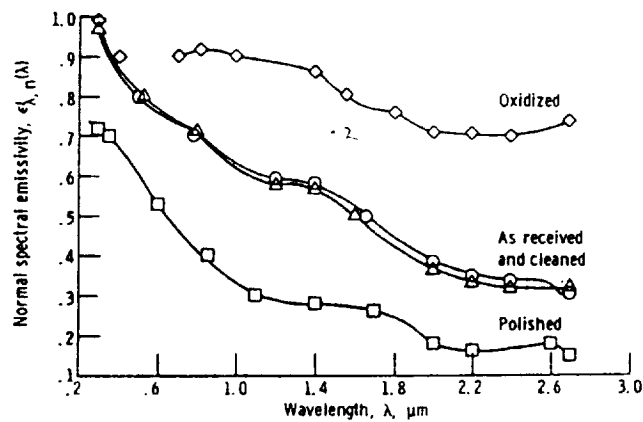


Figure 16. Effect of oxidation on normal spectral emissivity of Inconel X. (Data from [5]).

As a recommendation for future work it would be valuable to study alternative absorber optical surface characteristics. However, this time we recommend sand blasting the absorber dome to maximize the solar absorption and minimize the specular reflection components. This would also encourage oxidation of the rough surfaces. Encouraging oxidation of such a thin wall under conditions where U.V. exposure may also enhance oxidation, could be the wrong approach.

The objective of a surface coating would be to produce a passivating oxide layer over the base material. This would produce both desired effects-improved optical performance and oxidation resistance. Appendix C contains some recommendations for such coatings.

In a future program it would be beneficial to stochastically model and make optical measurements of the performance of various surfaces. It should be re-emphasized that durability of this shell is the primary goal and that the efficiency issue only amounts to a few percentage points either way.

The natural convection and wind effects on the cavity performance have been qualitatively observed in previous DOE open cavity dish systems. In the organic Rankine cycle (ORC) solar tests conducted at SNLA substantial transient reductions in generated power have been observed during periods of high wind. To our knowledge, no meaningful analysis based on correlation of test data exists. The recommended Stirling receiver is likely to also suffer from these effects. The most significant advantage the Stirling receiver has is its smaller aperture. However, this is determined by the concentrator and is offset by the higher operating temperature and a smaller cavity of the proposed receiver. In 1977 Sanders correlated convection losses with wind velocity for a Central Receiver design. Unfortunately, specific features of this receiver were quite different than those of the cavity heat pipe design. Therefore no direct extrapolation of the results can be readily applied to our present design.

This is in a sense a retraction from the figures presented by Sanders in the PDR. Convection losses for the Stirling receiver were estimated using the earlier Sanders data for our Brayton central tower receiver. We no longer believe that this previous work is relevant due to several key thermofluid differences. Briefly, this receiver was characterized before installation in the field using an innovative dimensional similitude approach which provided pertinent data without the complications of heat addition. In this receiver design, the engine working fluid was pumped through the open cavity to be heated at nominally atmospheric pressure. To simulate this while monitoring the exchange of the working fluid with the ambient, a low molecular weight gas was substituted which matched the dimensionless constraints of the hot working fluid. However, the pressure field

in the vicinity of the aperture for this case is likely to be significantly different from what we expect for the new Stirling design. In the Central Receiver the wind interacts with Euler-n type pressure gradients established by the working fluid flowing through the cavity. Also, the effect of pressure gradients driven by thermal induced density variations within the cavity was not present. A detailed description of these experiments is provided in references 3 and 4.

A direct measurement of convective mass transfer between the cavity and ambient should be conducted during initial characterization of the solar receiver. Our recommended approach is to employ a technique perfected by Sanders for the 1/4 MW receiver tests at the GIT facility (ref 4). This approach involves diluting the oxygen concentration within the cavity with nitrogen. Since the properties of nitrogen are very similar to air, there would be little effect on flow conditions. The mass efflux from the receiver could then be determined by measuring the rise in oxygen concentration during a controlled experiment. Sanders has developed the sensors and related instrumentation to conduct such tests during solar operation on the dish.

An alternate approach to deriving the convection losses is to indirectly calculate this loss component by subtracting the contribution of all other losses from the total losses. However, with such an energy balance it is difficult to measure all other losses with the necessary accuracy. Reflection losses for example would be much more difficult to measure than the convection losses. Also for a total energy balance it is necessary to integrate the effects over a sufficiently long time period to be assured of thermal equilibrium. However, wind conditions and hence cavity convection would respond to a much shorter time constant. To properly understand the aerodynamic interactions it would be necessary to directly analyze the convection phenomenon with the previously described method. This information would provide valuable insight for developing approaches to reduce losses in this area.

Section 6 Receiver Mechanical Layout

The overall mechanical design of the ASPS solar receiver has been carefully considered to minimize life cycle cost. This has resulted in a very simple design with careful attention to mechanical and thermal stresses and ease of manufacture and field service.

Solar Receiver with Heat Pipe Transport System: CDR

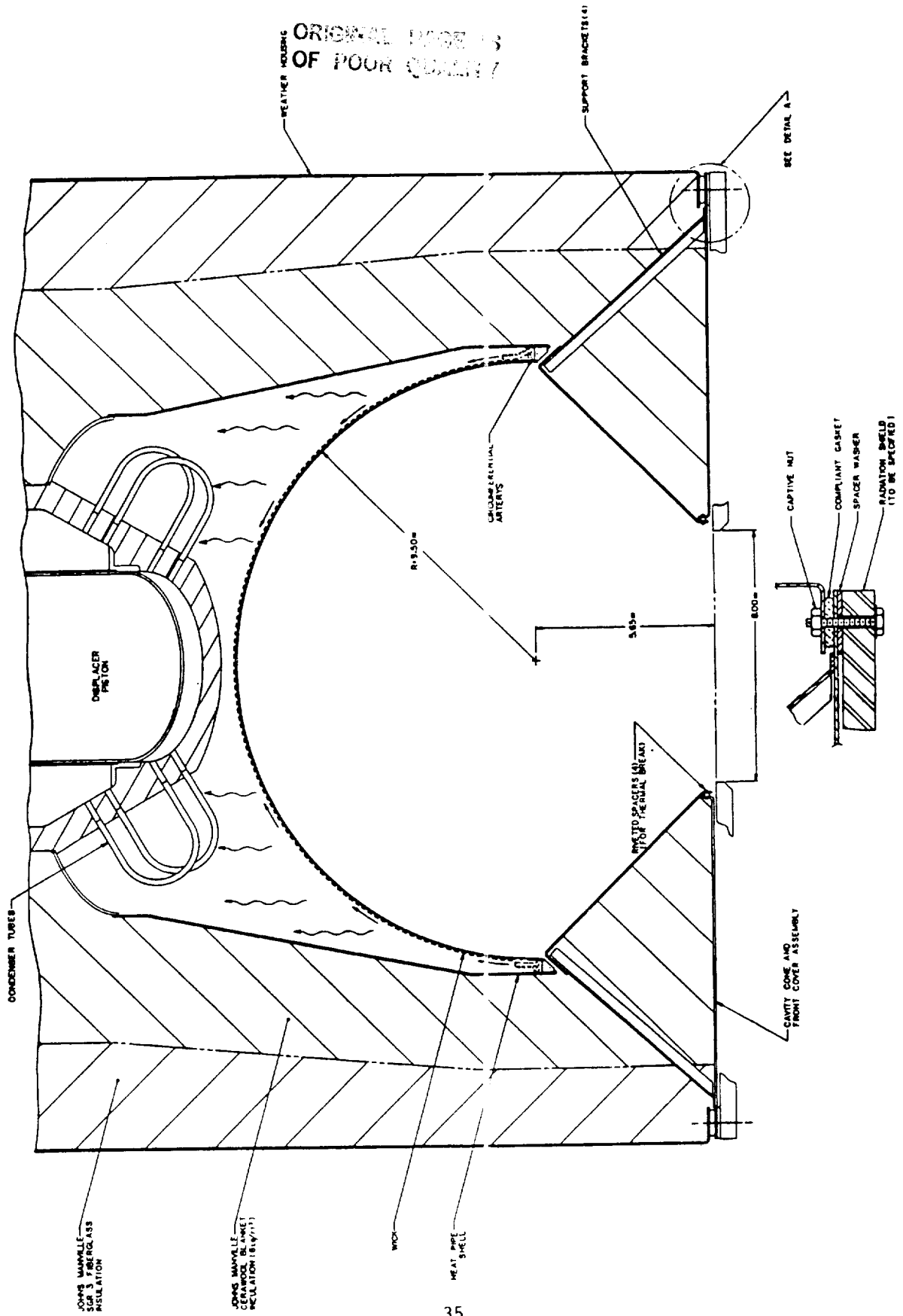


Figure 18.

The solar receiver as illustrated in figure 18 is composed of two major subassemblies: The absorber/heat pipe subassembly and the housing and insulation subassembly. These two subassemblies are physically independent to facilitate manufacture and maintenance.

To illustrate this, we will describe the receiver assembly process. The first step in the assembly process would be to weld the heat pipe shell/absorber dome assembly to the mating flange on the engine heater head and charge the heat pipe cavity with sodium. The heat pipe assembly can then be tested and inspected while it is totally accessible.

The next step would be to apply the two layers of blanket insulation to the engine and heat pipe assembly and slide on and fasten the cylindrical weather housing. Then the cavity cone and front cover assembly with its insulation would be bolted to the open end of the weather housing with four bolts. The final step is simply mounting the radiation shield disk over the front cover with an additional four machine screws. Disassembly is the reverse of the assembly process.

Heat Pipe Mechanical Design

The shape and size of the heat pipe subassembly is determined by its function. The absorber dome diameter is defined by the allowable flux and stress levels. The conical taper of the heat pipe shell is required to insure that the liquid sodium will always return to the distribution arteries at the base of the absorber dome even when the receiver assembly is oriented with its axis horizontal.

The triangular cross section ring which joins the absorber dome to the heat pipe shell is required to bridge the radial gap necessary for the circumferential arteries. It also transfers to the heat pipe shell the considerable force resulting from the subatmospheric pressure within the heat pipe cavity. This condition also requires a substantial wall thickness for the heat pipe shell to transfer the compressive load down to the heater head flange. The triangular cross section ring also facilitates the application of the arteries and wicking structure to the absorber dome by stabilizing the mouth of the dome and providing a shoulder against which to form the circumferential wick arteries.

The three joints involved in this assembly are welded to produce a hermetic seal for the heat pipe. These welds are illustrated in greater detail in figure 19. An objective of these weld designs is to minimize the possibility of crevice corrosion by the sodium. Should it be necessary to remove the heat pipe assembly from the heater head the weld between the heat pipe shell and the heater head flange would be severed. This process of cutting and rewelding could be repeated several times without affecting the clearance between the dome and the heater head.

Each of these three welds is circular and therefore suited to automated welding processes such as electron beam or laser welding. This permits the welds to be located so as to avoid crevices.

Outer Housing and Insulation Subassembly

To minimize manufacturing cost two types of insulation are used. The inner layer which contacts the heat pipe is Johns Mansville Cerawool blanket which is rated for use up to 1600°F while the outer layer is a much less expensive SGR3 fiberglass insulation rated at 1000°F. A sufficient thickness of the Cerawool blanket is applied to bring the temperature down to below 1000°F for the fiberglass.

The weather housing is a cylinder fabricated of 20 gauge Galvalume coated sheet steel. It slides on over the insulation and bolts to the engine assembly.

The key element of the cavity cone and front cover assembly is the stainless steel cone which forms part of the cavity surface. It is made of stainless steel as it operates at essentially the same temperature as the absorber surface due to radiant heat transfer from the absorber. To minimize conductive heat loss from this surface, it is attached to the front cover ring by just four riveted spacers. Similarly, four small support brackets are used to connect the outside diameter of the cone with the outside diameter of the front cover to create a geometrically stable configuration. Cerawool insulation is fitted into the resulting triangular cross section.

Another feature may be required for the applications where the receiver may be stored in a near horizontal attitude, where rain could enter the cavity through the aperture. To accommodate this problem a short segment of a ring of trough shaped cross section would be welded to the return flange on the major diameter of the cavity cone as shown in figure 20. A short drain tube would then conduct any accumulated water out through the insulation and spill it overboard. Typically, two of these gutter assemblies would be required to accommodate the receiver being tipped to the east or to the west.

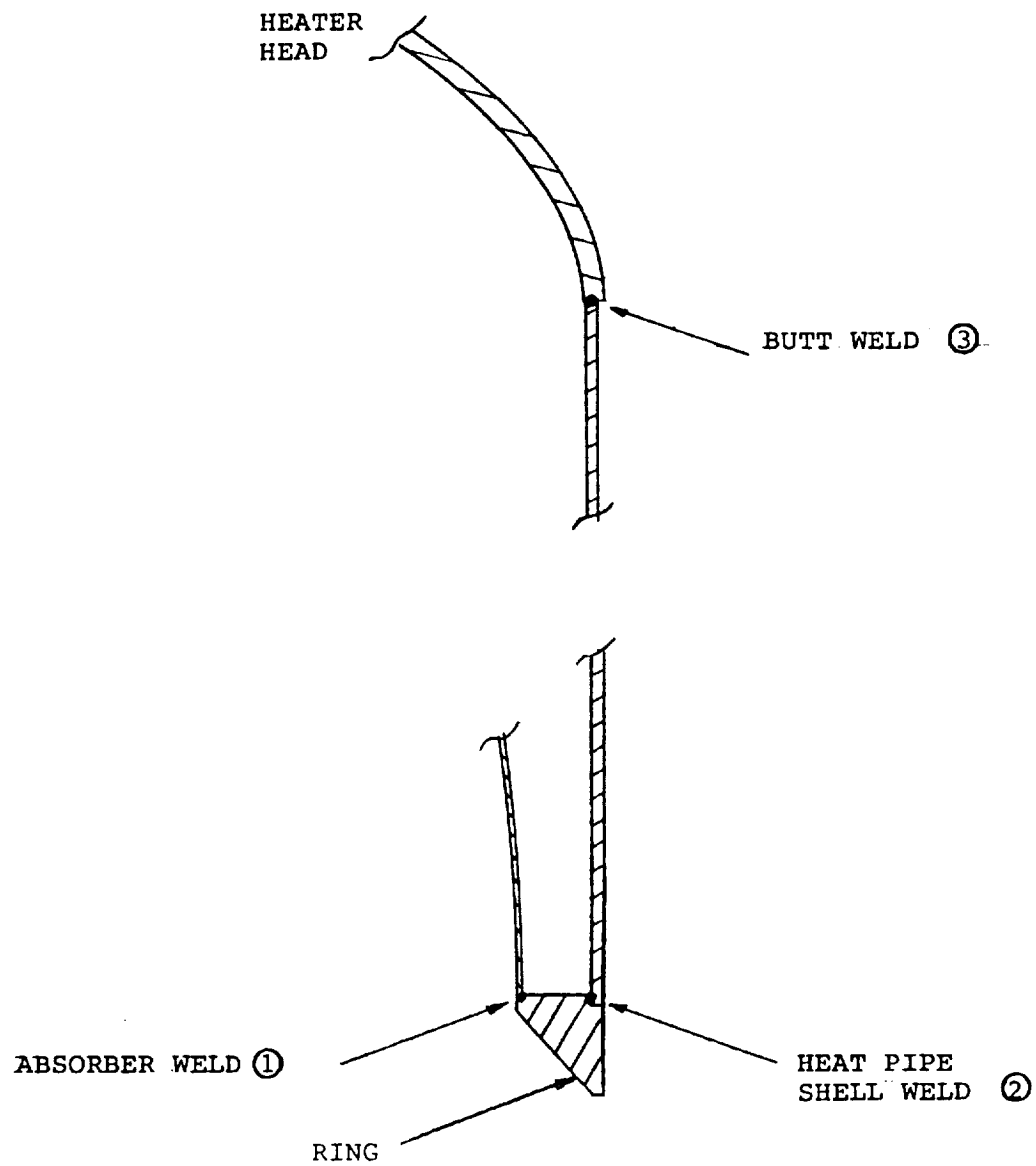


Figure 19. Cavity Heat Pipe Weld Designs.
Numbers Indicate Weld Sequence.

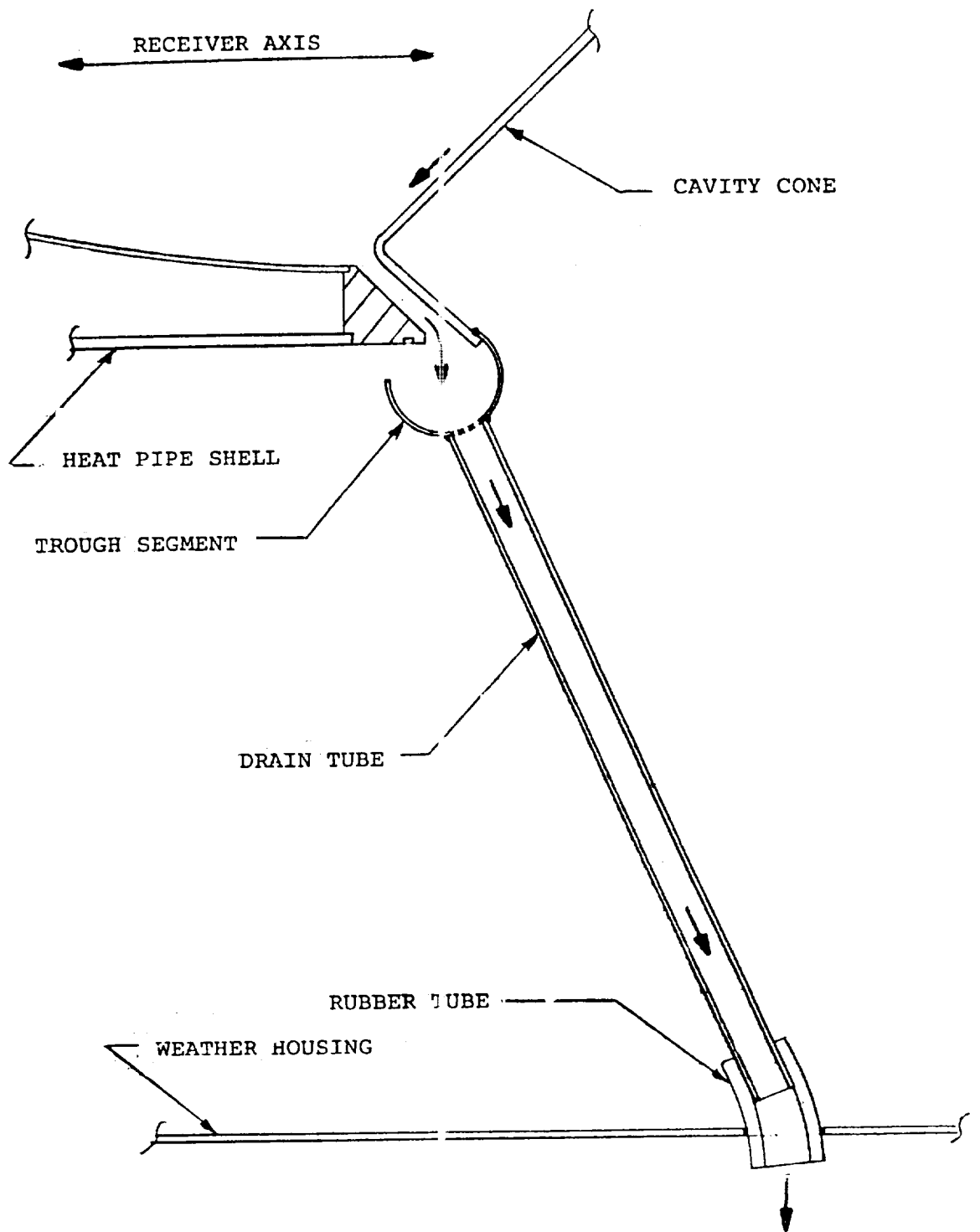


Figure 20. Cavity Water Drain.

The front cover ring is stamped from 20 gage stainless steel with a short flange at its inside diameter to accept the spacer rivets for the cavity cone. It may be necessary to form Annular Corrugation in this cover to avoid buckling due to differential thermal expansion. Both ends of the four support brackets are spot welded.

The front assembly is bolted to the weather housing using a compliant gasket which prevents the entry of moisture and provides a thermal break. Four additional bolts are used to secure the radiation shield ring in place over the front cover. Generous clearance holes in both the cover and the radiation shield accommodate manufacturing tolerances and differential thermal expansion.

Both the heat pipe and the housing subassemblies are mounted to the engine assembly which in turn is attached to the TBC mounting ring. The receiver extends through the inside diameter of the TBC mounting ring and may be equipped with several small wearpads if there is a tendency for it to rub against the ring I.D. during operation.

7. Receiver Cold Starting Requirements

"Cold Starting" the solar receiver is the procedure for elevating the sodium inventory temperature to a point where quasi-steady dynamic heat pipe performance initiates. At ambient temperature, up to the melting point at 98°C , the sodium is solidified. The initial energy input is therefore absorbed in the melting sodium. Once melted, the normal sodium mass transport mechanisms will begin. However, at temperatures well below the design point, the liquid sodium viscosity is substantially greater than the design value. This translates to an increase in frictional pressure drop in the wick which limits the tolerable local solar flux levels. In an extreme transient condition, viscous flow in the large arteries might not be sufficient to replenish local zones in the thin, thermally responsive wick exposed to a high solar flux.

The second starting issue involves controlling the stresses introduced by the volumetric expansion of the sodium. As the sodium changes phase, the material will increase its volume by about 5%. If this volume is somehow confined within a pore or crack, substantial pressures can arise. A cyclic occurrence of this phenomenon is often referred to as thermal ratcheting. Thermal ratcheting of a crack in the artery or the absorber could lead to catastrophic failure of the wick system.

The safest way to avoid the transient wick dry-out and the thermal ratcheting effects is to warm the system slowly. Low level heating will produce a more uniform temperature distribution in the sodium and wick. With sodium melted uniformly at its boundaries, there is a greater tendency for the liquid to find paths to seep out of cavities.

It should be pointed out that some relatively small heat pipes have been operated from frozen to full power in only a few seconds without problems. However, due to the unique geometry of this heat pipe and the requirement for 20,000 cycles, special precautions should be taken.

In the early development phases it is recommended that electric heating elements be employed to preheat the heat pipe evaporator section. The electric heater would be positioned to melt the radial and circumferential arteries as well as the liquid reservoir. To provide heat to the arteries on the dome it is necessary to use a radiant source within the solar cavity. A conductively coupled heater element could efficiently melt the circumferential arteries and reservoir, but this would not effectively influence the radial arteries on the shell. A radiant source of a few hundred watts located in the solar cavity could adequately preheat the sodium in about an hour.

Fortunately, it appears that this starting procedure would not be required for day to day operations. A transient cool-down analysis shows that it is possible to maintain the cavity above the sodium melting point through a typical night period. Figure 21 presents the transient SINDA model results. This shows that either the incorporation of a reasonable quantity of thermal mass within the receiver or a fused silicon window can yield the required thermal time constant.

Thermal mass in general is regarded as a receiver loss. For the most part energy put into thermal mass is essentially lost at the night. However, in this case energy stored in thermal mass can be used to displace electrical preheat. For this reason, an economic trade off should be conducted. At this time, this is believed to be a trivial issue and warrants attention only after some receiver characterization on the concentrator.

An alternate approach might be to provide some thermal storage in a phase change material (PCM) with a melting point just slightly above the sodium melting point of 98°C. Losses from the PCM would be lower than losses from sensible thermal storage at higher temperatures.

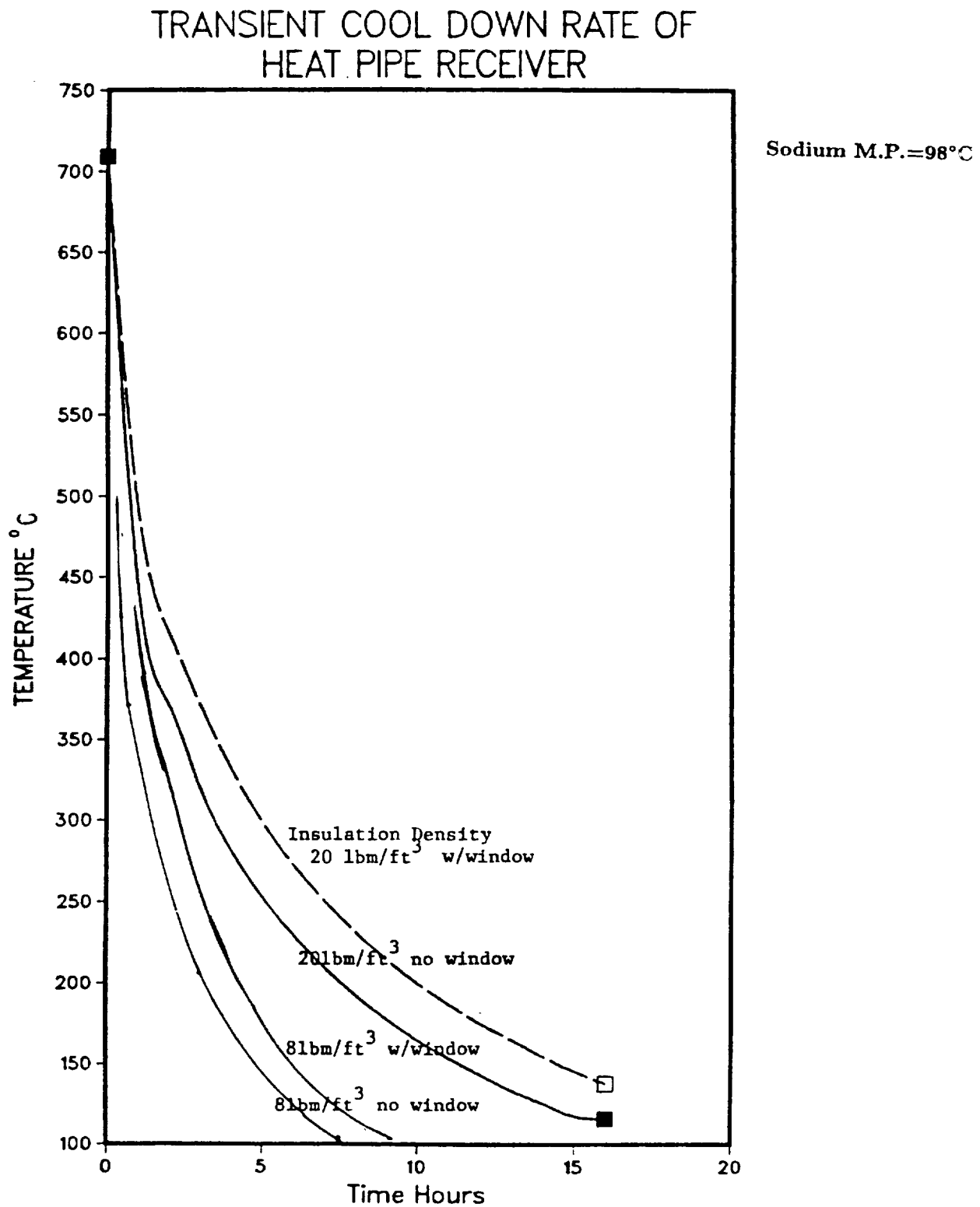


Figure 21. Transient SINDA analysis assuming step function interruption in solar. The sodium free zinc point is 98°C.

Assuming the sodium can be passively maintained in the liquid state through the night period, it is then reasonable to project that the less intense morning sun could safely power-up the system. The criteria for determining when auxiliary electric heating is required is best worked out in field tests.

8. Conclusions and Recommendations

Although the principles by which this heat pipe receiver has been designed are well established, many new features are embodied in the concept. The key issue, simply put, is to demonstrate that the cavity heat pipe receiver can provide sufficient operating life to achieve economic viability. Because of the initial cost projections for the heat pipe and the impracticality of refurbishing the unit after a failure, the target operating life is expected to be approximately 20 to 30 years. Over this period of about 80,000 hours of operation, one must expect something on the order of 20,000 thermal and pressure cycles.

For these reasons accelerated life testing procedures must be developed first for components and then for a complete receiver. Thermacore's powdered metal wick process appears to have an excellent applicability to this set of design problems. However, they have not had the opportunity to demonstrate these techniques on anything in this size range.

Long term corrosion related issues continue to be a key concern of NASA specialists. To address these concerns a composite wick, artery and absorber should be tested. Representative welds should also be present and dynamic sodium mass transfer must occur. We would suggest using a small 1" diameter tubular configuration which could be produced with existing Thermacore tooling. Unwicked end caps should incorporate welds similar to those recommended for the receiver. Having operated such a test for 6 months to a year, the tube should be dissected and analyzed. Some measurable corrosion will be detectable by a scanning electron microscope or other specialized instruments.

To establish confidence in the integrity and functionality of the powdered metal wick sintered to the solar absorber, the next step in the development should involve testing a segment of the evaporator. It is recommended that a representative test specimen be prepared by sintering wick and arteries to a 15 inch x 10 inch rectangular piece of the absorber sheet. For this first demonstration, the sheet would be formed to a 90° arc with only a lengthwise plane of curvature. The 15 inch dimension represents approximately the distance from base to apex of the proposed

hemispherical dome while the 10 inch width is about the distance between arteries. Two or more radial arteries and the joining section of the circumferential arteries should be also attached. This scale should reveal any problems associated with the fabrication technique without an excessive amount of tooling costs. It is believed at this time that the extra non-recurring expense for making mandrels with both planes of curvature would be less cost effective.

Once the specimen has been fabricated the critical procedures and cost related risks should be well understood. The next step should be to perform some mechanical endurance tests. A test rig could be designed to induce comparable stress levels in the composite structure by mechanical means. A bending stress in such a thin shell is similar to the actual thermal stress profile.

The FEM model developed under this contract could be also used to predict the deflection needed to simultaneously induce wick tensile and absorber compressive stresses. Switching the displacement to a smaller amount in the opposite direction would simulate the cold condition. It is not possible to duplicate the exact operating stress conditions, but this approach would make it possible to compile a large number of cycles quickly. Various fabrication parameters (pressures, temperatures, rates, cleaning preparation, alloys etc.) could be efficiently compared on a quantitative basis.

Early indications of the required engine development schedule project that it will be about one year longer than that of the receiver. This would then permit sufficient time to conduct the tests recommended above and build and characterize a complete receiver. Receiver characterization would be conducted first in the lab and then on the Test Bed Concentrator. The heater head tubes, as part of the receiver, would be cooled with a pumped working fluid. This gas would be pumped unidirectionally in the test for simplicity and to allow for an accurate energy balance.

These tests would also incorporate an extensive number of thermocouples and strain gauges secured to the heat pipe. Presolar characterization and check out could be effectively conducted in the laboratory environments.

Figure 22 illustrates a scheme which could be quickly implemented which uses Sanders existing solar test equipment. Producing 75Kw from radiant electric sources within this small cavity would require a more sizable investment. This simple approach would use our microprocessor controlled propane combustor to impinge hot gas on the cavity dome. This combustor is designed to be controlled by a thermocouple mounted in a critical location on the test unit. In this case it could be set to maintain the absorber surface temperature at nominally 700°C. As more or less heat is extracted from the engine simulation loop, the combustor would automatically maintain the surface temperature within very tight limits.

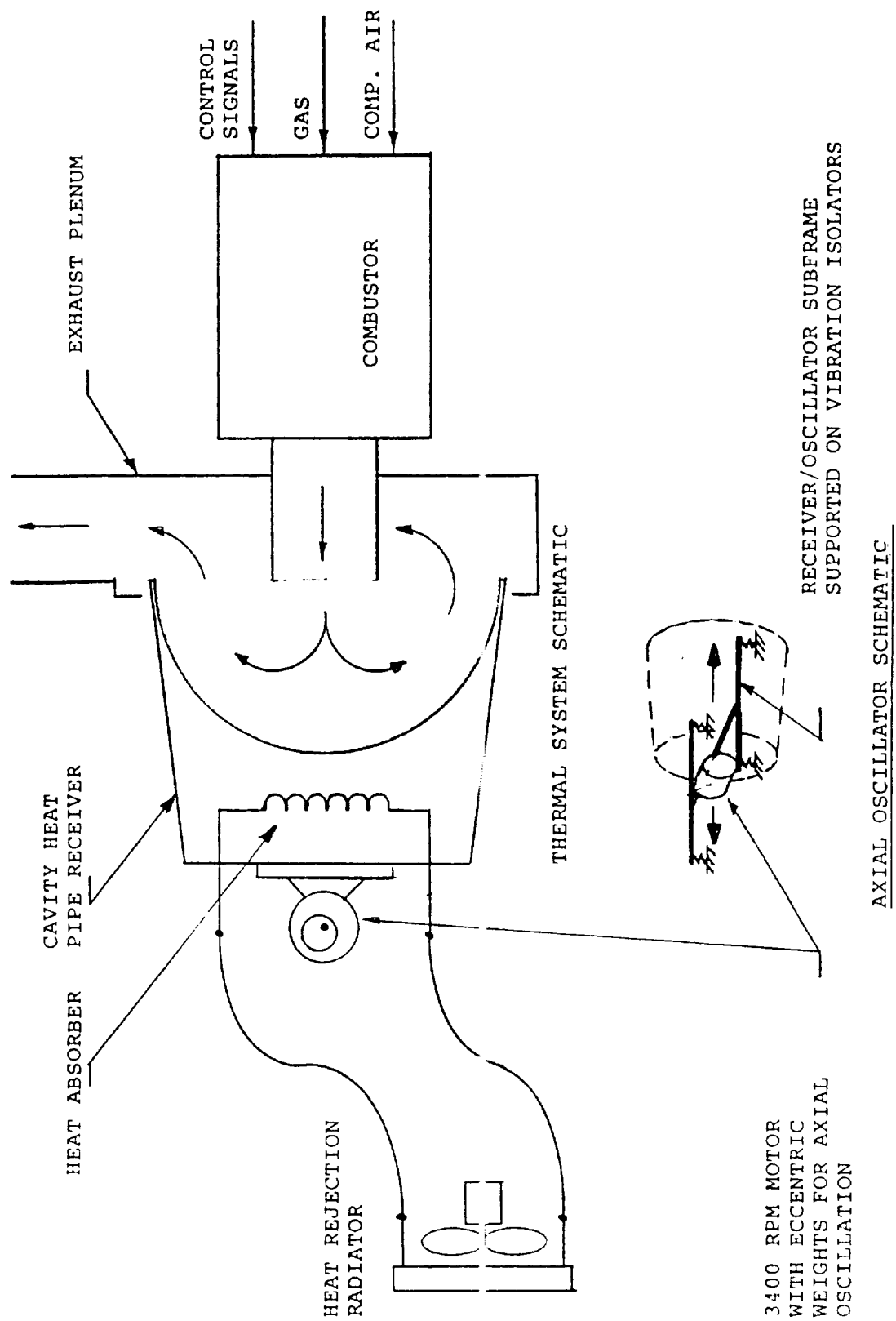


Figure 22. Receiver Thermal Cycling Test Rig Schematic.

In addition to the performance characterization and operations checkout, the forced hot air approach could be used to relatively quickly accumulate thermal cycles on the unit. Simply extinguishing and relighting the combustor while maintaining air flow would produce alternate heating and cooling cycles. With the radiant heaters it would take a very long time to cool the system down between cycles thus making it impractical to consider a moderate number of cycles. The gas cooled sequence would quickly cool down the heat pipe making accelerated life testing feasible.

This testing can also incorporate a means for simulating the axial vibration of the engine to observe its effect on heat pipe performance. The lower sketch on figure 22 illustrates how the receiver can be mounted on a subframe supported on vibration isolators and excited in the axial direction by a small motor with eccentric weights on its shaft.

The final phase of the receiver development should be to test the receiver on the TBC without the engine. Performance characterization, starting methodology and engine controlled transient response tests can only be effectively conducted under actual solar conditions.

Receiver performance related issues include studies of convection losses from the cavity and designing the cavity for sufficient thermal capacitance to maintain molten sodium in the arteries and reservoir for 16 hours. A brief outline of a method for experimentally analyzing cavity convection effects was provided in section 5. This experimental work should also be integrated with a computational analysis in order to provide a better understanding of the phenomenon. It is very conceivable that changes to the receiver in the vicinity of the aperture plate could reduce the severity of wind effects.

Sanders recommends that the option phase of this program should focus on developing a test plan which includes presolar activities and comprehensive solar tests. A summary of the recommended development phases is presented in figure 23.

Recommended Receiver/HTS Development Phases

Fabrication Development

- Develop process for sintering wick and artery to a sector of the dome
- Conduct flexure tests on suitable specimen to insure integrity of wick and interfacial bond (@700°C)

Model I Receiver/HTS

- Assemble shell, insulation, structure
- Fabricate heatpipe with simulated engine heater head
- Conduct auxiliary combustor checkout test in lab with simulated engine heat extraction (test vibration and orientation sensitivity)

Test Equipment on TBC with Simulated Engine

- Start up procedure/methodology/accessories
- Survivability demonstration (strain gauge, calorimetry, thermocouples)
- Characterization of losses (data reduction/analytical modeling/optimization)

Build Model II Receiver/HTS

- Integrated with engine



Figure 23

7

LIST OF REFERENCES

- 1 PAFEC LTD, 40 Broadgate, Beeston,
Nottingham NG9 2FW England
- 2 Halford, G.R. Manson, S.S. "Application of
Method of Estimating High-Temperature Low-
Cycle Fatigue Behavior of Materials",
American Society of Metals Transactions,
Vol. 61, No.1, Mar. 1968
- 3 Convective Loss Experiment, Sanders Assoc.
Contract to ERDA #EO-77-C03-1533
2/22/78
- 4 1/4 MW Solar Receiver, Sanders Assoc. ERDA
Contract AC03-77SF90506, DOE//SF/90506-1
10/1979
- 5 Wood, W.D. Deem, H., Lucks, C, "Thermal Radiative
Properties", Plenum Press, Plenum Publishing Co. NY,
1964
- 6 Siegel, R., Howell, J. "Thermal Radiation Heat
Transfer", McGraw-Hill Book Co, 1972
- 14 Torrance, K and Sparrow, E., "Theory of Off-Specular
Reflection from Roughened Surfaces", OPT. Soc. Am., Vol.
57, No 9, 1967

APPENDIX A

Hand stress calculations for heat pipe vessel
and attachment points to evaporator dome and engine.

The Solar Receiver Design Concept has been reviewed for potential problem areas. The change from a 160 ° spherical section to a full 180 ° section has improved the structural design and will tend to reduce the stresses due to the pressure loading at the joint with the cylindrical section. (see location 3 in Figure 1).

There are a few areas that should be analyzed more thoroughly. Due to the internal vacuum inside the cooling chamber and the relatively large size of the chamber, the resulting stresses could be quite high. Every joint or shape discontinuity in the structure is a potential stress riser. To get a rough idea of the magnitude of some of these stresses some hand calculations were run. These calculations can be found in Appendix A. The following table summarizes the results.

Location	Thickness	Cylinder(C) End plate(E)	Max Stress (k.s.i.)
1	.125	E	20.7
1	.25	E	4.0
2	.125	C	29.5
2	.25	C	7.1
3	.125	C	7.3
3	.25	C	1.7
3	.125	E	86.4
3	.25	E	21.6
3	.375	E	9.6
3	.5	E	5.4

****NOTE:** The cases selected from Roark to calculate the stresses were not exactly representative of the structure proposed. To get more accurate results a finite element analysis is recommended.

RECOMMENDATIONS

The following changes will help reduce the stresses:

1. Increasing the material thickness in the areas of concern.
2. Decreasing the diameter of the cylindrical section at location 3 (see figure 1) so that it is as close as it can be to the diameter of the spherical section (see figure 2).
3. To reduce the stresses location 2, it would help if the plate is shaped more spherical or with a generous radius to form an o-give shape. (see figure 2)
4. Welded joints should be acceptable but should be looked at in more detail when the design is analyzed more thoroughly. .

Solar Receiver with Heat Pipe Transport System: CDR

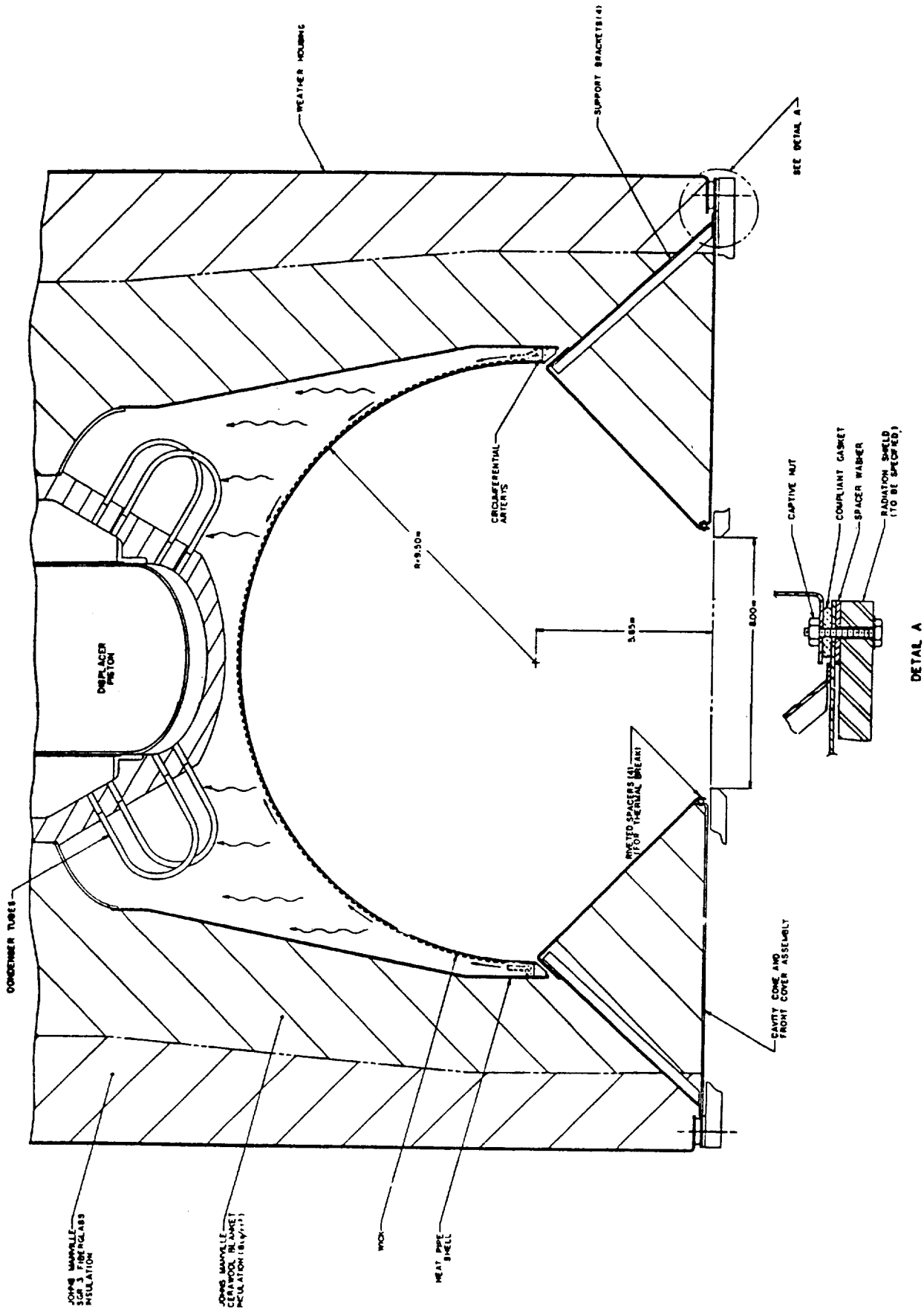
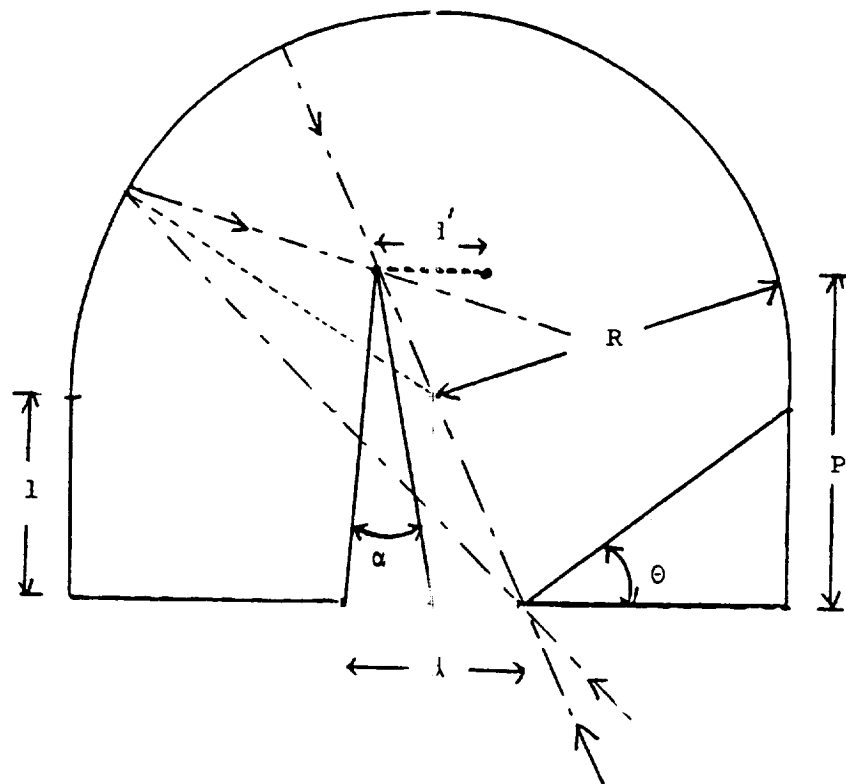


Figure A2

Appendix B.1

All specularly reflected rays entering the spherical cavity through the aperture (d) will pass through the image "disk" (d).



The magnification ratio $M = \frac{d}{d'} = \frac{s}{s'}$,

Were $\frac{1}{s} + \frac{1}{s} = \frac{2}{R}$

and $s = 1 + R$

$$\frac{1}{s'} = \frac{2}{R} - \frac{1}{s}$$

$$s' = \frac{sR}{2s-R} = \frac{(1+R)R}{2(1+R)-R} = \frac{R1+R^2}{21+R}$$

$$M = \frac{s'}{s} = \frac{sR}{2s-R} \cdot \frac{1}{s} = \frac{R}{2s-R}$$

$$= \frac{R}{2(1+R)-R} = \frac{R}{21+R}$$

$$P = s - s' = 1+R - \frac{R1+R^2}{21+R}$$

$$= \frac{21^2 + 21R + 1R + R^2 - 1R - R^2}{21+R}$$

$$= \frac{21^2 + 21R}{21+R} = \frac{21(1+R)}{21+R}$$

α = exit angular acceptance

$$= \sin^{-1}(d/2P)$$

$$= \sin^{-1} \left[\frac{d(21+R)}{41(1+R)} \right]$$

Fraction light that escapes = $F = \frac{\sin \alpha}{\sin \theta'}$

θ = concentrator rim angle

$$d \sin \theta = d' \sin \theta'$$

$$\sin \theta' = \frac{d}{d'} \sin \theta = (\sin \theta) / M$$

$$= \frac{(21+R) \sin \theta}{R}$$

Therefore

$$F = \frac{\frac{d(2l+F)}{4l(1+F)}}{\frac{2l+R}{R} \sin \theta} = \frac{d R}{4l(1+R) \sin \theta}$$

For the case where all reflections are lost, $F=1$, find l

$$d R = 4l(1+F) \sin \theta$$

$$4l^2 + 4lR - Rd = 0$$

$$l^2 + lR - \frac{Rd}{4} = 0$$

$$l = \frac{-R + \sqrt{R^2 + Rd}}{2}$$

For our case, $R=9.5$ inches, $d=8$ inches

$$l_{\min} = 1.70 \text{ inches}$$

In our case, $l = R-d/2 = 5.5$ inches

Therefore some specular reflections will hit conical cavity wall. This percentage of the reflected power = $1-F$

$$F = \frac{4 \times 9.5}{4 \times 5.5 + (5.5 + 9.5) \sin 45^\circ}$$

= 16.3% escapes on first reflection

If the average (spectrally integrated) reflectivity of the absorber surface is 15%, the emitted power on the first reflection is $.163 \times .15 = 2.44\%$

Secondary reflections, assumed to be diffuse, with F_v as the view factor of the cone to the aperture, calculated in appendix B.2.

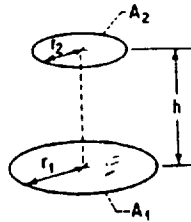
$$= (1-F) \times \rho_a \times \rho_c \times F_v$$

$$= (1-.163) (.15) (.15) (.239) = 0.45\%$$

The total for the specular absorber is therefore 2.9% which compares to Appendix B.2 diffuse calculation of 2.3%

Appendix B.2

Calculation of cavity reflection losses assuming purely diffuse optical characteristics of a spherical section absorber and conical cavity walls.



In diffuse reflections the direct transfer between the absorber and aperture can be represented by the geometric view factor from plane 3 to plane 1.

$$FV_{12} = 1/2 \left[X - \sqrt{X^2 - 4 \left(\frac{R_2}{R_1} \right)^2} \right] \quad (\text{reference 6})$$

$$\text{where } X = 1 + \frac{1 + R_2^2}{R_1^2}$$

$$R_2 = r_2/x$$

$$R_1 = r_1/x$$

For $r_1 = 19$ inches and $r_2 = 4$ inches, $x = 5.5$ inches

$$X = 1.512$$

$$R_1 = 1.727$$

$$R_2 = 0.727$$

$$FV_{12} = 12.89\%$$

$$\text{and } FV_{13} = 1 - FV_{12} = 87.11\%$$

Using reciprocity relations

$$\begin{aligned} FV_{32} &= FV_{23} A_2/A_3 \\ FV_{23} &= 1 - FV_{21} = 1 - FV_{12} A_1/A_2 \end{aligned}$$

$$= 1 - 0.1289 \frac{19^2}{8^2}$$

$$A_3 = \pi \frac{19}{2} \sqrt{\frac{19^2}{2} + (5.5+4)^2} - 4\pi \sqrt{4^2+4^2}$$

$$= 329.9 \text{ in}^2$$

$$A_2 = \pi \left(\frac{19}{2}\right)^2 = 283.0 \text{ in}^2$$

$$FV32 = .278 + \frac{283}{329.9} = 0.239$$

Direct flux from absorber through aperture

$$\dot{Q}_{12} = \rho_a \cdot FV_{12} \cdot P_c$$

Indirect flux from absorber to cavity cone, then through aperture.

$$\dot{Q}_{132} = \rho_a \cdot FV_{13} \cdot \rho_c \cdot FV_{32} \cdot P_c$$

All other internal reflections are much higher order terms

$\rho_a = \rho_c$	\dot{Q}_{12}/P	\dot{Q}_{132}/P	$\dot{Q} \text{ total}/P$
0.15	1.92%	0.34%	2.26%
0.10	1.27%	0.15%	1.43%
0.30	3.84%	1.36%	5.2%

P_c = Total solar power incident on absorber

ρ_a = Reflectivity of absorber, total hemispherical

ρ_c = Reflectivity of cavity walls, total hemispherical

A_3 = Area of conical cavity walls

A_2 = Aperture area

**Absorber Coatings to Minimize
Oxidation/Corrosion
and Improve Cavity Performance**

- Cr_2O_3 or ZrO_3 + Cobalt Nitrate
 - Have good absorptivity/
emissivity ratio
 - .005 to .010 inches atomized spray
coating has good resiliency
 - Can be cheaply applied or
reapplied in the field
- $Ni-Co-Cr-Al-Y$ or $Co-Cr-Al-Y$
 - Oxidation/corrosion resistant
coatings for gas turbine blades



APPENDIX II

**HEAT-TRANSPORT SYSTEM FOR A 25 kWe
ADVANCED STIRLING CONVERSION SYSTEM**

FINAL REPORT

Period Covered: November 1986 - June 1987

Prepared For:

Mechanical Technology Incorporated
Latham, New York

Prepared By

Thermacore, Inc.
Lancaster, Pennsylvania

CONTENTS

	<u>Page</u>
1.0 INTRODUCTION.....	1
2.0 CONCLUSIONS.....	3
3.0 RECOMMENDATIONS.....	4
4.0 WORK EFFORT.....	5
4.1 TASK 1: ESTABLISH DESIGN REQUIREMENTS.....	5
4.2 TASK 2: EVALUATE SINGLE AND MULTIPLE HEAT PIPE DESIGNS.....	6
4.3 TASK 3: SELECT HEAT PIPE WORKING FLUID AND CONTAINMENT/WICK MATERIAL.....	9
4.4 TASK 4: HEAT PIPE DESIGN.....	16
4.5 TASK 5: ESTABLISH START-UP AND SHUT-DOWN PROCEDURES.....	27

1.0 INTRODUCTION

The overall objective of the MTI Advanced Stirling Cycle Conversion System (ASCS) Program is to provide a low-cost free-piston Stirling engine system to generate electrical power. The ASCS will be a ground-based system used to convert approximately 75 kW of concentrated solar energy into 25 kW of electrical energy. The solar energy will be collected by an 11 meter diameter test bed concentrator and directed into a solar receiver. The solar energy will be transferred to the Stirling engine by a heat pipe system. An illustration of a proposed system arrangement using a single heat pipe is shown in Figure 1.

Thermacore was under contract with MTI to design the heat pipe system for the ASCS. Specific objectives include designing the wick structure, evaluating heat pipe wick and pressure boundary materials, and analyzing the heat-transport characteristics of the heat pipe system. This report documents the work done by Thermacore under the MTI contract.

ORIGINAL PAGE IS
OF POOR QUALITY

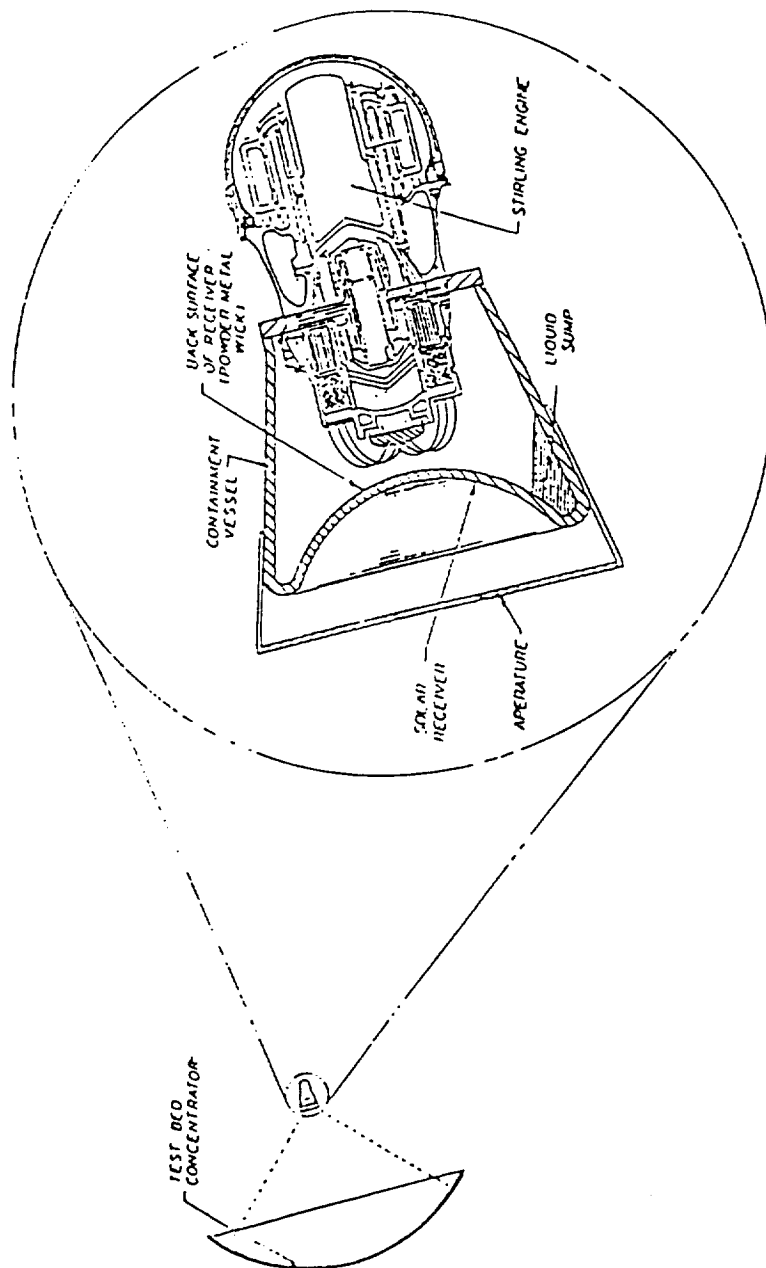


Figure 1. Single heat pipe concept

2.0 CONCLUSIONS

Several conclusions were reached as a result of the work effort for this program. These conclusions are briefly summarized below:

1. Single and multiple heat pipe concepts were evaluated for the ASCS. The single heat pipe design was selected because it exceeds the design requirements and provides a lower cost heat-transport/receiver system. These designs are both described in Section 4.2.

2. Sodium was selected as the working fluid for the receiver heat-transport system. Sodium provides a high liquid-transport factor and, based on existing life-test data, shows the potential for compatibility with Inconel 600 series alloys. An evaluation of sodium and of alternative working fluids is given in section 4.3.1.

3. Inconel 600 series alloys have been selected for the absorber surface. These alloys were selected because they have:

- o good high-temperature mechanical properties
- o high oxidation-resistance characteristics
- o potential for compatibility with sodium
- o good sinterability to the nickel wick structure
- o relatively low-cost for superalloy materials

These factors are discussed in more detail in Section 4.3.2.

4. Two artery designs were evaluated for the absorber surface. These designs are a radial and a parallel artery configuration. The radial configuration was selected primarily based on ease of fabrication.

The selected design provides two fully-redundant artery systems such that if one system fails, the other system can meet the load requirements. This design is described in Section 4.4.

5. As a conservative measure, an electric heater has been incorporated in the receiver design to liquify the sodium before heat pipe start-up. This helps to assure that liquid sodium will be available to supply the wick structure during the start-up transient. This feature is discussed in Section 4.5

3.0 RECOMMENDATIONS

This program has identified a heat pipe design that will meet the ASCS design requirements. The design analyses are based on well-established heat pipe calculational methods. The proposed fabricational methods are based on Thermacore's sintered powdered metal wick technology. This technology has been successfully demonstrated in many liquid metal heat pipe development programs. However, the geometry requirements for the ASCS application are unique: a working heat pipe of this geometry has not been conclusively proved by test. Consequently, Thermacore recommends that a full-scale, truncated-width section of the absorber surface be fabricated and tested. This work is believed to be one of the next steps to help assure the operational success of a full-scale heat pipe receiver.

4.0 WORK EFFORT

The work effort for this program has been divided into 5 inter-related tasks, as follows:

- o Task 1: Establish Design Requirements
- o Task 2: Evaluate Single and Multiple Heat Pipe Designs
- o Task 3: Select Heat Pipe Working Fluid and
Containment/Wick Materials
- o Task 4: Heat Pipe Design
- o Task 5: Establish Start-up and Shut Down Procedures

These tasks are described in the following sections:

4.1 TASK 1: ESTABLISH DESIGN REQUIREMENTS

The design requirements for the ASCS heat-transport system are summarized in Table 1.

TABLE 1. Design Requirements

<u>Parameter</u>	<u>Magnitude</u>
Transport Power (kW)	75
Evaporator Diameter (in.)	14 - 24
Evaporator Heat-Flux (W/cm^2)	25 - 75
Vapor Temperature ($^{\circ}\text{C}$)	700
Working Fluid	Sodium
Operating Life (hr)	60,000
Operating Cycles	20,000

The evaporator heat flux profile on the absorber surface has been determined by Sanders Associates. This profile is presented graphically later in this report, Figure 12.

4.2 TASK 2: EVALUATE SINGLE AND MULTIPLE HEAT PIPE DESIGNS

Two methods to transport heat from the solar receiver to the Stirling engine have been proposed. One method uses a single heat pipe and the other method uses multiple heat pipes. These concepts are shown in Figures 2 and 3.

The two heat pipe concepts have several advantages and disadvantages as outlined in Table 2. These items are discussed below:

TABLE 2. Evaluation of Heat Pipe Concepts

		<u>Single Heat Pipe Design</u>	<u>Multiple Heat Pipe Design</u>
1.	Integration with ASCS	Easy to Integrate	More Difficult to Integrate
2.	Redundancy	Provides no Heat Pipe System Redundancy	Provides Individual Pipe Redundancy
3.	Integration with Thermal Energy Storage	Can Be Integrated	Can Be Integrated
4.	Cost	Low	More Expensive Than Single Heat Pipe Design

- o Integration with ASCS. The single heat pipe concept is somewhat easier to integrate with the Stirling engine. It has fewer weld joints and consequently fewer failure points.

ORIGINAL PAGE IS
OF POOR QUALITY

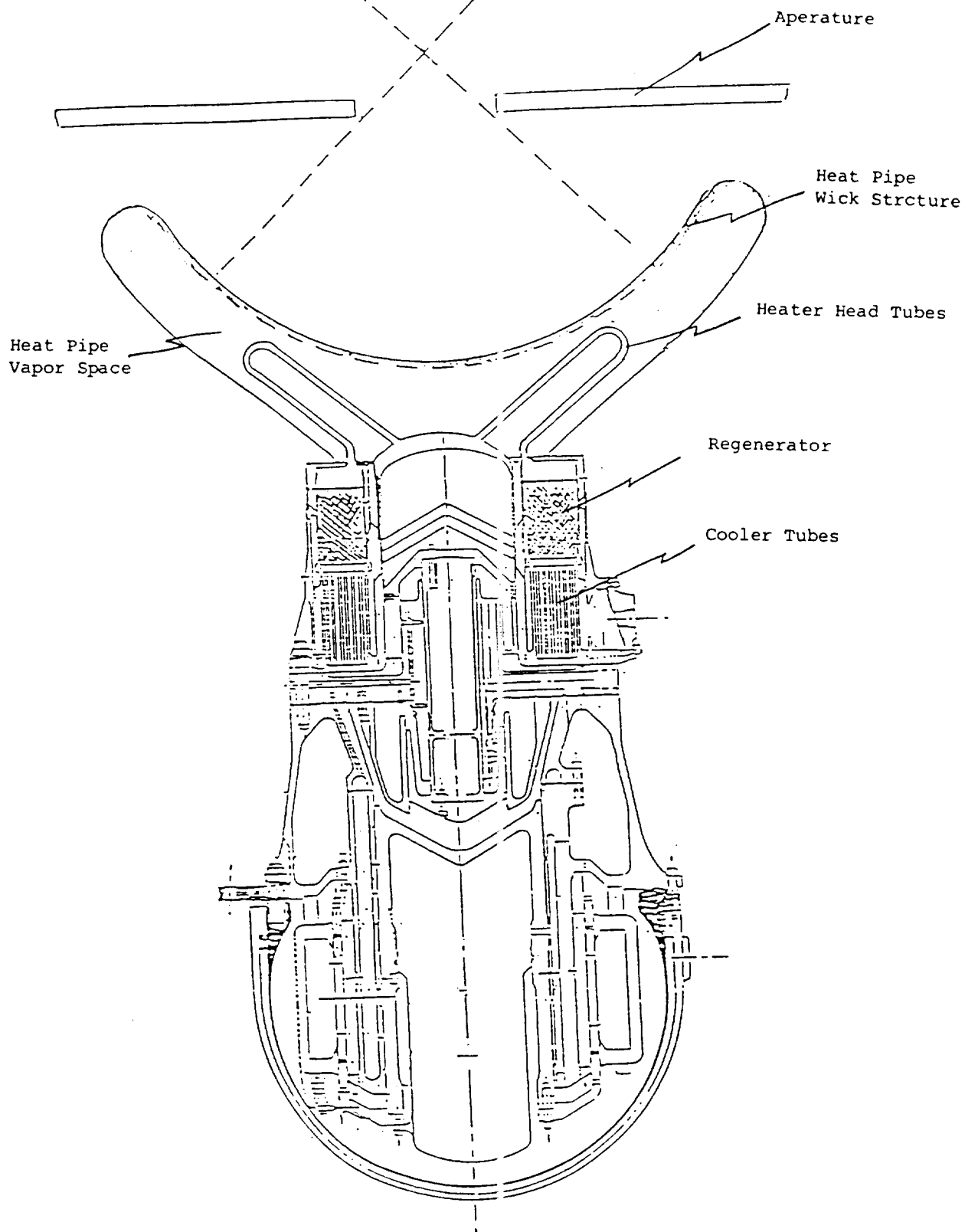


Figure 2. Single heat pipe design

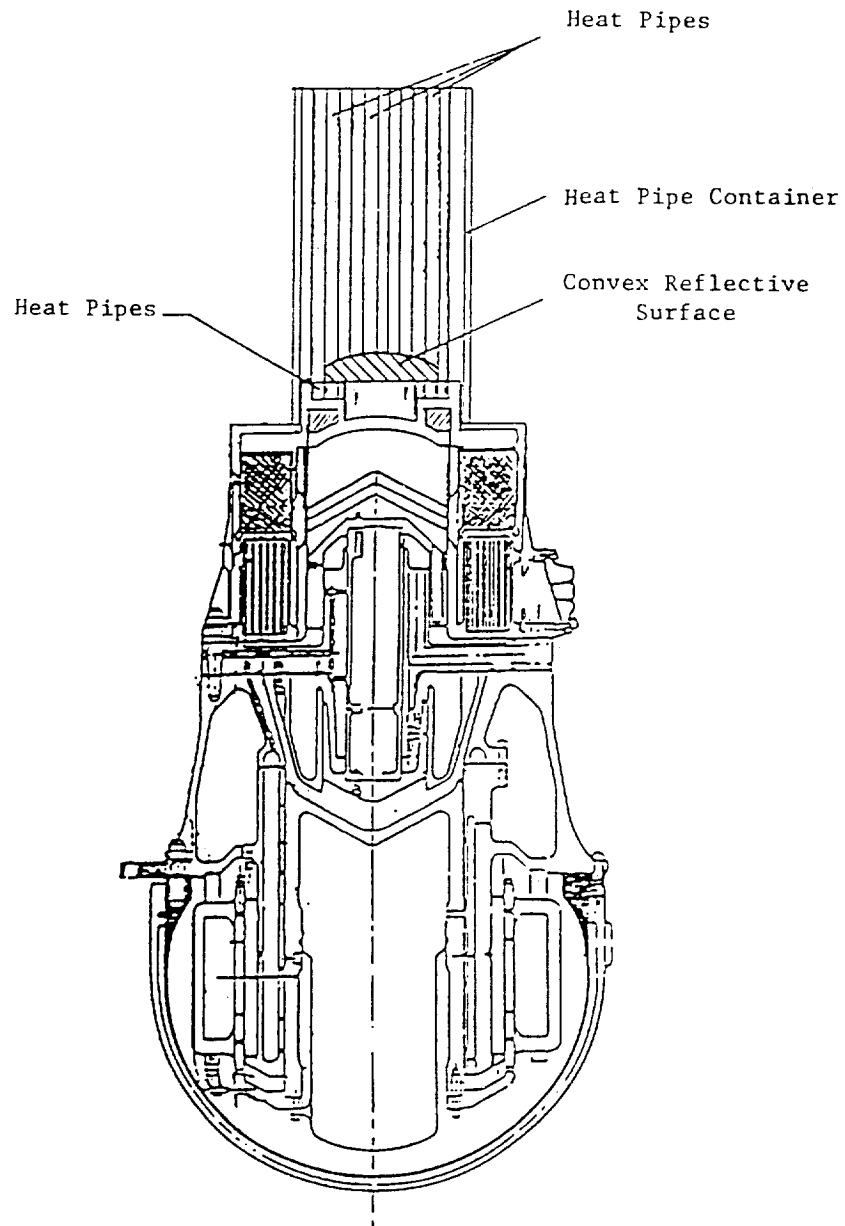
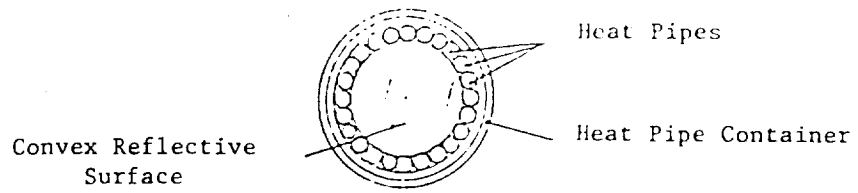


Figure 3. Multiple heat pipe design

- o Redundancy. The multiple heat pipe design provides the advantage of individual heat pipe redundancy. This system can be designed to continue operating after a heat pipe failure.
- o Integration with thermal storage. Both the multiple and single heat pipe design can be integrated with thermal storage techniques. For example, sealed canisters of thermal storage material could be integrated into the heat pipe vapor space. However, the detailed design of thermal storage is not within scope of this effort.
- o Cost. The single heat pipe design provides a lower cost design than the multiple heat pipe design. This results primarily because of the sintering and processing costs associated with the heat pipes. These costs are labor intensive and not directly related to the heat pipe size. Consequently, in this case, the multiple number of smaller heat pipes will be more expensive to sinter and process than a single large heat pipe.

The single heat pipe design was selected for this program. This design will meet the performance requirements and provide the most cost-effective heat-transfer system for the AACS.

4.3 TASK 3: Select Heat Pipe Working Fluid And Containment/Wick Materials

This section describes the selection of the heat pipe working fluid and the criteria for selecting the heat pipe containment and wick materials.

4.3.1 Working Fluid Selection

In a heat pipe, the ability of a working fluid to transport heat is a function of its physical properties. The relative amount of heat that the working fluid will transport can be determined from the liquid transport factor. The factor is given by the equation:

$$T = \rho_l \sigma h_{fg} / \mu_l$$

Where: T - Liquid Transport Factor
 ρ_l - Liquid Density
 σ - Surface Tension
 h_{fg} - Enthalpy of Vaporization
 μ_l - Liquid Viscosity

The properties of a good working fluid are:

- o High surface tension to provide a high capillary pumping pressure.
- o High enthalpy of vaporization and liquid density to provide a high heat absorption/rejection during phase change.
- o Low liquid viscosity to minimize the liquid pressure drop.

These properties are dependent on temperature and consequently the liquid transport factor is a strong function of temperature. This factor is shown in Figure 4 for several working fluids as a function of temperature.

At the expected operating temperature range, 700-800°C (973-1073K), liquid metal working fluids have the highest liquid transport factors.

ORIGINAL PAGE IS
OF POOR QUALITY

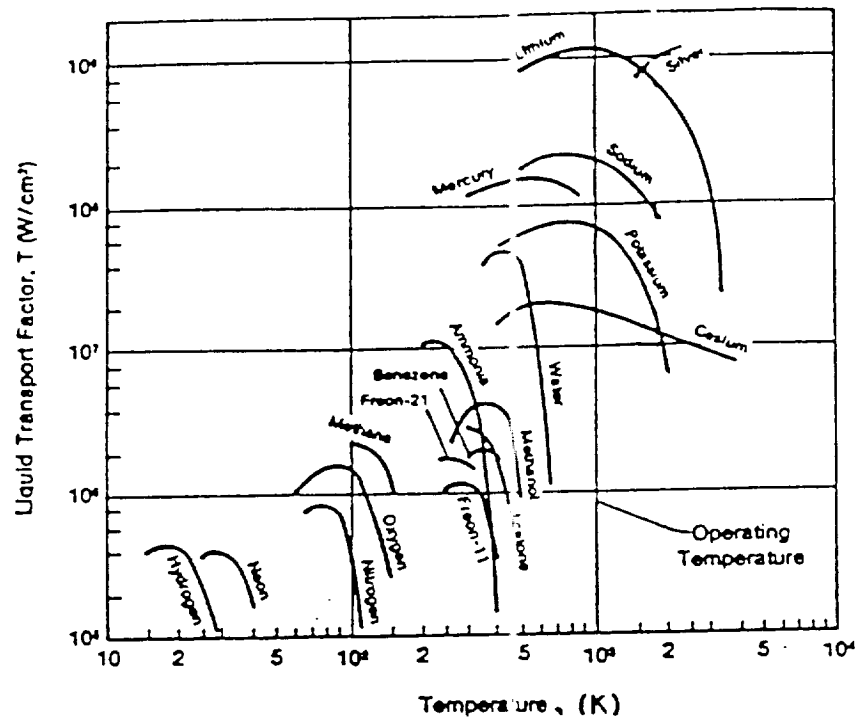


Figure 4. Liquid transport factors for various working fluids

Lithium has the highest liquid transport factor at the expected operating temperature, but there is limited data showing lithium to be compatible with superalloy and stainless steel materials. Lithium is generally used with refractory wall materials. However, superalloys or stainless steels are preferred for this application because they provide a lower cost containment vessel than refractory metals.

Sodium has the next highest liquid transport factor at the expected operating temperature and shows the potential for meeting the operating-life requirement when used with stainless steel or superalloy wall materials. Several examples of demonstrated life-test data of stainless steel and superalloys with sodium are shown in Table 3.

Consequently, sodium has been selected as the heat pipe working fluid for this program.

4.3.2 Containment and Wick Materials Selection

This section describes the basis for selecting nickel as the wick material and a 600 series Inconel as the containment material for the heat pipe.

The wick structure provides a means of transporting the working fluid, by capillary action, to the evaporator surface. Screen, grooves and sintered powder metal are alternative wick structures that were evaluated for this program.

Screen wicks are difficult to bond to the evaporator surface and consequently leave gaps at the wall. These gaps allow vapor generation in the wick which disrupts the liquid flow. This effect reduces the heat-flux limit on the generator surface. A grooved wick structure was

TABLE 3. Life-Test Data

<u>Wall Material</u>	<u>Working Fluid</u>	<u>Temp., °C</u>	<u>Operating</u>	<u>Reference</u>
304 S.S.	Sodium	800	12,760	1
304 S.S.	Sodium	732	11,500	2
304 S.S.	Sodium	700	10,000	3
Haynes 25	Sodium	732	12,000	2
Hastalloy-X	Sodium	715	33,100	1
Ni	Sodium	800	13,755	1
Incoloy 800	Sodium	820	24,000	4

References

1. Eastman, G. Y., "The Heat Pipe - A Progress Report," 4th Intersociety Energy Conversion Engineering Conference, Washington, D.C., September 1969, pp. 873-8.
2. Busse, C. A., Geiger, F., Strub, H., Poteschke, M., and Kraft, G., "High Temperature Lithium Heat Pipes," 2nd International Conference on Thermionic Electrical Power Generation, Euratom Rept. EUR 4210 f.e., 1969, pp. 495-506.
3. Ewell, G. J., Basiulis, A., Larp, T. R., "Reliability of Low-Cost Liquid Metal Heat Pipes," 3rd International Heat Pipe Conference, Palo Alto, California, May 22-24, 1978.
4. Thermacore, Life-Test Heat Pipe, test is currently being conducted.

also evaluated. However, the grooves can not provide enough capillary pumping pressure to overcome gravity and the liquid flow resistance.

The sintered powder metal wick structure overcomes these disadvantages. Because it is sintered to the receiver wall, it does not provide any wall/wick gaps. Additionally, the powdered metal wick provides a high capillary pumping pressure and, by incorporating arteries, provides a low liquid pressure drop. Previous experience at Thermacore has shown a heat-flux capability of 400 W/cm^2 with sintered powder metal wick structures and sodium as the working fluid. Details of the wick design are given in Section 4.4.

The powdered metal wick materials must be sinterable to the containment vessel and be compatible with sodium, the working fluid. In addition, the thermal conductivity and thermal expansion of the wick material are important properties.

The thermal conductivity of the wick is important because it affects the boiling limited heat flux. A wick structure that has a high thermal conductivity will be less likely to boil at a given heat flux than a wick structure with a low thermal conductivity.

The thermal expansion coefficients of the wall and wick materials have also been considered. Large differences in these coefficients provide shear stresses at the wall-to-wick interface. These shear stresses can be minimized by selecting materials that have similar thermal expansion coefficients.

Thermal expansion coefficients of nickel, Inconel 600, Inconel 601, 304 Stainless Steel, Incoloy 800H and Inconel X-750 are plotted in Figure 5. This plot shows that the thermal expansion of a nickel wick

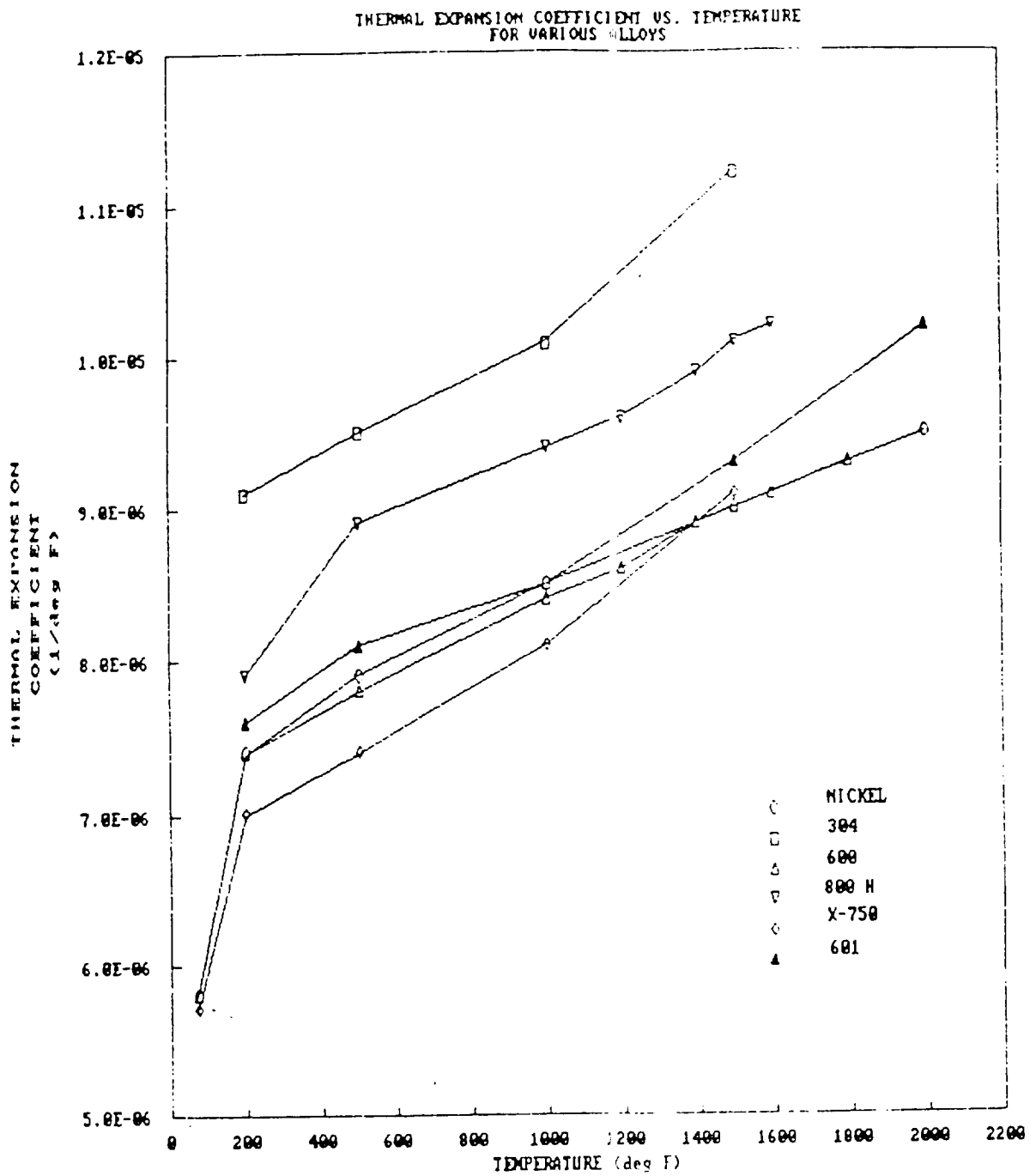


Figure 5. Thermal expansion coefficient versus temperature

material closely matches the thermal expansion of the Inconel 600 series alloys.

The Inconel 600 series appears to have the most potential for meeting the requirements of the ASCS. The specific alloys identified include Inconel 600, 601, and 625. Any of these alloys will most likely meet the heat pipe wall material requirements. However, the 601 and 625 alloys may provide a reduction of hydrogen permeability over the 600 alloy. This permeability reduction results from the formation of an aluminum oxide layer on the exterior surface of the absorber.

4.4 TASK 4: HEAT PIPE DESIGN

Heat pipes are sealed, evacuated devices that transfer heat by evaporating and condensing a working fluid. They are passive devices and do not require external power for their operation. Figure 6 illustrates a cut-away view of a typical heat pipe. Heat is input to the evaporator section and evaporates some of the working fluid. This increases the local vapor pressure and causes the vapor to flow to the other end where it condenses. The condensed liquid flows back to the evaporator section by the capillary pressure which is developed by the wick structure.

The thermal transport system for the ASCS is a hybrid heat pipe and reflux boiler. In this design, the working fluid liquid is distributed over the evaporator surface by a wick structure, as in a heat pipe. The working fluid is evaporated from this surface and is condensed on the evaporator section by draining from the tubes as in a pool boiler. The proposed design is shown schematically in Figure 2.

ORIGINAL PAGE IS
OF POOR QUALITY

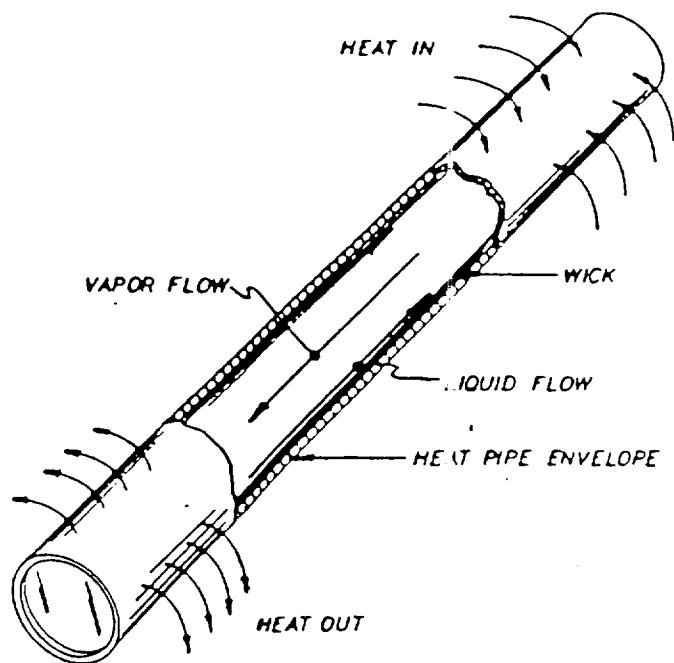


Figure 6. Cutaway view of a heat pipe

In order for the liquid working fluid to be distributed over the evaporator surface, the capillary pressure supplied by the pores in the wick structure, ΔP_c , minus the gravitational head, ΔP_g , must exceed the sum of the opposing liquid and vapor pressure drops.

$$\Delta P_c - \Delta P_g \geq \Delta P_v + \Delta P_\ell$$

where:

$$\Delta P_c = 2 \sigma / r_c$$

$$\Delta P_g = \rho g h$$

$$\Delta P_v = (8 \mu \dot{m} / \rho \pi r_{ev}^4) L_{ev}$$

$$\Delta P_\ell = (\mu L_{eff} \dot{m} / \rho K A)$$

The vapor pressure drop, ΔP_v , is negligible in this design because the effective area for vapor flow is large and the mass flow rate is relatively small.

The liquid pressure drop through the wick, ΔP_ℓ , is a significant term and provides the limiting heat flux factor. This pressure drop is caused by viscous drag in the liquid as it passes through the sintered porous flow passages.

Two wick structure concepts were evaluated for this program. These wick structures use either radial or parallel artery arrangements. Both concepts use a circumferential artery which allows the heat pipe to operate in any orientation. This is accomplished by providing continuity between the working fluid pool and the artery structure. As shown in Figure 7, the artery is fed by the pool of liquid regardless of the receiver orientation.

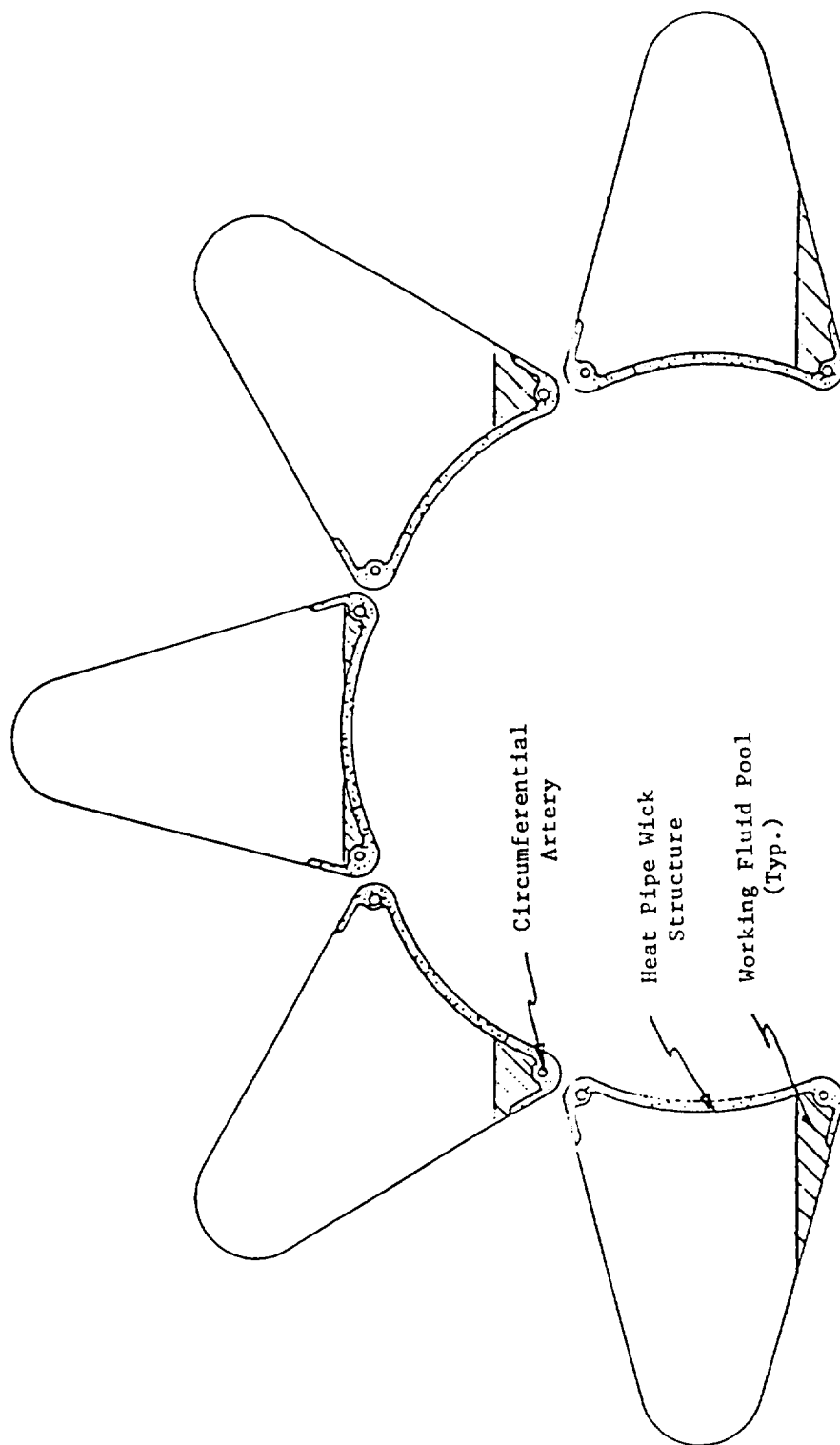


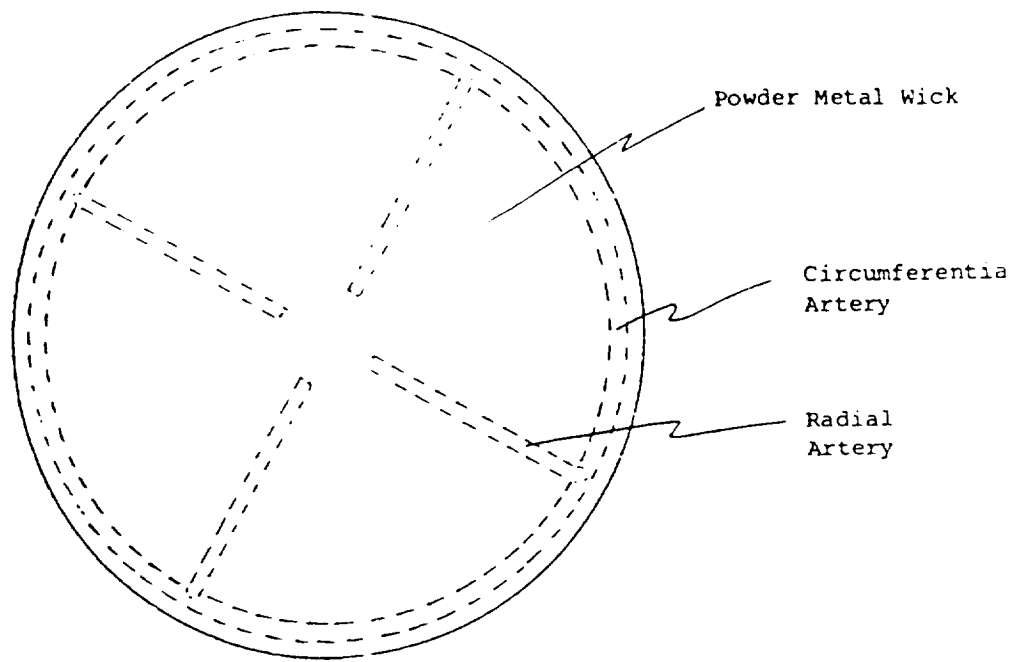
Figure 7. Single heat pipe design in various orientations

The radial artery design is shown in Figure 8. The inner surface of the hemispherical shell is coated with a sintered powder metal wick. The porous powder metal provides the capillary pumping force to distribute liquid over the entire surface. Arteries that radiate from the center are joined to the circumferential artery at the outer perimeter.

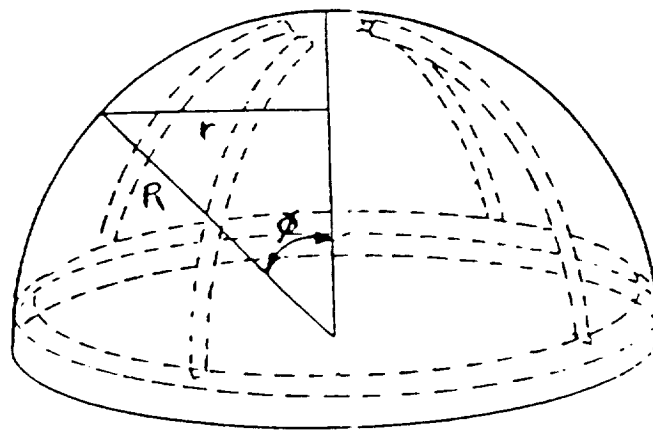
The maximum heat flux that the evaporator surface can sustain is limited mostly when the liquid viscous pressure drop exceeds the wick capillary pumping capability. This condition causes insufficient liquid to return to the wick structure causing local dry out and a "hot spot".

Figure 9 shows the results of wick dry-out calculations for the radial artery design. The maximum heat flux is a function of the angle ϕ , which is defined in Figure 8. The effective distance that the liquid must travel is function of ϕ and therefore the dry out limit is also a function of ϕ . Points in the wick that are close to an artery are easily fed with the working fluid. However, as the distance between a point in the wick and an artery becomes larger, the viscous forces in the liquid make it harder for the wick to be fed. This result is illustrated in Figure 9. Near the center of the evaporator surface, $\phi=0$, the point is near to radial arteries and the allowable heat flux is high. Also, near the circumferential artery the allowable heat flux is large. The point at which the allowable heat flux is a minimum, is the point at the greatest distance from any artery.

The maximum heat flux is also potentially limited by boiling in the arteries. If a vapor bubble nucleates below an artery, pushes into the artery and displaces the liquid, the artery will fail to deliver liquid

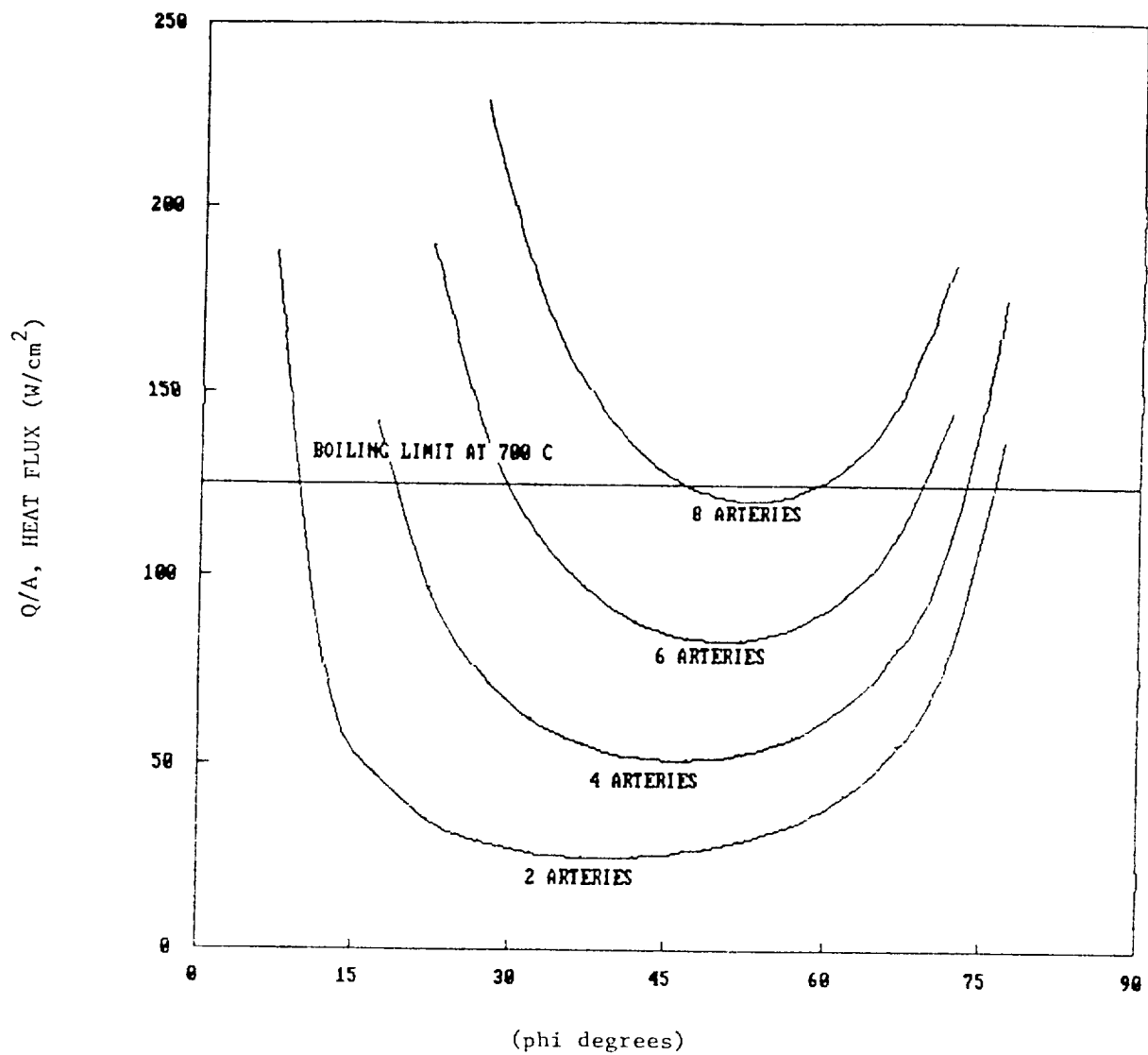


a) Top View



b) Side View

Figure 8. Radial artery design

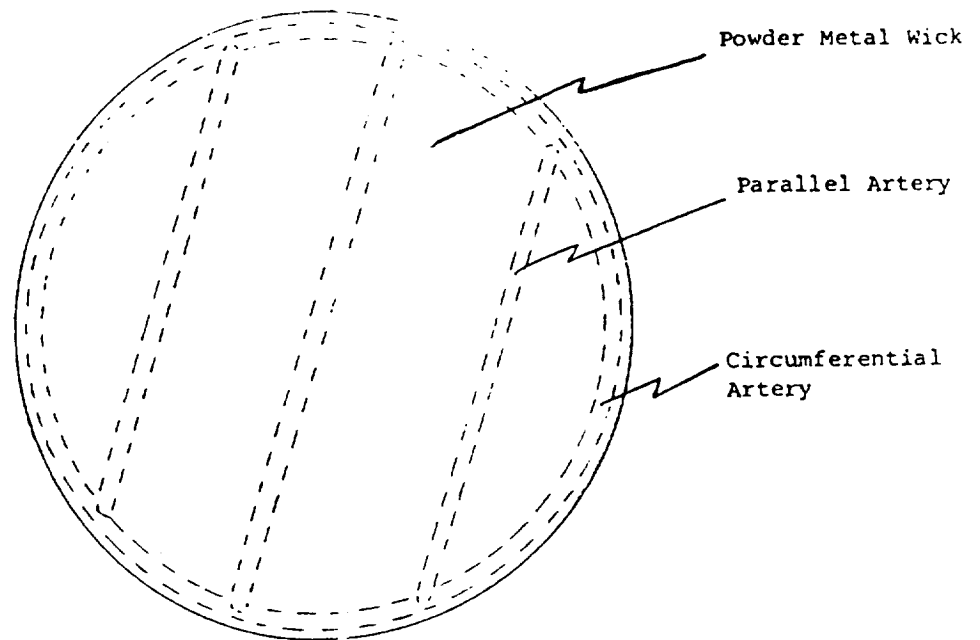


LEGEND:

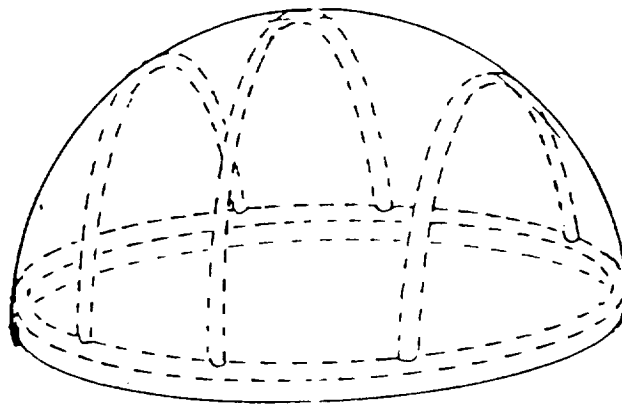
WORKING FLUID = SODIUM	TEMPERATURE = 700°C
DOME RADIUS = 9.5 in.	PORE RADIUS = 0.000019 m
WICK THICKNESS = 0.06 in.	WICK PERMEABILITY = 6.0E -12 m ²

Figure 9. Results of preliminary capillary limited calculations for radial artery design

ORIGINAL PAGE IS
OF POOR QUALITY



a) Top View



b) Side View

Figure 10. Parallel artery design

throughout the wick. This will cause the wick to dry out. The boiling limit is also shown on Figure 9.

Figure 10 illustrates the parallel artery design. The arteries are equally spaced and attached to a circumferential artery as shown. Because the arteries are equally spaced, the allowable heat flux is a function of the number of arteries. The allowable heat fluxes for varying numbers of arteries for the parallel design are shown in Table 4.

TABLE 4. Results of Preliminary Dry-out Calculations
for Parallel Artery Design

Working Fluid	Sodium
Wick Material	Nickel
Temperature	700°C
Dome Radius	9.5 in.
Wick Thickness	0.06 in.
Wick Permeability	$6 \times 10^{-12} \text{ m}^2$
Pore Radius	$1.9 \times 10^{-5} \text{ m}$
Boiling Limit	125 W/cm^2
<u>Number of Arteries</u>	<u>Heat Flux q/A (W/cm^2)</u>
2	19.7
4	54.8
6	107.5
8	177.6

The radial artery design, as illustrated in Figure 8, has been selected for the ASCS program. This design appears to be more compliant than the parallel design and consequently will be more tolerant to thermal stresses. Additionally, the radial design will be somewhat easier to fabricate than the parallel artery design.

Table 5 summarizes the heat pipe design features. Figure 11 is a schematic of the artery design. Two fully-independent sets of arteries are provided for redundancy. Consequently, if one artery system fails the other system will be able to handle the heat load.

TABLE 5. Heat Pipe Design Features

<u>PARAMETER</u>	<u>MAGNITUDE</u>
Evaporator Diameter (in)	19
Wick Thickness (in)	0.060
Wick Material	Sintered Nickel Powder
Mesh Size	-250 + 325
Pore Radius (m)	2.0×10^{-5}
Permeability (m^2)	5.0×10^{-12}
Number of Radial Arteries	8
Number of Circumferential Arteries	2
Artery Inside Diameter (in)	0.093
Working Fluid	Sodium
Mass of Working Fluid (g)	400
Maximum Heat Flux (W/cm^2)	40
Average Heat Flux (W/cm^2)	20

ORIGINAL PAGE IS
OF POOR QUALITY

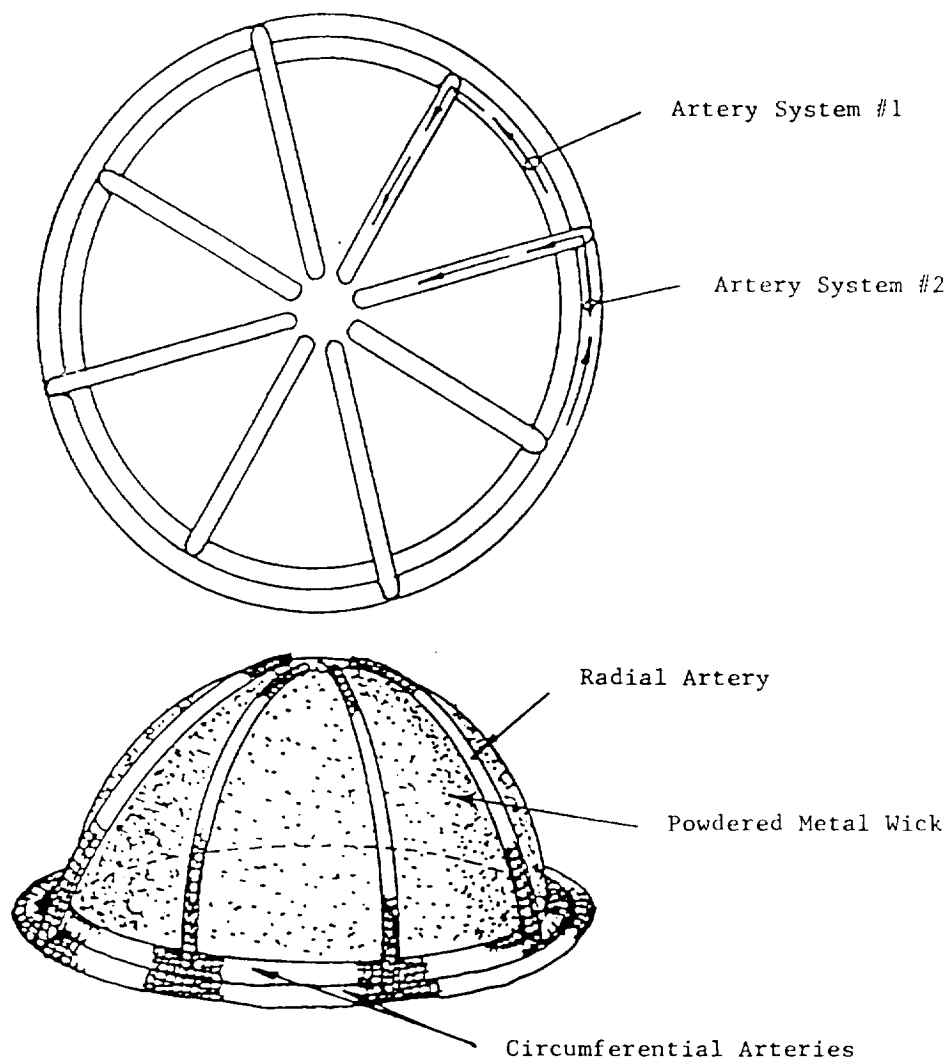


Figure 11. ASCS heat pipe receiver artery structure

The results of the heat pipe performance calculations are shown in Figure 12 along with the expected incident heat flux as calculated by Sanders Associates.

The predicted boiling limit heat flux at 700°C is about 125 W/cm^2 , which is a factor of 3.1 above the maximum incident heat flux.

The wick capillary pumping limit is shown in this figure for the artery system of one circumferential and four radial arteries and for the artery system of two circumferential and eight radial arteries. This figure also shows that if one of the two artery systems should deprime, the wick structure will have sufficient margin to operate on the other artery system.

4.5 TASK 5: ESTABLISH START-UP AND SHUT-DOWN PROCEDURES

This section describes the preliminary work effort to define the start-up and shut-down procedures.

During steady-state operation, liquid sodium is present at the wick-to-sump interface such that the liquid can enter the wick structure. However, during the start-up transient, the sodium in the sump may be frozen. As heat is input to the evaporator, liquid in the sump will begin to melt and enter the wick structure.

As the liquid melts, a void may form between the wick surface and the unmelted sodium mass. This void could potentially prevent liquid from returning to the wick structure. This condition is illustrated in Figure 13.

ORIGINAL PAGE IS
OF POOR QUALITY

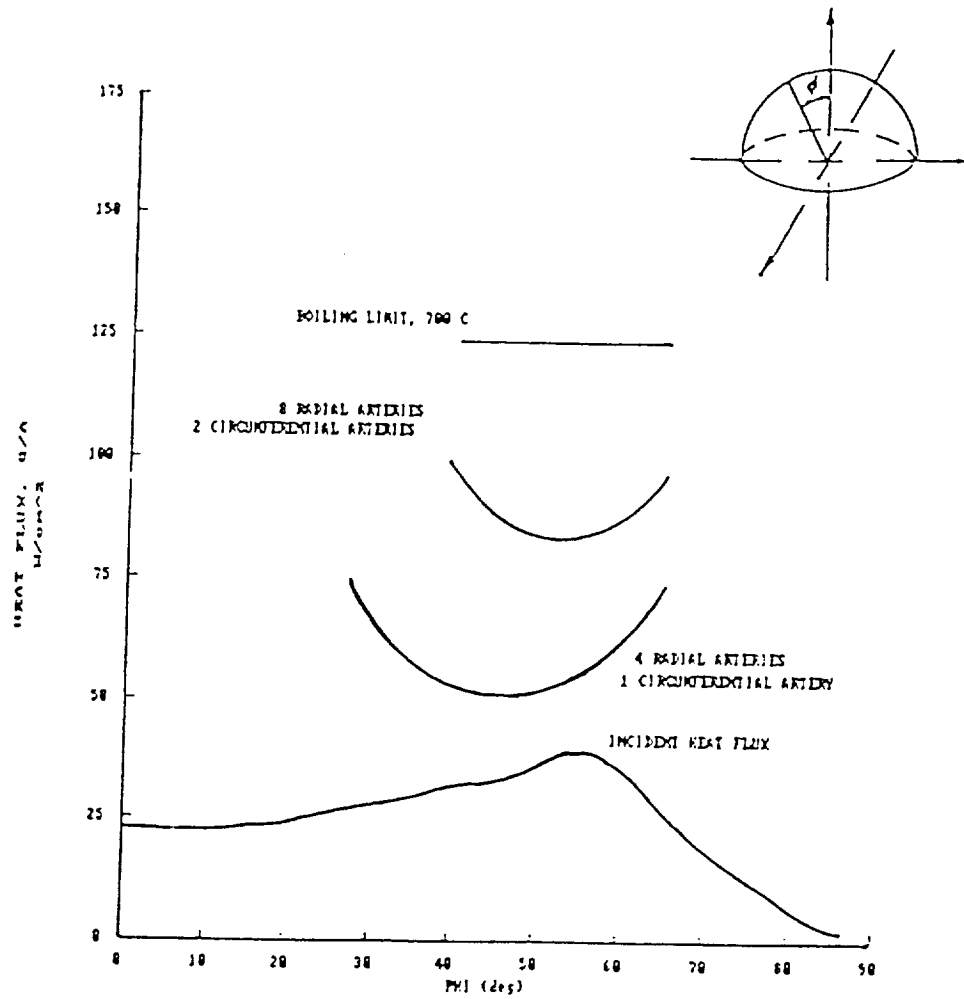


Figure 12. Results of heat pipe performance calculations

CHARACTERISTICS OF FOAM QUALITY

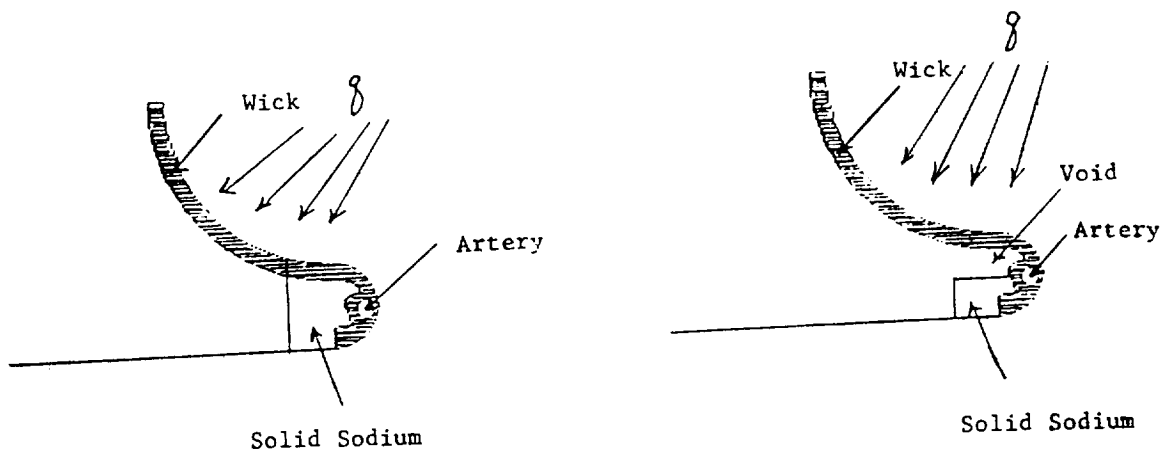


Figure 13. Schematic showing potential void formation during start-up

Two potential methods to prevent this problem have been identified. One method uses fins to provide a conduction path from the wick surface to the unmelted sodium and the other method uses an electrical resistance heater to melt the sodium before start-up.

The resistance heater approach has been selected for this program. It provides a simple method to insure that liquid sodium is available for start-up. Preliminary calculations show that about 160 watts of power are required to maintain the circumferential liquid pool at 150°C while the ambient temperature is -6°C . The resistance heater arrangement is shown schematically in Figure 14. Future development work should evaluate alternative design approaches, such as fins, to assure proper start-up operation.

During the shut-down procedure the receiver should be oriented in a vertical position so that the sodium uniformly fills the sump. This will minimize the time required to melt the frozen sodium before the next start-up cycle.

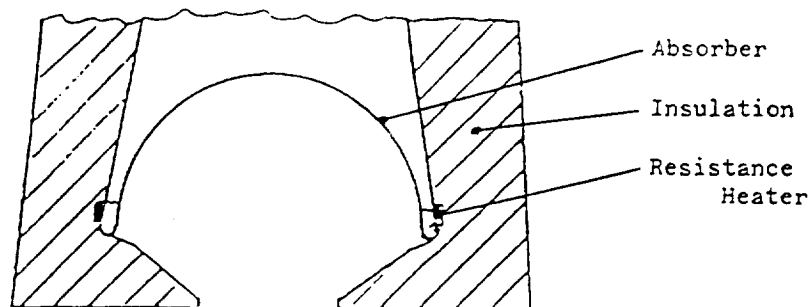


Figure 14. Schematic of resistance heater placement

APPENDIX III

COST PERFORMANCE TRADE-OFF BASIS

BASIS FOR TRADEOFFS BETWEEN MFG COSTS, REPLACEMENT COSTS, O&M COSTS, LIFE AND EFFICIENCY FOR SOLAR/STIRLING POWER MODULE.

The objective of the proposed program is to develop a conceptual design and cost estimate for a SOLAR/STIRLING Power Conversion System from which the economical potential of the concept can be determined. (i.e. the average annual cost of producing electric power in \$/kwh with such a system.)

There are several design decisions in which the best trade-off between initial cost, replacement cost and replacement interval, and efficiency are not self evident. A trade off basis is required to select the detail design parameters or characteristics.

The following are design decisions requiring such trade offs:

(1) Selection of hot side temperature

The initial cost and performance of the engine is a strong function of the material selected and the operating temperature of the hot side components. The cost of the receiver and heat transport components are also a function of the material selected to meet the temperature requirements.

In the temperature range 700C to 800C the number of materials available with useful creep strength is quite small and both the raw material and fabrication costs increase as the product of temperature and life increase.

The trade off basis will be used to select the

operating temperature and determine if there is an economic advantage to designing for replacement at intervals less than the full design life of 30 years (90000 hrs).

During the temperature selection process the engine pressure will also be selected and the potential of an active pressure control system assessed.

(2) Selection of alternator concept and characteristics

There are two basic alternator types being considered. One type uses permanent magnets to generate the flux and the second induces the flux with a d.c. coil.

There are variations in manufacturing cost and efficiency for which a trade off is required to select the best design.

(3) Seal characteristics

(a) For the initial reference non contacting seals will be evaluated. The manufactured cost is a function of the clearances and tolerances specified. The goal is the development of an inherently producible design which minimizes tolerance stack ups on clearances. There will still be a trade off between manufacture cost and efficiency in setting the final clearances.

(b) If acceptable cost or efficiency cannot be achieved with non contacting seals the potential of contact seals to meet the goals will be evaluated. This will require a trade off between initial cost, efficiency and replacement cost/seal life.

(4) Cooling System

The radiator size, fan size (power) and coolant pump size (power) will be selected to optimize the cold side temperature to give a balance between efficiency and cost.

UNIT COST FORMULATION

The basis for the trade offs will be a simplified estimate of the average unit cost of producing electric power .

The total unit cost is given by:

$$UT = \frac{\text{Average annual cost (\$)}}{\text{Annual production (kwhe)}}$$

The total unit cost is assumed to be made up of the following components:

UC = Unit cost required to recover the initial installation cost of the collector/receiver/engine-alternator.

UB = Unit cost required to recover capital cost of the balance of plant.

UR = Unit cost required to cover the average annual cost of replacements (major overhaul) on the engine.

UOMS = Annual operating and maintenance cost for the solar module, excluding major overhaul.

UOMB = annual operating and maintenance cost for the balance of plant.

$$UT = UC + UB + UR + UOMS - UOMB$$

UB and UOMS are assumed independent of the engine cost and performance

UOMS is assumed to be small compared to UC and UR

For the trade off analyses the basis will thus be to minimize US

where $US = UC + UR$.

For this study the heat delivered to the receiver of one solar module is defined in the attached table. This is based on the Test Bed Collector at Sandia.

i.e. 75 kwt at design point

191725 kwt/year

2978 operating hours per year

The peak input to the collector is assumed to be 100 kwt and the installed cost is assumed to be \$150/kwt for a total of \$15000.

The installed cost of the engine-alternator plus receiver is expected to be in the range \$10000 to \$15000. For the trade off analyses a nominal value for US of \$27500 will be used initially.

This will be updated after the first cost estimate is made.

The annualized cost of the initial installation is assumed to be given by:

$$US = F * CS$$

CS = installation cost of the solar module.

F = A capital recovery factor.(assumed to be 0.1 for the long life equipment.)

The annualized cost of major overhauls involving replacements is assumed given by:

$$UR = G * CR \quad \text{where } G = TR ** -(1+F)$$

CR = The cost of the major overhaul (\$)

TR = The time between replacements (years)

G = a factor to adjust the average from the simple CR/TR to account for the cost advantage in delaying expenditures.

The annual energy output of a solar module is given by:

$$ETAA * QIN \quad (\text{kwe/yr})$$

ETAA = The seasonal average efficiency of the receiver plus engine-alternator.

QIN = The seasonal input to the receiver (kwt)

ETAA is assumed to be $.92 * ETAD$ where ETAD is the efficiency at the design point input of 75kwt.

The annual energy output is thus:

$$AKWH = ETAD * .92 * 196000 = ETAD * 172600 \text{ kwe/yr}$$

The unit cost US is given by:

$$US = \frac{F * CS + G * CR}{AKWH} = \frac{F * CS + G * CR}{ETAD * 172600}$$

The trade off basis is the minimization of US.

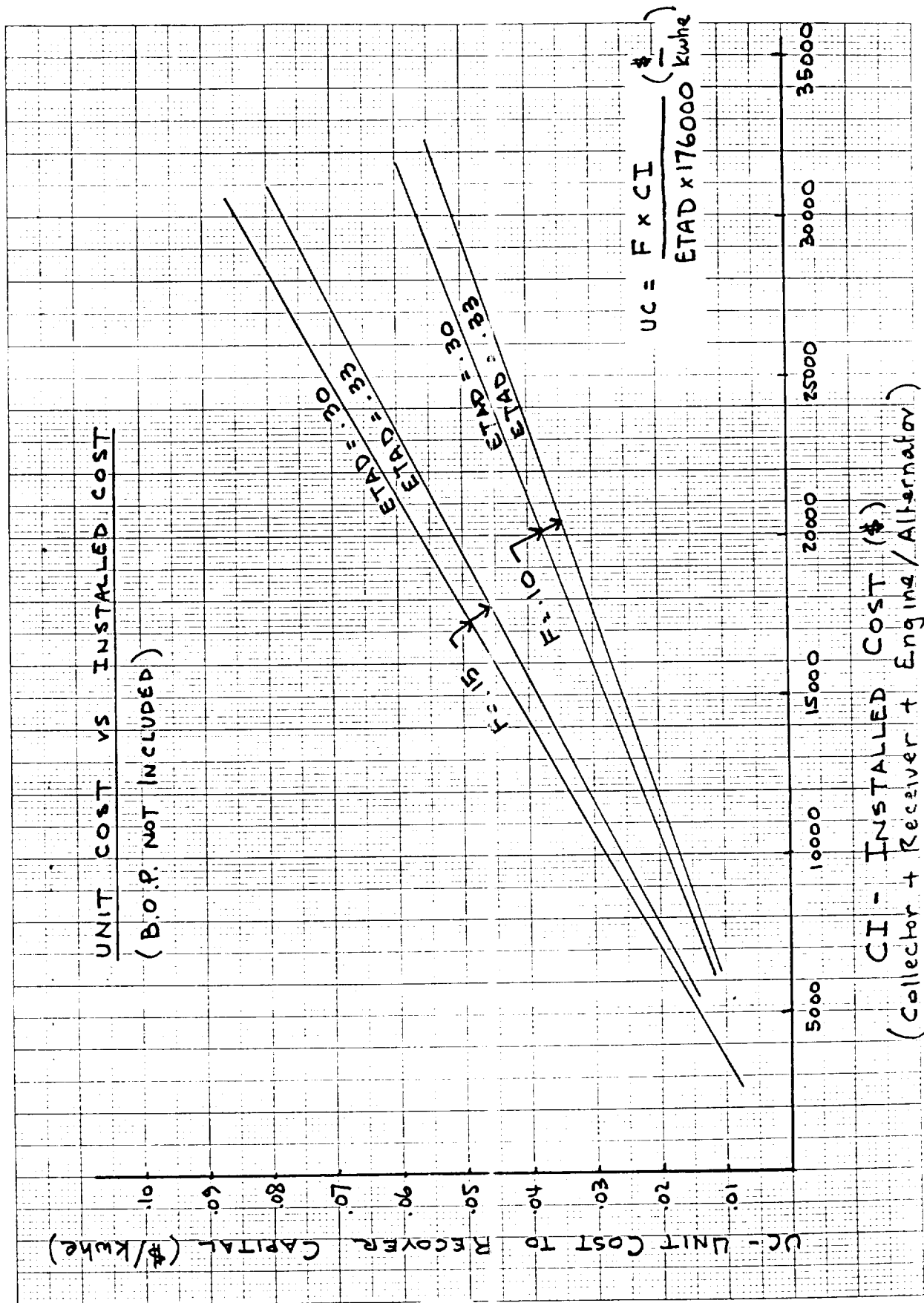
ORIGINAL PAGE IS
OF POOR QUALITY

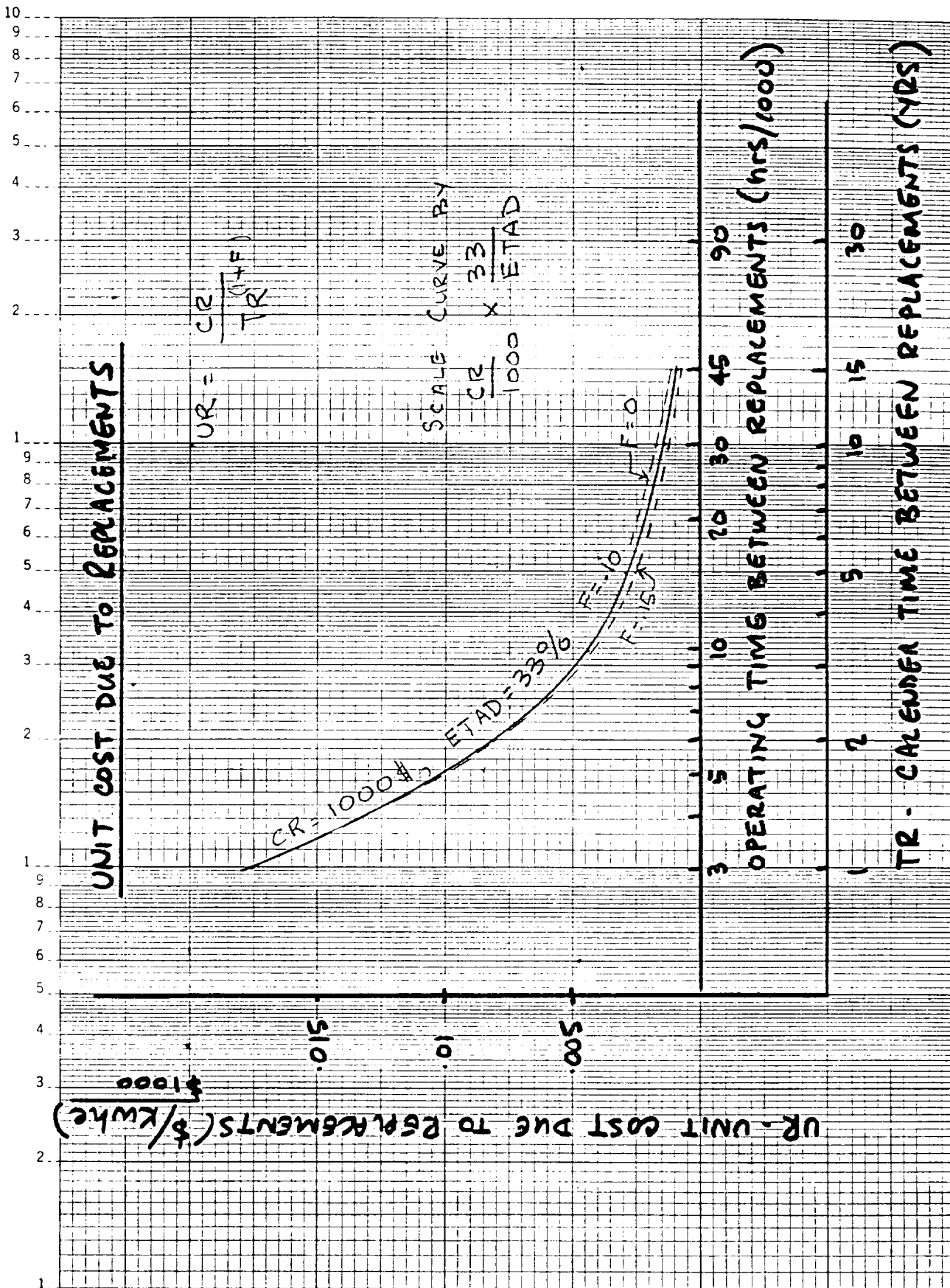
TABLE 2-1
CALCULATION OF YEARLY KILOWATT-HOURS

(Receiver) Solar Insolation (kW _t)	Power Conversion Efficiency (%)	Hours	output kW-hr	Input kWhr
4	Engine assumed off	5091	0	20364
11.8	Engine assumed off	276	0	3257
19.7	Engine assumed off	201	0	3459
27.6	Engine assumed off	216	0	5961 (3354)
35.5	21	181	1349	6426
43.3	25	229	2485	9915
51.3	27	261	3615	13389
59.2	29	444	7623	26285
67.1	31	674	14020	45225
75.	33	1021	25270	76575
82.8	31	168	4312	13910
TOTAL			58,666	191725

$$\frac{58666}{191725} = 30.6\%$$

$$\frac{30.6}{330} = 92\%$$





TRADE OFF BETWEEN INSTALLED COST AND EFFICIENCY. (with no replacements)

The cost to produce one kilowatt hour of electricity is:

$$UC = (F * CI) / (ETAD * 176000)$$

For an incremental increase in installed cost $\Delta(CI)$ and an incremental increase in system efficiency $\Delta(ETAD)$

The increment in unit cost is :

$$\Delta(UC) = (F * \Delta(CI) / 176000) / (\Delta(CI)/CI - \Delta(ETAD)/ETAD)$$

For $\Delta(UC)$ to be less than zero

$$\Delta(CI)/CI \text{ must be less than } \Delta(ETAD)/ETAD$$

For CI about \$30000 and ETAD about 33%

ONE POINT IN EFFICIENCY IS WORTH ABOUT \$900 IN INSTALLED COST.

Table A-6. Current Technology and Long-Term Component Goals — Continued

	Long-Term Component Goals ^(a)	
	Electric ^(b)	
	Annual Efficiency (%)	Cost (1984 \$)
OPTICAL MATERIALS	92	10/m ²
CONCENTRATORS		
Central Receiver	64	40/m ^{2(d)}
Dish	78	130/m ²
Trough	(e)	—
RECEIVERS		
Central Receiver	90	30/m ²
Dish	90	40 30 /m ²
Trough	—	—
TRANSPORT		
Central Receiver	99	25/m ²
Dish	99	7/m ²
Trough	—	—
STORAGE		
Central Receiver	98	20/kWht
Dish	—	—
Trough	—	—
CONVERSION ^(f)		
Central Receiver	39	350/kWe
Dish	41	300/kWe
Trough	—	—
BALANCE OF PLANT		
Central Receiver	NA ^(h)	30/m ²
Dish	NA	20/m ²
Trough	—	—
SYSTEM ^(g)		
Central Receiver	22	1000/kWe
Dish	28	1200/kWe
Trough	—	—
OPERATIONS & MAINTENANCE		
Central Receiver	NA	9/m ² -year
Dish	NA	10/m ² -year
Trough	—	—
ENERGY COST ⁽ⁱ⁾		
Central Receiver	NA	0.04/kWhe
Dish	NA	0.05/kWhe

Table A-6. Current Technology and Long-Term Component Goals — Continued

	Long-Term Component Goals ^(a)	
	Electric ^(b)	Assumptions
	Annual Efficiency (%)	Cost (1984 \$)
		Collector Net Power 100 m ² 25 kWe
OPTICAL MATERIALS	92	10/m ² ← ~\$15000
CONCENTRATORS	64	40/m ^{2(d)}
Central Receiver	78	130/m ² ←
Dish	(e)	—
Trough		
RECEIVERS	90	30/m ²
Central Receiver	90	10 30/m ² ←
Dish	—	—
Trough	—	—
TRANSPORT	99	25/m ²
Central Receiver	99	7/m ² ←
Dish	—	—
Trough	—	—
STORAGE	98	20/kWh
Central Receiver	—	—
Dish	—	—
Trough	—	—
CONVERSION ^(f)	39	350/kWe
Central Receiver	41	300/kWe ← ~\$8000
Dish	—	—
Trough	—	—
BALANCE OF PLANT	NA ^(h)	30/m ²
Central Receiver	NA	20/m ² ← ~\$2000
Dish	—	—
Trough	—	—
SYSTEM ^(g)	22	1000/kWe
Central Receiver	28	1200/kWe ← ~\$30000
Dish	—	—
Trough	—	—
OPERATIONS & MAINTENANCE	NA	9/m ² ·year
Central Receiver	NA	10/m ² ·year ← ~1000 \$/yr
Dish	—	—
Trough	—	—
ENERGY COST ⁽ⁱ⁾	NA	0.04/kWhe
Central Receiver	NA	0.05/kWhe
Dish	—	—

OBSERVATIONS ON COST GOALS IN TABLE A6

- The cost goal for the receiver plus HTS
plus engine/alternator is ~\$13,000
or ~500\$/kWe
- Engine/alternator and receiver performance vs. cost trade-off
is about 1200\$/kWe
i.e. 1 point in receiver efficiency (90% nominal) is worth ~\$300
1 point in E/A efficiency (35% nominal) is worth ~\$850
- For 65,000 kWh/year and 2000\$/yr
O&M cost in Table \equiv .015\$/kWh out of total of .05\$/kWh
(Proposed system excluding collector and BOP is projected
to be very small)
- Trade-off between O&M and capital cost
100\$ O&M ~1000\$ Capital Cost

SIMPLIFIED COST/PERFORMANCE TRADE OFF

$$UC = (F * C) / (Ne * Pdes)$$

UC = \$/kwh to recover capita

C = Capital cost per collector-engine system

F = Capital recovery factor

Ne = Operating hours per year * (Pav/Pdes)

Pdes = Design power output

$$Del(UC) = (F/Ne) * (C * Del(P) - P * Del(C)) / (P * P)$$

Del(UC) must be less than zero for acceptable trade off.

For Ne and F constant

$$Del(C) / Del(P) \text{ must be less than } C / P$$

For C = \$30000 and P = 25 kw

$$DEL(C) / Del(P) \text{ MUST BE LESS THAN } 1200\$/kwh$$

(Note: Trade off is independent of absolute values of F or Ne.

O&M versus CAPITAL COST

Total unit cost is given by

$$U(\text{tot}) = U(\text{O\&M}) + U(\text{CAP})$$

$$= (C(\text{O\&M}) + F * C(\text{CAP})) / (N * P)$$

For N and P constant

$$\text{Del}(U(\text{tot})) = \text{Del}(C(\text{O\&M})) + F * (\text{Del}(C(\text{CAP})))$$

$\text{Del}(U(\text{tot}))$ must be less than zero for acceptable tradeoff

For $F = .01$ UP TO \$1000 IN CAPITAL COST COULD BE SPENT TO SAVE 100 \$/yea IN O&M COSTS.

APPENDIX IV

PRELIMINARY DESIGN DESCRIPTION

This appendix is included for completeness and summarizes the design presented at the Preliminary Design Review. Some of the features, such as foil regenerators and/or a ceramic piston, might be considered for future designs.

Figure A4.1 is a cross section through the engine alternator. By comparing with Figure 4.1 the differences between the preliminary and final conceptual design layouts can be seen.

The major differences are:

1. The foil regenerator is smaller in diameter (9.5 in. vs. 10.5 in.) and longer (5.0 in. vs. 3.0 in.) The hot vessel diameter is correspondingly smaller and the hot vessel and displacer dome are correspondingly shorter.
2. The vessel head wall thickness is somewhat larger reflecting the higher design temperature (800°C vs. 700°C) in the preliminary design.
3. Minor changes were made in the receiver shell to reduce the joints exposed to sodium.
4. The reference joint in the vessel wall outboard of the cooler was selected to be a friction weld. Due to cost and technical uncertainties this was changed to a "wedged braze joint" at the bottom of the cooler.
5. The displacer assembly was unchanged except for the geometry of the piston to body joint.
6. The power piston and piston cylinder were made from a structural ceramic with silicon carbide the tentative selection. This permitted a

lighter piston. The stuffers and static seal at the stator support, which are included in the final design, were not required to adjust the power piston gas spring volume.

7. Alternator cooling is not shown in Figure A3.1, but a cooling jacket around the vessel was intended. This is replaced by internal air cooling coil on the final design.

Figures A4.2 through A4.10 show the subassemblies and the assembly procedures.

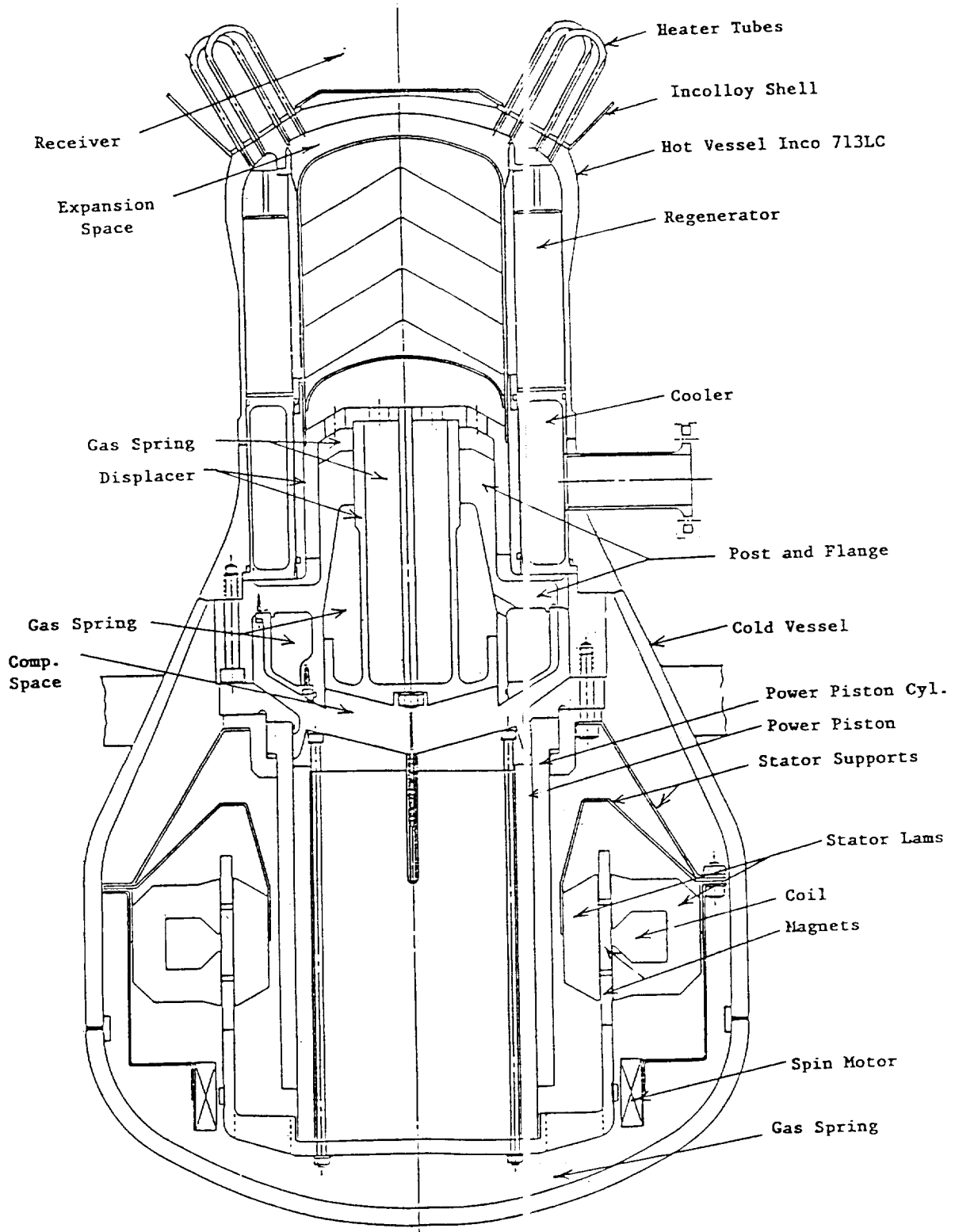


Fig A4.1

ASCS ENGINE ALTERNATOR

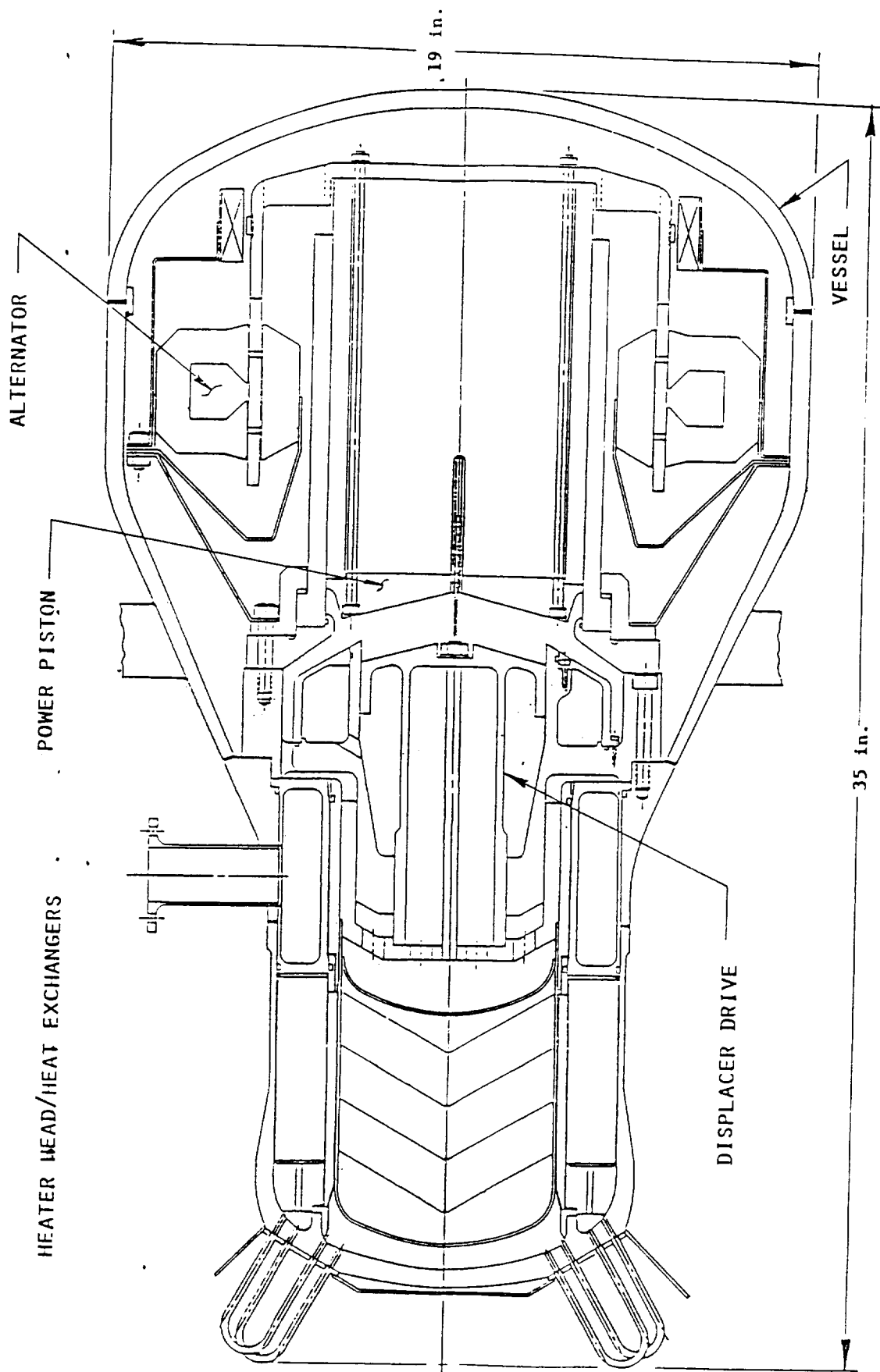


Fig. A4.2
 ASCS ENGINE/ALTERNATOR SYSTEM BREAKDOWN

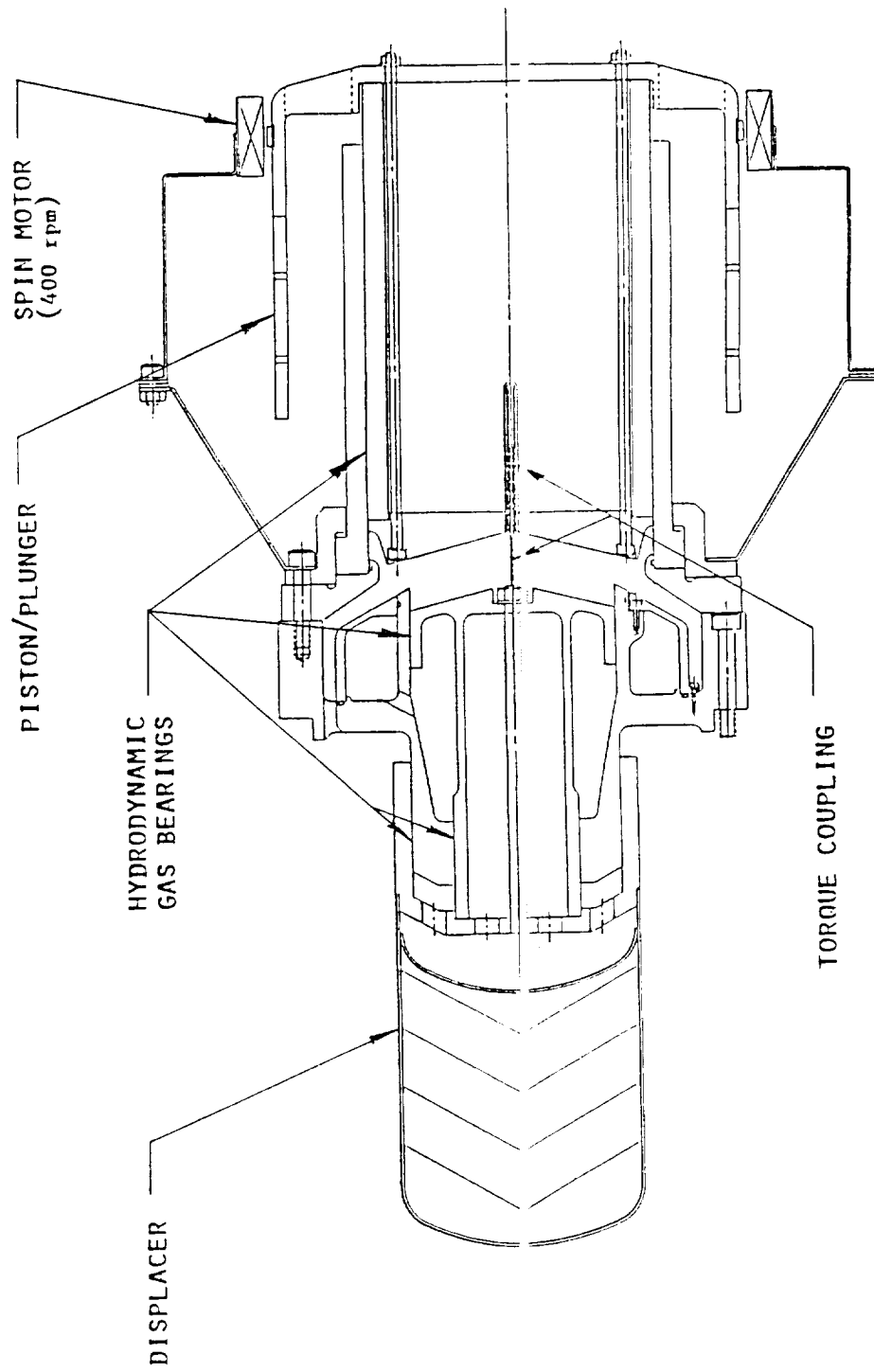


Fig. A4.4

HYDRODYNAMIC BEARINGS ARRANGEMENT

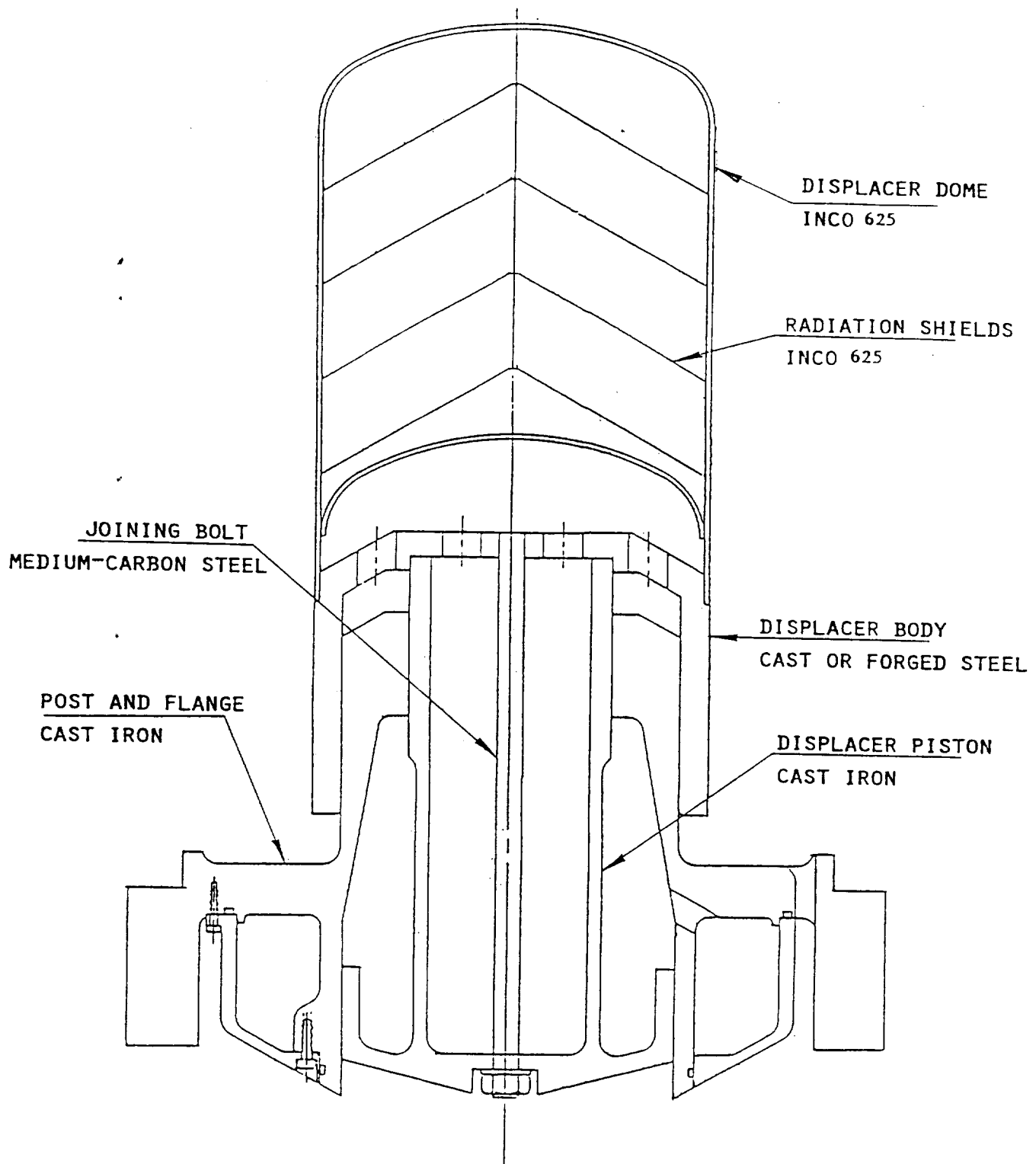


Fig. A4.5

DISPLACER DRIVE ASSEMBLY

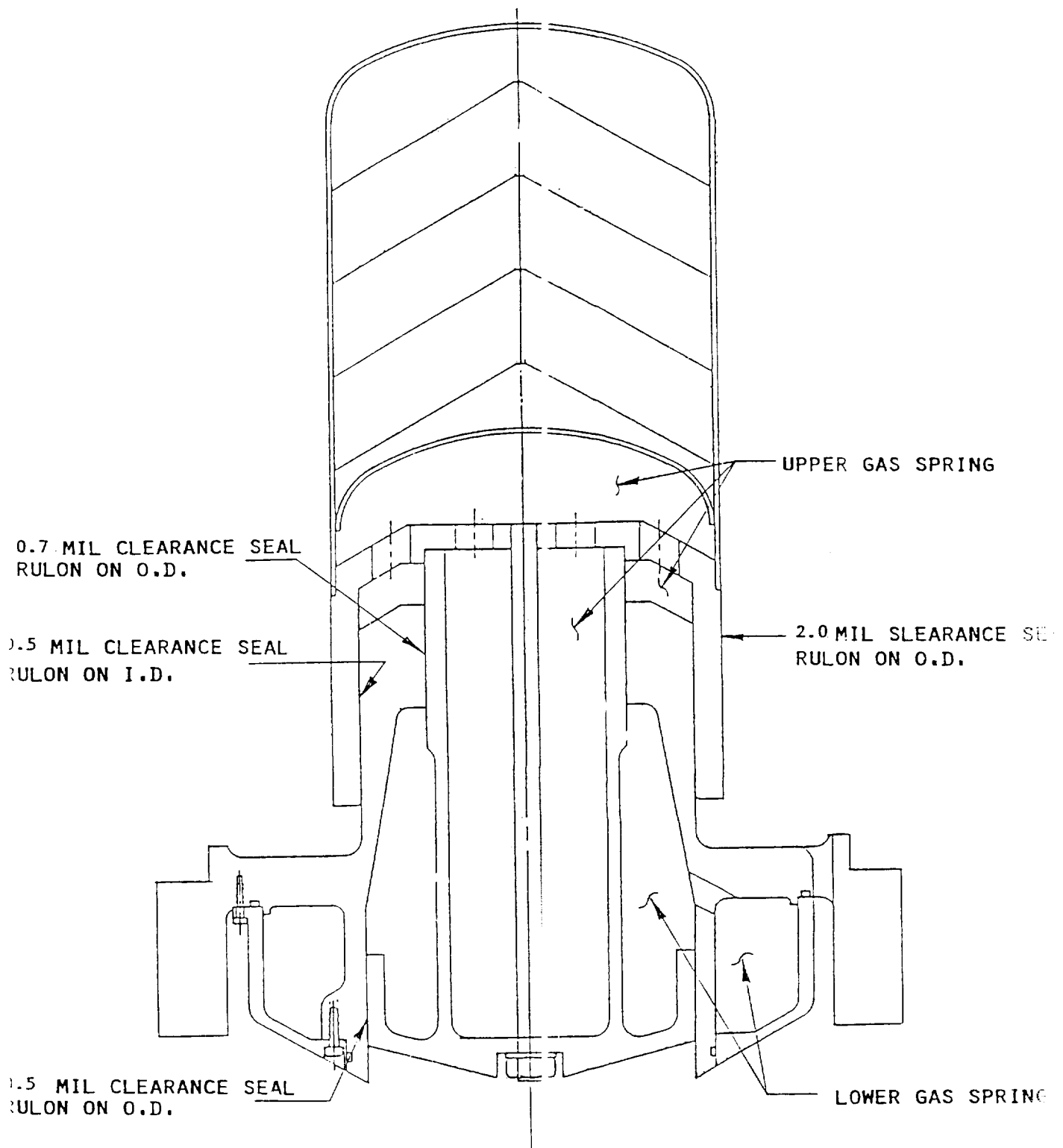


Fig. 4.6

DISPLACER DRIVE ASSEMBLY - SEALS

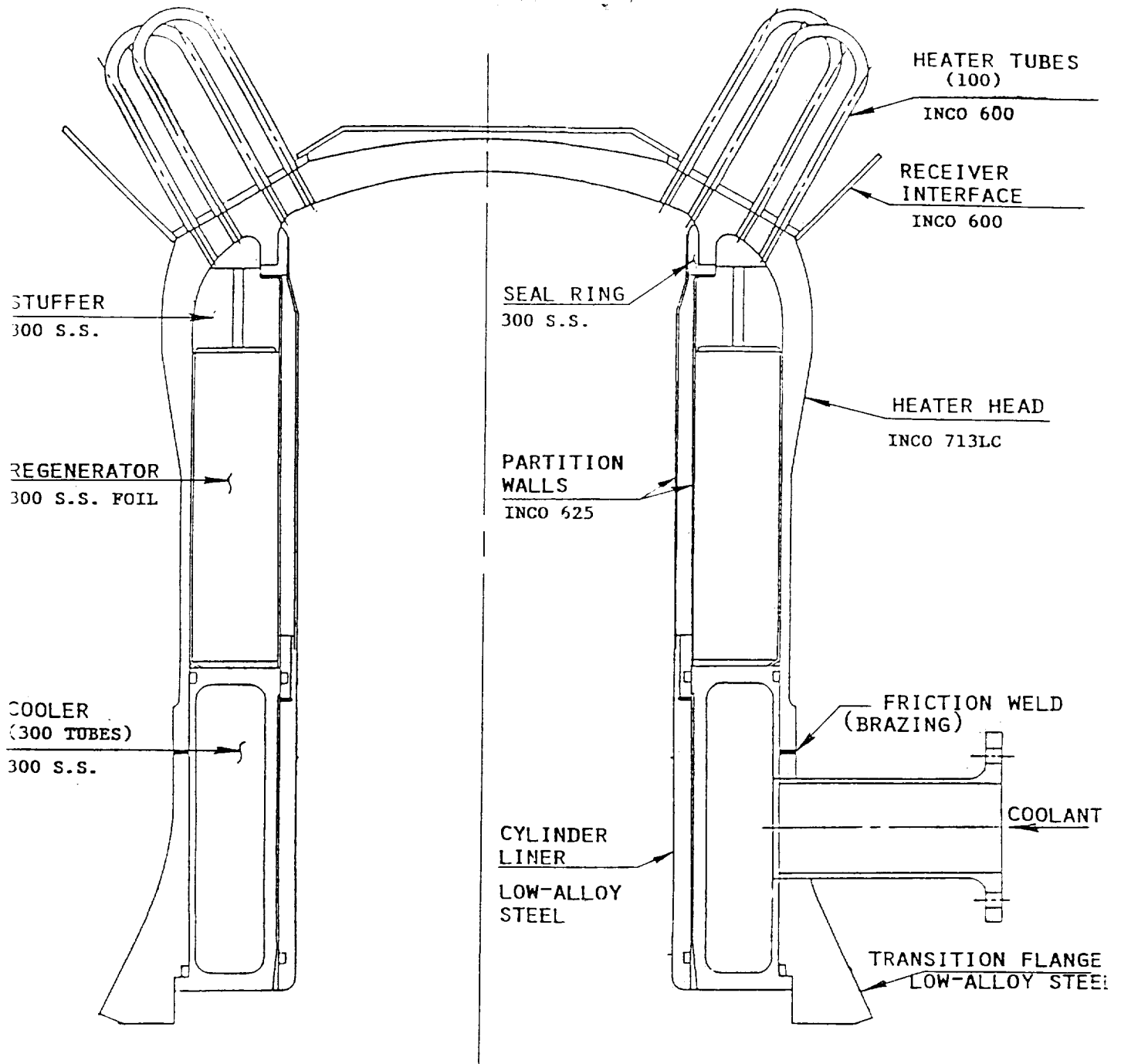


Fig. A4.7

HEATER HEAD/HEAT EXCHANGERS ASSEMBLY

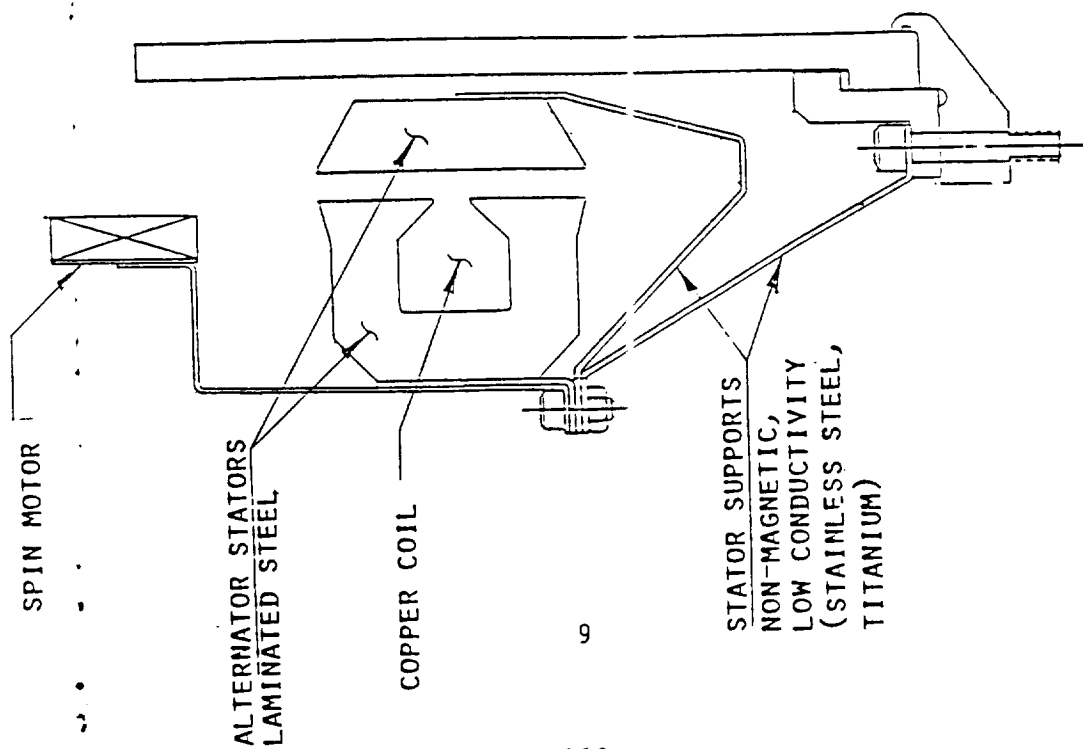
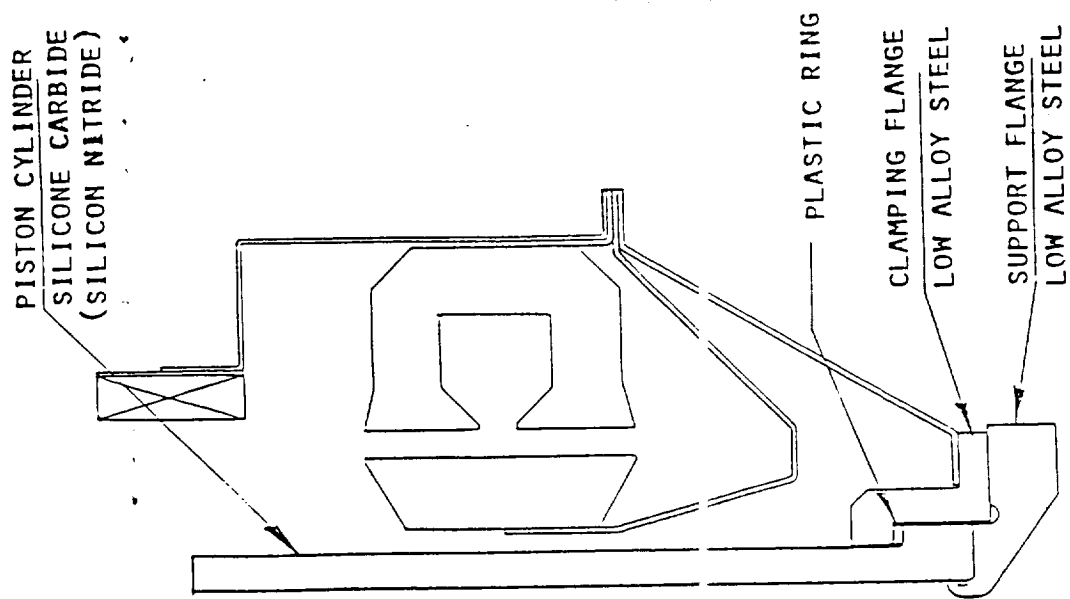


Fig. A4.8

PISTON CYLINDER/ALTERNATOR ASSEMBLY

ORIGINAL PAGE IS
OF POOR QUALITY

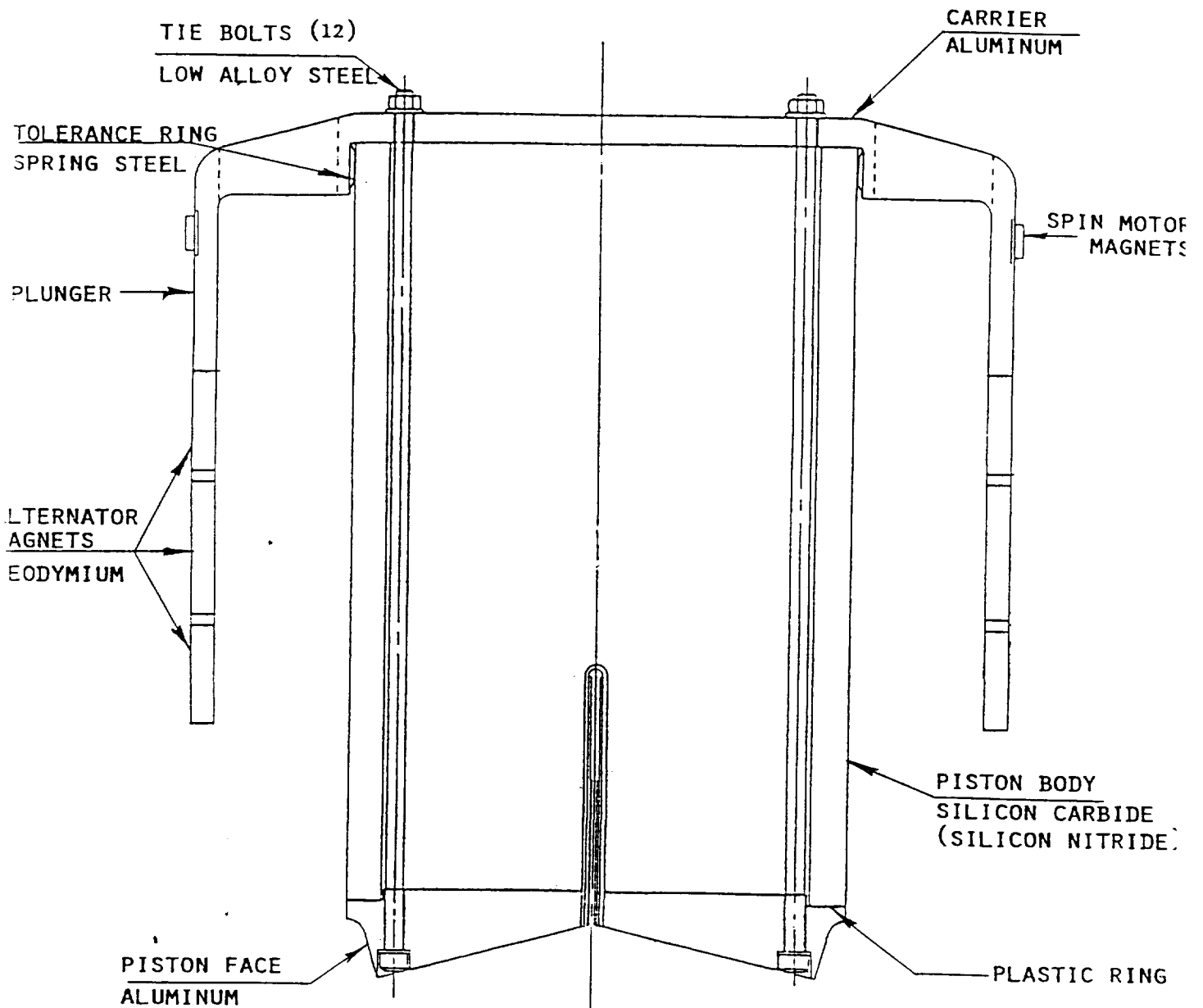


Fig. A4.9

POWER PISTON/PLUNGER ASSEMBLY

1. WELD VESSEL MINUS END CAP
2. INSTALL HEAT EXCHANGERS
3. INSTALL DISPLACER DRIVE
4. INSTALL PISTON CYLINDER, STATORS, AND SPIN MOTOR

5. INSERT FIXTURE TO ALIGN ALTERNATOR
6. TIGHTEN BOLTS
7. INSERT POWER PISTON/PLUNGER

8. WELD END CAP IN PLACE
9. EVACUATE AND CHARGE VESSEL WITH H_e

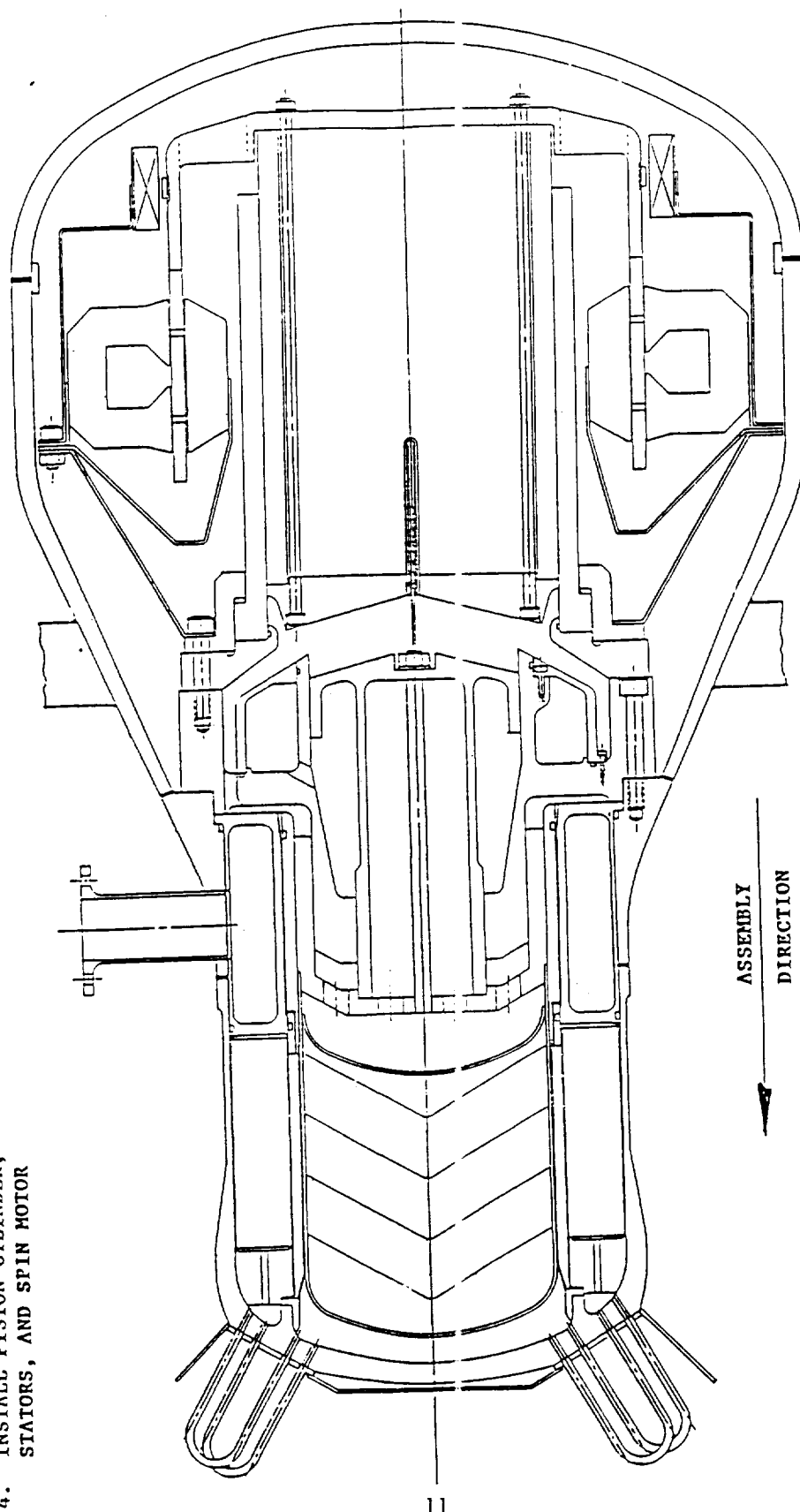


Fig. A4.10

ASCS ENGINE: GENERAL ASSEMBLY

APPENDIX V

COST ANALYSIS FOR MECHANICAL TECHNOLOGY 25 KW SOLAR DRIVE
ELECTRICAL GENERATOR AS FORECAST UTILIZING PARETO'S LAW

FINAL REPORT

October 1967

Prepared For:

Mechanical Technology Incorporated/NASA Lewis Research Center

G. Dockett
Mechanical Technology Incorporated
968 Albany-Shaker Road
Latham, New York 12110

R.K. Shaltens
Project Manager
NASA Lewis Research Center
21000 Brookpark Road
Cleveland, Ohio 44135

Prepared By:

A. Wurfel, R. Gladstone, R. Osen, and R. Heitsch

Pioneer Engineering and Manufacturing Company
Research and Development Division
32384 Edwards
Madison Heights, Michigan 48071

RESEARCH SUMMARY

Title Cost Analysis For Mechanical Technology 25 KW Solar Drive Electrical Generator As Forecast Utilizing Pareto's Law

Contractor Pioneer Engineering & Manufacturing Company, Research & Development Division

Principle Investigators A. Wurfel, R. Gladstone,
R. Osen, R. Heitsch

Objective To analyze cost by functional groupings for competitive comparison. This costing technique to utilize Pareto's Law, where deemed applicable. 10,000 units per annum was the given volume.

AREAS OF COMPARISON

<u>M.T.I.</u>		<u>S.T.C.</u>
	RECEIVER	
Receiver Shell		Receiver Shell
Arteries		Reflex Boiler
Wicking		
	CONVERSION SYSTEM	
Stirling Engine With		Stirling Engine
Vibration Assembly		
	POWER GENERATION	
Linear Alternator		Hydraulic Output and Generator
	POWER CONDITIONING AND CONTROLS	
Temperature Sensors		Capacitor Banks
Accelerometers		Synchronous Machine
Auto Transformer		
Tuning Capacitors		
	AUXILIARIES	
Radiator		Filter 2/10 Micron
Fan and Driver		Isolation Valve
Water Pump and Driver		Fan and Driver
		Pump and Driver
		Radiator

Results This device was processed and costed from undimensioned layouts and detail drawings. Tolerance discussions were held with the design contractor and applicable tolerances were assigned to each manufacturing operation; these tolerances are reflected in the costing. Where exotic materials were encountered and quantities currently available on the open market were not found, extrapolations were made to predict cost based on a driven market assumption. All costs for this exercise are based on a 10,000 unit volume. All processes utilized are current state-of-the-art and do not reflect any forecast outreach. Final costs, as estimated by Pioneer, are based upon Pareto's Law which basically states that 20% of the major items constitutes 80% of the whole. Identical approaches were taken on the competitive designs with the exception on tolerances; the competitive design exercise included detail drawing of components which were costed.

iii

Technical
Approach

Components were analyzed for complexity and 20% of the total detail were selected to be cost representative, utilizing Pareto's Law. These selected components were detail processed and costed utilizing Pioneer's computerized asset center costing method. Verbal and written dialogues were maintained with design contractors. Total costs were generated utilizing Pareto's Law and these cost reflect Michigan labor and material cost as we know for the year 1986. Extrapolations were made to reflect 1984 cost as well.

CONTENTS

	<u>PAGE</u>
RESEARCH SUMMARY	iii
COST SUMMARIES	1
DETAIL COSTING AND PROCESS	5
COMPARISON OF 713LC VERSUS XF-818 HEATER HEAD DOME	99
PATENT INFORMATION	108
EQUIPMENT COST ANALYSIS BY VOLUME	116
COSTING METHODOLOGY	118

RECAP OF MANUFACTURING COST FOR
MTI 25 KW SOLAR DRIVEN STIRLING ENGINE ELECTRICAL GENERATOR

1986 COST

PAGE KEY		MATERIAL COST	DIRECT LABOR COST	BURDEN COST	SCRAP ALLOWANCE	MANUFACTURING COST	LABOR MINS.
5	1. Receiver Shell Arteries Wicking	\$ 592.07	\$ 8.66	\$ 53.35	\$ 6.51	\$ 660.59	39.50
15&59	2. Stirling Engine With Vibration Absorber	3,958.13	111.23	284.06	41.94	4,395.36	504.15
68	3. Linear Alternator	863.27	31.58	161.04	10.56	1,066.45	141.60
86	4.* Temperature Sensors Accelerometers Auto Transformer Tuning Capacitors	453.01	7.54	31.18	.40	492.13	7.54
98	5.** Radiator Fan & Driver Water Pump & Driver	921.61				921.61	
		\$ 6,788.09	\$159.01	\$529.63	\$59.41	\$ 7,536.14	692.79
	Praeto's Extension @ 125% On Cost	\$ 8,485.11	\$198.76	\$662.04	\$74.26	\$ 9,420.18	692.79

* As quoted from engineering information as supplied.

**Cost adjusted for comparison, engineering information not complete for direct comparison.

Estimated Tooling Cost: \$802,200

Estimated Capital Equipment: \$4,108,200

RECAP OF MANUFACTURING COST FOR
MTI 25 KW SOLAR DRIVEN STIRLING ENGINE ELECTRICAL GENERATOR
1984 COST

PAGE KEY		MATERIAL COST	DIRECT LABOR COST	BURDEN COST	SCRAP ALLOWANCE	MANUFACTURING COST	LABOR MINS.
5	1. Receiver Shell Arteries Wicking	\$ 521.02	\$ 7.88	\$ 46.95	\$ 5.79	\$ 581.64	39.50
15&59	2. Stirling Engine With Vibration Absorber	3,483.15	101.22	252.81	37.33	3,874.51	504.15
68	3.*** Linear Alternator	863.27	28.73	141.72	9.40	1,043.12	141.60
86	4.* Temperature Sensors Accelerometers Auto Transformer Tuning Capacitors	398.65	6.86	27.44	.35	433.30	7.54
98	5.** Radiator Fan & Driver Water Pump & Driver	811.02				811.02	
		\$ 6,077.11	\$144.69	\$468.92	\$52.87	\$ 6,743.59	692.79
	Pareto's Extension @ 125% On Cost	<u>\$ 7,596.39</u>	<u>\$180.86</u>	<u>\$586.15</u>	<u>\$66.09</u>	<u>\$ 8,429.49</u>	<u>692.79</u>

* As quoted from engineering information as supplied.

** Cost adjusted for comparison, engineering information not complete for direct comparison.

***No material cost adjustment as magnetic materials not quotable in 1984.

Estimated Tooling Cost: \$802,200

Estimated Capital Equipment: \$4,108,200

RECAP OF MANUFACTURING COST FOR
MTI 25 KW SOLAR DRIVEN STIRLING ENGINE ELECTRICAL GENERATOR WITH XF818 HEATER HEAD
1986 COST

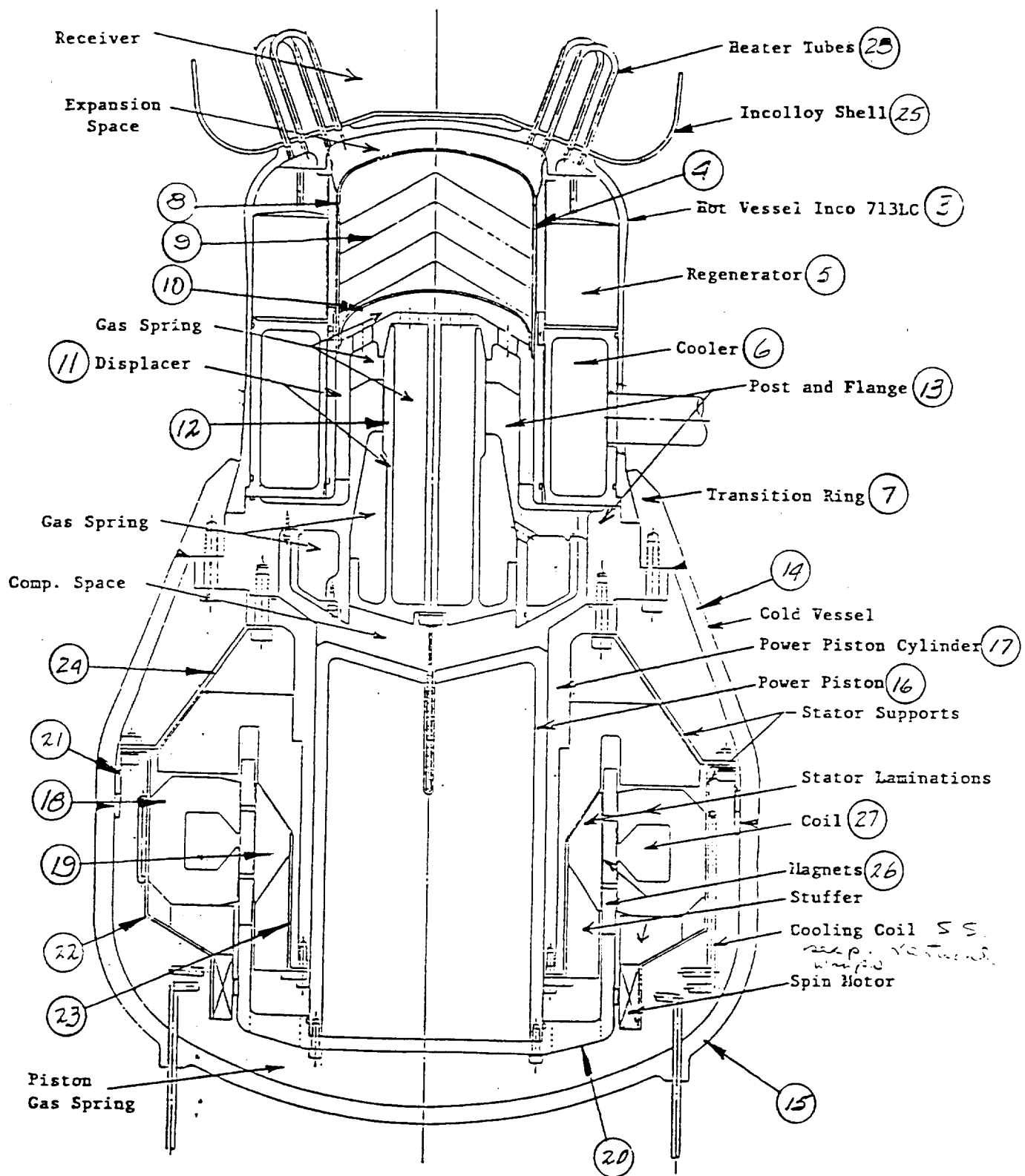
PAGE KEY		MATERIAL COST	DIRECT LABOR COST	BURDEN COST	SCRAP ALLOWANCE	MANUFACTURING COST	LABOR MINS.
5	1. Receiver Shell Arteries Wicking	\$ 592.07	\$ 8.66	\$ 53.35	\$ 6.51	\$ 660.59	39.50
15&59	2. Stirling Engine With Vibration Absorber	4,499.93	111.23	284.06	47.36	4,942.58	504.15
68	3. Linear Alternator	863.27	31.58	161.04	10.56	1,066.45	141.60
86	4.* Temperature Sensors Accelerometers Auto Transformer Tuning Capacitors	453.01	7.54	31.18	.40	492.13	7.54
98	5.** Radiator Fan & Driver Water Pump & Driver	921.61				921.61	
		\$ 7,329.89	\$159.01	\$529.63	\$64.83	\$ 8,083.36	692.79
	Praeto's Extension @ 125% On Cost	\$ 9,162.36	\$198.76	\$662.04	\$81.04	\$ 10,104.20	692.79

* As quoted from engineering information as supplied.

**Cost adjusted for comparison, engineering information not complete for direct comparison.

Estimated Tooling Cost: \$802,200

Estimated Capital Equipment: \$4,108,200



ASCS ENGINE ALTERNATOR

4

26741-ENGINE
A ALTERNATOR

RT6021		PROJECT - 1K		PIONEER ENGINEERING BILL OF MATERIAL WITH COST			PAGE 1 57/09/31		
VOLUME - 10,000		PART - 26741-1		DESC - ASSY RECEIVER			VENDOR		
COMPONENT	DESC - TRUNCATED TOOLING	QTY WEIGHT	MATERIAL	LAB MIN	LABOR \$	PLATEIN	SCRAP	MARK-UP	TOT COST
26741-1-A VENDOR	ARTERY - RADIAL 2.0	8 .0000	8.64	1.60	.32V M	.00 .48	.00 .08	.00	9.52 *
26741-1-B VENDOR	ARTERY CIRCUM 2.0	2 .0000	12.26	.50	.10V M	.00 .18	.00 .12	.00	12.66 *
26741-1C VENDOR	ASSY RECEIVER 67.0	1 16.2300	343.17	24.00	5.31V M	.00 43.34	.00 3.92	.00	395.74 *
26741-2. VENDOR	HEAT PIPE SHELL 60.0	1 14.9000	228.00	13.30	2.93V M	.00 8.35	.00 2.39	.00	241.67 *
COMPONENT TOTAL COST		31.1300	592.07	39.4	8.66V M	.00 52.35	.00 6.51	.00	592.07 659.59
131.0									
ASSEMBLY COST			.00	.0	.00 V M	.00 .00	.00 .00	.00	.00 .00
.0									
TOTAL COST		31.1300	592.07	39.4	8.66 V M	.00 52.35	.00 6.51	.00	592.07 659.59
TOOLING			131.0						

ORIGINAL PAGE IS
OF POOR QUALITY

RT5024 PROJECT - 1K PIONEER ENGINEERING PAGE 1
MANUFACTURING COST ANALYSIS 3.21.27 87/09/31

VOLUME- 10,000 P/A- B
PART # 25741-1-A DESC- ARTERY - RADIAL UPG-

OPER	OPERATION DESCRIPTION		EQUIP	M	STD	LAB COST	SEC HRS	BURDEN	BURDEN	VAR COST	TOOLING
			P	MIN	LAB RATE			RATE	COST	MFG COST	
010			1A	1.0	.100	.0212	.0017 V	.00	.0000	.0000	.0
						.2124	M 16.71		.0284	.0496	
020			5B	1.0	.100	.0212	.0017 V	.00	.0000	.0000	2.0
						.2124	M 20.23		.0344	.0556	

ANNUAL REQ-	80,000		LAB MIN -	.2000	
MAT CODE -	ST/STL	ECOM YR-LOC	LABOR \$ -	.0424	
COST/LB -	.000	PT TYPE - VENDOR	BURDEN V-	.0000	TOOL \$000 2.0
SCRAP FAC -	1.0%	MARK-UP FAC-	BURDEN M-	.0628	
ROUGH WT -	.0000	MARK-UP -	SCRAP -	.0119	TOTAL VAR 1.1971
FINAL WT -	.0000	OTHER -	MATERIAL-	1.0800	TOTAL MFG 1.1971

ORIGINAL PAGE IS
OF POOR QUALITY

ORIGINAL PAGE IS
OF POOR QUALITY

RT6024 PROJECT - 1K PIONEER ENGINEERING MANUFACTURING COST ANALYSIS 3.21.27 PAGE 1 67/08/31

VOLUME- 10,000 P/A- 2 UPE-
PART - 26741-1-B DESC- ARTERY CIRCUM

OPER	OPERATION DESCRIPTION										TOOLING
	EQUIP	M	STD	LAB COST	DOC HAS	BURDEN	BURDEN	VAR COST			
		P	MIN	LAB RATE		RATE	COST	MFG COST			

[illegible]

ANNUAL REQ-	20,000			LAB MIN -	.2500		
MAT CDGE -	ST/STL	ECON YR-LCC		LABOR \$ -	.0531		
COST/LB -	.000	PT TYPE -	VENDOR	BURDEN V-	.0000	TOTL \$000	2.0
SCRAP FAC -	1.0%	MARK-UP FAC-	0.0%	BURDEN M-	.0850		
ROUGH WT -	.0000	MARK-UP -	.0000	SCRAP -	.0627	TOTAL VAR	6.3308
FINAL WT -	.0000	OTHER -	5.1%	MATERIAL-	6.1300	TOTAL MFS	6.3308

RT6024 PROJECT - 1K PIONEER ENGINEERING PAGE 1
MANUFACTURING COST ANALYSIS 3.21.27 87/02/31

VOLUME- 10,000 P/A- 1
PART # 26741-1C DESC- ASSY RECIEVER UPE-

OPER	OPERATION DESCRIPTION		EQUIP	M	STD	LAB COST	DOC HRS	BURDEN	BURDEN	VAR COST	TOOLING
			P	MIN	LAB RATE			RATE	COST	MFG COST	
010			8A	1.0	.400	.0943 .2357	.0067 V M 25.28	.00	.0000 .1694	.0000 .2637	.0
020			BR	1.0	.500	.1179 .2357	.0083 V M 39.76	.00	.0000 .3300	.0000 .4479	50.0
030			7E4C	1.0	1.500	.3291 .2194	.0250 V M 39.89	.00	.0000 .9723	.0000 1.3014	5.0
040			14B	1.0	.500	.1073 .2146	.0093 V M 35.79	.00	.0000 .2971	.0000 .4044	.0
050			7E4C	1.0	4.000	.8776 .2194	.0667 V M 39.89	.00	.0000 2.5940	.0000 3.4716	5.0
060			14D1	1.0	3.000	.5500 .2200	.0500 V M 18.12	.00	.0000 .9060	.0000 1.5560	2.0
070			1A	1.0	2.000	.4248 .2124	.0333 V M 16.71	.00	.0000 .5564	.0000 .9812	5.0
080			2A2	1.0	4.000	.8936 .2234	.0667 V M 25.14	.00	.0000 1.6768	.0000 2.5704	.0
090			20A7	.5	11.000	1.2089 .2198	.1533 V M160.12	.00	.0000 29.3500	.0000 30.5589	.0
100			13A2	1.0	2.000	.4424 .2212	.0333 V M 84.65	.00	.0000 2.8188	.0000 3.2612	.0
110			20A7	.5	1.375	.1511 .2198	.0229 V M160.12	.00	.0000 3.6667	.0000 3.8176	.0

ORIGINAL PAGE IS
OF POOR QUALITY

RT6024 PROJECT - 1K PIONEER ENGINEERING PAGE 2
MANUFACTURING COS ANALYSIS 3.21.27 87/08/31

VOLUME- 10,000 P/A- 1
PART # 26741-10 DESC- ASSY RECEIVER UPG-

OPER	OPERATION DESCRIPTION	EQUIP	M	STD	LAB COST	CCC HRS	BURDEN	BURDEN	VAR COST	TOOLING
				P	MIN	LAB RATE	RATE	COST	MFG COST	

ANNUAL REQ-	10,000						LAB MIN -	24.0875		
MAT CODE -	ST/STL						LABOR \$ -	5.3070		
COST/LB -	9.500						BURDEN V-	.0000	TOOL \$000	67.0
SCRAP FAC -	1.0%						BURDEN M-	43.3375		
ROUGH WT -	25.0700						SCRAP -	3.9181	TOTAL VAR	395.7276
FINAL WT -	14.2300						MATERIAL-	343.1650	TOTAL MFG	395.7276

RTS024 PROJECT - 1K PIONEER ENGINEERING PAGE 1
MANUFACTURING COST ANALYSIS 3.21.27 87/06/31

VOLUME- 10,000 P/A- 1
PART # 26741-2 DESC- HEAT PIPE SHELL UPE-

OPER	OPERATION DESCRIPTION									
	EQUIP	M	STD	LAB COST	CCO HAS	BURDEN	BURDEN	VAR COST	TOOLING	
	P	MIN	LAB RATE			RATE	COST	MFG COST		
010	BC2	2.0	.200	.0943	.0033 V	.00	.0000	.0000	.0	
				.2357	M 82.17		.2712	.3655		
020	BR	2.0	.200	.0943	.0033 V	.00	.0000	.0000	50.0	
				.2357	M 39.76		.1312	.2255		
030	7E4C	1.0	2.000	.4398	.0333 V	.00	.0000	.0000	5.0	
				.2194	M 38.89		1.2950	1.7338		
040	7E4C	1.0	10.000	2.1940	.1667 V	.00	.0000	.0000	5.0	
				.2194	M 35.89		6.4830	8.6770		
050	1441	1.0	.500	.1073	.0023 V	.00	.0000	.0000	.0	
				.2146	M 26.97		.1741	.2814		

ANNUAL REQ-	10,000	LAB MIN -	13.3000		
MAT CODE -	ST/STL	LABOR \$ -	2.5287		
COST/LB -	9.500	PT TYPE -	VENDOR	BURDEN V-	.0000
SCRAP FAC -	1.0%	MARK-UP FAC-	0.0%	BURDEN M-	9.3545
ROUGH WT -	24.0900	MARK-UP -	.0000	SCRAP -	2.3928
FINAL WT -	14.9900	OTHER -	.000	MATERIAL-	228.0000
				TOTAL VAR	241.6760
				TOTAL MFG	241.6760

ORIGINAL PAGE IS
OF POOR QUALITY

ESTIMATING DEPARTMENT OPERATION SHEET

ORIGINAL PAGE IS
OF POOR QUALITY

[illegible]

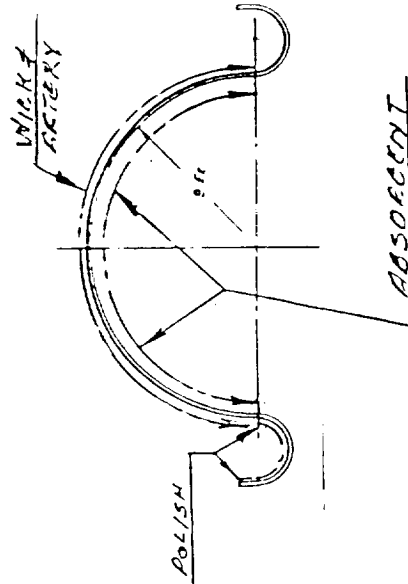
ESTIMATING DEPARTMENT

OPERATION SHEET

[illegible]

ESTIMATING DEPARTMENT OPERATION SHEET

VOLUME		PART NO.	PART NAME		PCS. REQ.	
PPG/UPG NO.	MATL. CODE	COST/LB	OTHER COST	HGH. WT.	FIN. WT.	MARK-UP
10,000/YR	26741-1C	9.50	10500	25.07	16.23	1%
OPER		041	RECEIVER ASSY		EQUIP RATE V <input checked="" type="checkbox"/> C <input type="checkbox"/>	
OPERATION DESCRIPTION			EQUIP. CODE	M/P	LABOR MINS.	TOOLING \$(000)
SHEAR BLANK			BA	1	0.40	—
DRAW FORM.			BR	1	0.50	50.0
TRIM EDGE & DEBUR			TEAC	1	1.50	5.0
WASH			148	1	0.50	—
POLISH I.D. OF ANNULAR RING TO #2 FINE FINISH			TEAC	1	4.00	5.0
MARK I.D. OF RING & GRIT BLAST I.D. OF HEMISPHERE			1401	1	3.00	2.0
POSITION (2) 1-B (13) 1-A ARTERIES TO O/S OF DOME (LOCATING TEMPLATE)			1A	1	2.0	5.0
TACK WELD (40) PLACES - TIG WELD			2A2	1	4.00	—
MASK 1/5 OF ANNULAR SURFACE AND COAT O.D. OF DOME WITH NICKEL POWDER			20A7	5	11.00	—
WELD TACK (2) STATION (1) TORCH AUTOMATIC MACHINE			13A2	1	2.00	—
ENTER			20A7	15	1.375	—
MAGK O/S ANNULAR SURFACE AND PLASMA SPRAY 1/5 OF DOME WITH CR203 - (2) 1005 THICK (2) STATION - (1) TORCH AUTOMATIC						
NEXT ASM.			JOB NO.		DATE	
6/16/87			21154		7/9/87	
DWG. DATE			ENGINEER		PART NO.	
21154			AW		26741-1C	



OPERATION SHEET

PEM 8-83 DF

ORIGINAL PAGE IS
OF POOR QUALITY

RT6021		PROJECT - 1K		PIONEER ENGINEERING BILL OF MATERIAL WITH COST				15.21		PAGE 1 87/11/14	
VOLUME - 10,000		PART - 1000		DESC - CONVERSION ASSY				VENDOR			
COMPONENT	DESC - TRUNCATED TOOLING	QTY WEIGHT	MATERIAL	LAB MIN	LABOR \$	BURDEN	SCRAP	MARK-UP	TOT COST		
26741-3 VENDOR	HEATER DOME 52.0	1 26.0000	1461.000	64.00	13.86V M	.00 31.21	.00 15.06	.00	1521.13 *		
26741-4 VENDOR	PARTITION INNER 16.0	1 1.5400	20.350	2.5	.59V M	.00 1.51	.00 .22	.00	22.67 *		
27641-5 VENDOR	REGENERATOR DISC 32.0	12 7.2360	758.700	5.16	1.20V M	.00 5.28	.00 7.68	.00	772.86 *		
26741-6 VENDOR	COOLER HSG 9.0	1 16.1000	103.700	146.10	31.48V M	.00 63.16	.00 1.98	.00	200.32 *		
26741-7 VENDOR	TRANSITION RING 5.0	1 32.6000	108.800	13.80	3.10V M	.00 9.54	.00 1.21	.00	122.65 *		
26741-8 VENDOR	DISPLACER DOME 16.0	1 4.2000	43.700	2.15	.48V M	.00 1.27	.00 .45	.00	45.90 *		
26741-9 VENDOR	RADIATION SHIELD 6.0	4 1.6400	5.900	.24	.04V M	.00 .24	.00 .08	.00	6.26 *		
26741-10 VENDOR	DISPLACER DOME 8.0	1 1.9700	20.900	.15	.48V M	.00 1.23	.00 .23	.00	22.84 *		
27641-11 VENDOR	DISPLACER 29.0	1 12.0000	21.050	12.21	4.01V M	.00 11.41	.00 .36	.00	36.83 *		
26741-12 VENDOR	PISTON 54.0	1 4.1000	12.584	11.00	2.39V M	.00 5.62	.00 .21	.00	20.80 *		
276741-13 VENDOR	POST & FLANGE 92.7	1 40.5000	38.760	9.26	8.64V M	.00 27.32	.00 .75	.00	75.47 *		
26741-14 VENDOR	SHELL HSG .0	1 63.0000	217.800	5.35	1.17V M	.00 3.23	.00 2.22	.00	224.42 *		
SKE 7761-15 VENDOR	SHELL HEAD 9.0	1 121.0000	405.900	10.10	2.18V M	.00 4.94	.00 4.13	.00	417.15 *		
26741-16 VENDOR	POWER PISTON 37.0	1 30.3000	189.800	11.00	2.38V M	.00 5.72	.00 1.98	.00	199.88 *		
26741-17 VENDOR	CYLINDER POWER PISTON 17.0	1 30.3000	159.200	21.60	4.74V M	.00 13.55	.00 1.77	.00	179.26 *		
26741-28 VENDOR	HEATER TUBE 5.0	94 2.8800	24.000	43.20	9.60V M	.00 18.24	.00 .96	.00	52.80		
26741-25 VENDOR	HEAD PLATE 50.0	1 10.6000	132.050	6.42	1.42V M	.00 4.21	.00 1.38	.00	139.06 *		

RT6021 PROJECT - 1K PIONEER ENGINEERING PAGE 2
 BILL OF MATERIAL WITH COST 15.21 87/11/14

VOLUME - 10,000 PART - 1000

DESC - CONVERSION ASSY

VENDOR

COMPONENT	DESC - TRUNCATED TOOLING	QTY WEIGHT	MATERIAL	LAB MIN	LABOR \$	BURDEN	SCRAP	MARK-UP	TOT COST
26741-29	COOLING TUBE	360.	20.880	28.80	7.20V	.00	.00		
VENDOR	.0	2.1600			M 21.60	.00	.00	.00	49.68 *

COMPONENT TOTAL COST	408.1260	3745.074	431.19	94.96V	.00	.00		3745.07
437.7				M 229.28	40.67	.00		4109.98

ASSEMBLY COST		.00	.00	.00 V	.00	.00		.00
.0				M .00	.00	.00	.00	.00

TOTAL COST	408.1260	3745.074	431.19	94.96 V	.00	.00		3745.07
				M 229.28	40.67	.00		4109.98

TOOLING 437.7

EQUIPMENT 4,861,200

ORIGINAL PAGE IS
 OF POOR QUALITY

ORIGINAL PAGE IS
OF POOR QUALITY

RT6021	PROJECT - 1K	PIONEER ENGINEERING BILL OF MATERIAL WITH COST					1.51.38	PAGE 1 87/10/13
VOLUME -	10,000 PART - 1030	DESC - ABSORBER ASSY					VENDOR	
COMPONENT	DESC - TRUNCATED TOOLING	QTY WEIGHT	MATERIAL	L-B MIN	LEADS \$	BURDEN	SCRAP	MARK-UP TOT COST
1031	ABSORBER	1	37.50	8.00	1.71V	.00	.00	
VENDOR	.0	75.0000			M	3.82	.43	.00 43.46 *
1032	POST	28	22.12	33.88	7.56V	.00	.00	
VENDOR	4.0	26.6840			M	26.60	.56	.00 56.84 *
1033	CAP	28	7.84	31.08	7.60V	.00	.00	
VENDOR	.0	7.9240			M	24.36	.28	.00 39.48 *
1034	SPRING	56	145.60	.00	.00V	.00	.00	
PURCHASED	.0	71.6800			M	.00	.00	.00 145.60 *
COMPONENT TOTAL COST		181.2880	213.06	72.96	16.27V	.00	.00	213.06
4.0					M	54.78	1.27	.00 265.38
ASSEMBLY COST			.00	.00	.00 V	.00	.00	.00
.0					M	.00	.00	.00 .00
TOTAL COST		181.2880	213.06	72.96	16.27 V	.00	.00	213.06
					M	54.78	1.27	.00 265.38
TOOLING		4.0						
EQUIPMENT		4,440,200						

RT6024 PROJECT - 1K PIONEER ENGINEERING PAGE 1
MANUFACTURING COST ANALYSIS 3.21.27 87/09/31

VOLUME- 10,000 P/A- 1
PART # 26741-3 DESC- HEATER DOME UPE-

OPER #	OPERATION DESCRIPTION	EQUIP	M	STD	LAB COST	OCC HRS	BURDEN	BURDEN	VAR COST	TOOLING
		P	MIN	LAB RATE			RATE	COST	MF6 COST	
010		7E3A	1.0	3.300	.7300 .2212	.0550 V M 41.31	.00	.0000 2.2721	.0000 3.0021	.0
020		7E3A	1.0	7.900	1.7475 .2212	.1317 V M 41.31	.00	.0000 5.4405	.0000 7.1880	10.0
030		7P3	1.0	3.000	.6702 .2234	.0500 V M 41.17	.00	.0000 2.0585	.0000 2.7287	5.0
040		14H	1.0	2.000	.4248 .2124	.0333 V M 16.71	.00	.0000 .5564	.0000 .9812	.0
060		7B2	1.0	2.000	.4282 .2146	.0333 V M 22.93	.00	.0000 .7636	.0000 1.1928	7.0
070		7B4	1.0	25.500	5.5208 .2165	.4250 V M 32.75	.00	.0000 13.9188	.0000 19.4396	20.0
080		14H	1.0	18.000	3.8232 .2124	.3000 V M 16.71	.00	.0000 5.0130	.0000 8.8362	.0
090		3C	1.0	2.000	.4468 .2234	.0333 V M 30.23	.00	.0000 1.0067	.0000 1.4535	10.0
100		14B	1.0	.300	.0644 .2146	.0050 V M 35.79	.00	.0000 .1790	.0000 .2434	.0

RT6024 PROJECT - 1K PIONEER ENGINEERING PAGE 2
MANUFACTURING COST ANALYSIS 3.21.27 87/08/31

VOLUME- 10,000 P/A- 1
PART # 26741-3 DESC- HEATER DOME UPG-

OPER	OPERATION DESCRIPTION	EQUIP	M	STD	LAB COST	DEC HRS	BURDEN	BURDEN	VAR COST	TOOLING
		P	MIN	MIN	LAB RATE		RATE	COST	MFG COST	

ANNUAL REQ-	10,000					LAB MIN -	64.0000			
MAT CODE -	ST/STL					LABOR \$ -	13.8569			
COST/LB -	42.000	ECON YR-LOC				BURDEN V-	.0000	TOOL \$000	52.0	
SCRAP FAC -	1.0%	PT TYPE -	VENDOR			BURDEN M-	31.2086			
ROUGH WT -	34.0000	MARK-UP FAC-		0.0%		SCRAP -	15.0607	TOTAL VAR	1,521.1262	
FINAL WT -	26.0000	MARK-UP		.0000		MATERIAL-	1,461.0000	TOTAL MFG	1,521.1262	
		OTHER			33.000					

ORIGINAL PAGE IS
OF POOR QUALITY

RT6024 PROJECT - 1K PIONEER ENGINEERING PAGE 1
MANUFACTURING COST ANALYSIS 3.21.27 87/08/31

VOLUME- 10,000 P/A- 1
PART # - 26741-4 DESC- PARTITION INNER UPG-

OPER	OPERATION DESCRIPTION	EQUIP	M	STD	LAB COST	OCC HRS	BURDEN	BURDEN	VAR COST	TOOLING
		P	MIN	LAB RATE			RATE	COST	MFG COST	
010		BB	1.0	.250	.0589	.0042 V	.00	.0000	.0000	.0
					.2357	M 26.71		.1122	.1711	
020		BC1	1.0	.250	.0589	.0042 V	.00	.0000	.0000	6.0
					.2357	M 61.48		.2582	.3171	
030		BC1	1.0	.250	.0589	.0042 V	.00	.0000	.0000	5.0
					.2357	M 61.48		.2582	.3171	
040		7E4B	1.0	1.500	.3291	.0250 V	.00	.0000	.0000	5.0
					.2194	M 29.93		.7483	1.0774	
050		1A	1.0	.200	.0425	.0033 V	.00	.0000	.0000	.0
					.2124	M 15.71		.0551	.0976	
060		14A2	1.0	.200	.0429	.0033 V	.00	.0000	.0000	.0
					.2146	M 23.42		.0773	.1202	

ANNUAL REQ-	10,000	LAB MIN -	2.6500
MAT CODE -	NICKEL	LABOR \$ -	.5912
COST/LB -	9.250	BURDEN V-	.0000
SCRAP FAC -	1.0%	BURDEN M-	1.5093
ROUGH WT -	2.2000	SCRAP -	.2245
FINAL WT -	1.5400	MATERIAL-	20.3500
			TOTAL VAR
			22.6750
			TOTAL MFG
			22.6750

ORIGINAL PAGE IS
OF POOR QUALITY

RT6024 PROJECT - 1K PIONEER ENGINEERING 3.21.27 PAGE 1
MANUFACTURING COST ANALYSIS 87/09/31

VOLUME- 10,000 P/A- 12
PART # 27641-5 DESC- REGENERATOR DISC UPE-

OPER	OPERATION DESCRIPTION	EQUIP	M	STD	LAB COST	SEC HRS	BURDEN	BURDEN	VAR COST	TOOLING
		P	MIN	LAB RATE			RATE	COST	MFG COST	

010		BC1	1.0	.330	.0778	.0055	V .00	.0000	.0000	25.0
					.235		M 61.48	.3381	.4159	

020		BC1	1.0	.100	.023	.0017	V .00	.0000	.0000	7.0
					.235		M 61.48	.1045	.1281	

ANNUAL REQ-	120,000					LAB MIN -	.4300			
MAT CODE -	ST/STL	ECOM YR-LCC				LABOR \$ -	.1014			
COST/LB -	75.000	PT TYPE - VENDOR				BURDEN V-	.0000	TOOL \$000	32.0	
SCRAP FAC -	1.0%	MARK-UP FAC-	0.01			BURDEN M-	.4426			
ROUGH WT -	.8430	MARK-UP -	.0000			SCRAP -	.6377	TOTAL VAR	64.4067	
FINAL WT -	.6030	OTHER -	.000			MATERIAL-	63.2250	TOTAL MFG	64.4067	

ORIGINAL PAGE IS
OF POOR QUALITY

RT6014 PROJECT - 1A PIONEER ENGINEERING PAGE 1
MANUFACTURING COST ANALYSIS 1.38.13 07/10/13

VOLUME- 10,000 F/A- 1
PART #- 26741-6 DESC- COOLER HSS TUP6-

OPER	OPERATION DESCRIPTION		EQUIP	M	STD	LAS COST	DCC HRS	BURDEN	BURDEN	VAR COST	TOTLINE
			F	MIN	LAS RATE			RATE	COST	MFG COST	
010			7E2	1.0	4.900	1.0780	.0817 V	.00	.0000	.0000	1.0
						.2200	M 35.46		2.8971	3.9751	
020			7E2	1.0	5.600	1.2760	.0967 V	.00	.0000	.0000	.0
						.2200	M 35.46		3.4290	4.7050	
030			7F2	1.0	1.400	.3072	.0233 V	.00	.0000	.0000	.0
						.2194	M 21.95		.5114	.8186	
040			7E2	1.0	40.000	8.6600	.6667 V	.00	.0000	.0000	4.0
						.2165	M 29.94		19.9810	28.6210	
050			7E2	1.0	40.000	8.6600	.6667 V	.00	.0000	.0000	4.0
						.2165	M 29.94		19.9810	28.6210	
060			2F2	1.0	1.000	.2198	.0167 V	.00	.0000	.0000	.0
						.2198	M 52.08		.2657	1.0595	
070			142	1.0	1.000	.2146	.0167 V	.00	.0000	.0000	.0
						.2146	M 35.79		.5977	.8123	
080			14	1.0	50.000	10.6200	.8333 V	.00	.0000	.0000	.0
						.2124	M 16.71		13.9244	24.5444	
090			30	1.0	2.000	.4448	.0333 V	.00	.0000	.0000	.0
						.2234	M 30.23		1.0067	1.4535	

ORIGINAL PAGE IS
OF POOR QUALITY

RT6014 PROJECT - 1K PIONEER ENGINEERING 1.38.13 PAGE 2
MANUFACTURING COST ANALYSIS 87/10/13

VOLUME- 10,000 P/A- 1
PART # 26741-6 DESC- COOLER HSB UFG-

OPER	OPERATION DESCRIPTION	EQUIP	M	STD	LAB COST	CCC HRS	BURDEN	BURDEN	VAR COST	TOOLING
		P	MIN	LAB RATE			RATE	COST	MFG COST	

ANNUAL REQ-	10,000					LAB MIN -	146.1000			
MAT CODE -	ST/STL					LABOR \$ -	31.4824			
COST/LB -	3.400	ECGN YR-LCC				BURDEN V-	.0000	TDDL \$000	9.0	
SCRAP FAC -	1.0%	PT TYPE -	VENDOR			BURDEN M-	63.1580			
ROUGH WT -	30.5000	MARK-UP FAC-	0.0%			SCRAP -	1.9634	TOTAL VAR	200.3238	
FINAL WT -	16.1000	MARK-UP	-	.0000		MATERIAL-	103.7000	TOTAL MFG	200.3238	
		OTHER	-	.000						

RT6024 PROJECT - 1K PIONEER ENGINEERING PAGE 1
MANUFACTURING COST ANALYSIS 3.21.27 87/08/31

VOLUME- 10,000 P/A- 1
PART #- 26741-7 DESC- TRANSITION RING UP6-

OPER	OPERATION DESCRIPTION	EQUIP	M	STD	LAB COST	DOC HRS	BURDEN	BURDEN	VAR COST	TOOLING
		P	MIN	LAB RATE			RATE	COST	MFG COST	
010		7E3C	1.0	3.600	.8273 .2298	.0500 V M 51.46	.00	.0000 3.0876	.0000 3.9149	.0
020		7E3C	1.0	5.500	1.2639 .2298	.0917 V M 51.46	.00	.0000 4.7189	.0000 5.9828	.0
030		7B3	1.0	.800	.1740 .2175	.0133 V M 24.19	.00	.0000 .3217	.0000 .4957	4.0
040		7B2	1.0	.800	.1717 .2146	.0133 V M 22.93	.00	.0000 .3050	.0000 .4767	1.0
050		14B	1.0	.100	.0215 .2146	.0017 V M 35.79	.00	.0000 .0608	.0000 .0823	.0
060		14A1	1.0	3.000	.6438 .2146	.0500 V M 20.97	.00	.0000 1.0485	.0000 1.6923	.0

ANNUAL REQ-	10,000			LAB MIN -	13.8000		
MAT CODE -	ST/STL	ECON YR-LOC		LABOR \$ -	3.1022		
COST/LB -	2.720	PT TYPE -	VENDOR	BURDEN V-	.0000	TOOL \$000	5.0
SCRAP FAC -	1.0%	MARK-UP FAC-	0.0%	BURDEN M-	9.5425		
ROUGH WT -	40.0000	MARK-UP -	.0000	SCRAP -	1.2144	TOTAL VAR	122.6591
FINAL WT -	32.6000	OTHER -	.000	MATERIAL-	108.8000	TOTAL MFG	122.6591

ORIGINAL PAGE IS
OF POOR QUALITY

ORIGINAL PAGE IS
OF POOR QUALITY

RT6024 PROJECT - 1K PIONEER ENGINEERING 3.21.27 PAGE 1
MANUFACTURING COST ANALYSIS 87/08/31

VOLUME- 10,000 P/A- 1
PART #- 26741-B DESC- DISPLACER DOME UPB-

OPER	OPERATION DESCRIPTION	EQUIP	M	STD	LAB COST	DEC HRS	BURDEN	BURDEN	VAR COST	TOOLING
		P	MIN	LAB RATE			RATE	COST	MFG COST	
010		8B	1.0	.250	.0589 .2357	.0042 V M 26.71	.00 .1422	.0000 .1711	.0000	.0
020		8C1	1.0	.400	.0943 .2357	.0067 V M 61.48	.00 .4119	.0000 .5062	.0000	15.0
030		7E4B	1.0	1.500	.3291 .2194	.0250 V M 29.93	.00 .7483	.0000 1.0774	.0000	1.0
040		14B	1.0	.000	.0000 .2146	.0000 V M 35.79	.00 .0000	.0000 .0000	.0000	.0

ANNUAL REQ-	10,000	ECON YR-LOC	LAB MIN -	2.1500
MAT CODE -	ST/STL	PT TYPE - VENDOR	LABOR \$ -	.4823
COST/LB -	9.500	MARK-UP FAC- 0.0%	BURDEN V-	.0000
SCRAP FAC -	1.0%	MARK-UP -	BURDEN M-	1.2724
ROUGH WT -	4.6000	OTHER -	SCRAP -	.4545
FINAL WT -	4.2000		MATERIAL-	43.7000
			TOTAL VAR	45.9092
			TOTAL MFG	45.9092

RT6024 PROJECT - 1K PIONEER ENGINEERING PAGE 1
MANUFACTURING COST ANALYSIS 3.21.27 87/05/31

VOLUME- 10,000 P/A- 4
PART # 26741-9 DESC- RADIATION SHIELD UPG-

OPER	OPERATION DESCRIPTION	EQUIP	M	STD	LAB COST	CCC HRS	BURDEN	BURDEN	VAR COST	TOOLING
		P	MIN	LAB RATE			RATE	COST	MFG COST	
010		BL1	.5	.030	.0035	.0005 V	.00	.0000	.0000	.0
					.2357	M 30.81		.0154	.0189	
020		BC1	.5	.030	.0035	.0005 V	.00	.0000	.0000	6.0
					.2357	M 61.48		.0307	.0342	
030		14B	1.0	.030	.0064	.0005 V	.00	.0000	.0000	.0
					.2143	M 35.79		.0179	.0243	

ANNUAL REQ-	40,000	LAB MIN -	.0600
MAT CODE -	ST/STL	LABOR \$ -	.0134
COST/LB -	2.500	BURDEN V-	.0000
SCRAP FAC -	1.0%	BURDEN M-	.0640
ROUGH WT -	.5900	SCRAP -	.0155
FINAL WT -	.4100	MATERIAL-	1.4750
		TOTAL VAR	1.5579
		TOTAL MFG	1.5679

ORIGINAL
OF POOR QUALITY

ORIGINAL PAGE IS
OF POOR QUALITY

RT6024 PROJECT - 1K PIONEER ENGINEERING 3.21.27 PAGE 1
MANUFACTURING COST ANALYSIS 97/08/31

VOLUME- 10,000 P/A- 1
PART # 26741-10 DESC- DISPACER CONE UPE-

OPER	OPERATION DESCRIPTION										TOOLING	
	EQUIP	M	STD	LAB	COST	ODD	HRS	BURDEN	BURDEN	VAR	COST	
	F	MIN	LAB	RAT				RATE	COST	MFG	COST	
010	SB	1.0	.250	.058		.0042	V	.00	.0000	.0000		.0
				.235		M	26.71	.1122	.1711			
020	BC1	1.0	.300	.070		.0050	V	.00	.0000	.0000		7.0
				.235		M	61.48	.3074	.3791			
030	7E4B	1.0	1.500	.325		.0250	V	.00	.0000	.0000		1.0
				.214		M	29.93	.7493	1.0774			
040	14B	1.0	.100	.021		.0017	V	.00	.0000	.0000		.0
				.214		M	35.79	.0608	.0823			

ANNUAL REQ-	10,000			LAB MIN -	2.1500		
MAT CODE -	NICKEL			LABOR \$ -	.4802		
COST/LB -	9.500	ECGN YR-LOC		BURDEN V-	.0000	TOOL \$000	9.0
SCRAF FAC -	1.8%	PT TYPE -	VENDOR	BURDEN M-	1.2287		
ROUGH WT -	2.2000	MARK-UP FAC-	0. %	SCRAP -	.2261	TOTAL VAR	20.9350
FINAL WT -	1.9700	MARK-UP	-	MATERIAL-	20.9000	TOTAL MFG	22.8050
		OTHER	-				

RT6024

PROJECT - 1Y

PIONEER ENGINEERING
MANUFACTURING COST ANALYSIS

3.21.27

PAGE 1
87/08/31VOLUME- 10,000
PART # 27641-11P/A- 1
DESC- DISPLACER

UP6-

OPER	OPERATION DESCRIPTION		EQUIP	M	STD	LAB COST	OCC HRS	BURDEN	BURDEN	VAR COST	TOTLING
			P		MIN	LAB RATE		RATE	COST	MFG COST	
010			7E3B	1.0	1.360	.3038 .2234	.0227 V M 46.75	.00 1.1066	.0000 1.4104	.0000	.0
020			7B6	1.0	1.200	.2542 .2118	.0200 V M 34.74	.00 .6948	.0000 .9490	.0000	5.0
030			7E3B	1.0	1.450	.3239 .2234	.0242 V M 46.75	.00 1.1798	.0000 1.5037	.0000	.0
040			7SB	1.0	4.100	.8918 .2175	.0683 V M 33.05	.00 2.2573	.0000 3.1491	.0000	.0
050			7E3B	1.0	1.500	.3351 .2234	.0250 V M 46.75	.00 1.2188	.0000 1.5539	.0000	7.5
060			14B	1.0	.050	.0107 .2146	.0008 V M 35.79	.00 .0286	.0000 .0393	.0000	.0
070			2K2	1.0	1.200	.2660 .2400	.0200 V M 62.62	.00 1.2524	.0000 1.5404	.0000	5.0
080			7E3B	1.0	1.300	.2604 .2234	.0217 V M 46.75	.00 1.0579	.0000 1.3483	.0000	.0
090			14D1	1.0	1.000	.2200 .2200	.0167 V M 19.12	.00 .3026	.0000 .5226	.0000	.0
100			1A	1.0	1.500	.3196 .2124	.0250 V M 16.71	.00 .4178	.0000 .7364	.0000	4.0
110			7SB	1.0	3.000	.6525 .2175	.0500 V M 33.05	.00 1.6525	.0000 2.3050	.0000	7.5
120			14B	1.0	.050	.0107 .2146	.0008 V M 35.79	.00 .0286	.0000 .0393	.0000	.0
130			14F	1.0	.500	.1062 .2124	.0083 V M 25.55	.00 .2121	.0000 .3183	.0000	.0

RTS024 PROJECT - 1K PIONEER ENGINEERING PAGE 1
MANUFACTURING COST ANALYSIS 3.21.27 87/08/31

VOLUME- 10,000 P/A- 1
PART # - 26741-12 DESC- PISTON UFG-

OPER	OPERATION DESCRIPTION		EQUIP	M	STD	LAB COST	DCC HRS	BURDEN	BURDEN	VAR COST	TOOLING
			P	MIN	LAB RATE			RATE	COST	MFG COST	
010			7E2	1.0	1.700	.3740 .2200	.0283 V M 35.46	.00 1.0035	.0000 1.0035	.0000 1.3775	.0
020			7E2	1.0	1.800	.3960 .2200	.0300 V M 35.46	.00 1.0638	.0000 1.0638	.0000 1.4598	.0
030			14A1	1.0	3.000	.6438 .2146	.0500 V M 29.97	.00 1.0485	.0000 1.0485	.0000 1.6923	5.0
040			75B	1.0	4.000	.8700 .2175	.0667 V M 33.05	.00 2.2044	.0000 2.2044	.0000 3.0744	49.0
050			14B	1.0	.500	.1073 .2146	.0083 V M 35.79	.00 .2971	.0000 .2971	.0000 .4044	.0

ANNUAL REQ-	10,000		LAB MIN -	11.0000	
MAT CODE -	CST IRON	ECON YR-LOC	LABOR \$ -	2.3911	
COST/LB -	.520	PT TYPE -	BURDEN V-	.0000	TOOL \$000 54.0
SCRAP FAC -	1.0%	MARK-UP FAC-	BURDEN M-	5.6173	
ROUGH WT -	9.2000	MARK-UP -	SCRAP -	.2059	TOTAL VAR 20.7983
FINAL WT -	4.1000	OTHER -	MATERIAL-	12.5840	TOTAL MFG 20.7983

ORIGINAL PAGE IS
OF POOR QUALITY

ORIGINAL PAGE IS
OF POOR QUALITY

RT6024 PROJECT - 1K PIONEER ENGINEERING PAGE 1
MANUFACTURING COST ANALYSIS 3.21.27 87/08/31

VOLUME- 10,000 P/A- 1
PART # 276741-13 DESC- POST & FLANGE UP6-

OPER	OPERATION DESCRIPTION	ESQUIP	M	STD	LAB COST	DOC HRS	BURDEN	BURDEN	VAR COST	TOOLING
		P	MIN	LAB RATE			RATE	COST	MFG COST	
010		7813	1.0	12.890	2.8745 .2230	.2148 V M 47.25	.00 10.1493	.0000 13.0238		4.0
020		7218	1.0	6.670	1.4874 .2230	.1112 V M 47.25	.00 5.2542	.0000 6.7416		3.0
030		20A3	1.0	2.300	.5855 .2198	.0383 V M 75.00	.00 2.8725	.0000 3.3780		3.0
040		7E38	1.0	3.000	.6702 .2234	.0500 V M 42.75	.00 2.4375	.0000 3.1077		5.5
050		1A	1.0	4.000	.8496 .2124	.0667 V M 16.71	.00 1.1146	.0000 1.9642		1.0
060		734	1.0	1.100	.2382 .2165	.0183 V M 32.75	.00 .5993	.0000 .8375		6.0
070		734	1.0	1.200	.2598 .2165	.0200 V M 32.75	.00 .6550	.0000 .9149		3.6
080		724	1.0	.800	.1732 .2165	.0133 V M 32.75	.00 .4356	.0000 .6088		6.0
090		754	1.0	.800	.1732 .2165	.0133 V M 32.75	.00 .4356	.0000 .6088		3.6
100		753	1.0	3.000	.6525 .2175	.0500 V M 33.05	.00 1.6525	.0000 2.3050		57.0
110		1443	1.0	3.000	.6436 .2146	.0500 V M 25.38	.00 1.4190	.0000 2.0628		.0
120		149	1.0	.500	.1077 .2146	.0083 V M 35.79	.00 .2971	.0000 .4044		.0

RTE024 PROJECT - 1K PIONEER ENGINEERING PAGE 2
MANUFACTURING COST ANALYSIS 3.21.27 87/09/31

VOLUME- 10,000 P/A- 1
PART # 276741-13 DESC- POST & FLANGE UFG-

OPER	OPERATION DESCRIPTION	EQUIP	M	STD	LAB COST	OCG HRS	BURDEN	BURDEN	VAR COST	TOOLING
		P	MIN	LAB RATE			RATE	COST	MFG COST	

ANNUAL REQ-	10,000					LAB MIN -	39.2600			
MAT CODE -	EST IRON					LABOR \$ -	9.6352			
COST/LB -	.510					BURDEN V-	.0000	TOOL \$000	92.7	
SCRAP FAC -	1.0%					BURDEN M-	27.3222			
ROUGH WT -	64.0000					SCRAP -	.7472	TOTAL VAR	75.4646	
FINAL WT -	40.5000					MATERIAL-	39.7600	TOTAL MFG	75.4646	

ORIGINAL PAGE IS
OF POOR QUALITY

PIONEER ENGINEERING
MANUFACTURING COST ANALYSIS

RTB024 PROJECT - 1K

3.21.27

P/A- 1
DESC- SHELL H56

105-

OPERATION	DESCRIPTION	EQUIP	M	STD	LAB COST	CCC HRS	BURDEN	BURDEN	VAR COST	TOOLING
			P	MIN	LAB RATE		RATE	COST	MFG COST	
010		7E4C	1.0	4.250	.9325 .2194	.1708 V M 35.89	.00 2.7534	.0000 3.6559	.0000	.0
020		14D2	1.0	1.000	.2200 .2200	.1167 V M 25.80	.00 .4309	.0000 .6509	.0000	.0
030		14A3	1.0	1.100	.0215 .2145	.0017 V M 25.38	.00 .0492	.0000 .0697	.0000	.0

ANNUAL REQ-	10,000
MAT CODE -	ST/STL
COST/LB -	3.300
SCRAP FAC -	1.0%
ROUGH WT -	66.0000
FINAL WT -	63.0000

ECON YR-LCC

PT TYPE - VENDOR

MARK-UP FAC-

MARK-UP -

OTHER -

L: B MIN - 5.3500

L: BOR \$ - 1.1740

GREEN V- .0000

B IRDEN M- 3.2325

5056P - 2.2221

MATERIAL-	217.3000
-----------	----------

TOTAL \$600

TOTAL VAR

TOTAL LIFE

1015-1100

.0

224.4286

224.4265

1998, 1999, 2000, 2001, 2002, 2003, 2004, 2005, 2006, 2007, 2008, 2009, 2010, 2011, 2012, 2013, 2014, 2015, 2016, 2017, 2018, 2019, 2020, 2021, 2022, 2023, 2024, 2025, 2026, 2027, 2028, 2029, 2030, 2031, 2032, 2033, 2034, 2035, 2036, 2037, 2038, 2039, 2040, 2041, 2042, 2043, 2044, 2045, 2046, 2047, 2048, 2049, 2050, 2051, 2052, 2053, 2054, 2055, 2056, 2057, 2058, 2059, 2060, 2061, 2062, 2063, 2064, 2065, 2066, 2067, 2068, 2069, 2070, 2071, 2072, 2073, 2074, 2075, 2076, 2077, 2078, 2079, 2080, 2081, 2082, 2083, 2084, 2085, 2086, 2087, 2088, 2089, 2090, 2091, 2092, 2093, 2094, 2095, 2096, 2097, 2098, 2099, 2100, 2101, 2102, 2103, 2104, 2105, 2106, 2107, 2108, 2109, 2110, 2111, 2112, 2113, 2114, 2115, 2116, 2117, 2118, 2119, 2120, 2121, 2122, 2123, 2124, 2125, 2126, 2127, 2128, 2129, 2130, 2131, 2132, 2133, 2134, 2135, 2136, 2137, 2138, 2139, 2140, 2141, 2142, 2143, 2144, 2145, 2146, 2147, 2148, 2149, 2150, 2151, 2152, 2153, 2154, 2155, 2156, 2157, 2158, 2159, 2160, 2161, 2162, 2163, 2164, 2165, 2166, 2167, 2168, 2169, 2170, 2171, 2172, 2173, 2174, 2175, 2176, 2177, 2178, 2179, 2180, 2181, 2182, 2183, 2184, 2185, 2186, 2187, 2188, 2189, 2190, 2191, 2192, 2193, 2194, 2195, 2196, 2197, 2198, 2199, 2200, 2201, 2202, 2203, 2204, 2205, 2206, 2207, 2208, 2209, 2210, 2211, 2212, 2213, 2214, 2215, 2216, 2217, 2218, 2219, 2220, 2221, 2222, 2223, 2224, 2225, 2226, 2227, 2228, 2229, 2230, 2231, 2232, 2233, 2234, 2235, 2236, 2237, 2238, 2239, 2240, 2241, 2242, 2243, 2244, 2245, 2246, 2247, 2248, 2249, 2250, 2251, 2252, 2253, 2254, 2255, 2256, 2257, 2258, 2259, 2260, 2261, 2262, 2263, 2264, 2265, 2266, 2267, 2268, 2269, 2270, 2271, 2272, 2273, 2274, 2275, 2276, 2277, 2278, 2279, 2280, 2281, 2282, 2283, 2284, 2285, 2286, 2287, 2288, 2289, 2290, 2291, 2292, 2293, 2294, 2295, 2296, 2297, 2298, 2299, 2300, 2301, 2302, 2303, 2304, 2305, 2306, 2307, 2308, 2309, 2310, 2311, 2312, 2313, 2314, 2315, 2316, 2317, 2318, 2319, 2320, 2321, 2322, 2323, 2324, 2325, 2326, 2327, 2328, 2329, 2330, 2331, 2332, 2333, 2334, 2335, 2336, 2337, 2338, 2339, 2340, 2341, 2342, 2343, 2344, 2345, 2346, 2347, 2348, 2349, 2350, 2351, 2352, 2353, 2354, 2355, 2356, 2357, 2358, 2359, 2360, 2361, 2362, 2363, 2364, 2365, 2366, 2367, 2368, 2369, 2370, 2371, 2372, 2373, 2374, 2375, 2376, 2377, 2378, 2379, 2380, 2381, 2382, 2383, 2384, 2385, 2386, 2387, 2388, 2389, 2390, 2391, 2392, 2393, 2394, 2395, 2396, 2397, 2398, 2399, 2400, 2401, 2402, 2403, 2404, 2405, 2406, 2407, 2408, 2409, 2410, 2411, 2412, 2413, 2414, 2415, 2416, 2417, 2418, 2419, 2420, 2421, 2422, 2423, 2424, 2425, 2426, 2427, 2428, 2429, 2430, 2431, 2432, 2433, 2434, 2435, 2436, 2437, 2438, 2439, 2440, 2441, 2442, 2443, 2444, 2445, 2446, 2447, 2448, 2449, 2450, 2451, 2452, 2453, 2454, 2455, 2456, 2457, 2458, 2459, 2460, 2461, 2462, 2463, 2464, 2465, 2466, 2467, 2468, 2469, 2470, 2471, 2472, 2473, 2474, 2475, 2476, 2477, 2478, 2479, 2480, 2481, 2482, 2483, 2484, 2485, 2486, 2487, 2488, 2489, 2490, 2491, 2492, 2493, 2494, 2495, 2496, 2497, 2498, 2499, 2500, 2501, 2502, 2503, 2504, 2505, 2506, 2507, 2508, 2509, 2510, 2511, 2512, 2513, 2514, 2515, 2516, 2517, 2518, 2519, 2520, 2521, 2522, 2523, 2524, 2525, 2526, 2527, 2528, 2529, 2530, 2531, 2532, 2533, 2534, 2535, 2536, 2537, 2538, 2539, 2540, 2541, 2542, 2543, 2544, 2545, 2546, 2547, 2548, 2549, 2550, 2551, 2552, 2553, 2554, 2555, 2556, 2557, 2558, 2559, 2560, 2561, 2562, 2563, 2564, 2565, 2566, 2567, 2568, 2569, 2570, 2571, 2572, 2573, 2574, 2575, 2576, 2577, 2578, 2579, 2580, 2581, 2582, 2583, 2584, 2585, 2586, 2587, 2588, 2589, 2590, 2591, 2592, 2593, 2594, 2595, 2596, 2597, 2598, 2599, 2600, 2601, 2602, 2603, 2604, 2605, 2606, 2607, 2608, 2609, 2610, 2611, 2612, 2613, 2614, 2615, 2616, 2617, 2618, 2619, 2620, 2621, 2622, 2623, 2624, 2625, 2626, 2627, 2628, 2629, 2630, 2631, 2632, 2633, 2634, 2635, 2636, 2637, 2638, 2639, 2640, 2641, 2642, 2643, 2644, 2645, 2646, 2647, 2648, 2649, 2650, 2651, 2652, 2653, 2654, 2655, 2656, 2657, 2658, 2659, 2660, 2661, 2662, 2663, 2664, 2665, 2666, 2667, 2668, 2669, 2670, 2671, 2672, 2673, 2674, 2675, 2676, 2677, 2678, 2679, 26

RT5024 PROJECT - 1K PIONEER ENGINEERING PAGE 1
MANUFACTURING COST ANALYSIS 3.21.27 87/03/31

VOLUME- 10,000 P/A- 1
PART # SKE 7751-15 DESC- SHELL HEAD UFG-

OPER	OPERATION DESCRIPTION	EQUIP	M	STD	LAB COST	SEC HRS	BURDEN	BURDEN	VAR COST	TOOLING
		P	MIN	LAB RATE			RATE	COST	MFG COST	
010		7E4C	1.0	3.600	.7898 .2194	.0600 V M 38.69	.00 2.3334	.0000 3.1232	.0	
020		766	1.0	1.400	.2965 .2118	.0233 V M 34.74	.00 .8094	.0000 1.1059	9.0	
030		762	1.0	2.000	.4292 .2146	.0333 V M 22.93	.00 .7636	.0000 1.1928	.0	
040		1A	1.0	2.000	.4248 .2124	.0333 V M 16.71	.00 .5564	.0000 .9812	.0	
050		14D2	1.0	1.000	.2260 .2200	.0157 V M 25.80	.00 .4309	.0000 .6509	.0	
060		14A3	1.0	.100	.0215 .2146	.0017 V M 28.38	.00 .0482	.0000 .0697	.0	

ANNUAL REQ-	10,000								
MAT CODE -	ST/STL	ECON YR-LDC		LAB MIN -	10.1000				
COST/LB -	3.300	PT TYPE -	VENDOR	LABOR \$ -	2.1818				
SCRAP FAC -	1.0%	MARK-UP FAC-	0.0%	BURDEN V-	.0000	TOOL \$000	9.0		
ROUGH WT -	123.0000	MARK-UP -	.0000	BURDEN M-	4.9419				
FINAL WT -	121.0000	OTHER -	.000	SCRAP -	4.1302	TOTAL VAR	417.1539		
				MATERIAL-	405.9000	TOTAL MFG	417.1539		

ORIGINAL TO BE
OF POOR QUALITY

RTE024 PROJECT - 1K

PIONEER ENGINEERING
MANUFACTURING COST ANALYSIS

3.21.27 PAGE 1
87/08/31

VOLUME- 10,000
PART # 26741-16

P/A- 1
DESC- POWER PISTON

UPG-

OPER	OPERATION DESCRIPTION	EQUIP	M	STD MIN	LAB COST LAB RATE	OCC HRS	BURDEN RATE	BURDEN COST	VAR COST MFG COST	TOOLING
010		7E3B	1.0	2.700	.6032 .2234	.0450 V M 48.75	.00	.0000 2.1938	.0000 2.7970	.0
020		766	1.0	1.100	.2330 .2118	.0 83 V M 34.74	.00	.0000 .6357	.0000 .8687	7.0
030		782	1.0	1.200	.2575 .2146	.0200 V M 22.93	.00	.0000 .4586	.0000 .7161	.0
040		148	1.0	.050	.0107 .2146	.008 V M 35.79	.00	.0000 .0286	.0000 .0393	.0
050		1482	1.0	.500	.1100 .2200	.0083 V M 25.80	.00	.0000 .2141	.0000 .3241	.0
060		1A	1.0	3.000	.6372 .2124	.0500 V M 16.71	.00	.0000 .8355	.0000 1.4727	5.0
070		758	1.0	2.400	.5220 .2175	.0400 V M 33.05	.00	.0000 1.3220	.0000 1.8440	25.0
080		148	1.0	.050	.0107 .2146	.0008 V M 35.79	.00	.0000 .0286	.0000 .0393	.0

RT6024 PROJECT - 1K PIONEER ENGINEERING PAGE 2
MANUFACTURING COST ANALYSIS 3.21.27 87/08/31

VOLUME- 10,000 P/A- 1
PART # 26741-16 DESC- POWER PISTON UFG-

OPER	OPERATION DESCRIPTION	EQUIP	M	STD	LAB COST	CCC HRS	BURDEN	BURDEN	VAR COST	TOOLING
		P	MIN	LAB RATE			RATE	COST	MFG COST	

ANNUAL REQ-	10,000					LAB MIN -	11.0000			
MAT CODE -	57/STL					LABOR \$ -	2.3643			
COST/LB -	4.000					BURDEN V-	.0000	TOOL \$000	37.0	
SCRAP FAC -	1.0%					BURDEN M-	5.7169			
ROUGH WT -	39.0000					SCRAP -	1.9790	TOTAL VAR	199.8802	
FINAL WT -	30.3000					MATERIAL-	189.8000	TOTAL MFG	199.8802	

OE FROM QUALITY

ORIGINAL PAGE IS
OF POOR QUALITY

RT6024 PROJECT - JK PIONEER ENGINEERING MANUFACTURING COST ANALYSIS 3.21.27 PAGE 1 87/08/31

VOLUME- 10,000 P/A- 1 URE-
PART 4- 26741-17 DESC- CYLINDER POWER PISTON

OPER	OPERATION DESCRIPTION	EQUIP	M	STD	LAP	COST	DC	MRS	BURDEN	BURDEN	VAR	COST	TOOLING
			P	MIN	LAE	RATE			RATE	COST	MFG	COST	
010		7E3B	1.0	2.600	.5808	.0433	V	.00	.0000	.0000			.0
					.2234		M	48.75	2.1109	2.6917			
020		7E3B	1.0	5.000	1.1170	.0833	V	.00	.0000	.0000			.0
					.2234		M	48.75	4.0609	5.1779			
030		7B6	1.0	1.100	.2530	.0183	V	.00	.0000	.0000			7.0
					.2118		M	34.74	.6357	.8687			
040		75B	1.0	10.300	2.2403	.1717	V	.00	.0000	.0000			10.0
					.2175		M	33.05	5.6747	7.9150			
050		7V2	1.0	2.000	.4325	.0333	V	.00	.0000	.0000			.0
					.2194		M	23.95	.7975	1.2363			
060		14B	1.0	.100	.0215	.0017	V	.00	.0000	.0000			.0
					.2148		M	35.79	.0608	.0823			
070		14F	1.0	.500	.1052	.0023	V	.00	.0000	.0000			.0
					.2124		M	25.55	.2121	.3183			
ANNUAL REQ-	10,000					LAB MIN -		21.6000					
MAT CODE -	5T/STL	ECON YR-LEC				LABOR \$ -		4.7376					
COST/LB -	4.000	PT TYPE -	VENDOR			BURDEN V-		.0000	TOOL \$000		17.0		
SCRAP FAC -	1.0%	MARK-UP FAC-	0.0%			BURDEN M-		13.5526	TOTAL VAR		179.2651		
ROUGH WT -	39.8000	MARK-UP -	.0000			SCRAP -		1.7749	TOTAL MFG		179.2651		
FINAL WT -	30.3000	OTHER -	.000			MATERIAL-		159.2000					

RTS:24 PROJECT - 1K PIONEER ENGINEERING PAGE 1
MANUFACTURING COST ANALYSIS 3.21.27 87/09/31

VOLUME- 10,000 P/A- 96
PART # 26741-29 DESC- HEATER TUBE UPS-

OPER	OPERATION DESCRIPTION	EQUIP	M	STD	LAB COST	OOD HRS	BURDEN	BURDEN	VAR COST	TOOLING
		P	MIN	LAB RATE			RATE	COST	MFS COST	
010		7A1	1.0	.200	.0437	.0033 V	.00	.0000	.0000	.0
					.2185	M 23.42		.0773	.1210	
020		8B	1.0	.200	.0471	.0033 V	.00	.0000	.0000	5.0
					.2357	M 26.71		.0881	.1352	
030		14B	1.0	.050	.0107	.0005 V	.00	.0000	.0000	.0
					.2146	M 35.79		.0286	.0393	

ANNUAL REQ-	950,000			LAB MIN -	.4500				
MAT CODE -	NICKEL	ECON YR-LDC		LABOR \$ -	.1015				
COST/LB -	5.330	PT TYPE -	VENDOR	BURDEN V-	.0000	TOOL \$000	5.0		
SCRAP FAC -	1.0%	MARK-UP FAC-	0.0%	BURDEN M-	.1940				
ROUGH WT -	.0300	MARK-UP -	.0000	SCRAP -	.0055	TOTAL VAR	.5509		
FINAL WT -	.0300	OTHER -	.000	MATERIAL-	.2499	TOTAL MFS	.5509		

ORIGINAL PAGE 78
OF POOR QUALITY

ORIGINAL PAGE IS
OF POOR QUALITY

RT6014 PROJECT - 1K PIONEER ENGINEERING PAGE 1
MANUFACTURING COST ANALYSIS 4.01 07/11/17

VOLUME- 10,000 P/A- 360
PART # 26741-29 DESC- COOLING TUBE UPE-

OPER	OPERATION DESCRIPTION	EQUIP	M	STD	LAB COST	STD HRS	BURDEN	BURDEN	VAR COST	TOLLING
		P	MIN	LAB RATE			RATE	COST	MFG COST	
010		781A	1.0	.083	.0185	.0014	V .00	.0000	.0000	.0
					.2230		M 44.18	.0619	.0804	

ANNUAL REQ-	3,600,000					LAB MIN -	.0830			
MAT CODE -	ST/STL	ECON YR-LOC				LABOR \$ -	.0185			
COST/LB -	8.330	PT TYPE -	VENDOR			BURDEN V-	.0000	TOOL \$000	- .0	
SCRAP FAC -	1.0%	MARK-UP FAC-	0.0%			BURDEN M-	.0619			
ROUGH WT -	.0070	MARK-UP	-	.0000		SCRAP -	.0014	TOTAL VAR	.1401	
FINAL WT -	.0060	OTHER	-	.000		MATERIAL-	.0583	TOTAL MFG	.1401	

RT6024 PROJECT - 1K PIONEER ENGINEERING PAGE 1
MANUFACTURING COST ANALYSIS 3.21.27 87/06/31

VOLUME- 10,000 P/A- 1
PART # 26741-25 DESC- HEAD PLATE UFG-

OPER	OPERATION DESCRIPTION	EQUTP	M	STD	LAB COST	SEC HRS	BURDEN	BURDEN	VAR COST	TOOLING
		P	MIN	LAB RATE			RATE	COST	MFS COST	
010		BC1	1.0	.120	.0283	.0020 V	.00	.0000	.0000	10.0
					.2357	M 61.48		.1230	.1513	
020		BR	1.0	.500	.1179	.0083 V	.00	.0000	.0000	30.0
					.2357	M 39.76		.3300	.4479	
030		7E4C	1.0	4.000	.8776	.0667 V	.00	.0000	.0000	5.0
					.2194	M 38.89		2.5940	3.4716	
040		7E4C	1.0	1.700	.3730	.0283 V	.00	.0000	.0000	5.0
					.2194	M 38.89		1.1006	1.4708	
050		14B	1.0	.100	.0215	.0017 V	.00	.0000	.0000	.0
					.2146	M 35.79		.0608	.0823	

ANNUAL REQ-	10,000	LAB MIN -	6.4200
MAT CODE -	NICKEL	LABOR \$ -	1.4183
COST/LB -	9.500	BURDEN V-	.0000
SCRAP FAC -	1.0%	BURDEN M-	4.2084
ROUGH WT -	13.9000	SCRAP -	1.3768
FINAL WT -	10.6000	MATERIAL-	132.0500
		TOTAL VAR	139.0535
		TOTAL MFS	139.0535

ORIGINAL 8/20/87
OF POOR QUALITY

ORIGINAL PAGE IS
OF POOR QUALITY

RTG014 PROJECT - 1K PIONEER ENGINEERING MANUFACTURING COST ANALYSIS 1.38.13 PAGE 1
E7/10/13

VOLUME- 10,000 P/A- 300
PART # 26741-25 DESC- COOLING TUBE UFG-

OPER	OPERATION DESCRIPTION	EQUIP	Q	STD	LAB COST	CCO HR	BURDEN	BURDEN	VAR COST	TOOLING
		P		MIN	LAB RATE		RATE	COST	MF6 COST	
010		761A	1.0	.083	.0185	.001	V .00	.0000	.0000	.0
					.2236		M 44.19	.0619	.0604	

ANNUAL REQ-	3,000,000					LAB MIN -	.0830			
MAT CODE -	ST/STL	EDCN YR-LGC				LABOR \$ -	.0185			
COST/LB -	8.330	FT TYPE - VENDOR				BURDEN V-	.0000	TOOL \$000	7.0	
SCRAP FAC -	1.0%	MARK-UP FAC-	0.0%			BURDEN M-	.0619			
ROUGH WT -	.0070	MARK-UP	-	.0000		SCRA -	.0014	TOTAL VAR	.1401	
FINAL WT -	.0060	OTHER	-	.000		MATERIAL-	.0583	TOTAL MF6	.1401	

OPERATION SHEET

PEM 8-83 DF

[illegible]

SKETCH -

OPERATION SHEET

PEM 0-83 DE

ESTIMATING DEPARTMENT

OPERATION SHEET

VOLUME 10,000/42		PART NO. 27641-5		PART NAME REGENERATOR DISC		PCS. REQ. 12	
PPG/UPG NO.		MATERIAL CODE 41		COST/LB. 75.00		OTHER COST	
FIN. WT. 0.603		RGH. WT. 0.843		SCRAP 1%		MARK-UP	
EQUIP. RATE V <input checked="" type="checkbox"/> C <input type="checkbox"/>							

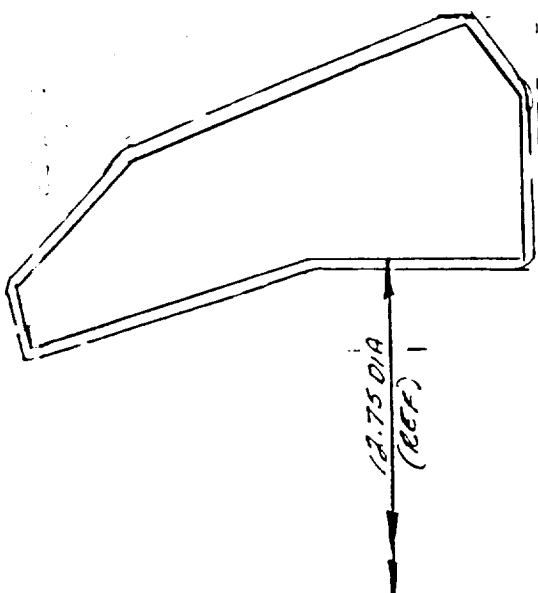
OPER	OPERATION DESCRIPTION	EQUIP. CODE	M/P	LABOR MINS.	TOOLING \$(000)	MATERIAL SPECS & BACK-UP DATA
10	BLANK CAT 1/2 CIRCLES - (36) HITS	801	1	0.33	25.0	MAT 1/4" METAL FLUT (BRUNSWICK)
20	TRIM 1/2" SECTIONS TO 90° (8) HITS	801	1	0.10	7.0	@ 13% DENSITY = 1.404# / FT. @ 10.5% = 75.0# / LB. SHEET OF 32 X 95 = (16) CIRCLES SETS DIE CUT - MAXIMUM EDGE CRUSH - 1/8" MAY REQUIRE (1) ADDL DISC FOR LOSS.
						--- SKETCH ---

NEXT ASM.	DWG. DATE 6/16/87	JOB NO. 21454	ENGINEER AN	DATE 7/13/87	PAGE OF 1	PART NO. 27641-5
-----------	----------------------	------------------	----------------	-----------------	--------------	---------------------

ESTIMATING DEPARTMENT OPERATION SHEET

VOLUME	PART NO.	PART NAME	PCS. REQ.							
10,000/YR	26741-6	COOLER HSG	1							
PPG/UPG NO.	MATL. CODE	COST/LB.	OTHER COST	RGH. WT. #	FIN. WT. #	SCRAP %	MARK-UP %	EQUIP. RATE V	EQUIP. RATE C	
041	3.40	950.25	30.5	16.1	1			<input checked="" type="checkbox"/>		
OPER	OPERATION DESCRIPTION		EQUIP. CODE	M/P	LABOR MINS.	TOOLING \$(000)	MATERIAL SPECS & BACK-UP DATA			
10	ROUGH TURN "B" DIA, RIGHT FIN "C" DIA AND FACE END "D"		7P2	1	4.90		STAINLESS STEEL C576-700 SERIES			
20	ROUGH BORE "A" DIA, FACE "D"		7P2	1	5.80					
30	FINISH BORE "A", THEN "B" AND FACE "E" HOLD "A" & "B" TO .0005 OF NOMINAL & CONCENTRIC TO EACH OTHER TO .0002 TIR.									
30	BORE (E) COOLER PORT HOLES		7P2	1	1.40					
40	BURE COMP - THERMAL DEBUR		20A1	1	1.00		PATT-85022			
50	WASH.		19B	1	0.50		SKETCH			
NEXT ASM.	DWG. DATE	JOB NO.	ENGINEER	DATE	PAGE	OF	PART NO.			
	6/16/57	2145-1	AA	6/18/57	26741-6					

ESTIMATING DEPARTMENT OPERATION SHEET

VOLUME		PART NO.		PART NAME		PCS. REQ.	
10,000 LR-		26741-7		TRANSITION RING		/	
PPG/UPG NO.	MATL. CODE	COST/LB.	OTHER COST	RGH. WT.	FIN. WT.	SCRAP	MARK-UP
	41	2.72		40	32.6	1	%
OPER	OPERATION DESCRIPTION			EQUIR. CODE	M/P	LABOR MINS.	TOOLING \$(000)
10	CHECK ON OLD, ROUGH & FINISH			73C	1	3.60	—
20	RGR & FINISH THEN O.D.			73C	1	5.50	—
30	DRILL (10) 5/16 DIA X 1" DEEP			763	1	0.80	4.0
40	TAP (10) 3/8-16 X 3/4 DEEP			762	1	0.80	1.0
50	WASH			14B	1	0.10	—
60	REMOVE BURRS			14A	1	3.0	—
<div style="text-align: center;"> <p>— MATERIAL SPECS & BACK-UP DATA —</p> <p>310 ST. STEEL CASTING</p> <p>— SKETCH —</p>  </div>							

ORIGINAL PAGE IS
OF POOR QUALITY

PART NO. 26741-7

PAGE — OF —

DATE 6/24/87

ENGINEER AH

JOB NO. 21454

DWG. DATE 6/16/87

NEXT ASM.

[illegible]

ESTIMATING DEPARTMENT

ESTIMATING DEPARTMENT

[illegible]

ESTIMATING DEPARTMENT OPERATION SHEET

VOLUME		PART NO.		PART NAME		PCS. REQ.	
PPG/UPG NO.	MAIL. CODE	COST/LB.	OTHER COST	RGH. WT.	FIN. WT.	SCRAP	MARK-UP
10,000/YR	27641-11	8.90	8.45	14#	12#	1%	1%
<div style="display: flex; justify-content: space-between;"> <div> <p>OPER</p> <p>10 REAR FIN TURN DIA "A" 1 STEP</p> <p>20 CONTOUR TOP, FACE BOTTOM</p> <p>30 DRILL TOP</p> <p>40 REAR FIN. BORE "B" 1 TAPER "C"</p> <p>50 GRIND DIA "B" 1 TAPER "C"</p> <p>60 GRIND DIA "B" 1 TAPER "C"</p> <p>70 SUPER FINISH BORE</p> <p>80 WASH</p> <p>90 INCL TO DOME ASSY -</p> <p>100 FINAL TURN KNURE DISPLACER</p> <p>110 DOME</p> <p>120 TAPER BLAST O.D. OF DISPLACER</p> <p>130 APPLY. RULON WITH GLOXY PASTE</p> <p>140 FINAL GRIND "A" DIA OF RULON TO</p> <p>150 MATCH SLEAVE</p> <p>160 WASH.</p> <p>170 BURE COMPLETE</p> </div> <div> <p>EQUIP. RATE</p> <p>Y <input checked="" type="checkbox"/> C <input type="checkbox"/></p> </div> </div>							
OPERATION DESCRIPTION				EQUIP. CODE	M/P	LABOR MINS.	TOOLING \$(000)
MATERIAL SPECS & BACK-UP DATA				<p>100% STEEL CASTING</p> <p>RULON 3.60XV - 6.5 IN DIA 1.13"</p> <p>SKETCH</p>			

ORIGINAL PAGE IS OF POOR QUALITY

NEXT ASM.

27641-11

DWG. DATE

6/16/87

JOB NO.

21554

DATE

6/29/87

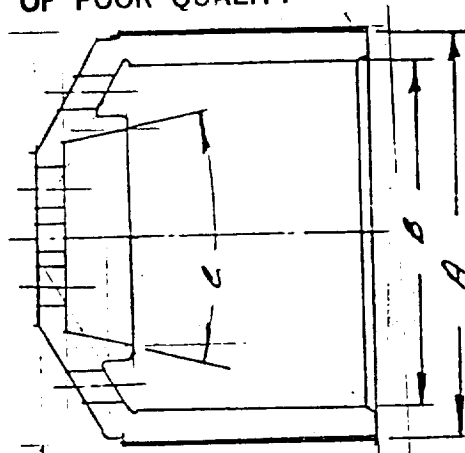
PAGE

OF

PART NO.

26741-11

ORIGINAL PAGE IS
OF POOR QUALITY



ESTIMATING DEPARTMENT OPERATION SHEET

VOLUME		PART NO.		PART NAME		PCS. REQ.		
10,000/YR		26741-12		PISTON		1		
PPG/UPG NO.	MATL. CODE	COST/LB.	OTHER COST	RGH. WT.	FIN. WT.	SCRAP	MARK-UP	EQUIP. RATE
	003	.52	7.80	9.24	4.14	1%	1%	V <input type="checkbox"/> C <input type="checkbox"/>
OPER	— OPERATION DESCRIPTION —							— MATERIAL SPECS & BACK-UP DATA —
20	FACE HEAD ANGLES END							MODULAR IRON- SAND CSIG
	DRILL 1/2" DIA. BOLT HOLE, CHAMFER							
	TURN 1/2" DIA. FACE BACK EDGE							
30	TURN 1/2" DIA. 1/2" TAPER, FACE END 1/2"							
	CHAMFER 1/2" DIA. FOR CENTER							
	APPLY RULON TO 1/2" DIA							RULON - 60 IN ² @ 13/N ²
40	GRIND 1/2" DIA. TO MATCH							INSPECTION AIR GAGE
	POST FLANGE & FINISH TAPER 1/2"							
50	WASH							— SKETCH —

NEXT ASM.	DWG. DATE	JOB NO.	ENGINEER	DATE	PAGE	OF	PART NO.
	6/16/87	21454	AA	6/27/87	26	741-12	

OPERATION SHEET

VOLUME		PART NO.		PART NAME		PCS. REQ.	
10,000 / YR		27641-13		POST FLANGE		1	
PPG/UPQ NO.	MATL. CODE	COST/LB.	OTHER COST	RGH. WT.	FIN. WT.	SCRAP	MARK-UP
	008	0.51	6.13	64#	40.5#	1%	1%
OPERATION DESCRIPTION							
10	RGH & FINISH TURN DIA - A, B, F, & G, FACES						
20	J.H. & END						
30	RGH & FINISH H.O.M., TURN FACE GROOVE						
40	K & L RGH & SEMI FIN D & E BORE						
50	FINISH GRIND C & D BORES & F DIA & G						
60	FACE L						
70	SUPER FINISH C & D DIAS						
80	APPLY EULON TO B DIA						
90	DRILL (Ø) Ø.12 P" HOLES						
100	DRILL (Ø) 1/8" Ø DR & C BORE (16) 1/8" HOLES						
110	TAP (Ø) Ø.12 P" HOLES						
120	TAP (Ø) 1/8" HOLES						
130	GRIND B DIA TO MATCH DISPLACER						
140	REMOVE ALL BURS						
150	WASH						
160							
170							
180							
190							
200							
210							
220							
230							
240							
250							
260							
270							
280							
290							
300							
310							
320							
330							
340							
350							
360							
370							
380							
390							
400							
410							
420							
430							
440							
450							
460							
470							
480							
490							
500							
510							
520							
530							
540							
550							
560							
570							
580							
590							
600							
610							
620							
630							
640							
650							
660							
670							
680							
690							
700							
710							
720							
730							
740							
750							
760							
770							
780							
790							
800							
810							
820							
830							
840							
850							
860							
870							
880							
890							
900							
910							
920							
930							
940							
950							
960							
970							
980							
990							
1000							

TOOLING \$ (000) 4.0

LABOR MINS. 12.89

M/P 1

EQUIR CODE 7010

FIN. WT. 40.5#

SCRAP 1%

MARK-UP 1%

EQUIR RATE V ☒ C ☐

— MATERIAL SPECS & BACK-UP DATA —

MODULAR IRON-SAND CAST

EULON - 47 IN. Ø 1.5"

— SKETCH —

NEXT ASM. 6-16-87

DWG. DATE 21454

ENGINEER AN

DATE 6-24-87

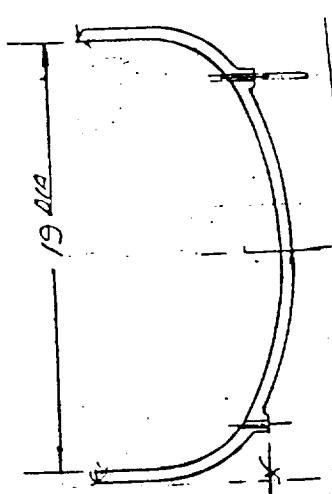
PART NO. 27641-13

PAGE 1 OF 1

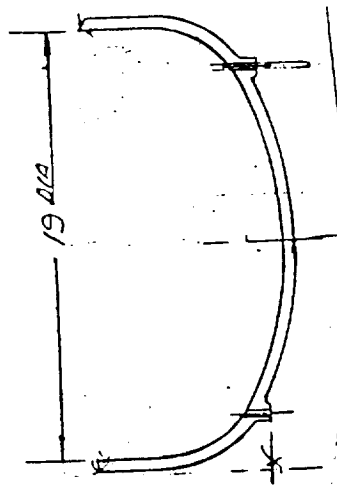
DEM 8-83 DF

OPERATION SHEET

OPERATION SHEET

VOLUME	PART NO.	PART NAME	PCS. REQ.				
10,000/YR PPG/UPG NO.	26741-15	SHELL-HEAD	/				
MATL. CODE	COST/LB.	OTHER COST	RGH. WT.	FIN. WT.	SCRAP	MARK-UP	EQUIP RATE C
041	3.30		123*	121*	— %	— %	[] V [x]
O P E R	OPERATION DESCRIPTION	EQUIP. CODE	M/P	LABOR MINS.	TOOLING \$(000)	MATERIAL SPECS & BACK-UP DATA —	
10	GRIND ON O.D. BORE 19" DIA X 1/2"	764C	1	3.60	—	A130 CASTING - HEAT TREAT TO RE-35-38	
20	FACE CHAMFER END,	766	1	1.40	9.0		
30	DRILL (10) 1/4 DIA HOLES (3/8 TURN)	76Z	1	2.00	—		
40	BURR CHAMFER (10) HOLES EACH SIDE	1A	1	2.00	—		
50	BURR LEVEL TOP.	140Z	1	1.00	—		
60	SAND BLAST	14A	1	0.10	—		
	WASH					SKETCH —	
							
						ORIGINAL PAGE IS OF POOR QUALITY	
NEXT ASM.	DWG. DATE	JOB NO.	ENGINEER	DATE	PAGE OF	PART NO.	
	6/12/87	26741	AH	6/29/87	— OF —	26741-15	

ORIGINAL PAGE IS
OF POOR QUALITY



ESTIMATING DEPARTMENT OPERATION SHEET

[illegible]

PEM 0-83 DF

OPERATION SHEET

[illegible]

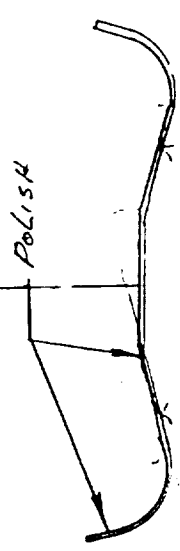
OPERATION SHEET

OPERATION SHEET

[illegible]

ORIGINAL PAGE IS
OF POOR QUALITY

ESTIMATING DEPARTMENT OPERATION SHEET

VOLUME		PART NO.		PART NAME		PCS. REQ.	
10,000/YR		26741-25		HEAD PLATE		1	
PPG/UPG NO.	MATL. CODE	COST/LB.	OTHER COST	RGH. WT.	FIN. WT.	SCRAP	EQUIP RATE
027	9.50	—	13.9	10.6	10.6	1 %	V <input type="checkbox"/> C <input type="checkbox"/>
OPER	OPERATION DESCRIPTION		EQUIP CODE	M/P	LABOR MINS.	TOOLING \$(000)	MATERIAL SPECS & BACK-UP DATA
10	BLANK TO 10" DIA		8C1	1	0.12	10.0	MAT-1064 INCB 800-1919 BLANK
20	FORM COMPLETE		8R	1	0.500	30.0	
30	POLISH INNER SURFACE - #2 FINE FINISH		7C4C	1	4.00	5.0	
40	TURN 190° CONE & TRIM TOP		7C4C	1	1.70	5.0	
50	WASH		140	1	0.10	—	
							— SKETCH —
							
NEXT ASM.	DWG. DATE	JOB NO.	ENGINEER	DATE	PAGE	OF	PART NO.
	6/16/87	21454	AW	7/7/87	—	—	26741-25

PEM 6-83 DF

RTS021 PROJECT - 1K		PIONEER ENGINEERING BILL OF MATERIAL WITH COST				PAGE 1 87/08/31	
VOLUME - 10,000 PART - 1030		DESC - ABSORBER ASSY				VENDOR	
COMPONENT	DESC - TRUNCATED TOOLING	QTY WEIGHT	MATERIAL	LAB MIN	LABOR \$	SCRAP	TOT COST
1031	ABSORBER	1	37.50	8.00	1.71V	.00	
VENDOR	.0	75.0000			M 3.82	.43	.00 43.46 *
1032	POST	28	22.12	33.88	7.56V	.00	
VENDOR	4.0	26.6840			M 26.60	.56	.00 56.84 *
1033	CAP	28	7.84	31.08	7.00V	.00	
VENDOR	.0	7.9240			M 24.36	.28	.00 39.49 *
1034	SPRING	56	145.60	.00	.00V	.00	
PURCHASED	.0	71.6800			M .00	.00	.00 145.60 *
COMPONENT TOTAL COST		181.2830	213.06	72.9	16.27V	.00	213.06
4.0					M 54.78	1.27	.00 285.38
ASSEMBLY COST			.00	.00	.00 V	.00	.00
.0					M .00	.00	.00
TOTAL COST		181.2830	213.06	72.95	16.27 V	.00	213.06
					M 54.78	1.27	.00 285.38
TOOLING		4.0					

-RTE024 PROJECT - 1K PIONEER ENGINEERING PAGE 1
MANUFACTURING COST ANALYSIS 3.21.27 67/08/31

VOLUME- 10,000 P/A- 1
PART # 1031 DESC- APSCREER UP6-

OPER	OPERATION DESCRIPTION		EQUIP	M	STD	LAE COST	CCS HRS	BURDEN	BURDEN	VAR COST	TOOLING
			P	MIN	LAE RATE			RATE	COST	MFG COST	
010			14H	1.0	5.000	1.0620	.0833 V	.00	.0000	.0000	.0
						.2124	M 16.71	1.3919	2.4539		
020			16B1	1.0	3.000	.6438	.0500 V	.00	.0000	.0000	.0
						.2146	M 48.60	2.4300	3.0738		

ANNUAL REQ-	10,000	LAE MIN -	8.0000
MAT CODE -	DST IRON	LABOR \$ -	1.7058
COST/LB -	.500	BURDEN V-	.0000
SCRAP FAC -	1.0%	BURDEN M-	3.8219
ROUGH WT -	75.0000	SCRAP -	.4303
FINAL WT -	75.0000	MATERIAL-	37.5000
		TOTAL VAR	43.4580
		TOTAL MFG	43.4580

ORIGINAL PAGE IS
OF POOR QUALITY

ORIGINAL PAGE IS
OF POOR QUALITY

RT6024 PROJECT - 1K PIONEER ENGINEERING PAGE 1
MANUFACTURING COST ANALYSIS 3.21.27 87/08/31

VOLUME- 10,000 P/A- 28
PART # - 1032 DESC- POST UPB-

OPER	OPERATION DESCRIPTION	EQUIP	Q	STD	LAB COST	CDL HRS	BURDEN	BURDEN	VAR COST	TOOLING
		P	MIN	LAB RATE			RATE	COST	MFG COST	
010		781B	1.0	.600	.1338 .2230	.0100 V M 47.25	.00 .4725	.0000 .4725	.0000 .6063	2.0
020		781B	1.0	.600	.1338 .2230	.0100 V M 47.25	.00 .4725	.0000 .4725	.0000 .6063	2.0
030		14B	1.0	.010	.0021 .2146	.0002 V M 35.79	.00 .0072	.0000 .0072	.0000 .0093	.0

ANNUAL REQ-	280,000	AB MIN -	1.2100
MAT CODE -	ST/STL	LABOR \$ -	.2697
COST/LB -	.700	BURDEN V-	.0000 TOOL \$000 4.0
SCRAP FAC -	1.0%	BURDEN M-	.9522
ROUGH WT -	1.1250	SCRAP -	.0201 TOTAL VAR 2.0295
FINAL WT -	.9530	MATERIAL-	.7875 TOTAL MFG 2.0295
		ECON YR-LCC	
		PT TYPE -	VENDOR
		MARK-UP FAC-	0.0%
		MARK-UP -	.0000
		OTHER -	.000

RT6024 PROJECT - 1K PIONEER ENGINEERING PAGE 1
MANUFACTURING COST ANALYSIS 3.21.27 87/09/31

VOLUME- 10,000 P/A- 28
PART #- 1033 DESC- CAP UPG-

OPER	OPERATION DESCRIPTION		EQUIP	M	STD	LAB COST	QCC HRS	BURDEN	BURDEN	VAR COST	TOOLING
			P	MIN	LAB RATE			RATE	COST	MFG COST	
010			7B1B	1.0	1.100	.2453	.0183 V	.00	.0000	.0000	.0
						.2230	M 47.25		.8647	1.1100	
020			14B	1.0	.010	.0021	.0002 V	.00	.0000	.0000	.0
						.2146	M 35.79		.0072	.0093	

ANNUAL REQ-	220,000		LAB MIN -	1.1100	
MAT CODE -	ST/STL	ECON YR-LDC	LABOR \$ -	.2474	
COST/LB -	.500	PT TYPE - VENDOR	BURDEN V-	.0000	TOOL \$000 .0
SCRAP FAC -	1.0%	MARK-UP FAC-	0.0%	BURDEN M-	.8719
ROUGH WT -	.5660	MARK-UP -	.0000	SCRAP -	.0140
FINAL WT -	.2830	OTHER -	.000	MATERIAL-	.2800
				TOTAL VAR	1.4133
				TOTAL MFG	1.4133

ORIGINAL PAGE IS
OF POOR QUALITY

PAGE 1
87/02/31

PIONEER ENGINEERING
MANUFACTURING COST ANALY IS

PAGE 1
87/02/31

U.S.-

311

RT6024 PROJECT - 1K PIONEER ENGINEERING PAGE 1
MANUFACTURING COST ANALYSIS 3.21.27 87/08/31

VOLUME- 10,000 P/A- 28
PART # 1035 DESC- NUT 1/2-20 HEVEY DUTY NYLOCK UFG-

OPER	OPERATION DESCRIPTION	EQUIP	M	STD	LAB COST	DEC HRS	BURDEN	BURDEN	VAR COST	TOLLING
		P	MIN	LAB RATE		RATE	COST	MFG COST		

ANNUAL REQ-	280,000					LAB MIN -		.0000		
MAT CODE -	ST/STL			ECON YR-LDC		LABOR \$ -		.0000		
COST/LB -	.000			FT TYPE - PURCHASED		BURDEN V-		.0000	TOOL \$000	.0
SCRAF FAC -	.0%			MARK-UP FAC-	0.0%	BURDEN M-		.0000		
ROUGH WT -	.0000			MARK-UP -	.0000	SCRAP -		.0000	TOTAL VAR	.1800
FINAL WT -	.1000			OTHER -	.180	MATERIAL-		.1800	TOTAL MFG	.1800

ORIGINAL PAGE IS
OF POOR QUALITY

ESTIMATING DEPARTMENT OPERATION SHEET

ORIGINAL PAGE IS
OF GOOD QUALITY

VOLUME			PART NO.		PART NAME		PCS. REQ.	
PPG/UPG NO.	MATL. CODE	COST/LB.	OTHER COST	RGH. WT.	FIN. WT.	SCRAP	MARK-UP	EQUIP. RATE
10,000/YR	8	1.50	—	75.0	75.0			
<div style="display: flex; justify-content: space-between;"> <div> <p>OPER — OPERATION DESCRIPTION —</p> <p>10 GRIND TO CLEAN BURS, ETC</p> <p>20 PAINT - (1) COAT</p> </div> <div> <p>EQUIP. CODE</p> <p>1414</p> <p>160</p> </div> <div> <p>LABOR MINS.</p> <p>5.0</p> <p>3.0</p> </div> <div> <p>TOOLING \$(000)</p> <p>—</p> </div> </div>								
<div style="display: flex; justify-content: space-between;"> <div> <p>— MATERIAL SPECS & BACK-UP DATA —</p> <p>IRON CASTING - CAST TO FINISH DIMENSIONS -</p> </div> <div> <p>— SKETCH —</p> </div> </div>								
<div style="display: flex; justify-content: space-between;"> <div> <p>— MATERIAL SPECS & BACK-UP DATA —</p> <p>IRON CASTING - CAST TO FINISH DIMENSIONS -</p> </div> <div> <p>— SKETCH —</p> </div> </div>								

ESTIMATING DEPARTMENT

OPERATION SHEET

[illegible]

DEM 8-83 DE

ESTIMATING DEPARTMENT OPERATION SHEET

[illegible]

~~ORIGINAL PAGE IS
OF POOR QUALITY~~

6'

RT5021 PROJECT - JK PIONEER ENGINEERING PAGE 1
BILL OF MATERIAL WITH COST 3.10.49 87/08/31

VOLUME - 10,000 PART - 1001 DESC - ASSY ALTERNATOR VENDOR

COMPONENT	DESC - TRUNCATED TOOLING	QTY WEIGHT	MATERIAL	LAB MIN	LABOR \$	BURDEN	SCRAP	MARK-UP	TOT COST
26741-18 VENDOR	OUTER LAMINATION 80.0	2670 85.4400	80.10	80.10	26.70V M 106.80	.00 .00	.00 .00	.00 .00	213.60 *
26741-19 VENDOR	INNER LAMINATION 30.0	1970 29.5500	19.70	39.40	.00V M 39.40	.00 .00	.00 .00	.00 .00	59.10 *
26741-20 VENDOR	ARMATURE CARRIER 8.0	1 6.3000	10.08	5.20	1.14V M 3.75	.00 .15	.00 .00	.00 .00	15.12 *
26741-21 VENDOR	SEAL RING 17.5	1 2.7000	1.17	9.15	2.01V M 5.52	.00 .09	.00 .00	.00 .00	8.79 *
26741-22 VENDOR	SUPPORT LOWER 39.0	1 9.0000	3.67	2.70	.61V M 2.01	.00 .06	.00 .00	.00 .00	6.35 *
26741-23 VENDOR	SUPPORT INNER 28.0	1 2.5000	.93	2.50	.56V M 1.74	.00 .03	.00 .00	.00 .00	3.26 *
26741-24 VENDOR	SUPPORT UPPER 35.0	1 8.7000	3.62	2.50	.56V M 1.82	.00 .06	.00 .00	.00 .00	6.06 *
26741-26 PURCHASED	MAGNET .0	270 5400.0000	702.00	.00	.00V M .00	.00 .00	.00 .00	.00 .00	702.00 *
26741-27 PURCHASED	COIL WIRE AWS-4 .0	1 60.0000	42.00	.00	.00V M .00	.00 .00	.00 .00	.00 .00	42.00 *
COMPONENT TOTAL COST		5604.1900	863.27	141.55	31.58V M 161.04	.00 .39	.00 .00	.00 .00	863.27 1056.28
ASSEMBLY COST			.00	.00	.00 V M .00	.00 .00	.00 .00	.00 .00	.00 .00
TOTAL COST		5604.1900	863.27	141.55	31.58 V M 161.04	.00 .39	.00 .00	.00 .00	863.27 1056.28
TOOLING			238.5						

ORIGINAL PAGE IS
OF POOR QUALITY

RT6024 PROJECT - 1K PIONEER ENGINEER NG MANUFACTURING COST ANALYSIS 3.21.27 PAGE 1
87/08/31

VOLUME- 10,000 P/A- 1
PART # 26741-22 DESC- SUPPORT LOWER VPS-

OPER	OPERATION DESCRIPTION	EQUIP	M	STD	LAB COST	LOC HRS	BURDEN	BURDEN	VAR COST	TOLLING
		P	KIN	LAB RATE			RATE	COST	MFG COST	
010		BA	1.0	.400	.0943 .2357	.0067 V M 25.22	.00	.0000 .1694	.0000 .2637	.0
020		BC2	1.0	.200	.0471 .2357	.0033 V M 82.17	.00	.0000 .2712	.0000 .3183	15.0
030		BC2	1.0	.200	.0471 .2357	.0033 V M 82.17	.00	.0000 .2712	.0000 .3183	15.0
040		7EAC	1.0	1.600	.3510 .2194	.0267 V M 35.89	.00	.0000 1.0384	.0000 1.3894	5.0
050		BC1	1.0	.200	.0471 .2357	.0033 V M 61.48	.00	.0000 .2029	.0000 .2500	4.0
060		14B	1.0	.100	.0215 .2146	.0017 V M 35.79	.00	.0000 .0608	.0000 .0823	.0

ANNUAL REQ-	10,000	ECON YR-LOC	LAB MIN -	2.7000
MAT CODE -	STEEL	PT TYPE - VENDOR	LABOR \$ -	.6081
COST/LB -	.270	MARK-UP FAC- 0.0%	BURDEN V-	.0000
SCRAP FAC -	1.0%	MARK-UP -	BURDEN M-	2.0139
ROUGH WT -	13.6000	OTHER -	SCRAP -	.0629
FINAL WT -	9.0000		MATERIAL-	3.6720
			TOTAL \$000	39.0
			TOTAL VAR	6.3569
			TOTAL MFG	6.3569

RT6024 PROJECT - 1X PIONEER ENGINEERING PAGE 1
MANUFACTURING COST ANALYSIS 3.21.27 87/08/31

VOLUME- 10,000 P/A- 1
PART # 26741-23 DESC- SUPPORT INNER UP6-

OPER	OPERATION DESCRIPTION		EQUIP	M	STD	LAB COST	CCC HRS	BURDEN	BURDEN	VAR COST	TOOLING
			P	MIN	LAB RATE			RATE	COST	MFG COST	
010			BA	1.0	.400	.0943	.0067 V	.00	.0000	.0000	.0
						.2357	M 25.28		.1694	.2637	
020			BC2	1.0	.200	.0471	.0033 V	.00	.0000	.0000	15.0
						.2357	M 82.17		.2712	.3183	
030			7E4C	1.0	1.600	.3510	.0267 V	.00	.0000	.0000	5.0
						.2194	M 38.89		1.0384	1.3894	
040			BD1	1.0	.200	.0471	.0033 V	.00	.0000	.0000	8.0
						.2357	M 61.48		.2029	.2500	
050			14B	1.0	.100	.0215	.0017 V	.00	.0000	.0000	.0
						.2146	M 35.79		.0608	.0823	

ANNUAL REQ-	10,000		LAB MIN -	2.5000	
MAT CODE -	STEEL	ECON YR-LOC	LABOR \$ -	.5610	
COST/LB -	.270	PT TYPE - VENDOR	BURDEN V-	.0000	TOOL \$000 28.0
SCRAP FAC -	1.0%	MARK-UP FAC-	0.0%	BURDEN M-	1.7427
ROUGH WT -	3.4400	MARK-UP -	.0000	SCRAP -	.0023
FINAL WT -	2.5000	OTHER -	.000	MATERIAL-	.9289
				TOTAL VAR	3.2648
				TOTAL MFG	3.2648

RT6024 PROJECT - 1K PIONEER ENGINEERING 3.21.27 PAGE 1
MANUFACTURING COST ANALYSIS 87/08/31

VOLUME- 10,000 P/A- 1
PART # 26741-24 DESC- SUPPORT UPPER UPS-

OPER	OPERATION DESCRIPTION		EQUIP	M	STD	LAB COST	DC	HAS	BURDEN	BURDEN	VAR COST	TOOLING
			P	MIN	LAB RATE				RATE	COST	MFG COST	
010			BA	1.0	.400	.0943 .2357		0067 V M 25.28	.00 .1694	.0000 .2637	.0000	.0
020			BC2	1.0	.200	.0471 .2357		.0033 V M 82.17	.00 .2712	.0000 .3183	.0000	15.0
030			7E4C	1.0	1.500	.3291 .2194		.0250 V M 38.89	.00 .9723	.0000 1.3014	.0000	5.0
040			BC1	1.0	.200	.0471 .2357		.0033 V M 61.48	.00 .2029	.0000 .2500	.0000	12.0
050			BC1	1.0	.200	.0471 .2357		.0033 V M 61.48	.00 .2029	.0000 .2500	.0000	4.0

ANNUAL REQ-	10,000		LAB MIN -	2.5600	
MAT CODE -	STEEL	ECON YR-LOC	LABOR \$ -	.5647	
COST/LB -	.270	PT TYPE - VENDOR	BURDEN V-	.0000	TOOL \$000 36.0
SCRAP FAC -	1.0%	MARK-UP FAC-	0.0%	BURDEN M-	1.8187
ROUGH WT -	13.4000	MARK-UP -	.0000	SCRAP -	.0600
FINAL WT -	8.7000	OTHER -	.000	MATERIAL-	3.6180
				TOTAL VAR	6.0614
				TOTAL MFG	6.0614

RT6024 PROJECT - 1K PIONEER ENGINEERING PAGE 1
MANUFACTURING COST ANALYSIS 3.21.27 87/08/31

VOLUME- 10,000 P/A- 270
PART # 26741-25 DESC- MAGNET UPG-

OPER	OPERATION DESCRIPTION		EQUIP	M	STD	LAB COST	DOC HRS	BURDEN	BURDEN	VAR COST	TOOLING
			P	MIN	LAB RATE			RATE	COST	MF6 COST	
ANNUAL REQ-	2,700,000					LAB MIN -		.0000			
MAT CODE -	STEEL	ECON YR-LOC				LABOR \$ -		.0000			
COST/LB -	.000	PT TYPE - PURCHASED				BURDEN V-		.0000	TOOL \$000		.0
SCRAP FAC -	.0%	MARK-UP FAC-			0.0%	BURDEN M-		.0000			
ROUGH WT -	.0000	MARK-UP -			.0000	SCRAP -		.0000	TOTAL VAR		2.6000
FINAL WT -	20.0000	OTHER -			2.600	MATERIAL-		2.6000	TOTAL MF6		2.6000

ORIGINAL PAGE IS
OF POOR QUALITY

ORIGINAL PAGE IS
OF POOR QUALITY

RTG024 PROJECT - 1K PIONEER ENGINEERING MANUFACTURING COST ANALYSIS 3.21.27 PAGE 1 87/08/31

VOLUME- 10,600 P/A- 1 USE-
PART 4- 26741-27 DESC- COIL WIRE AWG-4.

DEPT	OPERATION DESCRIPTION	EQUIP	M	STD	LAB COST	DOC HRS	BURDEN	BURDEN	VAR COST	TOOLING
			P	MIN	LAB RATE		RATE	COST	MFG COST	

ANNUAL REQ-	10,000			LAT MIN -	.0000		
MAT CODE -	COPPER	ECON YR-LOC		LAT DR \$ -	.0000		
CGST/LB -	.000	PT TYPE -	PURCHASED	BUDEN V-	.0000	TOOL \$000	.0
SCRAP FAC -	.0%	MARK-UP FAC-	0.0%	BUDEN M-	.0000		
ROUGH WT -	.0000	MARK-UP -	.0000	SC AP -	.0000	TOTAL VAR	42.0000
FINAL WT -	60.0000	OTHER -	42.000	MATERIAL-	42.0000	TOTAL MFG	42.0000

RT6024 . PROJECT - 1K PIONEER ENGINEERING PAGE 1
MANUFACTURING COST ANALYSIS 3.21.27 87/08/31

VOLUME- 10,000 P/A- 1
PART # 26741-20 DESC- ARMATURE CARRIER UFG-

OPER	OPERATION DESCRIPTION		EQUIP	M	STD	LAB COST	OCG HRS	BURDEN	BURDEN	VAR COST	TOOLING
			P	MIN	LAB RATE			RATE	COST	MFG COST	
010			7E3B	1.0	3.500	.7919 .2234	.0583 V M 48.75	.00 2.8421	.0000 3.6240	.0000	.0
020			766	1.0	1.100	.2330 .2118	.0183 V M 34.74	.00 .6357	.0000 .8687	.0000	8.0
030			14B	1.0	.100	.0215 .2146	.0017 V M 35.79	.00 .0608	.0000 .0823	.0000	.0
040			14F	1.0	.500	.1062 .2124	.0083 V M 25.55	.00 .2121	.0000 .3183	.0000	.0

ANNUAL REQ-	10,000			LAB MIN -	5.2000		
MAT CODE -	ALUMINUM	ECOR YR-LDC		LABOR \$ -	1.1426		
COST/LB -	1.440	PT TYPE -	VENDOR	BURDEN V-	.0000	TOOL \$000	8.0
SCRAP FAC -	1.0%	MARK-UP FAC-	0.0%	BURDEN M-	3.7507		
ROUGH WT -	7.0000	MARK-UP -	.0000	SCRAP -	.1497	TOTAL VAR	15.1230
FINAL WT -	6.3000	OTHER -	.000	MATERIAL-	10.0300	TOTAL MFG	15.1230

ORIGINAL PAGE IS
OF POOR QUALITY

RTE024 PROJECT - 1K
 VOLUME- 10,000 P/A- 1
 PART #- 26741-21 DESC- SEAL RING UPE-

OPER	OPERATION DESCRIPTION	EQUIP	M	STD	LBS COST	CCC LBS	BURDEN	BURDEN	VAR COST	TOOLING
			P	MIN	LBS RATE		RATE	COST	MFB COST	
010		5A1	1.0	.100	.0220 .2198	.0017 V M 26.26	.00 .0480	.0000 .0700	.0000	.0
020		5X2	1.0	.200	.0447 .2234	.0033 V M 27.82	.00 .0918	.0000 .1365	.0000	.0
030		2A2	1.0	.500	.1117 .2234	.0083 V M 25.14	.00 .2097	.0000 .3204	.0000	1.5
040		14H	1.0	.800	.1699 .2124	.0133 V M 16.71	.00 .2222	.0000 .3921	.0000	.0
050		5A1	1.0	.100	.0220 .2198	.0017 V M 26.26	.00 .0480	.0000 .0700	.0000	.0
060		5X2	1.0	.600	.1340 .2234	.0100 V M 27.82	.00 .2782	.0000 .4122	.0000	.0
070		2A2	1.0	.500	.1117 .2234	.0083 V M 25.14	.00 .2097	.0000 .3204	.0000	1.5
080		20A1	1.0	3.000	.6594 .2198	.0500 V M 52.08	.00 2.6040	.0000 3.2634	.0000	4.0
090		BC1	1.0	.150	.0354 .2357	.0025 V M 61.48	.00 .1537	.0000 .1891	.0000	4.0
100		2C	1.0	2.000	.4364 .2182	.0333 V M 27.14	.00 .9038	.0000 1.3402	.0000	1.5
110		7E4C	1.0	1.000	.2194 .2194	.0167 V M 39.89	.00 .6495	.0000 .8589	.0000	5.0
120		14B	1.0	.100	.0215 .2146	.0017 V M 35.79	.00 .0608	.0000 .0823	.0000	.0
130		14F	1.0	.100	.0212 .2124	.0017 V M 25.55	.00 .0434	.0000 .0646	.0000	.0

ORIGINAL PAGE IS
 OF POOR QUALITY

RTE024 PROJECT - 1K PIONEER ENGINEERING
 MANUFACTURING COST ANALYSIS 3.21.27
 VOLUME- 10,000 P/A- 1
 PART #- 26741-21 DESC- SEAL RING UFG-

PAGE 2
 87/08/31

OPER	OPERATION DESCRIPTION		EQUIP	M	STD	LAB COST	COO HRS	BURDEN	BURDEN	VAR COST	TOOLING
			#		MIN	LAB RATE		RATE	COST	MFG COST	
ANNUAL REQ-	10,000										
MAT CODE -	STEEL	ECON YR-LCC									
COST/LB -	.300	FT TYPE - VENDOR									
SCRAP FAC -	1.0%	MARK-UP FAC-			0.0%					TOOL \$000	17.5
ROUGH WT -	3.9000	MARK-UP -			.0000						
FINAL WT -	2.7000	OTHER -			.000					TOTAL VAR	8.7871
										TOTAL MFG	8.7871

ORIGINAL PAGE IS
 OF POOR QUALITY

ORIGINAL PAGE IS
OF POOR QUALITY

RT6024 PROJECT - JK PIONEER ENGINEERING MANUFACTURING COST ANALYSIS 3.21.27 PAGE 1
87/09/31

VOLUME- 10,000 P/A- 2,670
PART #- 26741-18 DESC- OUTER LAMINATION UPB-

OPER	OPERATION DESCRIPTION	EQUIP	M	STD	LAB COST	CCC HRS	BURDEN	BURDEN	VAR COST	TDC LINE
		P	MIN	LAB RATE			RATE	COST	MFG COST	
010		BL2	.5	.030	.0035	.0005 V	.00	.0000	.0000	.0
					.2357	M 29.04		.0145	.0180	
020		BE2	.5	.030	.0035	.0005 V	.00	.0000	.0000	80.0
					.2357	M 48.60		.0243	.0278	

ANNUAL REQ-	26,700,000					LFB MIN -	.0300			
MAT CODE -	ST/STL	ECON YR-LDC				LABOR \$ -	.0070			
COST/LB -	.620	PT TYPE -	VENDOR			BURDEN V-	.0000	TOOL \$000	80.0	
SCRAP FAC -	1.0%	MARK-UP FAC-	0.0%			BURDEN M-	.0388			
ROUGH WT -	.0520	MARK-UP	-	.0000		SCRAP -	.0008	TOTAL VAR	.0788	
FINAL WT -	.0320	OTHER	-	.000		MATERIAL-	.0322	TOTAL MFG	.0788	

RT8024 PROJECT - 1K PIONEER ENGINEERING PAGE 1
MANUFACTURING COST ANALYSIS 3.21.27 87/08/31

VOLUME- 10,000 P/A- 1,970
PART # 26741-19 DESC- INNER LAMINATION UPB-

OPER	OPERATION DESCRIPTION		EQUIP	M	STD	LAB COST	OCC HRS	BURDEN	BURDEN	VAR COST	TOOLING
			P	MIN	LAB RATE			RATE	COST	MFG COST	
010			2L2	.5	.015	.0018	.0003 V	.00	.0000	.0000	.0
						.2357	M 29.04		.0087	.0105	
020			BE2	.5	.015	.0018	.0003 V	.00	.0000	.0000	30.0
						.2357	M 48.60		.0146	.0164	

ANNUAL REQ-	19,700,000		LAB MIN -	.0150		
MAT CODE -	ST/STL	ECON YR-LDC	LABOR \$ -	.0036		
COST/LB -	.630	PT TYPE - VENDOR	BURDEN V-	.0000	TOOL \$000	30.0
SCRAP FAC -	1.0%	MARK-UP FAC-	0.0%	BURDEN M-	.0233	
ROUGH WT -	.0160	MARK-UP -	.0000	SCRAP -	.0004	TOTAL VAR
FINAL WT -	.0150	OTHER -	.000	MATERIAL-	.0101	TOTAL MFG
						.0374

ORIGINAL PAGE IS
OF POOR QUALITY

ESTIMATING DEPARTMENT OPERATION SHEET

ORIGINAL PAGE IS
OF POOR QUALITY

VOLUME		PART NO.	PART NAME		PCS. REQ.			
10,000/VR		26741-18	OUTER LAMINATION		2670			
PPG/UPG NO.	MATL. CODE	COST/LB.	OTHER COST	RGH. WT.	FIN. WT.	SCRAP	MARK-UP	EQUIP. RATE
							%	V C
	41	.62		0.052	0.032		1	
OPER	— OPERATION DESCRIPTION —		EQUIP. CODE	M/P	LABOR MINS.	TOOLING \$(000)	— MATERIAL SPECS & BACK-UP DATA —	
10	DECOR, STRAIGHTEN, FEED		822	.5	0.03		MAT- M19 STEEL-236A COIL	
							X 2 3/4 WIDE. COATED -	
20	PROGRESSIVE DIE:		822	.5	0.03	20.0		
	NOTCH							
	BLANK OPENING							
	EMBOS							
	OUTER							
							— SKETCH —	
NEXT ASM.	DWG. DATE	JOB NO.	ENGINEER	DATE	PAGE	OF	PART NO.	
	6/16/87	211514	JW	6/30/87			26741-18	

OPERATION SHEET

[illegible]

ESTIMATING DEPARTMENT OPERATION SHEET

[illegible]

OPERATION SHEET

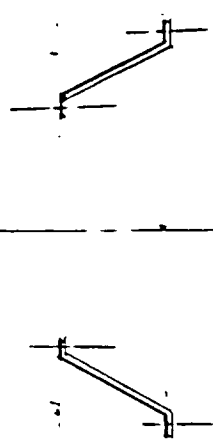
PEM 0-03 DF

[illegible]

OPERATION SHEET

[illegible]

ESTIMATING DEPARTMENT OPERATION SHEET

VOLUME		PART NO.		PART NAME		PCS. REQ.	
PPG/UPG NO.	10,000/YR	26741-24	042	0.27	SUPPORT - UPPER	13.4	8.7
MAIL. CODE		COST/LB.		OTHER COST		FIN. WT.	
042		0.27				8.7	
SCRAP		MARK-UP		EQUIP RATE		EQUIP RATE	
1%		1%		1%		1%	
OPER	DESCRIPTION	EQUIP CODE	M/P	LABOR MINS.	TOOLING \$(000)	MATERIAL SPECS & BACK-UP DATA	
10	SQUARE SHEAR BLANK	8A	1	0.40	—	MAT - 18 GA HRS - P30 21X21	
20	DRAW FORM	8C2	1	0.200	15M	BLANK	
30	TRIM TOP AND BOTTOM	7EAC	1	1.500	3M		
40	PURGE HOLES - SMALL FLANGE	8C1	1	0.200	18M		
50	PURGE HOLES - LARGE FLANGE	8C1	1	0.300	4M		
	(DIE COMMON TO 22 & 21)						
						— SKETCH —	
							
						<p>ORIGINAL PAGE IS OF POOR QUALITY</p>	

NEXT ASM.	DWG. DATE	JOB NO.	DATE	ENGINEER	PAGE	OF	PART NO.
	6/16/87	2454	7/2/87	AN	—	—	27641-24

RT6021 PROJECT - 1K PIONEER ENGINEERING PAGE 1
BILL OF MATERIAL WITH COST 3.11.01 87/10/14

VOLUME - 10,000 PART - MTI-100 DESC - POWER CONTR & COND PURCHASED

COMPONENT	DESC - TRUNCATED TOOLING	QTY WEIGHT	MATERIAL	LAB MIN	LABOR \$	BURDEN	SCRAP	MARK-UP	TOT COST
MTI-VC-50 VENDOR	VOLTAGE CONTROLLER A 87.5	1 19.5400	254.82	34.01	7.54V M	.00 31.18	.00 .40	.00	293.94 *
MTI-VC-51 PURCHASED	CAPACITOR .0	23 .0000	173.19	.00	.00V M	.00 .00	.00 .00	.00	173.19 *
COMPONENT TOTAL COST		19.5400	428.01	34.01	7.54V	.00	.00		428.01
		87.5			M	31.18	.40	.00	467.13
ASSEMBLY COST			.00	.00	.00 V	.00	.00		.00
		.0			M	.00	.00	.00	.00
TOTAL COST		19.5400	428.01	34.01	7.54 V	.00	.00		428.01
					M	31.18	.40	.00	467.13
TOOLING		87.5							
EQUIPMENT			4,790,200						

ORIGINAL PAGE IS
OF POOR QUALITY

RT6021		PROJECT - 1K		PIONEER ENGINEERING BILL OF MATERIAL WITH C-ST			3.11.01		PAGE 1 8/10/14	
VOLUME - 10,000		PART - MTI-VC-50		DESC - VOLTAGE CONTROLLER ASSY				VENDOR		
COMPONENT	DESC - TRUNCATED TODLING	QTY WEIGHT	MATERIAL	LAB MIN	LAPOR \$	BURDEN	SCPAD	MARK-UP	TOT COST	
MTI-VC-1 VENDOR	HOUSING 35.0	1 7.6000	.00	12.00	2.70V M	.00 20.20	.00 .23	.00	23.13 *	
MTI-VC-2 VENDOR	BRUSH SUPT 7.0	1 .5500	.00	3.01	.65V M	.00 1.53	.00 .02	.00	2.20 *	
MTI-VC-10 PURCHASED	BRUSH ASST 3/8 SQ .0	2 .0000	9.00	.00	.00V M	.00 .00	.00 .00	.00	9.00 *	
MTI-VC-3 VENDOR	BASE PLATE 9.0	1 3.7000	.00	.85	.19V M	.00 .62	.00 .01	.00	.82 *	
MTI-VC-4 VENDOR	TERMINAL COVER 8.0	1 1.0000	.44	1.01	.24V M	.00 .74	.00 .01	.00	1.43 *	
MTI-VC-5 VENDOR	TERMINAL BOARD .5	1 .1400	.81	.0	.01V M	.00 .06	.00 .01	.00	.87 *	
MTI-VC-6 PURCHASED	TERMINAL BLOCK .0	3 .0000	.90	.00	.00V M	.00 .00	.00 .00	.00	.90 *	
MTI-VC-7 VENDOR	CONTACT RING 3.0	1 1.1000	.00	3.15	.86V M	.00 1.88	.00 .00	.00	2.34 *	
MTI-VC-8 VENDOR	UPPER COVER 10.0	1 4.7000	1.82	5.15	1.17V M	.00 3.52	.00 .07	.00	6.58 *	
MTI-VC-9 PURCHASED	GEAR MOTOR .0	1 .0000	75.00	.00	.00V M	.00 .00	.00 .00	.00	75.00 *	
MTI-VC-15 PURCHASED	COIL ASSY .0	1 .0000	164.00	.00	.00V M	.00 .00	.00 .00	.00	164.00 *	
MTI-VC-13 VENDOR	MOTOR SUPPORT 15.0	1 .7500	.31	.65	.15V M	.00 .57	.00 .01	.00	1.04 *	
MTI-VC-12 PURCHASED	GASKET .0	1 .0000	.40	.00	.00V M	.00 .00	.00 .00	.00	.40 *	
MTI-VC-16 PURCHASED	GASKET .0	1 .0000	.90	.00	.00V M	.00 .00	.00 .00	.00	.90 *	
MTI-VC-17 PURCHASED	SCREW 1/4-20 X 5/8 F .0	24 .0000	.48	.00	.00V M	.00 .00	.00 .00	.00	.48 *	
MTI-VC-18 PURCHASED	SCREW 1/4-20 X 3/8 B .0	8 .0000	.16	.00	.00V M	.00 .00	.00 .00	.00	.16 *	
MTI-VC-19 PURCHASED	SCREW #10-24 X 5/8 F .0	8 .0000	.16	.00	.00V M	.00 .00	.00 .00	.00	.16 *	

RT6021 PROJECT - 1K PIONEER ENGINEERING PAGE 2
 BILL OF MATERIAL WITH COST 3.11.01 87/10/14

VOLUME - 10,000 PART - MTI-VC-50 DESC - VOLTAGE CONTROLLER ASSY VENDOR

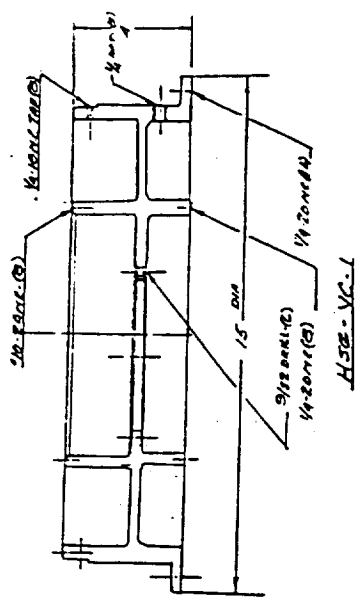
COMPONENT	DESC - TRUNCATED TOOLING	QTY WEIGHT	MATERIAL	LAB MIN	LABOR \$	BURDEN	SCRAP	MARK-UP	TOT COST
MTI-VC-20 PURCHASED	SCREW 1/4-20 X 5/8 H .0	8 .0000	.16	.00	.00V M	.00 .00	.00 .00	.00	.16 *
MTI-VC-21 PURCHASED	BOLT 1/4-20 X 1 HEX .0	4 .0000	.12	.00	.00V M	.00 .00	.00 .00	.00	.12 *
MTI-VC-22 PURCHASED	NUT 1/4-20 .0	4 .0000	.08	.00	.00V M	.00 .00	.00 .00	.00	.08 *
MTI-VC-23 PURCHASED	WASHER 1/4" LOCK .0	4 .0000	.04	.00	.00V M	.00 .00	.00 .00	.00	.04 *
MTI-VC-24 PURCHASED	FITTING .0	2 .0000	.04	.00	.00V M	.00 .00	.00 .00	.00	.04 *
COMPONENT TOTAL COST		19.5400	254.82	26.62	5.97V M	.00 29.12	.00 .36		254.82 290.27
ASSEMBLY COST			.00	7.39	1.57 V M	.00 2.06	.00 .04		.00 3.67
TOTAL COST		19.5400	254.82	34.01	7.54 V M	.00 31.18	.00 .40		254.82 293.94
TOOLING			87.5						

ORIGINAL PAGE IS
 OF POOR QUALITY

ESTIMATING DEPARTMENT OPERATION SHEET

VOLUME		PART NO.	PART NAME	PCS. REQ.	
PPG/UPG NO.	MATL. CODE	COST/LB.	OTHER COST	RGH. WT.	FIN. WT.
1010000/48	003			5.0 #	7.6 #
MACHINE BOTTOM COMPLETE					
10	78	0.5	11.9	10.0	
MACHINE TOP COMPLETE					
20	78	0.5	11.9	25.0	
MACHINE FIXTURE					
30	140	1.0	0.10		

DATE 10/2/87
 ENGINEER AN
 PART NO. MTI-VC-1
 PAGE 1 OF 1



OPERATION SHEET

DEM 0-03 DE

VOLUME		PART NO.		PART NAME		PCS. REQ.	
PPG/UPG NO.	MATL. CODE	COST/LB.	OTHER COST	RGH. WT.	FIN. WT.	SCRAP	MARK-UP
10.000	042	0.26	0.07	1.41	1.00	1%	1%
<p>OPERATION DESCRIPTION</p> <p>BLANK-9" DIA.</p> <p>STEEL RULE DIE</p> <p>PRE (B) 9/32 DIA HOLES</p> <p>PRE UNITS</p> <p>DEAD FORM</p> <p>(HYDRO FORM)</p> <p>WASH</p> <p>PAINT-PRIME</p>							
10			021	1.0	0.30	1.0	
20			BA	1.0	0.30	2.0	
30			BE	1.0	0.30	5.0	
40			148	1.0	0.05	-	
50			168	1.0	0.10	-	
<p>--- MATERIAL SPECS & BACK-UP DATA ---</p> <p>MAT. - 16GA CRS - 7" BLANK</p> <p>--- SKETCH ---</p>							

ORIGINAL PAGE IS
OF FOUR QUALITY

PART NO. MTI-VE.4
 DATE 10/2/87
 PAGE 1 OF 1
 ENGINEER AN

NEXT ASM.
 DWG. DATE
 JOB NO. 21454

DEM 8-83 OF

ORIGINAL PAGE IS
OF POOR QUALITY

OPERATION SHEET

ITEM 0-03 OF

OPERATION SHEET

OPERATION SHEET

[illegible]

~~ORIGINAL PAGE IS~~
~~OF POOR QUALITY~~

ESTIMATING DEPARTMENT OPERATION SHEET

VOLUME 10,000		PART NO. MTI-VE-13		PART NAME 110 TOL 5400000		PCS. REQ. 1	
PPG/UPG NO.	MATL. CODE 042	COST/LB. 0.26	OTHER COST	RGH. WT. 1.2	FIN. WT. 0.75	SCRAP 1 %	MARK-UP %
EQUIP. RATE C		EQUIP. RATE V <input checked="" type="checkbox"/>					
OPER	OPERATION DESCRIPTION		EQUIP. CODE	M/P	LABOR MINS.	TOOLING \$(000)	MATERIAL SPECS & BACK-UP DATA
10	CUT BLANK-STEEL RAIL DIC		8E1	1.0	0.20	1.0	MAT-16 GA-C25 - 8" BLANK
20	DRAW FORM		8R	1.0	0.20	4.0	
30	HYDRO FORM		8E1	1.0	0.10	5.0	
40	PRE (6) 7/32 IN LWR FEG		8E1	1.0	0.10	5.0	
50	PAG (4) 9/32 IN 3/4 IN TOP		8E1	1.0	0.10	5.0	
	WASH		1AB	1.0	0.05	-	
<div style="text-align: center;"> <p>— SKETCH —</p> </div>							
NEXT ASM.	DWG. DATE	JOB NO. 2145-1	ENGINEER AN	DATE 10/2/87	PAGE 1	OF 1	PART NO. MTI-VE-13

PEM 8-83 DF

ORIGINAL PAGE IS
OF POOR QUALITY

COOLANT CIRCUIT		
Coolant Radiator With Fan & Motor	41.6 BTU/Min Young #AV6005	<u>500 PCS.</u> \$1,995.00
		<u>OEM</u> \$897.75
Pump - Coolant	Grundfos 6.2 GPM	\$ 52.99
		<u>\$ 23.86</u>
		\$921.61

COMPARISON OF COSTS: 713LC vs. XF-818 HEATER DOME

Investigation of XF-818 has revealed only one (1) source for this material — Howmet Turbine Components Corp., Ann Arbor, Michigan.

Information received there indicated that this is a rarely used material which they developed for a specific customer and which is considered to be available only on special order in 2,000 lb. lots.

When pressed for a comparative cost with 713LC, they estimated 713LC at \$7.00 to \$7.50 per pound vs. XF-818 at \$4.00 to \$5.00 per pound for ingot materials.

With this information we contacted Bob Braden, Sales Manager at their LaPorte, Indiana plant, the only foundry they can recall having used it. Mr. Braden estimated the "as cast" cost would be about 70% of 713LC based on our discussions and assumptions.

It should be noted that this is a very broadly based estimate with possibility of wide variances when specific quotes are possible.

The part cost has been revised for XF-818 to the increased weight from 34 pounds to 67 pounds and the material cost to \$29.40 per pound, 70% of the \$42.00 shown for 713LC.

A review of previous Pioneer cost revealed that analysis costs were used for XF-818 not "as cast" cost.

RTS014 PROJECT - 1K PIONEER ENGINEERING PASE 1
MANUFACTURING COST ANALYSIS 3.18 87/11/13

VOLUME- 10,000 P/A- 1
PART #- 26741-3 DESC- HEATER DOME
BFB-

OPER	OPERATION DESCRIPTION	EQUIP	M	STD	LAB COST	ODD HRS	BURDEN	BURDEN	VAR COST	TOOLING
		P	MIN	LAB RATE			RATE	COST	MFG COST	
010		7E3A	1.0	3.300	.7300 .2212	.0551 V M 41.31	.00	.0000 2.2721	.0000 3.0021	.0
020		7E3A	1.0	7.900	1.7475 .2212	.1317 V M 41.31	.00	.0000 5.4405	.0000 7.1630	10.0
030		7F3	1.0	3.000	.6702 .2234	.0500 V M 41.17	.00	.0000 2.0585	.0000 2.7287	5.0
040		14H	1.0	2.000	.4245 .2104	.0375 V M 16.71	.00	.0000 .5564	.0000 .5812	.0
050		7E2	1.0	2.000	.4282 .2146	.0375 V M 28.83	.00	.0000 .7636	.0000 1.1928	7.0
070		7E4	1.0	25.500	5.5208 .2165	.4251 V M 32.75	.00	.0000 17.9188	.0000 19.4398	20.0
080		14H	1.0	18.000	3.8032 .2124	.3000 V M 16.71	.00	.0000 5.0130	.0000 9.8362	.0
090		3C	1.0	2.000	.4468 .2234	.0375 V M 30.23	.00	.0000 1.0067	.0000 1.4535	10.0
100		14B	1.0	.300	.0644 .2146	.0050 V M 35.79	.00	.0000 .1790	.0000 .2434	.0

ORIGINAL PAGE IS
OF POOR QUALITY

VOLUME- 10,000 P/A- 1
PART # 25741-3 DESC- HEATER DOME UFG-

OPER	OPERATION DESCRIPTION		M P	STD MIN	LAB COST LAB RATE	CON WTS	FURNEN RATE	FURNEN COST	VAR COST MPS COST	TOOLING
	EQUP									

ANNUAL REQ-	10,000	ECON YR-LOC		LABOR \$ -	13.9539		
MAT CODE -	ST/STL	PT TYPE -	VENDOR	SHRDN V-	.0000	TOTL \$000	52.0
COST/LB -	29.400	MARY-UP FAC-	0.0%	SHRDN M-	31.2053		
SCRAP FAC -	1.0%	MARY-UP -	.0000	SRGP -	20.4787	TOTAL VAR	2,068.3442
ROUGH WT -	67.0000	OTHER -	33.000	MATERIAL-	2,002.9000	TOTAL MFB	2,068.3442
FINAL WT -	54.0000						

ORIGINAL PAGE IS
OF POOR QUALITY

" ROUGH WEIGHT: 69.0 LBS.

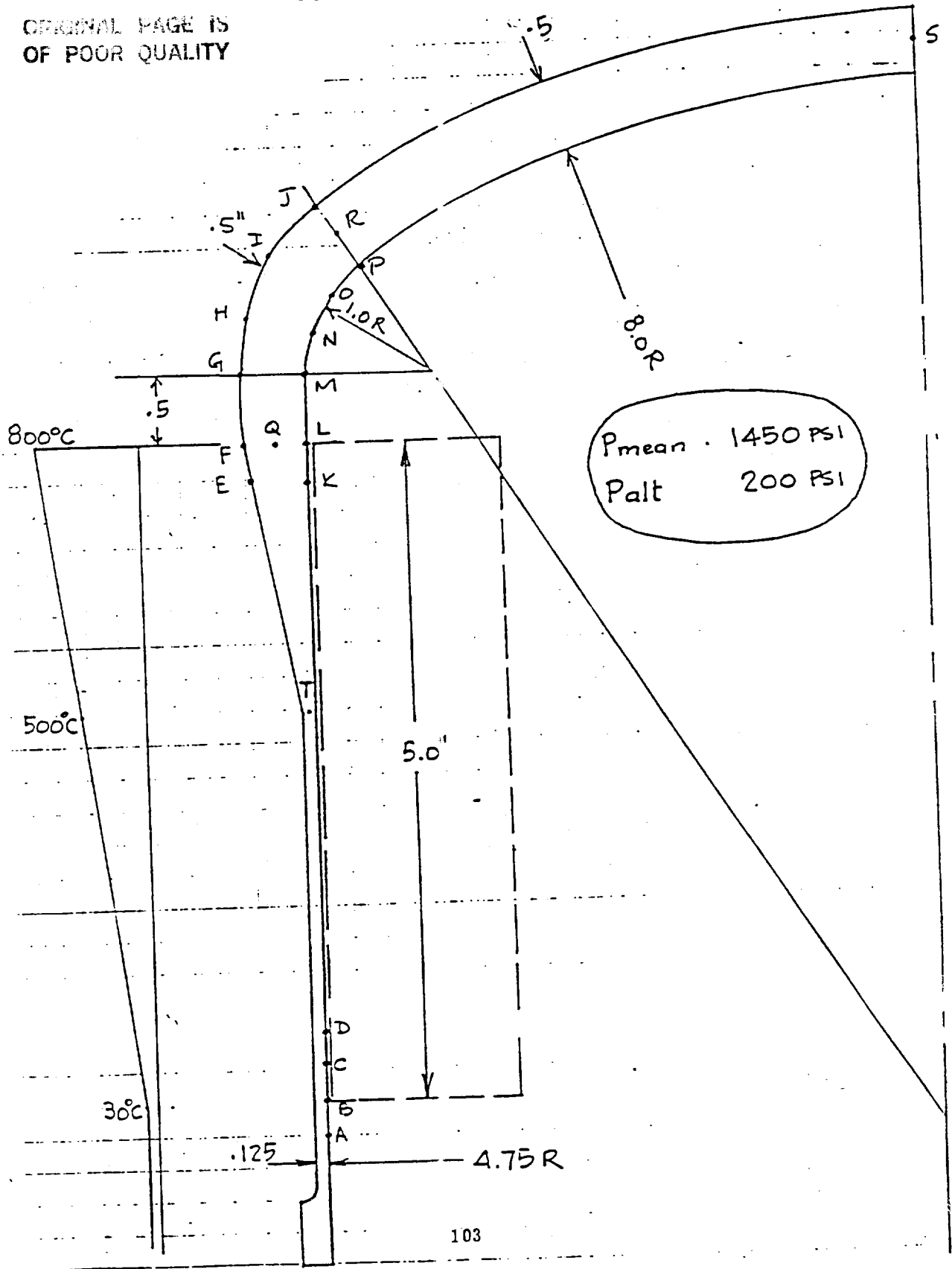


MTI SOLAR ENGINE

APPROX $1/2$ SCALE

HEATER HEAD 713LC

ORIGINAL PAGE IS
OF POOR QUALITY



RT6014 PROJECT - 31 PIONEER ENGINEERING PAGE 1
MANUFACTURING COST ANALYSIS 1.35.45 87/10/16

VOLUME- 10,000 P/A- 1
PART # 26741-3-A DESC- HEATER DOME (XF-818) UP6-

OPER	OPERATION DESCRIPTION		EQUIP	M	STD	LAB COST	OCC HRS	BURDEN	BURDEN	VAR COST	TOOLING
			P		MIN	LAB RATE		RATE	COST	MFG COST	
010		7E3A	1.0		3.300	.7300 .2212	.0550 V M 41.31	.00 2.2721	.0000 3.0021	.0000	.0
020		7E3A	1.0		7.900	1.7475 .2212	.1317 V M 41.31	.00 5.4405	.0000 7.1880	.0000	10.0
030		7P3	1.0		3.000	.6702 .2234	.0500 V M 41.17	.00 2.0585	.0000 2.7287	.0000	5.0
040		14H	1.0		2.000	.4248 .2124	.0333 V M 16.71	.00 .5564	.0000 .9812	.0000	.0
050		7B2	1.0		2.000	.4292 .2146	.0333 V M 22.93	.00 .7636	.0000 1.1928	.0000	7.0
070		7B4	1.0		25.500	5.5208 .2165	.4250 V M 32.75	.00 13.9188	.0000 19.4396	.0000	20.0
080		14H	1.0		18.000	3.8232 .2124	.3000 V M 16.71	.00 5.0130	.0000 8.8362	.0000	.0
090		3C	1.0		2.000	.4468 .2234	.0333 V M 30.23	.00 1.0067	.0000 1.4535	.0000	10.0
100		14B	1.0		.300	.0644 .2146	.0050 V M 35.79	.00 .1790	.0000 .2434	.0000	.0

ORIGINAL PAGE IS
OF POOR QUALITY

PIONEER ENGINEERING
MANUFACTURING COST ANALYSIS
PAGE 2
87/10/16
1.35.45

PROJECT - 31
VOLUME- 10,000 P/A- 1
PART # - 26741-3-A DESC- HEATER DOME (XF-B18) UP6-

OPER	OPERATION DESCRIPTION	EQUIP	M	STD	LAB COST	O C HRS	BURDEN	BURDEN	VAR COST	TOOLING
			P	MIN	LAE RATE		RATE	COST	MFG COST	

ANNUAL REQ-	10,000						LAB MIN -	64.0000		
MAT CODE -	ST/STL	ECON YR-LOC					LABOR \$ -	13.8569		
COST/LB -	34.000	PT TYPE -	VENDOR				BURDEN V-	.0000	TDDL \$000	52.0
SCRAP FAC -	1.0%	MARK-UP FAC-	0.0%				BURDEN M-	31.2086		
ROUGH WT -	69.0000	MARK-UP -	.0000				SCRAP -	24.2407	TOTAL VAR	2,448.3062
FINAL WT -	61.0000	OTHER -	33.000				MATERIAL-	2,379.0000	TOTAL MFG	2,448.3062

RT PROJECT - 1K PIONEER ENGINEERING PAGE 1
MANUFACTURING COST ANALYSIS 3.21.27 B7/08/31

VOLUME- 10,000 P/A- 1
PART #- 26741-3 DESC- HEATER DOME UPE-

OPER	OPERATION DESCRIPTION										TOOLING
	EQUIP	M	STD	LAB COST	COL FAS	BURDEN	BURDEN	VAR COST			
	P	MIN	LAB RATE			RATE	COST	MFB COST			
010	7E3A	1.0	3.300	.7300 .2212	.0550 V M 41.31	.00 2.2721	.0000 3.0621	.0000		.0	
020	7E3A	1.0	7.900	1.7475 .2212	.1317 V M 41.31	.00 5.4405	.0000 7.1880	.0000		10.0	
030	7P3	1.0	3.000	.6702 .2234	.0500 V M 41.17	.00 2.0585	.0000 2.7287	.0000		5.0	
040	14H	1.0	2.000	.4248 .2124	.0333 V M 16.71	.00 .5564	.0000 .5812	.0000		.0	
q	7E2	1.0	2.000	.4292 .2146	.0333 V M 22.93	.00 .7636	.0000 1.1928	.0000		7.0	
070	7B4	1.0	25.500	5.5208 .2165	.4250 V M 32.75	.00 13.9188	.0000 19.4396	.0000		20.0	
080	14H	1.0	18.000	3.8232 .2124	.3000 V M 16.71	.00 5.0130	.0000 8.8362	.0000		.0	
090	3C	1.0	2.000	.4468 .2234	.0333 V M 30.23	.00 1.0067	.0000 1.4575	.0000		10.0	
100	14B	1.0	.300	.0644 .2146	.0050 V M 35.79	.00 .1790	.0000 .2434	.0000		.0	

ORIGINAL FILED IN
OF POOR QUALITY

ORIGINAL PAGE IS
OF POOR QUALITY

RT PROJECT - 1Y PIONEER ENGINEERING PAGE 2
MANUFACTURING COST ANALYSIS 3.21.27 87/08/31

VOLUME- 10,000 P/A- 1
PART # 26741-3 DESC- HEATER DOME UPG-

OPER	OPERATION DESCRIPTION	EQUIP	M	STD	LAB COST	DEC HAS	BURDEN	BURDEN	VAR COST	TOOLING
		F	MIN	LAB RATE			RATE	COST	MF6 COST	

ANNUAL REQ-	10,000				LAB MIN -	64.0000				
MAT CODE -	ST/STL			ECON YR-LOC	LABOR \$ -	13.8569				
COST/LB -	42.000			PT TYPE -	BURDEN V-	.0000		TOOL \$000	52.0	
SCRAP FAC -	1.0%			MARK-UP FAC-	BURDEN M-	31.2086				
ROUGH WT -	34.0000			MARK-UP -	SCRAP -	15.0607		TOTAL VAR	1,521.1262	
FINAL WT -	26.0000			OTHER -	MATERIAL-	1,461.0000		TOTAL MF6	1,521.1262	

United States Patent [19]
Croat

[11] Patent Number: 4,496,395
[45] Date of Patent: Jan. 29, 1985

[54] HIGH COERCIVITY RARE EARTH-IRON
MAGNETS

[75] Inventor: John J. Croat, Sterling Heights,
Mich.

[73] Assignee: General Motors Corporation, Detroit,
Mich.

[21] Appl. No.: 274,070

[22] Filed: Jun. 16, 1981

[51] Int. Cl.³ C22C 33/00

[52] U.S. Cl. 75/123 E; 148/31.57;
164/462; 420/416

[58] Field of Search 75/170, 152, 123 E,
75/134 F; 148/31.57; 164/462, 463, 479, 423,
427, 429; 420/416

[56] References Cited

U.S. PATENT DOCUMENTS

3,102,002 8/1963 Wallace et al. 75/152
3,421,889 1/1969 Ostertag et al. 75/170
3,560,200 2/1971 Nesbitt et al. 75/170
3,615,911 10/1971 Nesbitt et al. 148/31.57
3,790,414 2/1974 Tawara et al. 75/170
3,845,805 11/1974 Kavesh 164/81
4,142,571 3/1979 Narasimhan 164/88
4,152,486 5/1979 Imamura et al. 75/123 E

4,190,095 2/1980 Bedell 164/463
4,192,696 3/1980 Menth et al. 75/170
4,197,146 4/1980 Frischman 148/31.55
4,308,474 12/1981 Savage et al. 75/123 E

FOREIGN PATENT DOCUMENTS

104862 3/1981 Japan .

OTHER PUBLICATIONS

Clark, "High-Field Magnetization and Coercivity of Amorphous Rare Earth-Fe₂ Alloys" Appl. Phys. Lett. vol. 23, No. 11, Dec. 1973, pp. 642-644.

Chaudhari et al., "Metallic Glasses" Scientific American Apr. 1980, pp. 98-117.

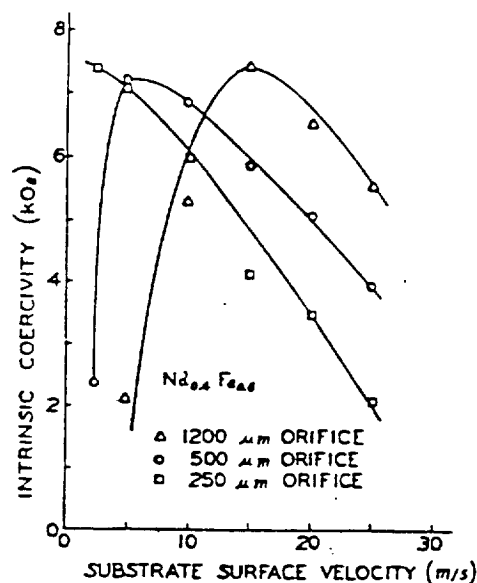
Primary Examiner—John P. Sheehan

Attorney, Agent, or Firm—E. F. Harasek

[57] ABSTRACT

Ferromagnetic compositions having intrinsic magnetic coercivities at room temperature of at least 1,000 Oersted are formed by the controlled quench of molten rare earth-transition metal alloys. Hard magnets may be inexpensively formed from the lower atomic weight lanthanide elements and iron.

21 Claims, 6 Drawing Figures



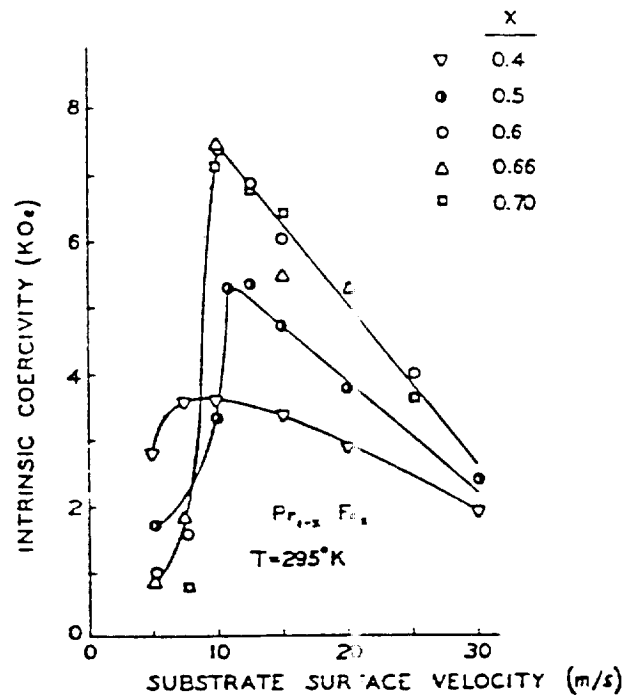
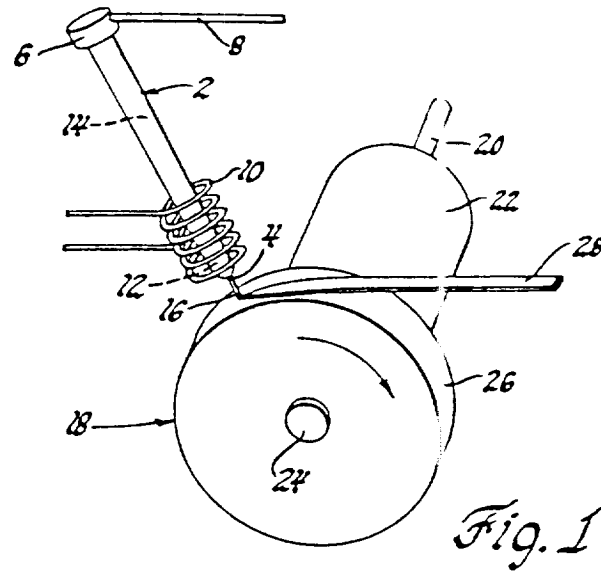


Fig. 6

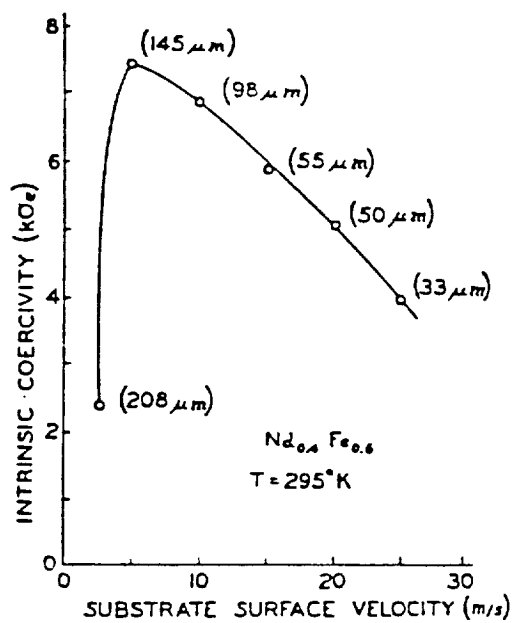


Fig. 2

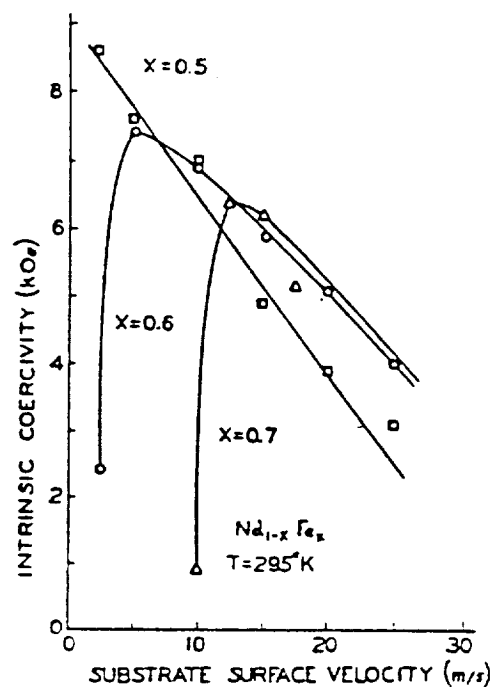


Fig. 3

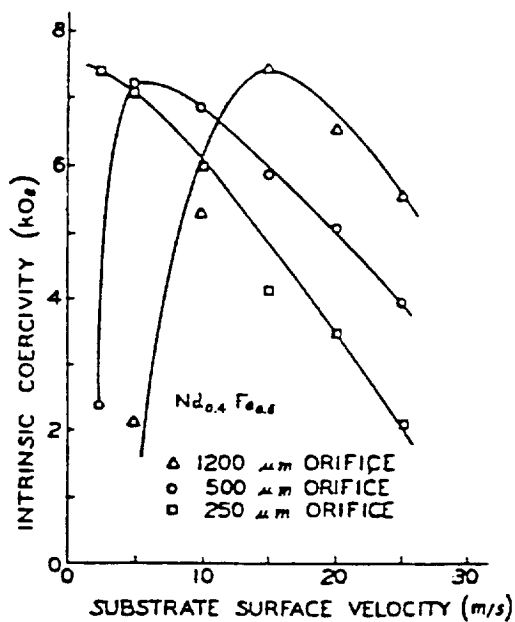


Fig. 4

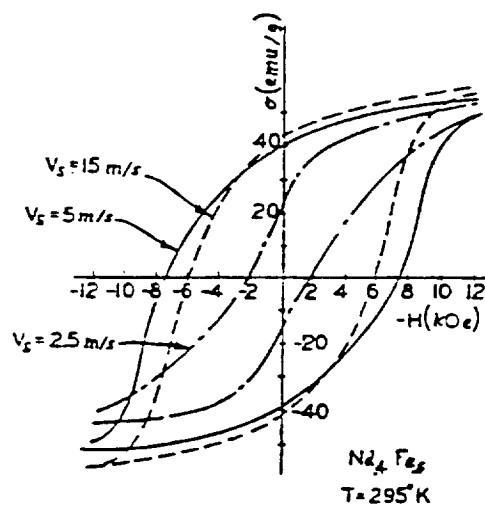


Fig. 5

HIGH COERCIVITY RARE EARTH-IRON MAGNETS

This invention relates to substantially amorphous rare earth-iron (Re-Fe) alloys with high room temperature magnetic coercivities and to a reliable method of forming such magnetic alloys from molten precursors.

BACKGROUND

Intermetallic compounds of certain rare earth and transition metals (RE-TM) can be made into magnetically aligned permanent magnets with coercivities of several thousand Oersteds. The compounds are ground into sub-crystal sized particles commensurate with single magnetic domain size, and are then aligned in a magnetic field. The particle alignment and consequently the magnetic alignment, is fixed by sintering or by dispersing the particles in a resinous binder or low melting metal such as lead. This is often referred to as the powder metallurgy process of making rare earth-transition metal magnets. When treated in this manner, these intermetallic compounds develop high intrinsic magnetic coercivities at room temperature.

The most common intermetallic compounds processable into magnets by the powder metallurgy method contain substantial amounts of the elements samarium and cobalt, e.g., SmCo_5 , $\text{Sm}_2\text{Co}_{17}$. Both of these metals are relatively expensive due to scarcity in the world market. They are, therefore, undesirable components for mass produced magnets. Lower atomic weight rare earth elements such as cerium, praseodymium and neodymium are more abundant and less expensive than samarium. Similarly, iron is preferred over cobalt. However, it is well known that the light rare earth elements and iron do not form intermetallic phases when homogeneously melted together and allowed to crystallize as they cool. Moreover, attempts to magnetically harden such rare earth-iron alloys by powder metallurgy processing have not been successful.

This invention relates to a novel, efficient and inexpensive method which can be used to produce magnetically coercive rare earth-iron alloys directly from homogenous molten mixtures of the elements.

OBJECTS

It is an object of the invention to provide magnetically hard RE-TM alloys, particularly Re-Fe alloys, and a reliable means of forming them directly from molten mixtures of the elements. A more particular object is to provide a method of making magnetically hard alloys from mixtures of rare earth elements and iron which do not otherwise form high coercivity intermetallic phases when allowed to crystallize as they cool. A further object of the invention is to control the solidification of molten rare earth-iron mixtures to produce ferromagnetic alloys with substantially amorphous microstructures as determined by X-ray diffraction. A more specific object is to provide hard magnetic alloys with room temperature coercivities of at least several thousand Oersteds directly from molten mixtures of low atomic weight rare earth elements such as Ce, Pr, Nd and, the abundant transition metal, Fe, by a specially adapted quenching process.

BRIEF SUMMARY

In accordance with a preferred practice of the invention, a magnetically hard rare earth-iron metal alloy

may be formed as follows. Mixtures of rare earth elements and iron are homogeneously alloyed in suitable proportions, preferably about 0.2 to 0.66 atomic percent iron and the balance rare earth metal. The preferred rare earth metals are the relatively low atomic weight elements which occur early in the lanthanide series such as cerium, praseodymium, and neodymium. These alloys have some room temperature coercivity, but it is generally less than 200 Oersteds. Herein, compositions with intrinsic coercivities less than about 200 Oersteds at room temperature (about 25° C.) will be referred to as soft magnets or as alloys having soft magnetic properties. The alloyed, magnetically soft Re-Fe mixture is placed in a cylindrical quartz crucible surrounded by an induction heating coil. The rare earth iron mixture is melted in the crucible by activating the induction heating coil. The crucible has an orifice at the bottom for expressing a minute stream of molten alloy. The top of the crucible is sealed and provided with means for introducing a pressurized gas above the molten alloy to propel it through the orifice. Directly adjacent the orifice outlet is a rotating chill disk made of highly heat conductive copper electroplated with chromium. Metal ejected through the orifice impinges on the perimeter of the rotating disk so that it cools almost instantaneously and evenly. The orifice diameter is generally in the range of 250-1200 microns. The preferred velocity of the perimeter of the rotating disk is about 2.5 to 25 meters per second. The disk itself, can be considered an infinitely thick chill plate. The cooling of the ejected molten alloy is, therefore, a function of heat transfer within the alloy itself onto the chill surface. I found that if the disk is maintained at room temperature, and the molten alloy is ejected through the orifice under a pressure of about 2.5 pounds per square inch, then the maximum thickness for cooled ribbon formed on the perimeter of the chill disk should be no more than about 200 microns. This provides a rate of cooling which produces the high coercivity magnetic alloys of this invention. Quench rate in spin melting can be controlled by adjusting such parameters as the diameter of the ejection orifice, the ejection pressure, the speed of the quench disk, the temperature of the disk and the temperature of the molten alloy. Herein the terms melt spinning and spin melting are used interchangeably and refer to the process of expressing a molten metal alloy through a small orifice and rapidly quenching it on a spinning chill surface.

Critical to the invention is controlling the quench rate of the molten Re-Fe alloys. Enough atomic ordering should occur upon solidification to achieve high magnetic coercivity. However, a magnetically soft crystalline microstructure should be avoided. While spin melting is a suitable method of quenching molten RE-TM to achieve hard magnetic materials, any other equivalent quenching means such as, e.g., spraying the molten metal onto a cooled substrate would fall within the scope of my invention.

I have, e.g., spun melt an alloy of $\text{Nd}_{0.5}\text{Fe}_{0.5}$ from an orifice 500 microns in diameter at an ejection pressure of 2.5 psi on a room temperature chill surface moving at a relative speed of 2.5 meters per second to directly yield an alloy with a measured coercivity of 8.65 kilo-Oersteds. The spun melt magnetic alloy had a substantially flat X-ray diffraction pattern.

DETAILED DESCRIPTION

My invention will be better understood in view of preferred embodiments thereof described by the following figures, descriptions and examples.

FIG. 1 is a schematic view of a spin melting apparatus suitable for use in the practice of the invention;

FIG. 2 is a plot of substrate surface velocity versus intrinsic coercivity for $\text{Nd}_{0.4}\text{Fe}_{0.6}$ at 295°K . The parenthetical numbers adjacent the data points are measured ribbon thicknesses.

FIG. 3 is a plot of substrate surface velocity versus intrinsic coercivity for three different spun melt neodymium-iron alloys;

FIG. 4 is a plot of chill substrate surface velocity versus intrinsic magnetic coercivity for spun melt $\text{Nd}_{0.4}\text{Fe}_{0.6}$ at ejection orifice diameters of 1200, 500 and 250 microns;

FIG. 5 is a hysteresis curve for $\text{Nd}_{0.4}\text{Fe}_{0.6}$ taken at 295°C . for four different chill substrate speeds.

FIG. 6 is a plot of substrate surface velocity versus intrinsic coercivity for 5 different alloys of spun melt praseodymium-iron alloys.

APPARATUS

FIG. 1 shows a schematic representation of a spin melting apparatus that could be used to practice the method of this invention. A hollow generally cylindrical quartz tube 2 is provided for retaining alloys of rare earth and transition metals for melting. The tube has a small orifice 4 in its bottom through which molten alloy is expressed. Tube 2 is provided with cap 6 which sealably retains inlet tube 8 for a pressurized inert gas such as argon. An induction type heating coil 10 is disposed around the portion of quartz tube 2 containing the metals. When the coil is activated, it heats the material within the quartz tube causing it to melt and form a fluid mass 12 for ejection through orifice 4. Gas is introduced into space 14 above molten alloy 12 to maintain a constant positive pressure so that the molten alloy is expressed at a controlled rate through orifice 4. The expressed stream 16 immediately impinges on rotating disk 18 made of copper metal plated with chromium to form a uniform ribbon 28 of alloy. Disk 18 is retained on shaft 20 and mounted against inner and outer retaining members 22 and 24, respectively. Disk 18 is rotated in a clockwise direction as depicted by a motor not shown. The relative velocity between expressed molten metal 16 and chill surface 26 is controlled by changing the frequency of rotation. The speed of disk 18 will be expressed herein as the number of meters per second which a point on the chill surface of the disk travels at a constant rotational frequency. Means may be provided within disk 18 to chill it. Disk 18 is much more massive than ribbon 28 and acts as an infinitely thick heat sink. The limiting factor for the rate of chill of the molten alloy of stream 4 is the thickness of ribbon 28. If ribbon 28 is too thick, the metal most remote from chill surface 26 will cool more slowly than that adjacent the chill surface. If the rare earth-iron alloy cools too slowly from the melt, it will solidify with a crystalline microstructure that is not permanently magnetic. If it cools too quickly, the ribbon will have relatively low coercivity (<1 koe). This invention relates to making hard RE-TM magnets by quenching molten mixtures of the elements at a rate between that which yields amorphous soft magnetic material and nonmagnetic crystalline materials. Herein, the term hard magnet or hard mag-

netic alloy will generally refer to an Re-Fe alloy with a room temperature coercivity greater than about 1,000 Oersteds that may be formed by quenching from the melt at a suitable rate. Generally, the intrinsic coercivity of these magnetic alloys will increase as the temperature approaches absolute zero.

The operational parameters of a spin melting apparatus may be adjusted to achieve optimum results by the practice of my method. For example, the rare earth and transition metals retained in the melting tube or vessel must be at a temperature above the melting point of the alloy to be in a sufficiently fluid state. The quench time for a spun melt alloy is a function of its temperature at expression from the tube orifice. The amount of pressure introduced into the melting vessel above a molten alloy will affect the rate at which metal is expressed through the orifice. The following description and examples will clearly set out for one skilled in the art methods of practicing and the results obtainable by my invention. In the above described spin melting apparatus, I prefer to use a relatively low ejection pressure, (about 2-3 psig). At such pressures the metal flows out of the orifice in a uniform stream so that when it impinges and is quenched on the cooling disk it forms a relatively uniform ribbon. Another parameter that can be adjusted is the orifice size at the outlet of the melting vessel. The larger the orifice, the faster the metal will flow from it, the slower it will cool on the chill surface and the larger will be the resultant ribbon. I prefer to operate with a round orifice with a diameter from about 250-1200 microns. Other orifice sizes may be suitable, but all other parameters would have to be adjusted accordingly for much smaller or larger orifice sizes. Another critical factor is the rate at which the chill substrate moves relative to the impingement stream of rare earth-iron alloy. The faster the substrate moves, the thinner the ribbon of rare earth transition metal formed and the faster the quench. It is important that the ribbon be thin enough to cool substantially uniformly throughout. The temperature of the chill substrate may also be adjusted by the inclusion of heating or cooling means beneath the chill surface. It may be desirable to conduct a spin melting operation in an inert atmosphere so that the Re-Fe alloys are not oxidized as they are expressed from the melting vessel and quenched.

PREFERRED COMPOSITIONS

The hard magnets of this invention are formed from molten homogeneous mixtures of rare earth elements and transition elements, particularly iron. The rare earth elements are the group falling in Group IIIA of the periodic table and include the metals scandium, yttrium and the elements from atomic number 57 (lanthanum) through 71 (lutetium). The preferred rare earth elements are the lower atomic weight members of the lanthanide series. These are the most abundant and least expensive of the rare earths. In order to achieve the high magnetic coercivities desired, I believe that the outer f-orbital of the rare earth constituents should not be empty, full, or half full. That is, there should not be zero, seven, or fourteen valence electrons in the outer f-orbital. Also suitable would be mischmetals consisting predominantly of these rare earth elements.

Herein, the relative amounts of rare earth and transition metals will be expressed in atomic fractions. In an alloy of $\text{Nd}_{0.4}\text{Fe}_{0.6}$ e.g., the alloyed mixture would contain proportionately on a weight basis 0.6 moles times the atomic weight of neodymium (144.24 grams/-

4,496,395

5

moles) or 86.544 grams and 0.4 moles times the atomic weight of iron (55.85 grams per mole) or 22.34 g. On a weight percent basis $\text{Nd}_{0.6}\text{Fe}_{0.4}$ would contain

$$\frac{\text{Wt Nd}}{\text{Wt Nd} + \text{Wt Fe}} \times 100 = 79.5\% \text{ Nd and}$$

$$\frac{\text{Wt Fe}}{\text{Wt Nd} + \text{Wt Fe}} \times 100 = 20.5\% \text{ Fe}$$

An atomic fraction of 0.4 would be equivalent to 40 atomic percent. The compositional range of the RE-TM alloys of this invention is about 20-70 atomic percent transition metal and the balance rare earth metal. Small amounts of other elements may be present so long as they do not materially affect the practice of the invention.

MAGNETISM

Magnetically soft, amorphous, glass-like forms of the subject rare earth-transition metal alloys can be achieved by spin melting followed by a rapid quench. Any atomic ordering that may exist in the alloys is extremely short range and cannot be detected by X-ray diffraction. They have high magnetic field saturations but low room temperature intrinsic coercivity, generally 100-200 Oe.

The key to practicing my invention is to quench a molten rare earth-transition metal alloy, particularly rare earth-iron alloy, at a rate slower than the cooling rate needed to form amorphous, glass-like solids with soft magnetic properties but fast enough to avoid the formation of a crystalline, soft magnetic microstructure. High magnetic coercivity (generally greater than 1,000 Oe) characterizes quenched RE-TM compositions formed in accordance with my method. These hard magnetic properties distinguish my alloys from any like composition previously formed by melt-spinning, simply alloying, or high rate sputtering followed by low temperature annealing. X-ray diffraction patterns of some of the Nd-Fe and Pr-Fe alloys to contain weak Bragg reflections corresponding to crystalline rare earths (Nd, Pr) and the $\text{RE}_2\text{Fe}_{17}$ intermetallic phases. Owing to the low magnetic ordering temperatures of these phases (less than 330° K.), however, it is highly unlikely that they could be the magnetically hard component in these melt spun alloys. The coercive force is believed due to an underlying amorphous or very finely crystalline alloy. The preferred $\text{Sm}_{0.4}\text{Fe}_{0.6}$ and $\text{Tb}_{0.4}\text{Fe}_{0.6}$ alloys also contain weak Bragg reflections which could be indexed to the REFe_2 intermetallic phases. These phases do have relatively high magnetic ordering temperatures (approximately 700° K.) and could account for the coercivity in these alloys. Magnets made by my invention not only have excellent magnetic characteristics, but are also easy and economical to produce. The following examples will better illustrate the practice of my invention.

EXAMPLE I

A mixture of 63.25 weight percent neodymium metal and 36.75 weight percent iron was melted to form a homogeneous $\text{Nd}_{0.4}\text{Fe}_{0.6}$ alloy. A sample of the alloy was dispersed in the tube of a melt spinning apparatus like that shown in FIG. 1. The alloy was melted and ejected through a circular orifice 500 microns in diameter with an argon pressure of 17 kPa (2.5 psi) onto a chill disk initially at room temperature. The velocity of the chill disk was varied at 2.5, 5, 15, 20 and 25 meters per

6

second. The intrinsic coercivities of the resulting alloys were measured at a temperature of 295° K. The alloy ribbons were pulverized to powder by a roller on a hard surface and retained in the sample tube of a magnetometer. FIG. 2 plots the measured intrinsic coercivity in kiloOersteds as a function of the substrate surface velocity for the chill member. The parenthetical numbers adjacent the data points correspond to measured ribbon thicknesses in microns. It is clear that a substrate velocity of 2.5 meters per second does not achieve the desired optimum coercivity. We believe that the ribbon layed down at this substrate surface velocity was too thick (208 microns). It cooled slowly enough to allow the growth of nonmagnetic crystal structures. The optimum quench rate appeared to be achieved at a disk surface velocity of 5 meters per second. At higher disk speeds (faster quench and thinner ribbon) the room temperature intrinsic coercivity decreased gradually indicating the formation of amorphous soft magnetic structures in the alloy.

EXAMPLE II

FIG. 3 shows a plot of measured intrinsic magnetic coercivity at 295° K. as a function of chill disk surface velocity for three different neodymium iron alloys. The alloys were composed of $\text{Nd}_{1-x}\text{Fe}_x$ where x is 0.5, 0.6 and 0.7. The maximum achievable coercivity seems to be a function of both the substrate surface velocity and the composition of the rare earth transition metal alloy. The greatest coercivity was achieved for $\text{Nd}_{0.5}\text{Fe}_{0.5}$ and a chill disk surface speed of about 2.5 meters per second. The other two neodymium iron alloys containing a greater proportion of iron showed lower maximum coercivities achieved at relatively higher substrate surface velocities. However, all of the materials had extremely good maximum room temperature coercivities (greater than 6 kiloOersteds).

EXAMPLE III

FIG. 4 shows the effect of varying the size of the ejection orifice of an apparatus like that shown in FIG. 1 for $\text{Nd}_{0.4}\text{Fe}_{0.6}$. The ejection gas pressure was maintained at about 2.5 psig and the chill disk was initially at room temperature. The figure shows that substrate surface velocity must increase as the orifice size increases. For the 250 micron orifice, the maximum measured coercivity was achieved at a substrate speed of about 2.5 meters per second. For the 500 micron orifice, the optimum measured coercivity was at a chill surface speed of 5 meters per second. For the largest orifice, 1200 microns in diameter, the optimum substrate surface speed was higher, 15 meters per second. Again, the process is limited by the thickness of the ribbon formed on the chill surface. That is, that portion of the metal most remote from the chill surface itself must cool by heat transfer through the balance the spun melt material at a rate fast enough to achieve the desired ordering of atoms in the alloy. Homogeneous cooling is desired so that the magnetic properties of the ribbon are uniform throughout. The faster the chill surface travels, the thinner the ribbon of RE-TM produced.

EXAMPLE IV

FIG. 5 shows hysteresis curves for $\text{Nd}_{0.4}\text{Fe}_{0.6}$ ejected from a 500 micron orifice at a gas pressure of 2.5 psi onto a chill member moving at rates of 2.5, 5, and 15 meters per second, respectively. Those alloys ejected

13

onto the substrate moving at a speed of 2.5 meters per second had relatively low room temperature coercivity. The narrow hysteresis curve suggests that this alloy is a relatively soft magnetic material. Alternatively, the relatively wide hysteresis curves for chill substrate velocities of 5 and 15 meters per second are indicative of materials with high intrinsic magnetic coercivities at room temperatures. They are good hard magnetic materials.

EXAMPLE V

FIG. 6 is a plot of chill disk velocity versus measured intrinsic coercivity in kiloOersteds for alloys of $\text{Pr}_{1-x}\text{Fe}_x$ where x is 0.4, 0.5, 0.6, 0.66 and 0.7. The alloys were ejected at a pressure of about 2.5 psig through a 500 micron orifice. The $\text{Pr}_{0.34}\text{Fe}_{0.66}$ and $\text{Pr}_{0.3}\text{Fe}_{0.7}$ quenched on a disk moving at about ten meters per second had measured intrinsic coercivities at 22° C. of greater than 7 kiloOersteds. The $\text{Pr}_{0.6}\text{Fe}_{0.4}$ alloy had a maximum measured coercivity of about 3.8 kiloOersteds at a quench disk surface velocity of about five meters per second.

I have also spun melt samples $\text{Tb}_{0.4}\text{Fe}_{0.6}$ and $\text{Sm}_{0.4}\text{Fe}_{0.6}$. The maximum coercivity measured for the terbium alloy was about three kiloOersteds. The samarium alloy developed a room temperature coercivity of at least 15 kiloOersteds, the highest coercivity measurable by the available magnetometer. Spun melt samples of $\text{Y}_{0.6}\text{Fe}_{0.4}$ did not develop high intrinsic coercivities. The measured coercivities of the yttrium samples were in the 100-200 Oersted range.

Thus I have discovered a reliable and inexpensive method of making alloys of rare earth elements and iron into hard magnetic materials. Heretofore, no one has been able to make such high coercivity magnets from low molecular weight rare earth elements, mischmetals, or even samarium and iron. Accordingly, while my invention has been described in terms of specific embodiments thereof, other forms may be readily adapted by one skilled in the art. Accordingly, my invention is to be limited only by the following claims.

The embodiments of the invention in which an exclusive property or privilege is claimed are defined as follows:

1. A method of making an alloy with permanent magnetic properties at room temperature comprising the steps of forming a mixture of iron and one or more rare earth elements;
 - heating said mixture to form a homogeneous molten alloy; and
 - quenching said molten alloy at a rate such that it solidifies substantially instantaneously to form an alloy having an inherent room temperature magnetic coercivity of at least about 5,000 Oersteds as quenched.
2. A method of making a permanent magnet comprising the steps of:
 - melting an alloy of 20 to 70 atomic percent iron and the balance one or more rare earth elements taken from the group consisting of praseodymium, neodymium, and samarium;
 - quenching said molten alloy at a rate such that it solidifies substantially instantaneously to form an alloy with a substantially amorphous to very finely crystalline microstructure as measured by X-ray diffraction having a room temperature intrinsic magnetic coercivity of at least about 1,000 Oersteds; and

comminuting and compacting said alloy into a magnet shape and magnetizing it in an applied magnetic field.

3. A method of making an alloy with permanent magnetic properties comprising the steps of:
 - alloying a mixture consisting essentially of 20 to 70 atomic percent iron and the balance of one or more rare earth elements taken from the group consisting of praseodymium, neodymium, and samarium;
 - melting said alloy to form a fluid mass;
 - withdrawing a small amount of said alloy from said fluid mass; and
 - instantaneously quenching said small fluid amount such that the as quenched alloy has an inherent intrinsic magnetic coercivity of at least 1,000 Oersteds at room temperature.
4. A method of making a magnetically hard alloy directly from a molten mixture of iron and rare earth elements comprising:
 - melting a mixture consisting essentially of 20 to 70 atomic percent iron and the balance one or more rare earth elements taken from the group consisting of neodymium, praseodymium, and mischmetals thereof;
 - expressing said molten mixture from an orifice; and
 - immediately impinging said expressed mixture onto a chill surface moving at a rate with respect to the expressed metal such that it rapidly solidifies to form an alloy ribbon with a thickness less than about 200 microns having a magnetic coercivity at room temperature of at least about 1,000 Oersteds.
5. A method of making an iron-rare earth element alloy having a magnetic coercivity of at least 1,000 Oersteds at room temperature comprising melting an alloy of 20 to 70 atomic percent iron and the balance one or more rare earth elements taken from the group consisting of praseodymium, neodymium, samarium, and mischmetals thereof; and ejecting said alloy through an orifice sized such that when the ejected alloy is impinged onto a chill surface traveling at a substantially constant velocity relative thereto, a ribbon having a thickness less than about 200 microns and a substantially amorphous to very finely crystalline microstructure as determinable by ordinary X-ray diffraction is formed.
6. A method of making an iron-rare earth element permanent magnet alloy having a Curie temperature above 295° K. and a coercivity greater than about 1,000 Oersteds at room temperature comprising melting an alloy consisting essentially of 20 to 70 atomic percent iron and the balance one or more rare earth elements taken from the group consisting of praseodymium, neodymium and samarium; expressing said alloy through an orifice; and impinging the expressed metal onto a chill surface traveling at a velocity relative thereto such that an alloy ribbon having a thickness less than about 200 microns is formed.
7. A friable ribbon of rare earth-iron alloy having been formed by melt-spinning a homogeneous mixture of iron and neodymium, said ribbon having an intrinsic magnetic coercivity at room temperature of at least 1,000 Oersteds as formed.
8. A method of making an alloy with permanent magnetic properties at room and elevated temperatures comprising the steps of:
 - mixing iron and one or more rare earth elements taken from the group consisting of praseodymium, neodymium and samarium;

4,496,355

9

melting said mixture; and
quenching said molten mixture at a rate such that it solidifies to form an alloy having a substantially flat X-ray diffraction pattern and an intrinsic magnetic coercivity at room temperature of at least about 1,000 Oersteds.

9. A method of making an alloy with permanent magnetic properties at room temperature comprising the steps of:

forming a mixture of iron and at least one rare earth element taken from the group consisting of praseodymium, neodymium, samarium and mischmetals thereof;

heating said mixture in a crucible to form a homogeneous molten alloy;

pressurizing said crucible to eject said mixture through an orifice in its bottom about 250-1200 micronmeters in diameter; and

impinging said ejected mixture onto the perimeter of a chill wheel rotating at a rate such that an alloy ribbon less than 200 microns thick with an intrinsic coercivity of at least 5,000 Oersteds at room temperature is formed.

10. A method of making an alloy which may be directly manufactured into a permanent magnet as it is quenched from the melt comprising:

melting an alloy of iron and one or more rare earth elements taken from the group consisting of neodymium, praseodymium, samarium and mischmetals thereof;

expressing said molten alloy from an orifice; and immediately impinging said expressed alloy onto a chill surface moving at a rate with respect to the expressed metal such that it solidifies substantially instantaneously to form a brittle ribbon with a thickness less than about 200 microns and a magnetic coercivity at room temperature of at least about 1,000 Oersteds.

11. A method of making an iron-rare earth element alloy having an inherent magnetic coercivity of at least 1,000 Oersteds at room temperature comprising:

alloying a mixture of iron and one or more rare earth elements taken from the group consisting of praseodymium, neodymium, samarium and mischmetals thereof;

melting said iron-rare earth alloy in a crucible having an outlet orifice through which said alloy may be expressed at a controlled rate;

expressing said alloy from said orifice and impinging the expressed molten stream onto the perimeter of a rotating chill surface traveling at a relative velocity with respect to the stream such that an alloy ribbon having a thickness less than about 200 microns and a substantially amorphous to very finely crystalline microstructure as determinable by X-ray diffraction is formed.

12. A permanent magnet having an inherent intrinsic magnetic coercivity of at least 5,000 Oersteds at room temperature comprising a rapidly quenched alloy of iron and one or more rare earth elements taken from the group consisting of neodymium, samarium and praseodymium.

10

13. A permanent magnet alloy having an inherent intrinsic magnetic coercivity of at least 5000 Oersteds at room temperature comprising iron and one or more rare earth elements taken from the group consisting of neodymium and praseodymium.

14. A permanent magnet having an inherent intrinsic magnetic coercivity of at least 5000 Oersteds at room temperature which comprises one or more light rare earth elements taken from the group consisting of neodymium and praseodymium and at least 50 atomic percent iron.

15. A permanent magnet having an inherent intrinsic magnetic coercivity of at least 5000 Oersteds at room temperature and a magnetic ordering temperature above about 295° K. which comprises one or more rare earth elements taken from the group consisting of neodymium and praseodymium, and at least about 50 atomic percent iron.

16. A permanent magnet alloy having an inherent intrinsic magnetic coercivity of at least 5000 Oersteds at room temperature and a magnetic ordering temperature above about 295° K. comprising one or more rare earth element constituents taken from the group consisting of neodymium, praseodymium or mischmetals thereof and iron or iron mixed with a small amount of cobalt where the iron comprises at least 50 atomic percent of the alloy.

17. A permanent magnet containing a magnetic phase based on one or more rare earth elements and iron, which phase has an intrinsic magnetic coercivity of at least 5,000 Oersteds at room temperature and a magnetic ordering temperature above about 295° K., the rare earth constituent consisting predominantly of neodymium and/or praseodymium.

18. A permanent magnet based on neodymium and iron, which phase has an intrinsic magnetic coercivity of at least 5,000 Oersteds at room temperature and a magnetic ordering temperature above about 295° K.

19. A magnetically hard alloy consisting essentially of at least 20 atomic percent iron and the balance one or more rare earth elements taken from the group consisting of praseodymium, neodymium and samarium, said alloy having been formed by instantaneously quenching a homogeneous molten mixture of the rare earth and iron to create a magnetic microstructure with an intrinsic magnetic coercivity of at least 1,000 Oersteds at room temperature.

20. A substantially amorphous to very finely crystalline alloy that therefor has a magnetic coercivity of at least about 1,000 Oersteds at room temperature comprising 20 to 70 atomic percent iron and the balance one or more rare earth elements taken from the group consisting of praseodymium and neodymium or mischmetals thereof.

21. A friable metal ribbon having a coercivity of at least about 1,000 Oersteds at room temperature that can be comminuted, pressed and magnetized as quenched from the melt to make permanent magnets comprising 20 to 70 atomic percent iron, and one or more rare earth elements taken from the group consisting of praseodymium, neodymium and mischmetals thereof.

* * * * *

RT6010

PROJECT - 1K

EQUIPMENT COST ANALYSIS BY VOLUME

3.59.41

PAGE 1

VOLUME	EQUIPMENT	DESCRIPTION	TOTAL HOURS	EQUIPMENT COST	TOTAL EQUIP COST
10,000	1A V	SMALL PARTS & BENCH ASM.	2,252.0	1,000	1,000
	2A2 V	MANUAL	633.0	3,000	3,000
	2C V	SEAM	333.0	8,000	8,000
	2K2 V	MEDIUM - PARTS 12" SQ MAX WT 10#	200.0	200,000	200,000
	3C V	FURNACE BRATING	333.0	40,000	40,000
	5A1 V	SMALL - UP TO 1" DIA. STOCK	34.0	8,000	8,000
	5B V	BENDING - HAND	220.0	1,000	1,000
	5X2 V	MEDIUM - 1/8" TO 3/8" SECTION	133.0	15,000	15,000
	7A1 V	1/8" TO 2" O.D. STOCK	3,168.0	20,000	20,000
	7B1B V	2AC	13,584.0	80,000	320,000
	7E2 V	S/SPDL TURRET (47A W/5) 2 5/8" MAX	2,367.0	60,000	60,000
	7E3A V	SMALL	1,667.0	80,000	80,000
	7E3B V	MEDIUM	3,735.0	120,000	120,000
	7E3C V	LARGE	1,517.0	200,000	200,000
	7E4B V	16" TO 18" SWING	750.0	30,000	30,000
	7E4C V	17" TO 40" SWING	6,126.0	50,000	100,000
	7E2 V	SINGLE SPINDLE	999.0	1,800	1,800
	7E3 V	MULTIPLE SPINDLE	133.0	2,400	2,400
	7E4 V	SPEC. MULTIPLE HEAD	4,899.0	10,000	10,000
	7E5 V	NATCO MOL. 5016-15 HF	952.0	75,000	75,000
	7P2 V	MEDIUM	233.0	25,000	25,000
	7P3 V	LARGE	500.0	70,000	70,000
	7S3 V	O.D. & I.D. GRINDER	4,467.0	40,000	40,000
	7V2 V	SGL. STROKE OVER 4" DIA.	333.0	20,000	20,000
	9A V	SNEAKS OR PRESS BRAKE	268.0	12,000	12,000
	8B V	SMALL - UP TO 36" X 48" BED AREA	3,294.0	25,000	25,000

PIONEER ENGINEERING

87/02/31

RT6010 PROJECT - 1K EQUIPMENT COST ANALYSIS BY VOLUME 3.59.41 PAGE 2

VOLUME	EQUIPMENT	DESCRIPTION	TOTAL HOURS	EQUIPMENT COST	TOTAL EQUIP COST
10,000	BC1 V	36" X 48" THRU 60" X 96" (W/AIR)	1,262.0	60,000	60,000
	BC2 V	36" X 48" THRU 60" X 120" (W/AIR)	165.0	70,000	70,000
	BE2 V	MEDIUM	19,260.0	40,000	200,000
	BL1 V	1 1/2 TON	20.0	8,000	8,000
	BL2 V	2 1/2 TON	19,260.0	18,000	90,000
	BR V	HYDROFORM	199.0	150,000	150,000
	13A2 V	MEDIUM PARTS	333.0	200,000	200,000
	14A1 V	SMALL	1,083.0	11,000	11,000
	14A2 V	MEDIUM	33.0	18,000	18,000
	14A3 V	LARGE	534.0	24,000	24,000
	14B V	WASH	1,450.0	41,000	41,000
	14D1 V	SMALL FACILITY	667.0	8,000	8,000
	14D2 V	LARGE FACILITY	417.0	22,000	22,000
	14F V	ELECTRICAL DEBURRING	266.0	17,000	17,000
	14H V	HAND BRINDER	4,299.0	1,000	1,000
	16B1 V	AIR DRY	500.0	100,000	100,000
	20A1 V	\$100,000	234.0	100,000	100,000
	20A3 V	\$300,000	383.0	300,000	300,000
	20A7 V	\$1,200,000	2,062.0	1,200,000	1,200,000
		TOTAL HOURS			106,987.0

ASSET CENTER MANUFACTURING COSTING METHODOLOGY

The methodology used in the development of manufacturing costs by Pioneer follows typical estimating procedures used in the auto industry. The specific approach is the application of burden and labor rates for each piece of equipment, or type of operation. This is labeled an "Asset Center Costing Methodology".

Some costing methodologies use department wide or plant wide burden rates. The later rates are average rates and do not reflect the costs of a specific operation. A particular operation may be the most expensive, or least expensive, in a department, or plant. A design may require a series of operations that are all above the "average" and therefore, an analysis conducted in this manner can be significantly above that of the "real" costs of producing a part.

The following paragraphs discuss the methodology in detail. Pioneer has developed computer programs utilizing micro-computers for the process and cost analyses. However, for clarification, the initial paragraphs describe an operation sheet used for manual process analysis. Later paragraphs discuss the current computerized version.

INITIAL EVALUATIONS

Manufacturing engineers analyze the part or assembly and list each of the manufacturing processes, or operations required to complete the fabrication cycle from the raw material to the finished product.

DETAILED PROCESSING AND COST ESTIMATING

Process engineers and cost estimators, under the direction of manufacturing engineers, conduct a detailed process and cost analysis for each part and assembly. All information developed during this analysis is recorded on the form shown in Figure 1. A Process/Cost Sheet is made out for each part and subassembly. The results are summarized to obtain the total assembly cost.

Two costs can be developed in this process, variable cost and manufacturing cost. The variable cost contains only those costs associated with the manufacture of the part or assembly. Manufacturing cost consists of the variable cost plus fixed burden costs.

An example of the process and cost estimating process shown in Figure 1 is discussed in the following paragraphs. This is a process sheet for forming a bumper face bar.

DRAWING DATE:

1 2 3 4 5 6 7 8 9 10 11 12

The process sheet entries include all operations, from straightening the sheet steel to the final forming of the bumper.

The column headings and other items of interest on the process sheet are:

- OPER (Upper left corner) Each operation is coded in this column. For this part seven distinct operations are required and are coded 10 through 70.
- VOL The production volume at which the items are being costed.
- P/A The number of pieces per assembly of the particular part being costed.
- REQ The number of pieces per year required of the piece being costed. It is a product of VOL (Volume Per Year) and P/A (Pieces Per Assembly).
- OPERATION DESCRIPTION Each distinct operation is described.
- TYPE OF EQUIPMENT Capital Equipment employed in each operation.
- M/P Number of men required for each operation.
- PCS/HR
 MINS PCS/HR is the pieces produced per hour per operation.
 MINS is the minutes per piece to process one piece through each operation.
- LABOR COST
 RATE LABOR COST is the direct labor dollars per piece.
 LABOR RATE is the direct labor dollars per minute (including fringes).
- OCC. HOURS The time, in hours, that it takes to process the part through the operation. For example, if the production rate is 400 pieces per hour, the occupancy hours is one hour divided by 400 pieces per hour or .0025 hours per piece.
- BURDEN RATE There are two burden rate entries, "V" for Variable Burden Rate and "M" for Manufacturing Burden Rate.

"V" (Variable Burden Rate) includes Set-Up Costs, In-Bound Freight, Perishable Production Tools, and other Miscellaneous Costs that vary with volume changes. "M" (Manufacturing Burden Rate) includes Variable and Fixed Burden. Fixed Burden covers Taxes, Insurance, Depreciation on Capital Equipment and Building, Maintenance Costs that do not vary with volume. See Figure 5 for a more definitive list of burden factors for both variable and fixed.

●BURDEN COST

Per piece burden cost is calculated by multiplying each burden rate by the occupancy hours.

● $\frac{\text{VAR COST}}{\text{MFG COST}}$

VAR COST is the variable burden plus direct labor cost. MFG COST is the cost of each operation including direct labor, variable burden, and fixed burden.

●DIE MODELS

Unique die models required for each operation.

●TOOLING

Dies, fixtures and other special tooling required for each operation. Tooling and equipment costs are summarized in the lower middle section.

●MATERIAL

Material is noted and cost calculated in the special box located on the lower left corner of the sheet. Column headings in this area are self explanatory. The type of material is determined in several ways; i.e., by specification on drawing, by chemical analysis, by contacting appropriate technical personnel responsible for material selection. Once the correct material specification is obtained appropriate sources are contacted to obtain the cost per pound of the material in the form and quantity required to produce the part.

●TOOLING COST SUMMARY

The total tooling cost for a given part is summarized in the lower middle section of the Process/Cost Sheet. The tooling cost is reported as a lump sum, leaving

specific amortization up to the client. Tooling is an expense item and may be amortized in the year of use. Competitive economics, however, may preclude this move, so that a more extended amortization period may be used. Since this is a variable subject to the client's marketing strategy, tooling amortization is not a standard entry on these sheets. As a general rule the automotive firms amortize major tools and dies over a three year period. Pioneer has reported consumer costs which include the amortized tooling cost, usually in summary documents, if requested by the client.

●EQUIPMENT COSTS

The lower middle section summarizes cost of equipment, equipment installation and freight, and the cost of all pieces of equipment required to meet the production schedule. For instance, if the annual requirement is 300,000 units, and the shop works two shifts (4000 hours, or 250 days times 16 hours per day), the planning rate of production per operation is 93 units per hour ($\frac{300,000}{4,000}$ divided by .8, inherent delay factor), and if the equipment selected for the particular process can only produce 50 pieces per hour it is assumed that two such processes, or pieces of equipment, will be installed to meet the schedule.

●PART OR ASSEMBLY COST SUMMARY

Costs for producing the part are totaled in the lower right side of the form. The entries are:

TOTAL VARIABLE LABOR AND BURDEN; direct labor plus variable burden.

TOTAL MANUFACTURING LABOR AND BURDEN; direct labor, variable burden and fixed burden.

MATERIAL; total material cost.

SCRAP; an allowance for scrap based on experience.
(% of Var. Cost)

MARKUP; since this is a part involving inter-divisional transfer, a markup is included.

TOTAL VARIABLE COST; the sum of items (a), (c) and (d).

TOTAL TRANSFER COST; the sum of (b), (c) (d) and (e). This part is obviously a very high material sensitive part since approximately 70% of the transfer cost is reflected in the cost of steel.

All sub-assembly and final assembly cost will also be developed on these process sheets. A work flow chart illustrating the methodology used to build up assembly cost is presented in Figure 2.

Figure 3 presents a flow diagram of the cost build up from basic cost items through consumer costs.

COST METHODOLOGY VIA COMPUTER PROGRAM

To permit more expeditious data processing, Pioneer uses a computer program to make all of the calculations discussed above.

Using the computer requires that the manufacturing engineer process the part being costed, select the equipment required, and define the operation cycle time. Figure 4 illustrates the Process/Cost Sheet prepared by the manufacturing engineer for the computer method. Note the equipment code specified for each operation. From this information the computer selects the appropriate labor and burden rates, as well as equipment costs. Using the specific cycle time, indicated manpower level and the equipment code, the computer calculates the labor cost, occupancy hours, variable burden, and manufacturing burden. It is also programmed to determine the multiples of a given machine required for an operation to produce the required number of pieces per hour. This is particularly important where costs are determined for a series of different production rates, where a process may not change from one rate to another, but only one machine may satisfy the requirement instead of two at a greater requirement. The scrap material costs are computed and the total cost is calculated.

Use of the computer permits error free accumulation of the total cost of a product, eliminating manual build up of sub-assembly to final assembly costs. Other cost data manipulations and extractions are possible using the computer which are cost prohibitive if attempted manually.

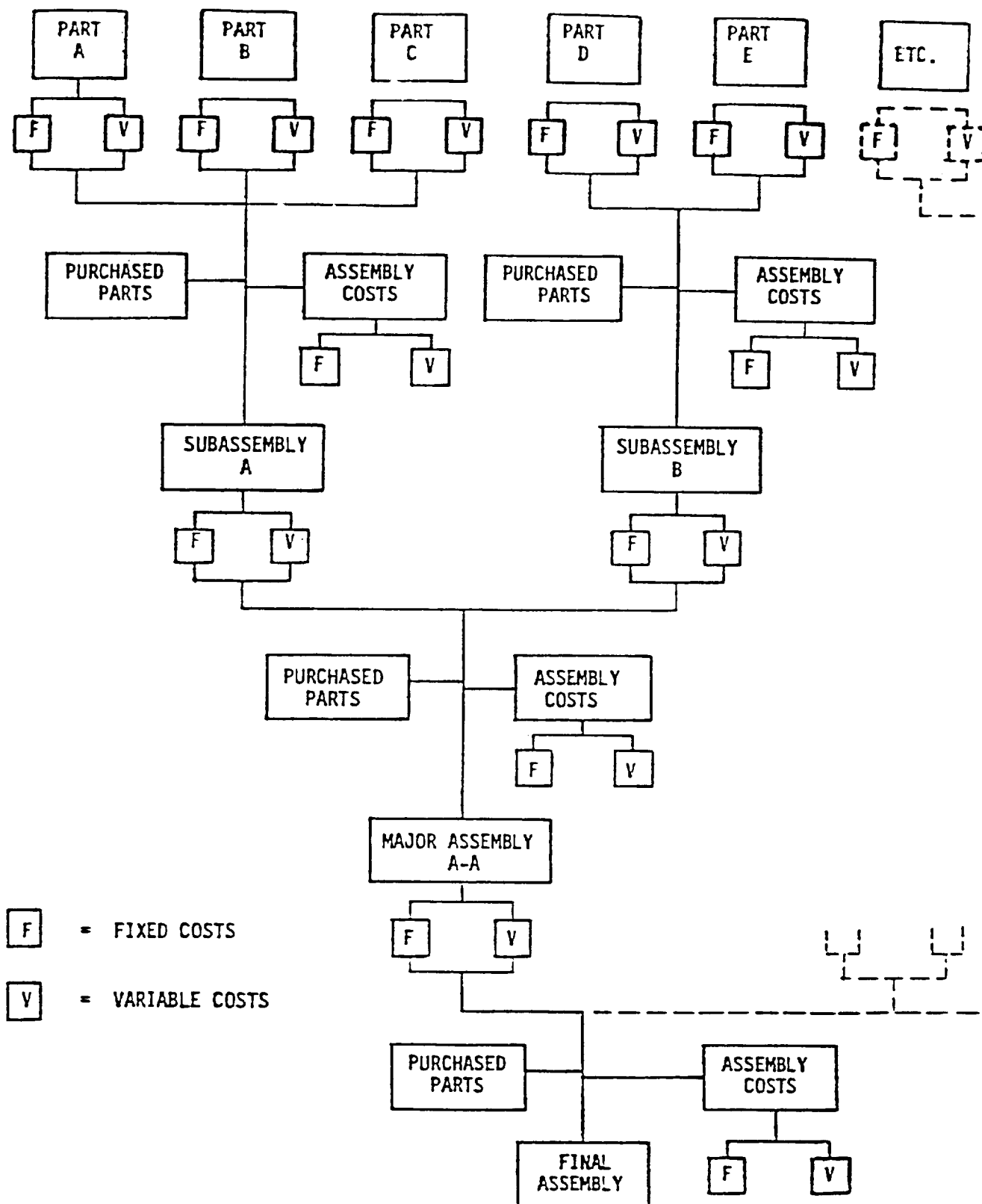


Figure 2

124

DETERMINATION OF MANUFACTURING AND CONSUMER COSTS

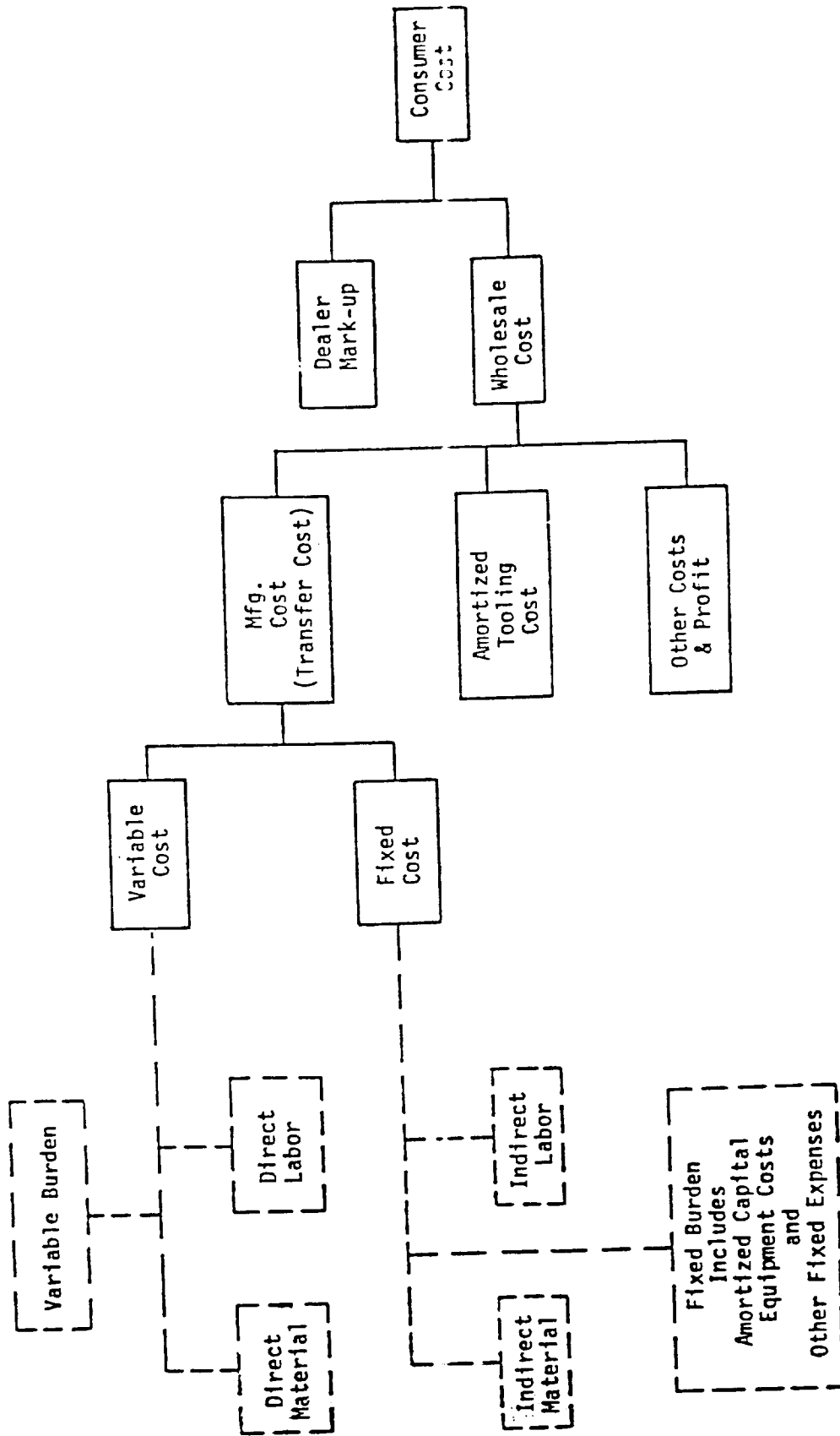


Figure 3

115

375

ORIGINAL PAGE IS
OF POOR QUALITY

PIONEER ENGINEERING
MANUFACTURING COST ANALYSIS

PROJECT - 1D

RT0005

VOLUME- 400,000
PART # - 1
P/A- 1
DESC- DOOR - OUTER PANEL - IN/WHITE

OPER	OPERATION DESCRIPTION	EQUIP	M	STD MIN	LAB COST LAB RATE	OCC HRS	BURDEN RATE	BURDEN COST	VAR COST HFG COST	DIE MODEL	TOT \$00
010	ROUGH BLANK FROM SHEET AUTO LOAD & EJECT	BD1	1.00	.12	.0381 .3174	.0020	V 66.12	.1322	.1703	0	
020	DRAW COMPL. AUTO LOAD, EJECT & TURNOVER	BD1	1.00	.16	.0508 .3174	.0027	V 66.12	.1785	.2293	0	
030	TRIM BINDER STK. & PIERCE LK. & HDL. HLS	BD1	.00	.16	.0000 .3174	.0027	V 66.12	.1785	.1785	0	
040	FORM HEM FLANGE 3 SIDES & BELT FLANGE	BD1	.00	.16	.0000 .3174	.0027	V 66.12	.1785	.1785	0	
050	FIN. FORM BELT FLANGE COMPLETE	BD1	1.00	.16	.0508 .3174	.0027	V 66.12	.1785	.2293	0	
ANNUAL REQ-	400,000										
MAT CODE -											
COST/LB -	.294										
SCRAP FAC -	.0%										
ROUGH WT -	16.69										
FINAL WT -	10.40										
LAB MIN -	.4400										
LABOR \$ -	.1397										
BURDEN V-	.8462										
SCRAP -	.0000										
MATERIAL-	4.9069										
OTHER-	.00										
TOTAL VAR											5.892

Figure 4

BURDEN RATE DERIVATION

Pioneer does its cost estimating using the "Asset Center" burden approach, as opposed to the more common, less demanding technique of deriving manufacturing cost by applying departmental or plant wide burden as a percentage of direct labor cost. The "Asset Center" approach is not normally used by most companies because it requires a more refined and sophisticated data collection system, the complexity of which is shunned by comptrollers. It is however, more accurate and for this and many other reasons is the approach used by Pioneer. The following paragraphs review some of the philosophical rationale for using "Asset Center" burden rates.

Classically burden rates are historically determined — the burden rates for this year's projected costs are based on what was accumulated last year. The resultant burden rates are closely guarded secrets by most companies. The question could easily be asked, then, how does Pioneer — a consultant house with manufacturing operations — come to possess burden rates, especially in an "Asset Center" format?

Pioneer has been applying the "Asset Center" costing methodology for well over a decade. The costing personnel is, and has been, composed of individuals who have had significant, in depth, experience in costing and manufacturing, especially in the automotive industry. This depth of exposure has been harnessed to quantify the factors contributing to the operation of a nominal manufacturing facility. This process is tedious and time consuming, requiring a number of iterations to verify the choice of coefficients. The results are variable and manufacturing burden rates that are representative of a reasonably well managed production facility. These rates are for obvious reasons considered proprietary.

The evidence of the sufficiency of the burden rates has been two-fold. First, Pioneer has had the opportunity to compare its costs for various items directly with those produced for various companies by their personnel. These comparisons have been made on the level of labor, material, and burden costs, not merely an end item summary.

Second, Pioneer routinely does purchase analysis, that is, checking the cost being paid for purchased items. Where a Pioneer cost estimate is below the purchase cost, Pioneer has gone out to qualified vendors for new quotations. Literally millions of dollars have been saved by Pioneer clients where Pioneer costs have indicated that the purchase price should be lower than that being paid.

As a result Pioneer has gained confidence in the reliability of its "Asset Center" burden rates.

PIONEER ENGINEERING & MANUFACTURING
BURDEN FACTORS

<u>FIXED</u>	<u>VARIABLE</u>
Salaries & Fringes	Salaries & Fringes
Maint. Repair (Grounds & External Bldg.)	Maint. Repair (Internal Bldg. & Production Equipt.)
Welding Equipment	Welding Equipment
Material Handling	Material Handling
Non Capitalized Project Expense	Power Tools
Preproduction Expense set up as a fixed cost	Expense Tools
 Dies (Maintenance)	Set-up
Operating Supplies	Dies
Office Supplies	Operating Supplies
 Janitor Supplies	Office Supplies
Misc. Supplies	Welding Supplies
Heating	Janitor Supplies
Transportation	Other Misc. Supplies
Electric Power & Light (Based on min. rate x usage set by Utility)	 Transportation
 Water	Electric Power & Light
Communications (Wats)	 Fuel
Plant Protection	Water
 Non Productive Freight	 Other Purchased Services (i.e. Kelly Girls)
Company Car & Travel Expense	Non Productive Freight
Executive Fringes & Services	
State & Local Taxes	
Insurance	
Depreciation	
Pensions & Leaseholds	

Figure 5

Figure 5 lists the factors that have been considered in the determination of the Pioneer burden rates. The ratio of application of these costs between fixed and variable burden are not shown inasmuch as this is considered proprietary.

COST METHODOLOGY VARIANCE

Estimating as the name implies, is not an exact science, rigidly controlled by natural laws. There are variables. The variables are:

1. The method manufacture of the part.
2. The skill of the estimator.
3. The applicable labor and burden rates used by the estimator.
4. The estimating methodology.

Each of these variables is capable of producing differences in cost estimates of the same part.

Much of estimating is based on judgement. The first variable, method of manufacture, is judgement dominated. How a part is to be made is conditioned by the estimator's background and work experiences. For example, because one estimator's background is stamping-intensive, chances are his judgements (opinions), reflecting a higher degree of skill, will produce a highly reliable estimate of a sheet metal part. The same man, estimating a machined part, will not produce as reliable an estimate.

In many cases, there is no single, best way to make a part. When the production volume is large enough to justify a double tool-up, for example, some manufacturers will deliberately tool the same part differently in order to gain operating experience in their search of optimum methods. For example: Today, door panels — both inner and outer — are produced singly by one automotive company, and doubly (two-at-a-time) by a competitor. In each case, production volumes are similar. What factors prompted these dissimilar tool-ups? Presumably, both methods were considered by each process engineer before the final choice. Each had to consider the "economics" of both methods. Is one "more right" than the other? What this illustrates, is the flexibility inherent in the estimating process.

Some men, cautious by nature, will play it safe and "throw in two or three more operations".⁽¹⁾ This generosity is, in turn, compounded by the multiplier effect —three to five times — when the burden cost is applied.

⁽¹⁾ Operations = Steps in the manufacturing sequence.

From these examples, it is easy to see how estimating variances can occur in the first two variables.

The third variable, labor and burden rates, is the most abused element in cost estimating. The reason is that most estimators are excellent mechanics and engineers, know manufacturing techniques, but are poor financiers — most have only a rudimentary comprehension of how burden rates and burden costs are developed and applied. Their principal interest is in developing the manufacturing sequence, and specifying the equipment and tooling. Of secondary importance (interest) is the selection of the proper labor and burden rates. This step, performed almost casually by most estimators, is perhaps the most important in the estimating process because of the multiplier effect (most estimators calculate the burden cost of an operation by multiplying the direct labor cost by a burden percentage factor, usually two to eight times the labor cost).

Most manufacturing operations involve a single machine, such as a punch press, run by a single operator. To illustrate how the typical estimator develops a cost estimate, assume such a machine, run by a single operator, performing a forming operation, a sheet metal part, 300 parts per hour are produced in this operation. The direct labor, therefore, is .2 minutes per part ($\frac{60}{300}$). Assuming a direct labor cost of \$10.00 per hour the labor cost for this operation comes to:

$$\frac{.2 \times 10.00}{60} = \$.033$$

The next step is the calculation of the burden or factory overhead. Estimating departments have a schedule of burden rates, a specific rate for a specific machine, developed by the plant comptroller.

One of the methods used in calculating burden is to multiply the direct labor cost for a given operation by a percentage factor: e.g., 300%, 400%, etc. These percentage factors are developed from historical data accumulated over a number of accounting periods. These factors usually are based on data covering a whole department (sometimes on data which is not broken down below that of a whole plant). Consequently, the factors can be influenced by departmental conditions not specifically related to the operation itself. Burden rates based on historical data can very easily include inefficiencies that get lost in the overall departmental or plant operation.

Burden costs developed as a percentage of labor are still related to the type of equipment. It should be noted that labor can vary relative to a piece of equipment

depending upon the complexity of the part and specific operation performed but the burden remains the same. As an illustration of this and expanding on the example discussed above:

$$\text{Labor Cost } (.033) \times \text{Burden Factor } (300\%) = \$.099.$$

The combined labor and burden cost for this operation, then, is $.033 + .099 = \$.132$.

Assume in our example that a second man, a helper, is required to man the stamping press. The labor cost now becomes \$.066 per operation per part. The unwary estimator will often assume that the burden cost should then be $300\% \times .066$, or \$.198.

This is obviously false, since the overhead doesn't double simply because another man has been added. Only the incremental costs, in this situation, associated with the addition of the second man should be added to the base cost calculated earlier. The estimator should "up the cost" of the operation by only the direct labor cost of the second man (\$.033). The burden cost would remain as it was when one man operated the press. The new cost for the press operation, now manned by an operator and a helper, is $.033 + .033 + .099 = \$.165$.

Another problem which occurs frequently in estimating, is the application of burden to an unmanned manufacturing operation. For example, assume a sequence of six press operations required to make a stamping. The first, or blanking operation, required two operators to remove the blank, dope it with lubricant and insert it in the draw die of the following operation, making sure that two blanks have not stuck together (a double blank could wreck the draw die). The next three operations are loaded and unloaded mechanically, the part is even inverted between operation 3 and 4, all without operator intervention. The final operation, a cam-piercing operation, requires one operator who removes the part, applies a dab of paint for identification, and hangs the part onto a conveyor.

What cost does the estimator assign to each operation? If he is using the burden percentage method, there is no problem with the first and final operations, since these have operators. The estimator simply calculates the direct labor cost for each of these, then multiplies these by the burden percentage rates to obtain the burden cost, making sure, of course, that he has not doubled the burden cost in the first operation which has two operators.

The problem arises when the estimator tries to apply his formula to those operations which are unmanned. There is no direct labor cost, nothing he can multiply by his

burden percentage rate. The unwary estimator will frequently assume that, since there is no labor cost, there can be no burden cost.

We know this to be false, since all of the burden elements — with the exception of fringe benefits — are still there whether an operator is present or not.

Another method of burden cost calculation used by Pioneer, is the "Burden Center" concept.

Whereas the "Burden Percentage" method covers a full department, sometimes an entire plant, the "Burden Center" approach considers a much smaller entity: a single machine plus only those expenses directly associated with the operation of the machine. These expenses are both variable (expenses which vary with product volume changes) and fixed (expenses which are unaffected by volume changes).

Typical variable expenses considered in burden would be (this is not a complete list):

- | | |
|--------------------|-------------------|
| — Indirect Labor | — Maintenance |
| — Perishable Tools | — Fringe Benefits |
| — Fuel | — Utilities |

Typical fixed and non-variable expenses would be:

- | | |
|--------------------------|----------------------|
| — Taxes | — Insurance |
| — Amortization | — Some Supervision |
| — Some Clerks & Janitors | — Some Utility Bills |

A pro rata share of each of these elements is assigned to each burden center. The result is a carefully-developed, localized cost for a specific machine or other asset, reflecting only those expenses unique to that machine. These costs are stated in "dollars per machine-hour" giving rise to the expression: Machine-hour rate.

"Burden Center" rates can be generated historical data, or they can be developed from equipment specifications and requirements for power, lubrication, light, heat, indirect labor, average maintenance, material handling, and other costs required to keep the equipment operating. The latter method of burden development is beneficial when developing costs for a new plant or facility where historical data has not been developed. Another advantage in the latter approach is that nominal burden costs can be developed around nominal equipment production rates.

Costs developed around nominal production rates for a piece of equipment are an important consideration when assessing production costs. For example, a piece of equipment has a theoretical production rate for which it is designed. This theoretical rate may not be achieved because of inherent equipment and human operational conditions. However, "nominal" rates have been established through experience of an acceptable "efficient" plant. Well managed plants can achieve these nominal rates. All cost analyses should be developed around burden rates based on "nominal" production standards. Costs developed with burden rates established with other than nominal standards should not be used for comparison because they include variances in production inefficiencies and do not have a common base. Pioneer costs are established around nominal production rates.

There are other cost methodologies. One such method uses the cost-per-pound approach. Under this method, the parts of a car, for example, are grouped by classes of material: steel stampings, castings, forgings, molded plastics, etc. The cost of each part is divided by its finished weight, and a cost-per-pound obtained: a "meat-market" approach. Pioneer does not endorse this method because of its dependence on a straight-line relationship between weight and cost. For example, if a seven-pound brake drum cost \$3.50, will a nine-pound drum cost \$4.50? (\$.50 per pound.) Unlikely. The labor and burden will remain essentially the same for each size of drum, but the material cost, obviously, will be different. In spite of its imprecision, the method has some utility: as a "rough-and-dirty" indicator of approximate cost, as a crude verification that the estimate is "in the ball park".

Report Documentation Page

1. Report No. NASA CR-180890		2. Government Accession No.		3. Recipient's Catalog No.	
4. Title and Subtitle Conceptual Design of an Advanced Stirling Conversion System for Terrestrial Power Generation				5. Report Date January 1988	
				6. Performing Organization Code	
7. Author(s)				8. Performing Organization Report No. MTI-87-TR57	
				10. Work Unit No.	
9. Performing Organization Name and Address Mechanical Technology Inc., Latham, New York; Sanders Associates, Inc., Nashua, New Hampshire; Thermacore Inc., Lancaster, Pennsylvania; and Pioneer Engineering Company, Madison Heights, Michigan				11. Contract or Grant No. DEN 3-372	
				13. Type of Report and Period Covered Contractor Report	
12. Sponsoring Agency Name and Address U.S. Department of Energy Office of Solar Heat Technologies Washington, D.C. 20545				14. Sponsoring Agency-Code Report No. DOE/NASA/0372-1	
15. Supplementary Notes Final Report. Prepared under Interagency Agreement DE-AT04-85AL33408. Project Manager, R.K. Shaltens, Power Technology Division, NASA Lewis Research Center, Cleveland, Ohio 44135.					
16. Abstract This report describes the conceptual design of a system for converting solar energy into electricity using a free-piston Stirling engine directly coupled to a linear alternator. The system is designed for mounting at the focal plane of a 100 m ² parabolic solar collector. It includes a receiver which is integrated with the engine heater head. Heat transfer from receiver to engine involves boiling liquid sodium at the heater surface of the receiver and condensing sodium vapor on the engine heater tubes. A sintered wick is located on the back surface of the receiver face to distribute the sodium and gravity is used to return the condensed sodium to a sump within the receiver. The system is connected to a utility power grid. The net power output from the system is 23.2 kWe at the design point (75 kWt into the receiver). Maximum power output is 26.7 kWe at the peak insolation level. Annual output is approximately 60 000 kWh for a site at Albuquerque, New Mexico. The manufacturing cost for the System has been esti- mated at approximately \$8500 (1984 dollars). The installed cost goal is \$13 000 (1984 dollars). Costs at the conceptual design level are only approximate but the estimates indicate that acceptable costs are attainable.					
17. Key Words (Suggested by Author(s)) Stirling engines Solar power conversion Distributed solar system			18. Distribution Statement Unclassified - Unlimited Subject Category 85 DOE Category UC-96		
19. Security Classif. (of this report) Unclassified		20. Security Classif. (of this page) Unclassified		21. No of pages 388	
				22. Price* A17	